Structure-Property Insights into Molybdenum Imido Alkylidene *N*-Heterocyclic Carbene Complexes for Olefin Metathesis

Von der Fakultät Chemie der Universität Stuttgart
zur Erlangung der Würde eines
Doktors der Naturwissenschaften (Dr. rer. nat.)
genehmigte Abhandlung

vorgelegt von

Mohasin Shamshuddin Momin
aus Karad, Indien

Hauptberichter:	Prof. Dr. Michael R. Buchmeiser
Mitberichter:	Prof. Dr. Biprajit Sarkar
Prüfungsvorsitz:	Prof. Dr. Dietrich Gudat

Tag der mündlichen Prüfung: 25.03.2021

Institut für Polymerchemie
Universität Stuttgart
2021

Dedicated to My Family

This work was carried out from April 2017 to January 2021 at the Institute of Polymer Chemistry (University of Stuttgart, Germany) under the supervision of Prof. Dr. M. R. Buchmeiser.

Erklärung über die Eigenständigkeit der Dissertation

Ich versichere, dass ich die vorliegende Arbeit mit dem Titel:

“Structure-Property Insights into Molybdenum Imido Alkylidene N-Heterocyclic Carbene Complexes for Olefin Metathesis”

selbständig verfasst und keine anderen als die angegebenen Quellen und Hilfsmittel benutzt habe; aus fremden Quellen entnommene Passagen und Gedanken sind als solche kenntlich gemacht.

Declaration of Authorship

I hereby certify that the dissertation entitled:

“Structure-Property Insights into Molybdenum Imido Alkylidene N-Heterocyclic Carbene Complexes for Olefin Metathesis”

is entirely my own work, unless indicated otherwise. Passages and ideas from other sources have been clearly indicated.

Name/Name: Mohasin Momin

Unterschrift/Signed: _____

Datum/Date: _____

Acknowledgment

First and foremost, I would like to express my deep regard, sincere gratitude and heartfelt thanks to Prof. Dr. Michael R. Buchmeiser for offering me a doctoral position in his magnificent research group. I absolutely admire your inspirational guidance, stimulating personality and encouragement throughout the thesis work. I would also like to thank you for providing the best working conditions and funding the conference visits.

I would like to thank Prof. Dr. Biprajit Sarkar for reviewing my work and Prof. Dietrich Gudat for chairing the examination committee.

Special thanks to Dr. Dongren Wang for his wholehearted support in administrative work and GC-MS troubleshooting throughout my Ph.D. studies. I would also like to thank Dr. Wolfgang Frey for measuring crystal structures and always cheerful attitude, Barbara Förtsch for measuring elemental analyses and the Institute of Organic Chemistry's analytics department for measuring mass spectra. I would like to thank Mike Wendel for his support in glove box maintenance and technical and safety matter in the laboratory.

I am thankful to Philipp, Janis and Mathis for proofreading my work and abstract translations. Mathis and former colleagues Iris and Roman deserve special thanks for always being there for invaluable scientific discussions and support. "SuperLab - 0.563: Jonas, Philipp, Pradeep, Hande and Alina; thank you very much all of you. It was a great time with a variety of good music. I would like to thank Hagen for helping me with the initial administrative formalities and visa extensions. Former colleagues Kathrina and Jessica, thank you for your moral support and for being a good friend. During my stay at the Buchmeiser group, I found everyone very special, helpful and cooperative. I would like to thank all of you for a great time, a pleasant atmosphere, the Wasen visit and the barbecues. I would also like to thank my colleagues cum friends, Abdul Wasif, Pradeep and Saravana, for Mughlai to South Indian cuisines and their valuable support.

Outside the lab, I would like to thank Swayam, Shreyash, Mohit, Vithavya, Hasan, Saad, Zulqarnain, Suleman, and Hajisaab for making my stay in Stuttgart more pleasant and enjoyable. I would like to thank my former colleagues from IOCL, India, Dr. Bhasker Bantu, Dr. Naresh Kumar, Dr. Sukhdeep Kaur and Dr. Gurmeet Singh, for their valuable support. Of course, the list of well-wishers will not be complete until I don't mention few names; Vinod, Ravi, Khudbuddin and Vinayak. I am thankful to them for their unconditional support and for being excellent friends.

Last but not least, I would like to thank my family – the best family, without their support, I could not have succeeded. My dear mother (late): who showed me the path to science; my father: grateful for his patience and believing in me; my sisters Shakoappa, Ranoappa and Sajida: the best sisters in the world; my brother Rajubhaiyya: the best brother one could have. I would also like to thank my brother in laws, sister in law, paternal and maternal uncles and aunts for their prayers and support. I am indebted to my wife Jasmin and both the sons, Abdul Ahad and Muhammad Saad, for their patience and am thankful to them for being a constant inspiration throughout the thesis. You have given me a lot of strength and support!

CURRICULUM VITAE

Mohasin Momin

Profile

Ph. D. student at the Institute of Polymer Chemistry, University of Stuttgart, Germany, under the supervision of Prof. Michael R. Buchmeiser since 2017. Research focus on organometallic Chemistry, polymer chemistry and catalysis.

Personal Data

Name	Mohasin Momin
Date of Birth	July 13th, 1984
Place of Birth	Karad, India

Education

Ph. D.	Since 04.2017	#Institute of Polymer Chemistry, University of Stuttgart, Germany #Thesis title: "*Structure-Property Insights into Molybdenum Imido Alkylidene N-Heterocyclic Carbene Complexes for Olefin Metathesis*" #Adviser: Prof. Dr. Michael R. Buchmeiser
M. Sc.	06.2004 – 05.2006	#Organic Chemistry, Shivaji University, Kolhapur, India #Thesis Title: "*Synthesis of novel α, β – unsaturated aromatic esters by Knoevenagel condensation reaction*" #Adviser: Prof. Dr. D. M. Pore #Grade Obtained – First-Class
B. Sc.	06.2001 – 04.2004	#Specialization – Chemistry, Shivaji University, Kolhapur, India #Minor Subjects – Botany, Zoology, Geology and Pollution #Grade Obtained – First-Class

Work Experience

Teaching Assistant	2018, 2019	Teaching assistant in practical courses for Master students in macromolecular chemistry
Senior Analyst	07.2015 – 03.2017	#Petrochemical & Polymer Dept., Research & Development Centre, Indian Oil Corporation Ltd. (IOCL), Faridabad, India # Ziegler-Natta catalysts for olefin polymerizations; ethylene, propylene and other alpha-olefins polymerization; Drag reducing polymers for product pipeline

Analyst	03.2012 – 06.2015	#Petrochemical & Polymer Dept., Research & Development Centre, Indian Oil Corporation Ltd. (IOCL), Faridabad, India # Ziegler-Natta catalysts for olefin polymerizations; ethylene, propylene and other alpha-olefins polymerization; Drag reducing polymers for product pipeline
Junior Research Fellow	02.2011 – 02.2012	#Polymer Science & Engineering Dept., National Chemical Laboratory (NCL), Pune, India # Development of high temperature materials, such as polyimide, phenolic resins, polyurethanes *etc.*
Project Assistant	10.2007 – 01.2011	#Polymer Science & Engineering Dept., National Chemical Laboratory (NCL), Pune, India # High Internal Phase Emulsion (HIPE) polymerization, Suspension polymerization techniques, Polymerization kinetics etc. Development of high temperature materials, such as polyimide, phenolic resins, polyurethanes etc.
Trainee	10.2006 – 04.2007	# Quality Control Dept., Cipla Pharma Ltd., Goa, India # Quality control analysis of finished products

Publications

2021 *"Tuning the Latent Behavior of Molybdenum Imido Alkylidene N-Heterocyclic Carbene Complexes in Dicyclopentadiene Polymerization"* M. Momin, J. V. Musso, W. Frey, M. R. Buchmeiser, *Organometallics,* **2021**, *40*, 253–265.

2020 *"Origin and Use of Hydroxyl Group Tolerance in Cationic Molybdenum Imido Alkylidene N-Heterocyclic Carbene Catalysts"* R. Schowner, I. Elser, M. Benedikter, M. Momin, W. Frey, T. Schneck, L. Stöhr, M. R. Buchmeiser, *Angew. Chem. Int. Ed.* **2020**, *59*, 951–958.

2019 *"Stereoselective Olefin Ring-Opening Cross Metathesis Catalyzed by Molybdenum Imido Alkylidene N-Heterocyclic Carbene Complexes"* M. Momin, G. M. Nagy, M. R. Buchmeiser, *Adv. Synth. Catal.* **2019**, *361*, 5596–5604.

2015 *"Thermotropic liquid crystalline polyesters derived from bis-(4-hydroxybenzoyloxy)-2-methyl-1,4-benzene and aliphatic dicarboxylic acid chlorides"* K. Mulani, M. Momin, N. Ganjave, N. Chavan, *Bull. Mater. Sci.*, **2015**, *38*, 1301–1308.

2014 *"Thermotropic liquid crystalline polyesters based on trimesogenic diol and flexible spacers"* K. Mulani, M. Momin, N. Ganjave and N. Chavan, *Malaysian Polymer Journal,* **2014**, *9*, 54-61,

Book Chapter

2021 N-*Heterocyclic and Mesoionic Carbene Complexes of Groups 5 and 6 Metals In: Comprehensive Organometallic Chemistry IV*
P. M. Hauser, F. Ziegler, J. Musso, P. Panyam, M. Momin, J. Groos, M. R. Buchmeiser*, Comprehensive Organometallic Chemistry IV,* in press (2021)

Patents (Granted)

2018 *"Process for preparation of Drag Reducing Polymer and usage thereof"*
S. Kaur, M. Momin, M. S. Negi, G. Singh, N. Kumar, B. Bantu, G. S. Kapur, S. Sharma, ***US 10094399B2***, *Oct. 2018*

2018 *"Catalyst process modification and polymerization thereof"*
G. Singh, N. Kumar, B. Bantu, S. Kaur, R. Rani, M. S. Negi, M. Momin, G. S. Kapur, S. Sharma, ***US 9873752B2****, Jan. 2018*

2017 *"Catalyst for olefin polymerization and polymerization thereof"*
G. Singh, N. Kumar, B. Bantu, S. Kaur, R. Rani, M. Momin, G. S. Kapur, S. Sharma, B. Basu, R. K. Malhotra, ***US 9758602B2****, Sep. 2017*

Poster Presentation

2019 *"Highly E- and Z-selective ring opening/cross metathesis catalyzed by molybdenum imido alkylidene N-heterocyclic carbene complexes",*
M. Momin, I. Elser, R. Schowner, M. Benedikter, M. R. Buchmeiser *International Symposium on Olefin Metathesis (ISOM) XXIII,* ***2019***, Barcelona, Spain.

Table of Contents

List of Abbreviations and Symbols

Å	Angstrom
ADMET	Acyclic Diene Metathesis
Ar	Aryl, Aromatic Substituent
ARCM	Asymmetric Ring-Closing Metathesis
AROCM	Asymmetric Ring-Opening Cross-Metathesis
ATR	Attenuated Total Reflection
$B(Ar^F)_4$	Tetrakis[3,5-bis(trifluoromethyl)phenyl]borate
BINOL	1,1´-Binaphthol-2-2´-ol
CM	Cross Metathesis
°C	Degree Celsius
δ	Chemical Shift
d	Doublet
DCMNBE	2,3-Dicarbomethoxynorborn-5-ene
DCPD	Dicyclopentadiene
DFT	Density Functional Theory
Dipp	2,6-Diisopropylphenyl
DME	1,2-Dimethoxyethane
DSC	Differential Scanning Calorimetry
EA	Elemental Analysis
equiv.	Equivalents
Et	Ethyl, C_2H_5
et al.	Et alia
g	Gram
GC-MS	Gas Chromatography - Mass Spectrometry
h	Hour
HM	Homometathesis
HMTO	2,6-Bis(2,4,6-trimethylphenyl)phenolate
HOMO	Highest Occupied Molecular Orbital
Hz	Hertz
HRMS	High Resolution Mass Spectroscopy
ICy	1,3-Dicyclohexylimidazol-2-ylidene
IMes	1,3-Dimesitylimidazol-2-ylidene
*i*Pr	Isopropyl

$IMesH_2$	1,3-Dimesitylimidazolin-2-ylidene
$IMesCl_2$	1,3-Dimesityl-4,5-dichloroimidazol-2-ylidene
IR	Infrared
it	*Isotactic*
I*t*Bu	1,3-Di-*tert*-butylimidazol-2-ylidene
J	Coupling Constant
K	Kelvin
KHMDS	Potassium Hexamethyldisilazide
LUMO	Lowest Unoccupied Molecular Orbital
λ	Wavelength
M	Molar Mass
m	meta
m	Multiplet
m/z	Mass/Charge ratio
MAP	Monoalkoxide-Pyrrolide
Me	Methyl
MeCN	Acetonitrile
Mes	Mesityl
min	Minute
mg	Milligram
MHz	Megahertz
mL	Milliliter
mmol	Millimole
MS	Mass Spectrometry
NBE	Norbornene
NHC	*N*-Heterocyclic Carbene
nm	Nanometer
NMR	Nuclear Magnetic Resonance
o	ortho
OTf	Trifluoromethanesulfonate
OTPP	2,3,5,6-Tetraphenylphenolate
p	para
Ph	Phenyl, C_6H_5
pm	Picometer

ppm	Parts Per Million
py	Pyridine
pyr	pyrrole
q	Quartet
quint	Quintet
RCM	Ring Closing Metathesis
ROCM	Ring-Opening Cross-Metathesis
ROMP	Ring-Opening Metathesis Polymerization
RIM	Reaction Injection Molding
RT	Room Temperature
s	Singlet
SM	Self-Metathesis
SP	Square Pyramidal
SPS	Solvent Purification System
st	*Syndiotactic*
T	Temperature
t	Triplet
*t*Bu	tert-Butyl
TBP	Trigonal Bipyramidal
T_c	Coalescence Temperature
TEP	*Tolmans* Electronic Parameter
T_g	Glass Transition Temperature
THF	Tetrahydrofuran
TMS	Trimethylsilane
TMSCl	Chlorotrimethylsilane
TON	Turn-Over Number
Triflate	Trifluoromethanesulfonate
V_{bur}	Buried Volume
VE	Valence Electrons
wt.	Weight
5-Me	1,3-Dimethylimidazol-2-ylidene
5-MeCl_2	1,3-Dimethyl-4,5-dichloroimidazol-2-ylidene

Objective

One of the revolutionary discoveries within the field of organometallic chemistry are the "Schrock Carbenes." They featured as well-defined catalysts in olefin metathesis, known as Schrock- and Grubbs-catalysts. Progress in catalyst development through catalyst synthesis, catalyst design and mechanistic investigations shaped olefin metathesis as a versatile tool for carbon-carbon bond formation. Olefin metathesis provides a wide range of applications, from the synthesis of complex natural products to the manufacturing of high-strength materials. However, many issues, such as catalyst stability, stereoselectivity, latency, functional group tolerance, etc., require further development. In 2014, *Buchmeiser* and coworkers developed a new class of molybdenum-based olefin metathesis catalyst by coordinating *N*-heterocyclic carbenes (NHC) to molybdenum imido alkylidene bistriflate dimethoxyethane complexes. In addition to the resulting neutral bistriflate NHC complexes, cationic-at-metal complexes could subsequently be prepared by replacing one of the triflate ligands with a weakly-coordinating anion. This class of complexes showed remarkable activity, productivity and functional group tolerance.

The aim of this work was to investigate and modify these molybdenum imido alkylidene NHC complexes to establish structure-property relations in olefin metathesis. Stereoselective ring-opening cross-metathesis (ROCM) was to be addressed by exploiting the influence of the disparity between the size of the imido and aryloxide ligands. Additionally, the influence of the catalysts on post-metathesis isomerization of the products was to be revealed by kinetic studies. Further, the ligands at the metal center should be varied to enrich the present latent catalyst portfolio with more cost-effective catalysts that allow for better control of polymerization. To accomplish this, novel molybdenum imido alkylidene NHC complexes bearing an *O*- and *N*-chelating alkylidene moiety were to be synthesized. Next, the utility of these novel complexes in ring-opening metathesis polymerization (ROMP) of dicyclopentadiene (DCPD) should be demonstrated. Additionally, molybdenum imido alkylidene NHC complexes with electron-poor imido ligand were to be synthesized to investigate their tolerance towards functional groups in olefin metathesis.

Zusammenfassung

In den vergangenen sechs Jahren wurden in unserer Gruppe Molybdän Imido Alkyliden *N*-heterozyklische Carben (NHC) Bistriflatkomplexe mit 16 Valenzelektronen, sowie die korrespondierenden kationischen Molybdän Imido Alkyliden NHC Monotriflat und Monoalkoxid Komplexe mit 14 Valenzelektronen, entwickelt. Die Komplexe zeichnen sich durch hohe Aktivitäten und Produktivitäten in der Olefinmetathese aus, sowie durch ihre Toleranz gegenüber funktionellen Gruppen. Im Rahmen dieser Arbeit konnte die bestehende Katalysatorbibliothek erweitert werden und somit stereoselektive Olefinmetathesereaktionen ermöglicht werden. Im Detail handelt es sich dabei um die ringöffnende Kreuzmetathesereaktion (ROCM) von 2,3-disubstituierten Norbornenderivaten. Mit Hilfe von maßgeschneiderten kationischen Molybdän Imido Alkyliden Monoalkoxid und Monopyrrolid Katalysatoren wurde eine Vielzahl unterschiedlicher linearer Olefine als Partner für die Kreuzmetathese eingesetzt.

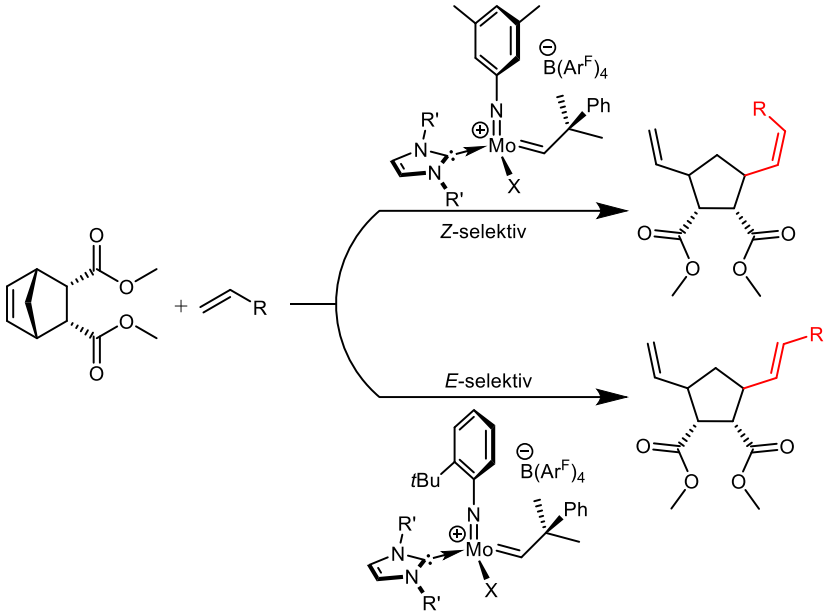

Schema 1. Repräsentative Darstellung der durch Molybdän Imido Alkyliden NHC Komplexe katalysierten stereoselektiven ringöffnenden Kreuzmetathese.

Durch die Wahl der Substitutenten des Imidoliganden kann dessen sterischer Anspruch, der typischerweise mit Hilfe des verdeckten Volumen $\%V_{bur}$ quantifiziert wird, maßgeschneidert werden. Durch Variation der anionischen Alkoxid und Pyrrolidliganden sowie des verdeckten Volumens des Imidoliganden konnten mit bis zu 99 % Selektivität *E*-Olefine sowie mit einer Selektivität von bis zu 96 % *Z*-Olefine hergestellt warden. Werden sterisch wenig anspruchsvolle allyl ether als Partner für

die Kreuzmetathese eingesetzt, so kommt es zur *O*-Chelatisierung des kationischen Metallzentrums, was wiederum zu einer hohen *E*-Selektivität führt. Der Reaktionsfortschritt von Reaktionen mit repräsentativen Katalysatoren, die hohe *E*- bzw. *Z*-Anteile produzieren, wurde mittels GC-MS verfolgt um festzustellen, ob es nach der Metathesereaktion zur Isomerisierung des Produkts kommt. Mit Ausnahme einer Reaktion konnte keinerlei Isomerisierung des Produkts beobachtet werden, obwohl der Katalysator auch nach der Metathesereaktion noch Aktivität zeigte. Die hohe Stereoselektivität der Komplexe ist daher auf thermodynamische, nicht auf kinetische Kontrolle zurückzuführen.

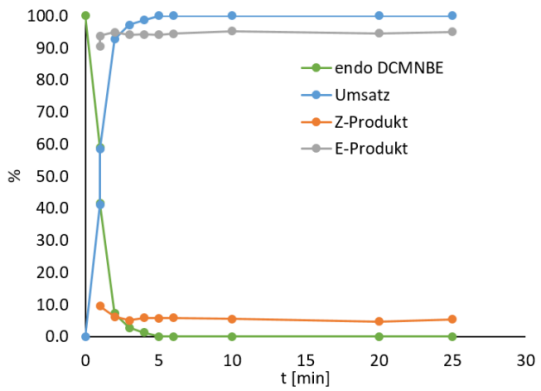

Abbildung 1. a) Kinetik der *E*-selektiven ROCM von *endo, endo*-2,3-Dicarbomethoxynorborn-5-en (DCMNBE) mit Allybenzylether.

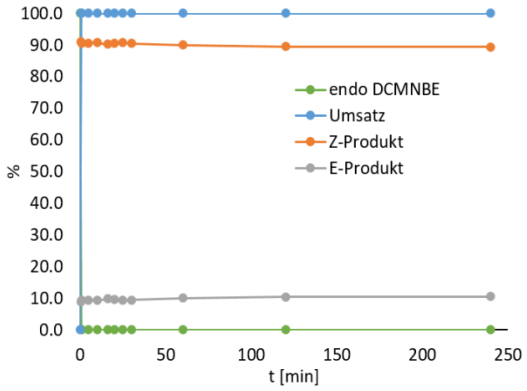

Abbildung 1. b) Kinetik der *Z*-selektiven ROCM von *endo, endo*-2,3-Dicarbomethoxynorborn-5-en (DCMNBE) mit Allybenzylether.

Als Nächstes wurden thermisch schaltbare, hexakoordinierte Molybdäninitiatoren mit chelatisierendem Alkyliden untersucht und als Präkatalysatoren für die ringöffnende Metathesepolymerisation (ROMP) von Dicyclopentadien (DCPD) eingesetzt. Das endgültige Ziel dieser Arbeit war die Entwicklung latenter Präkatalysatoren mit ausreichend niedrigem T_{onset} (die Temperatur, bei welcher die exotherme Reaktion beginnt) sowie quantitativer und schneller Initiierung nach erfolgter Aktivierung. Im Rahmen dieser Arbeit wurde eine Vielzahl neuer Molybdän(VI) Imido Alkyliden NHC Komplexe mit *O*- und *N*-chealtisierenden Alkylidenliganden, größtenteils auf Basis von kommerziell erhältlichen, kostengünstigen Olefinen wie *N*-Vinyl-2-pyrrolidon und 2-Vinylpyridin, hergestellt. Mit Hilfe der dynamischen Differenzkalorimetrie wurde die Eignung der Komplexe als Initiatoren für die ringöffnende Metathesepolymerisation von DCPD verglichen. Präkatalysatoren für die Olefinmetathese, deren Struktur sich von 2-Vinylpyridin ableitet, bildeten durch den chelatisierenden Alkylidenliganden einen viergliedrigen Ring und konnten mit Hilfe der Röntgenstrukturanalyse strukturell

charakterisiert werden. Die labile Beschaffenheit des viergliedrigen Chelats führt zu hoher Aktivität, wobei aufgrund des hexakoordinierten Metallzentrums eine ausreichender gewährleistet ist. Diese hexakoordinierten Komplexe wurden auch auf Ihre Luftstabilität als Feststoff untersucht. Die notwendige Feinjustierung von T_{onset} konnte durch maßgeschneiderte Präkatalysatoren erreicht werden. Neben den Bistriflatkomplexen ermöglichten auch Molybdän Imido Alkyliden NHC Monoalkoxid Monotriflatkomplexe hohe Aktivitäten ohne Verschlechterung der Latenz.

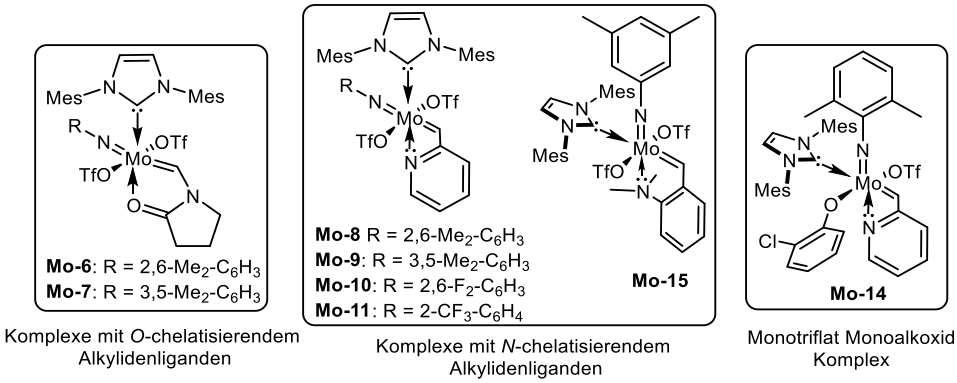

Abbildung 2. *O*- und *N*-chelatisierte Mo Imido Alkyliden NHC Komplexe.

Des Weiteren konnte ein seltenes Beispiel für einen Molybdän η^2-Olefin NHC Komplex durch Kreuzmetathese von 2-Vinylpyridin mit Mo(*N*-2,6-Me_2-C_6H_3)(CHCMe_2Ph)(IMes)(OTf)(O-2-Cl-C_6H_4) isoliert werden (Abbildung 3).

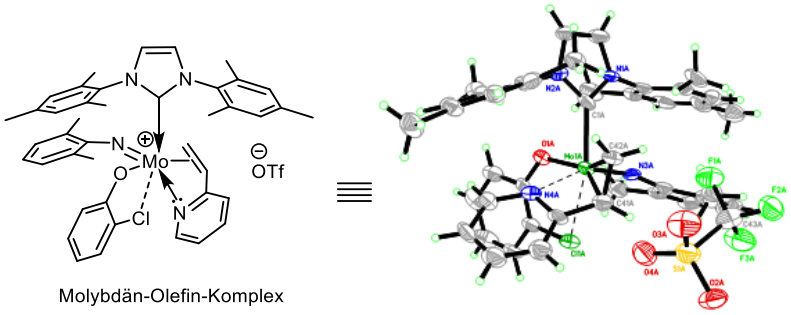

Abbildung 3. Mo η^2-Olefin NHC complex.

Schließlich konnte gezeigt werden, dass Komplexe mit elektronenarmen Imidoliganden nicht nur höhere Produktivitäten aufweisen als analoge Komplexe mit elektronenreichen Imidoliganden, sondern auch Hydroxylgruppen und Luft tolerieren. Daher wurden neutrale und kationische Molybdän 2,6-Difluorphenylimido Alkyliden NHC Komplexe **Mo-19** – **Mo-24** hergestellt (Schema 2).

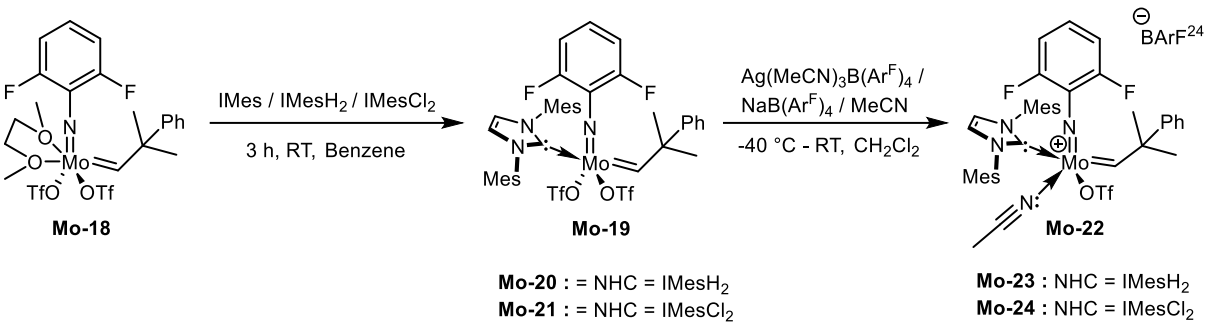

Mo-20 : = NHC = $IMesH_2$
Mo-21 : = NHC = $IMesCl_2$

Mo-23 : NHC = $IMesH_2$
Mo-24 : NHC = $IMesCl_2$

Schema 2. Synthese von Mo 2,6-Difluorphenylimido Alkyliden NHC Komplexen.

Abstract

In the past six years, our group has developed neutral, 16-valence electron (VE) molybdenum imido alkylidene *N*-heterocyclic carbene (NHC) bistriflates as well as the corresponding cationic 14-VE molybdenum imido alkylidene NHC monotriflate and monoalkoxide complexes, which display high activity, productivity and functional group tolerance in various olefin metathesis reactions. This thesis elaborates and extends the existing catalyst library, thereby enabling stereoselective olefin metathesis reactions, specifically ring-opening cross-metathesis (ROCM, Scheme 1). 2,3-Disubstituted norbornene derivatives and a variety of terminal olefins as cross-partners were evaluated, employing tailored cationic molybdenum imido alkylidene monoalkoxide and monopyrrolide catalysts.

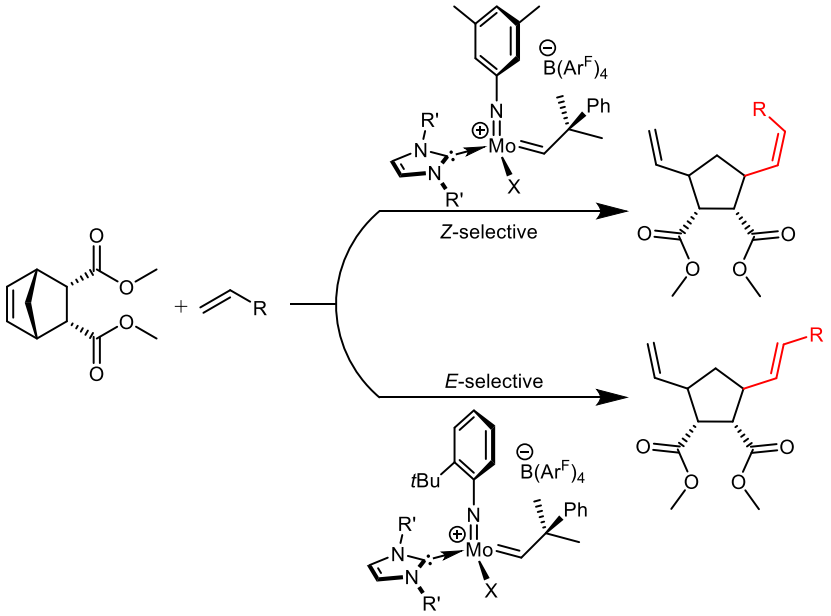

Scheme 1. Representation of stereoselective ring-opening cross-metathesis catalyzed by Mo imido alkylidene NHC complexes.

The choice of substituents at the imido ligand allows for tuning of its steric demand, typically expressed as the buried volume $\%V_{bur.}$ By variation of the buried volume of the imido ligand and the anionic alkoxide or pyrrolide ligands, high *E*-selectivity of up to 99% as well as high *Z*-selectivity of up to 96% could be achieved. “Sterically undemanding” allyl ethers used as a cross-partners experienced *O*-chelation to the cationic metal center, which led to high *E*-selectivity. The reaction progress of representative high *E*- and high *Z*-selective catalysts for all cross-partners was monitored via GC-MS to check for any post-metathesis isomerization (Figure 1). With only one single exception, no post-metathesis isomerization was observed, even

though the catalyst remained active after the metathesis reaction. The catalysts delivered high stereoselectivity under *thermodynamic* but not under *kinetic* control.

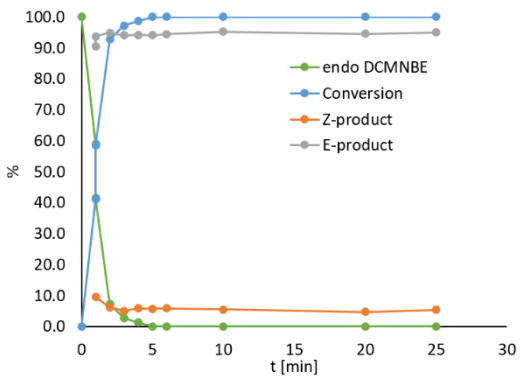

Figure 1. a) *E*-selective ROCM kinetics of *endo, endo*-2,3-dicarbomethoxynorborn-5-ene (DCMNBE) with allyl benzyl ether.

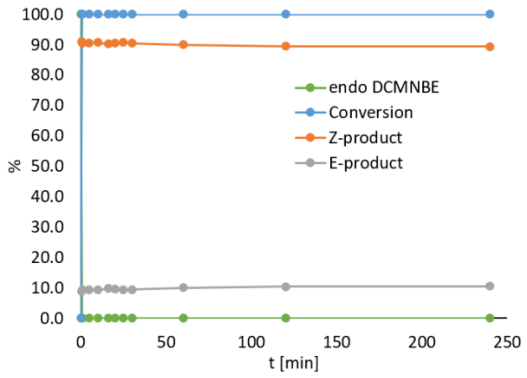

Figure 1. b) *Z*-selective ROCM kinetics of *endo, endo*-2,3-dicarbomethoxynorborn-5-ene (DCMNBE) with allyl benzyl ether.

Next, thermally switchable hexacoordinated molybdenum initiators bearing a chelating alkylidene were investigated as pre-catalysts for the ring-opening metathesis polymerization (ROMP) of dicyclopentadiene (DCPD). The ultimate aim of the current work was to achieve latent pre-catalysts with sufficiently low T_{onset} (temperature at which exotherm starts) along with quantitative and fast initiation once activated. In the present work, several new molybdenum(VI) imido alkylidene NHC complexes bearing *O*- as well as *N*-chelating alkylidene moieties (Figure 2), mostly derived from commercially available, inexpensive olefins viz. *N*-vinyl-2-pyrrolidone and 2-vinylpyridine, were synthesized and compared with respect to their ROMP behavior in the polymerization of DCPD by differential scanning calorimetry. Olefin metathesis pre-catalysts derived from 2-vinylpyridine provided 4-membered chelating alkylidene motifs and were structurally characterized by single-crystal X-ray analysis. The labile nature of the four-membered chelates provides high activity together with adequate latency caused by the hexacoordination of the metal center. These hexacoordinated complexes were subjected to air stability studies in the solid state. The necessary fine-tuning of T_{onset} was accomplished by the use of tailored pre-catalysts. In addition to bistriflate complexes, molybdenum imido alkylidene NHC monoalkoxide monotriflate complexes also delivered high activity without sacrificing latency.

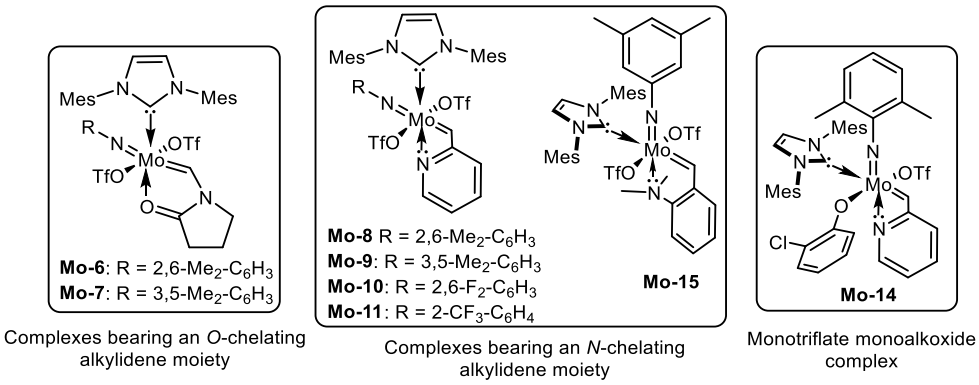

Figure 2. *O*- and *N*-chelated Mo imido alkylidene NHC complexes.

Furthermore, a rare example of a molybdenum η^2-olefin NHC complex obtained through the cross-metathesis of 2-vinylpyridine with Mo(*N*-2,6-Me_2-C_6H_3)(CHCMe_2Ph)(IMes)(OTf)(O-2-Cl-C_6H_4) is presented (Figure 3).

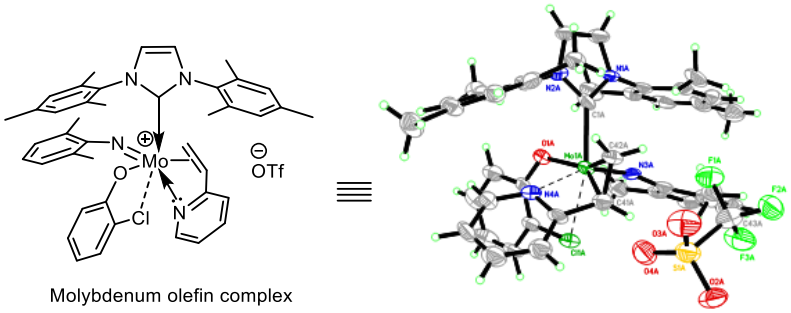

Figure 3. Mo η^2-olefin NHC complex.

Finally, complexes bearing electron-poor imido ligands were found to be more productive than their analogs bearing electron-rich imido ligands, while being tolerant towards hydroxyl groups and air. In this regard, the novel neutral or cationic molybdenum 2,6-difluorophenylimido alkylidene NHC complexes **Mo-19** – **Mo-24** were prepared (Scheme 2).

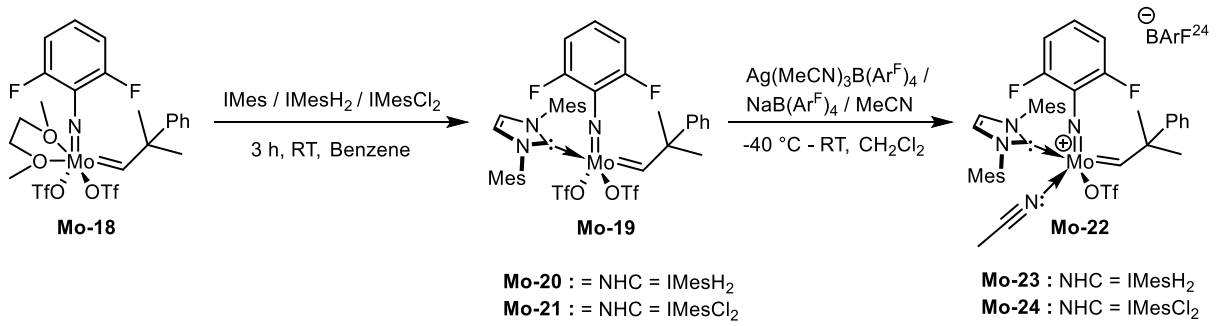

Scheme 2. Synthesis of Mo 2,6-difluorophenylimido alkylidene NHC complexes.

Chapter 1

Theoretical Background

1.1 *N*-Heterocyclic Carbenes

In general, a neutral carbene is a divalent carbon with only six valence electrons. Based on the distribution of these valence electrons in the frontier orbitals, carbenes are classified as singlet and triplet carbenes. In singlet carbenes the electrons are paired, with each pair occupying one of the sp^2 hybrid orbitals, while the p orbital remains empty. Triplet carbenes have unpaired electrons, one of which is occupying a p orbital while the other occupies one of the sp^2 orbitals.[1]

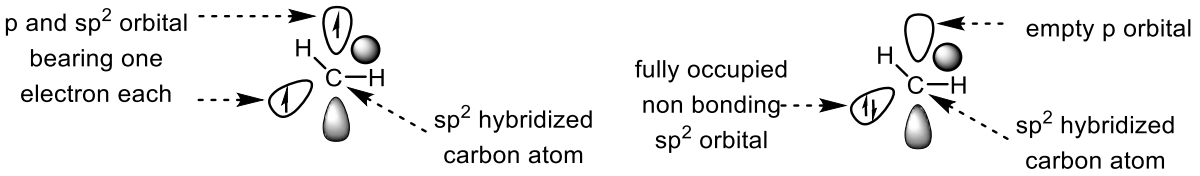

Figure 4. Triplet and singlet carbenes.

N-Heterocyclic carbenes (NHCs) are well-known examples of persistent carbenes and have found widespread use since their discovery.[2-5] NHCs bear at least one nitrogen atom, which is adjacent to the divalent carbon in a heterocyclic ring. As carbenes are electron-deficient species, they were initially thought to be too reactive and too unstable to be isolated. However, NHCs are stabilized by mesomeric effects, both nitrogen lone pairs strongly interact with the p_π orbital of the carbene center. The σ-electron-withdrawing effect of the nitrogen atoms also contributes to NHC stabilization. Both the mesomeric and the inductive effects help to maintain the electroneutrality of the carbene center. The phenomenon that involves inductive and mesomeric effects working together might induce a state of dynamic equilibrium (a push-pull mechanism) that helps NHC attain thermodynamic stability.

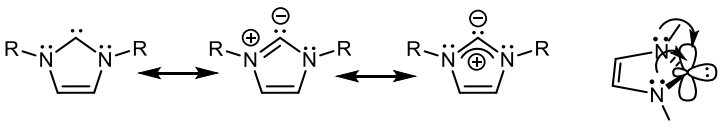

Figure 5. Mesomeric structures of NHCs and mesomeric stabilization of the singlet ground state.

Most NHCs are singlet carbenes, and their cyclic structure forces the carbene carbon to adapt a bent structure. Since NHCs are bent carbenes, the frontier orbitals are sp^2 hybridized and an empty p orbital is orthogonal to the sp^2 plane. Therefore, the singlet ground state σ^2 configuration is favored in NHCs. Thus, NHCs were initially considered to be pure σ-donor ligands and the π*-backdonation was considered insignificant. This might be due to a rather high occupancy of the formally empty pπ

orbital of the carbene carbon atom due to π-delocalization (mesomeric effect). However, *Meyer* and coworkers evidenced that NHCs also have some π*-backdonation capability.[6]

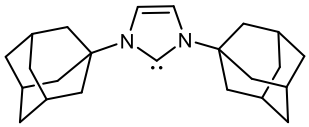

Figure 6. First isolated carbene by *Arduengo.*[7]

In 1991, *Arduengo* and coworkers isolated the first crystalline, storable, free *N*-heterocyclic carbene, thus laying the foundation for today's popularity of NHCs.[8] However, in the early 1960s, the first evidence for the formation of NHCs was reported by *Wanzlick,*[9] but the free carbene could not be isolated. Soon afterwards, *Wanzlick*[10, 11] and *Öfele*[12] independently revealed the nucleophilic nature of NHCs and their use as a ligand in metal complexes by trapping the free carbene with a mercury and chromium salt. The isolation of the first free NHC with sterically demanding adamantyl substituents at the nitrogen indicated that steric shielding of the carbene could be one of the aspects of NHC's stabilization. However, one year later, *Arduengo* and coworkers successfully isolated the stable 1,3,4,5-tetramethylimidazol-2-ylidene, which proved that the electronic stabilization of the carbene center in imidazol-2-ylidenes is sufficient to produce stable species.[13] Furthermore, they reported a stable, isolable carbene based on a saturated imidazolin-2-ylidene ring and demonstrated that the unsaturation in the imidazole ring is not required to obtain stable NHCs.[14] Soon after the stability of such carbenes was revealed, an entire family of imidazol-2-ylidenes with various substituents was synthesized. The most frequently used route for the synthesis of free NHC is by deprotonation of imidazolium or imidazolinium salts. Symmetrical and unsymmetrical imidazolium salts are distinguished depending on the substituents at the nitrogen atoms. Symmetrically substituted salts can be prepared straightforwardly by cyclization of 1,2-diimines with orthoformates,[15, 16] while the unsymmetrical ones can be synthesized by stepwise alkylation of imidazole with alkyl halides. If the free NHCs are unstable, their silver(I) salts can be used as carbene transfer agents. They can be prepared by reaction of the corresponding imidazolium salt with silver oxide.[6, 17] A wide variety of NHCs has been synthesized by varying the parent heterocycle as well as the substituents at the nitrogen atoms (Figure 7).

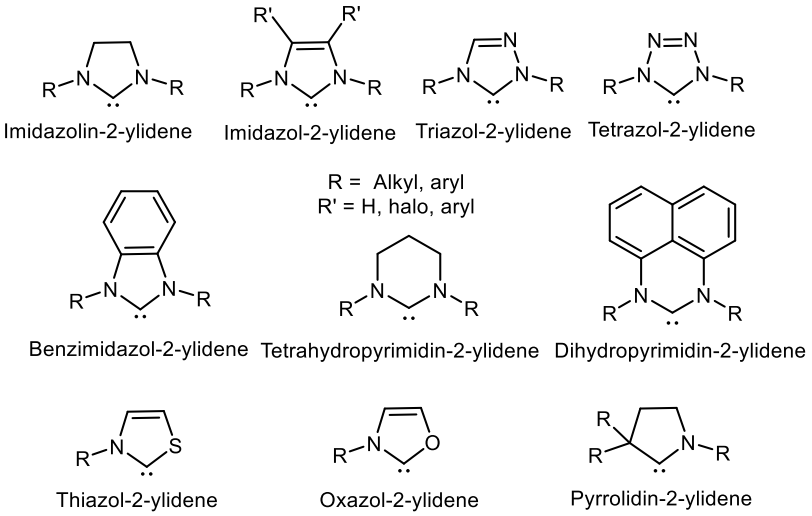

Figure 7. Selected examples of *N*-heterocyclic carbene skeletons.[3]

NHCs have emerged as the key ancillary ligands in organometallic chemistry. They bind more firmly to the metal center than their rival phosphine ligands.[18, 19] The different approaches to incorporate NHCs into metal complexes are depicted in Scheme 3. Route **A** describes the reaction of an isolated free carbene with metal complexes, which typically entails the displacement of a ligand or sometimes scission of a dimeric metal precursor. Route **B** is employed in the case of carbenes that are not stable enough to be isolated. The carbene is generated *in situ*, either by applying an external base or by proton transfer to a ligand of the metal complex. Route **C** demonstrates transmetallation as an effective route to generate metal NHC complexes *via* a carbene transfer agent. Electronic and steric parameters of NHCs have been introduced for the detailed understanding of the bonding properties of NHCs to transition metals.[20]

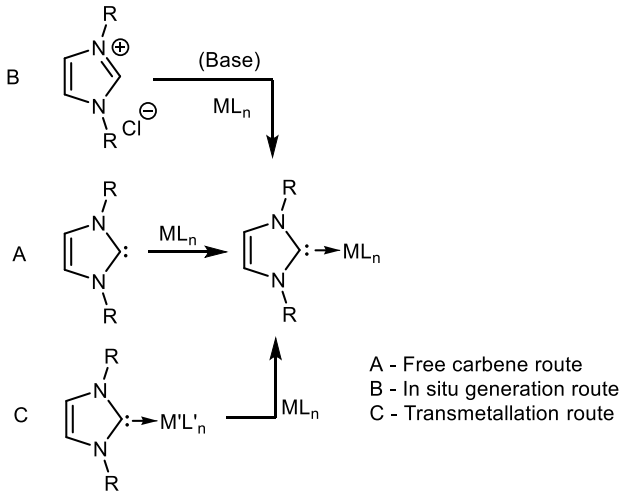

Scheme 3. Different approaches for the synthesis of metal-NHC complexes.

The electronic properties of NHCs are quantified by the *Tolman* electronic parameter (TEP). [21] TEP was originally developed for phosphine ligands by *Tolman* in 1977.[22] It is determined by coordinating a ligand to a metal carbonyl complex and measuring the IR stretching frequency of the carbonyl ligand *trans* to the NHC. The coordinated ligand changes the electron density at the metal, which, in turn, changes the order of carbon-oxygen triple bond in carbonyl ligand. An electron-rich metal center strengthens the metal-carbon bond due to π-backbonding but weakens the carbon-oxygen triple bond.[4, 21] However, the accuracy of TEP values is limited due to the solvent dependency of the IR spectrum, the resolution of the IR spectrometer and the effects imparted by other ligands. Nevertheless, some standards of measurements for assessing the electronic properties of NHCs such as the pK_a of the corresponding salts, the nucleophilicity parameter, IR and NMR spectroscopic data and electrochemical studies have been reported.[21] To quantify the steric impact of NHC ligands, the concept of percent buried volume ($\%V_{bur}$) was developed.[23-25] It measures the volume fraction of the coordination sphere of a metal that is occupied by atoms of the NHC ligand. To calculate the buried volume, the geometry of the ligand and metal complex must be known. It is usually obtained from crystallographic data or from DFT calculations. The excellent electronic and steric features of NHCs and their influence on the structure, stability and reactivity of the resulting complexes let them stand out from other donor ligands.

1.2 Metal-Carbene Complexes

Complexes containing a double bond between the metal and a carbon atom are called metal-carbene complexes. The first complex of this type was encountered in 1964, when *Fischer* and *Maasböl* reacted tungsten hexacarbonyl with an organolithium compound such as LiPh or LiMe. The resulting ionic complex, was protonated and the subsequent alkylation gave the first metal-carbene complex (Scheme 4).[26] A large family of stable metal-carbene complexes, usually containing transition metals in a low oxidation state, has been reported and dubbed *Fischer* carbenes.[27-29] The carbene carbon is electrophilic and stabilized by an adjacent heteroatom (O or N).[30]

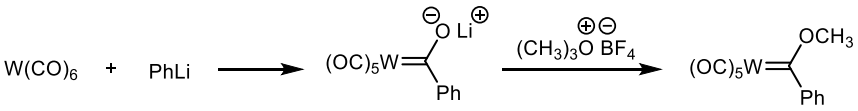

Scheme 4. Synthesis of the first *Fischer* carbene.[26]

In 1974, *Schrock* reported the first transition metal carbene complex that does not bear a stabilizing heteroatom substituent at the carbene carbon, and thus clearly contrasts Fischer carbenes. The tantalum complex, $Ta[CH_2C(CH_3)_3]_3Cl_2$ was reacted with two equivalents of neopentyllithium to yield two equivalents of lithium chloride, one equivalent of neopentane, and a stable metal carbene complex (Scheme 5). The reaction proceeds through an intramolecular α-hydrogen abstraction. Unlike *Fischer* carbenes, the carbene carbon is nucleophilic and the metal is more electrophilic.[31] Furthermore, *Fischer* carbenes are singlet carbenes, while *Schrock* carbenes are triplet carbenes.

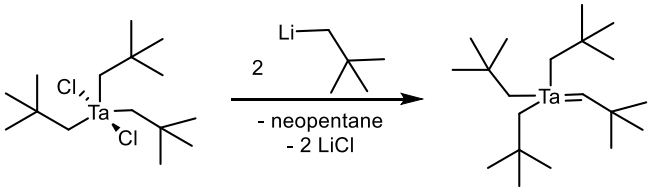

Scheme 5. Synthesis of the first *Schrock* carbene.[31]

1.3 Olefin Metathesis

Olefin metathesis is a reaction that involves redistribution of the substituents present on olefins by scission and formation of carbon-carbon double bond in presence of a transition metal catalyst (Scheme 6).[32] The first olefin metathesis reaction was

reported in 1957, when *Herbert S. Eleuterio* observed that, in the presence of molybdenum oxide supported on alumina and metal hydrides as a promoter, the C=C double bond present in cyclic olefin can be broken, resulting in the formation of high molecular weight polymers.[33, 34] In 1964, *Banks* and *Bailey* observed the disproportionation reaction of propylene in the presence of tungsten or molybdenum hexacarbonyl or cobalt molybdenum (VI) oxide on alumina, yielding a mixture of ethylene and 2-butene.[35, 36] They termed this reaction as an '*Olefin Disproportionation*'. In 1967, *Calderon* and coworkers were the first to name this novel skeletal transformation reaction of unsaturated hydrocarbons as the '*Olefin Metathesis*'.[37]

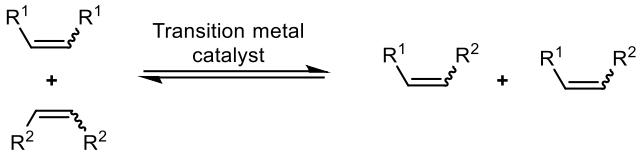

Scheme 6. The olefin metathesis reaction.

Olefin metathesis has been recognized as important and highly useful reaction in chemistry. In 2005, the Nobel Prize in Chemistry was awarded to *Yves Chauvin*, *Robert H. Grubbs,* and *Richard R. Schrock* for their involvement in the elucidation of the reaction mechanism and the design of highly active catalysts for olefin metathesis reactions.[38-40] In 1971, *Chauvin* and *Herisson* proposed the most convincing mechanism suggesting that the reaction is initiated by a metal carbene and also propagates through it (Scheme 7).[41] The mechanism entails the reaction of a catalyst bearing a metal carbon double bond i.e. a metal carbene with an olefin to form a metallacyclobutane intermediate via a [2+2] cycloaddition. This metallacyclobutane undergoes cycloreversion to give either the original species or a new olefinic product and a new metal carbene. Since the reaction is reversible, a mixture of the original species and product olefins is often obtained. Finally, this mechanism was well accepted and recognized.

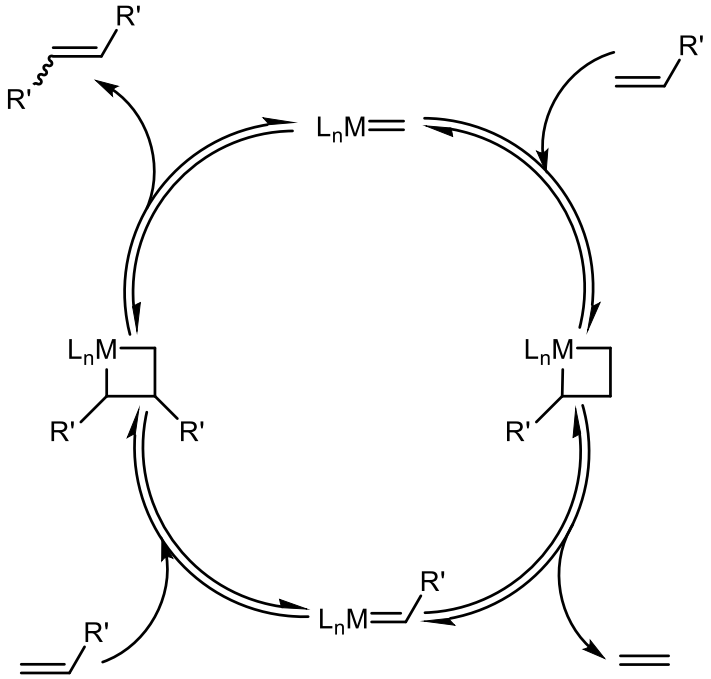

Scheme 7. *Chauvin's* olefin metathesis mechanism.

The first evidence for *Chauvin's* mechanism was provided by *Fred Tebbe*. He reported a bimetallic titanium and aluminum based compound with bridging methylene and chlorine linkers, which was later named *Tebbe's* reagent.[42] This compound is a versatile methylene transfer reagent for homologation of olefins and the formation of terminal olefins from ketones.[43] A metallacyclobutene was isolated and characterized when this reagent was reacted with diphenylacetylene.[44] Further evidence for the *Chauvin* mechanism was provided by *Grubbs* and coworkers when the reaction of *Tebbe's* reagent with neohexene in presence of a 4-vinylpyridine-styrene copolymer as a Lewis base yielded the titanacyclobutane shown in Figure 5.[45]

Tebbe's isolated -
First metallacyclobutene
1980

Grubbs' isolated -
First metallacyclobutane
1980

Figure 8. First isolated and fully characterized intermediates of olefin metathesis, reported by *Tebbe* and *Grubbs*

Kinetic investigations of titanium-based metathesis systems showed that the resting state is the metallacyclobutane rather than the metal alkylidene, as observed for

tantalum and tungsten metathesis systems, too.[46-48] Thus, a series of metallacycles was synthesized and their reactions with olefins provided more insights about the mechanism of titanium-catalyzed metathesis.

1.4 Types of Olefin Metathesis Reactions

Olefin metathesis reactions are categorized into different classes such as ring-opening metathesis polymerization (ROMP), acyclic diene metathesis (ADMET) polymerization, ring-closing metathesis (RCM), cross-metathesis (CM), ring-opening cross-metathesis (ROCM), as well as the metathesis of alkynes such as ene-yne metathesis (EYM), 1-alkyne polymerization and the cyclopolymerization of alkynes (Scheme 8). This classification of olefin metathesis reactions is mainly based on the substrates used and the product formed. Olefin metathesis reactions are driven by either the liberation of a volatile product, release of ring strain, or formation of an entropically favored product. ROMP and ROCM will be discussed in detail in the following sections.

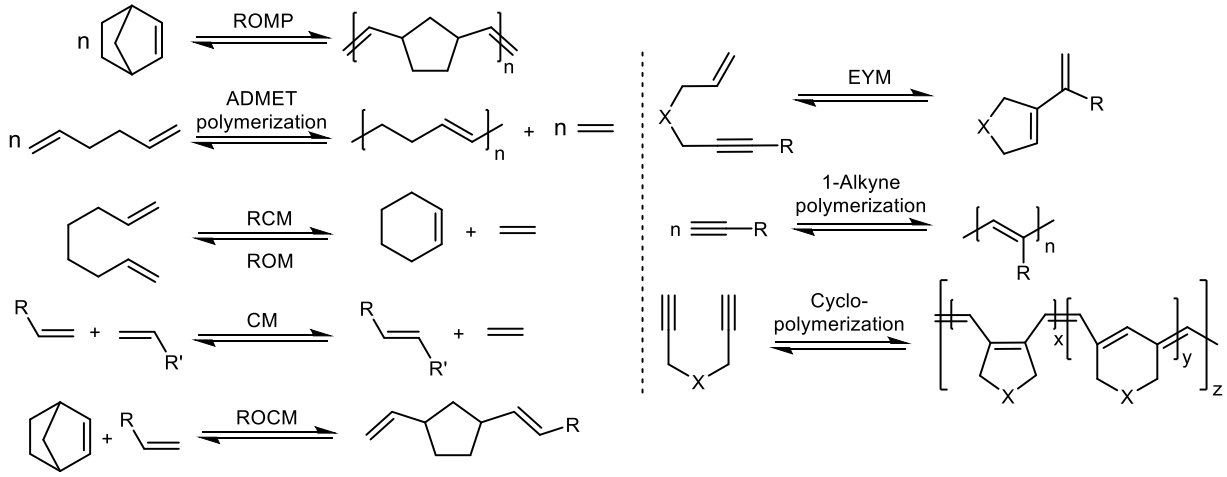

Scheme 8. Different types of olefin metathesis reactions.

1.4.1 Ring-Opening Metathesis Polymerization (ROMP)

ROMP polymers can be derived from a variety of cyclic olefins in the presence of a transition metal catalyst (Scheme 9). Primarily, strained cyclic monomers *viz.* norbornene or norbornene derivatives are used. The release of ring strain is the driving force for the propagation of polymerization. Along with the fundamental parameters of polymers such as molecular weight, molecular weight distribution, and

chemical composition, the microstructural features such as *cis*/*trans* isomerism and tacticity also play an important role in defining polymer properties.

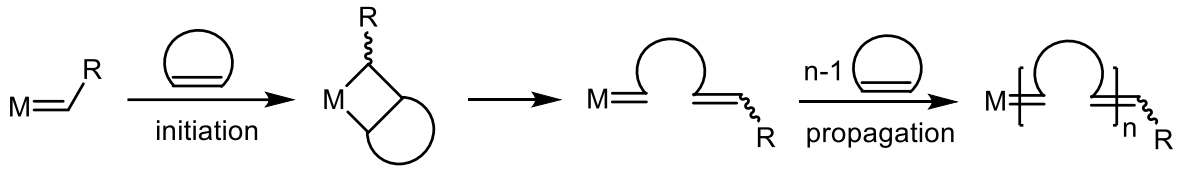

Scheme 9. Mechanism of the ROMP of cyclic olefins.

The four basic stereoregular structures derived from the ROMP of norbornene are depicted in Figure 6. Since ROMP-derived polymers contain carbon-carbon double bond in the backbone, *cis*/*trans* isomers are the basic structural feature of ROMP polymers. Tacticity is the next important microstructural parameter obtained from norbornenes or norbornadienes. If the configuration of the chiral carbon atoms in one repeat unit is identical with the configuration of the analogous chiral carbon atoms in the next repeat unit, the polymer is called *isotactic* (*it*). In the case of opposite chirality, the polymer is called *syndiotactic* (*st*). The synthesis of highly stereoregular polymer is of vast importance, since tacticity governs the physical properties of polymers such as the melting point (T_m), the glass transition temperature (T_g), solubility, etc. The catalyst plays an instrumental role in accessing polymers with regular structures.

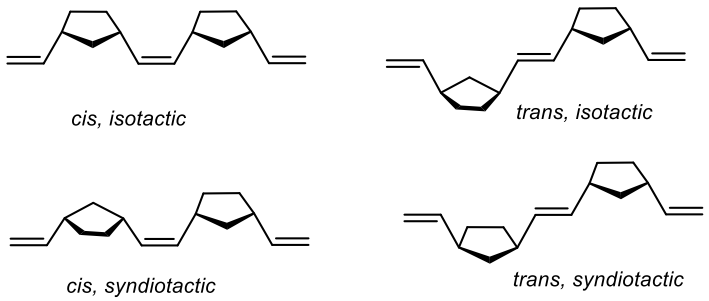

Figure 9. The four regular structures of polynorbornene.

Principally the *cis*/*trans* structure is the outcome of the systematic approach of incoming monomer molecules towards the *syn* or *anti* metal alkylidene. If the ring structure of norbornene pointing in the opposite direction compared to the substituent of the imido ligand, called as ene$_{anti}$ approach or the same direction, called as ene$_{syn}$ approach. When a monomer adds in ene$_{anti}$ fashion to the *syn* alkylidene or ene$_{syn}$ fashion to the *anti* alkylidene, a *trans* double bond with new *anti* alkylidene at the metal center will form. The ene$_{syn}$ approach of the monomer to the *syn* alkylidene or

the ene$_{anti}$ approach to the *anti* alkylidene will result into *cis* double bond and a new *syn* alkylidene at the metal center (Scheme 10).

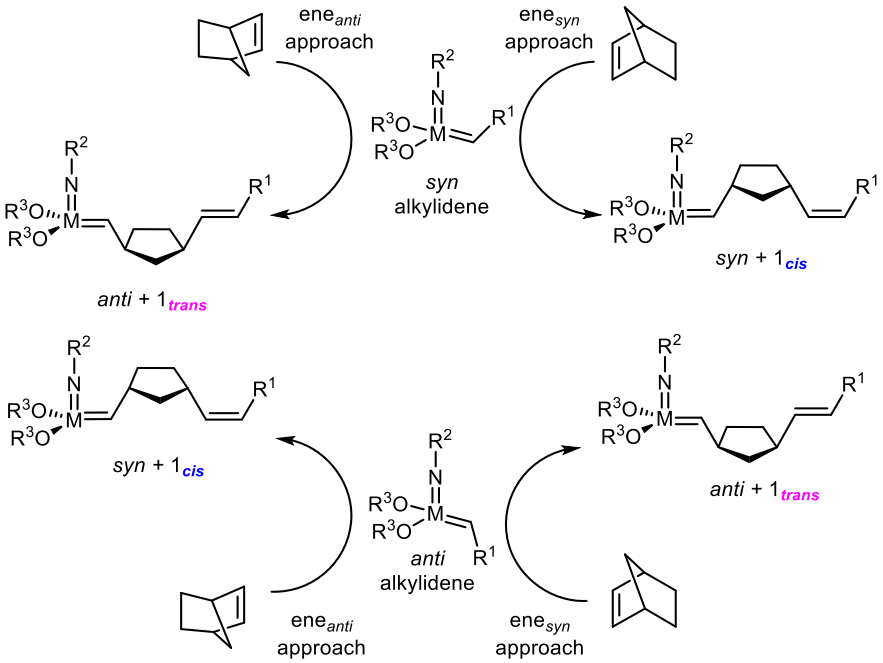

Scheme 10. First insertion products of addition of norbornene to the *syn* and *anti* alkylidene.

Concurrently, the CNO faces (rear and front) determine tacticity in the polymer. If the monomer approaches from the same face in every insertion step, an *isotactic* polymer will be formed while addition to the alternate faces will result in a *syndiotactic* polymer (Scheme 11).

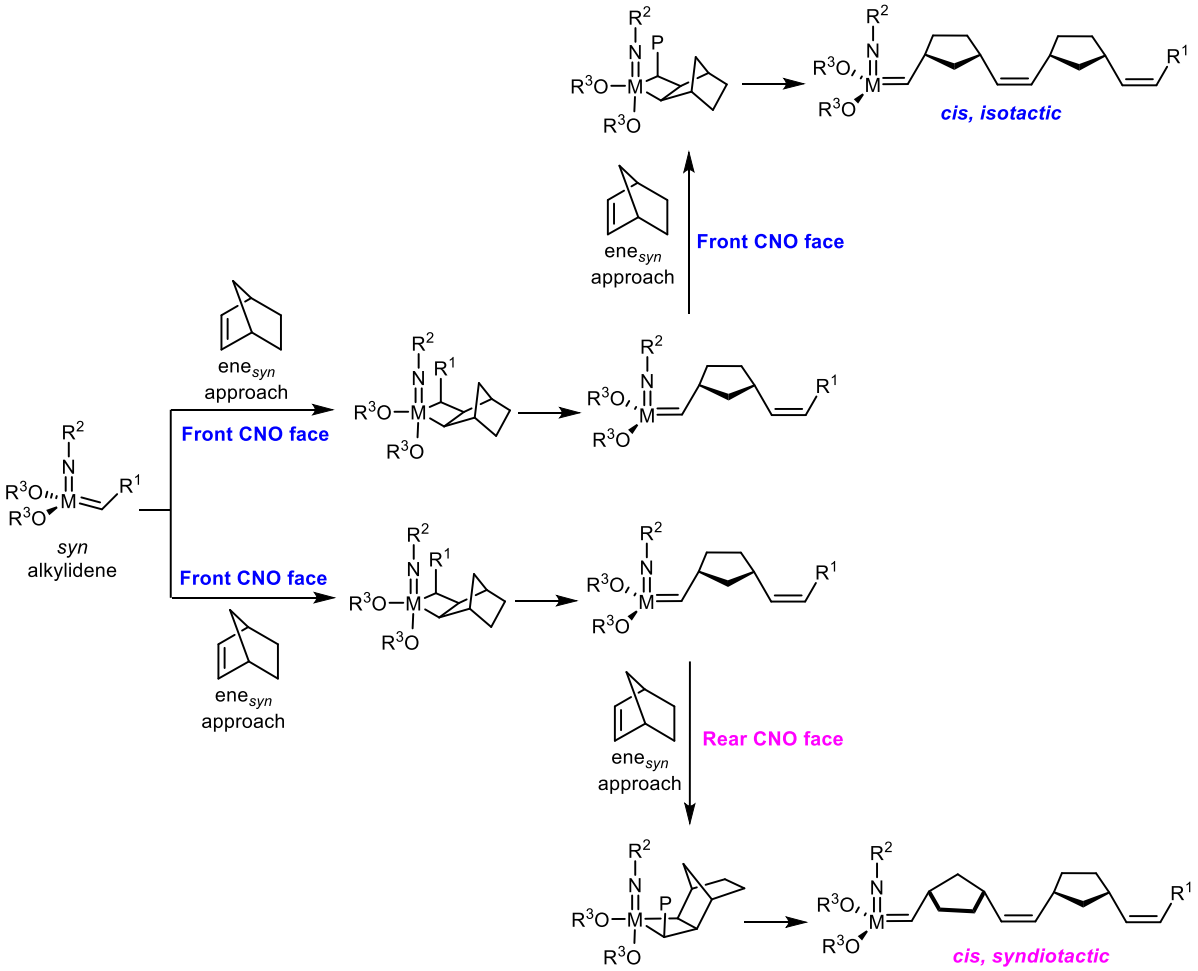

Scheme 11. Addition of norbornene to front and rear CNO faces of a metal alkylidene.

Hitherto, four different mechanisms have been identified that deliver four different stereoregular structures through ROMP, namely, chain-end control (*trans, st*), enantiomorphic site control (*cis*, *it*), stereogenic metal control (*cis*, *st*), and the turnstile rearrangement of the metallacyclobutane (*trans*, *it*).[49, 50]

1.4.2 Ring-Opening Cross-Metathesis (ROCM)

Ring-opening cross-metathesis is a tandem reaction, which involves the initial opening of a cycloolefin by a metathesis catalyst, followed by cross-metathesis of the opened ring with another alkene i.e. the cross-partner, generating a diene (Scheme 12). As shown in Scheme 12, either an end-differentiated monosubstituted diene or a symmetrically capped disubstituted diene can be obtained. If a relatively small amount of cross-partner is used or a readily polymerizable cycloolefin is used, ROMP can occur instead and telechelic polymers or oligomers will form.[51] Analogous to ROMP, ROCM utilizes the ring strain of cyclic olefins as the driving force for ring-

opening. However, to avoid polymerization, the reactions are carried out in dilute solutions (max. 0.1 M) and often a tenfold excess of cross-partner is employed.[52] The cycloolefins employed in ROCM reactions require bulky ring substituents to discourage the formation of oligomeric side products. The cross partners generally used are unhindered, relatively electron-rich terminal alkenes.

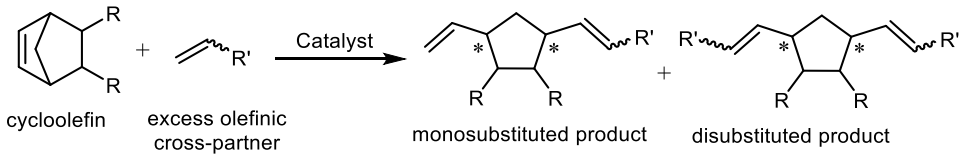

Scheme 12. Ring-opening cross-metathesis reaction of cyclic olefins.

A common product of ROCM reactions are substituted tetrahydrofurans, which are common motifs found in many biologically active natural products.[53-55] ROCM gained vital importance in organic synthesis as a synthetic tool for the preparation of functionalized alicyclic compounds. Several studies investigating the issues concerning chemoselectivity (ROCM *vs* ROMP), enantioselectivity (ee %) and stereoselctivity (*E/Z* isomerism) of ROCM reactions have been published.[56-58]

1.5 Catalyst Development for Olefin Metathesis

1.5.1 *Schrock* catalysts

The development of well-defined metal alkylidene complexes by *Schrock* and *Grubbs* has significantly extended the scope of olefin metathesis reactions as a valuable synthetic tool in organic synthesis and polymer synthesis.[59-63] Tantalum alkylidene complexes, such as the first isolable metal-alkylidene complex as discussed above, are in general not found in classical olefin metathesis system, mainly due to their bimolecular decomposition tendency.[64] Since 1983, the chemistry of molybdenum, tungsten, and rhenium has progressed considerably.[65] A breakthrough in olefin metathesis catalysts based on molybdenum and tungsten reported by *Schrock* and coworkers can be described by the general formula $M(NR)(CHR')(OR'')_2$, where M = Mo, W; R = alkyl or aryl; R' = $C(Me)_3$, CMe_2Ph or $SiMe_3$; R'' = alkyl, phenyl, diolate. The introduction of sterically demanding imido ligand provided relative stability towards bimolecular decomposition. Consequently, these complexes are known as *Schrock*-type catalysts. The metal centers in these complexes are relatively Lewis acidic due to their high oxidation state. These complexes showed significant

metathesis activity in olefin metathesis. The most conventional route to access these catalysts involves a four-step synthesis for molybdenum and a five-step synthesis for tungsten, as shown in Scheme 11.[59, 66-69]

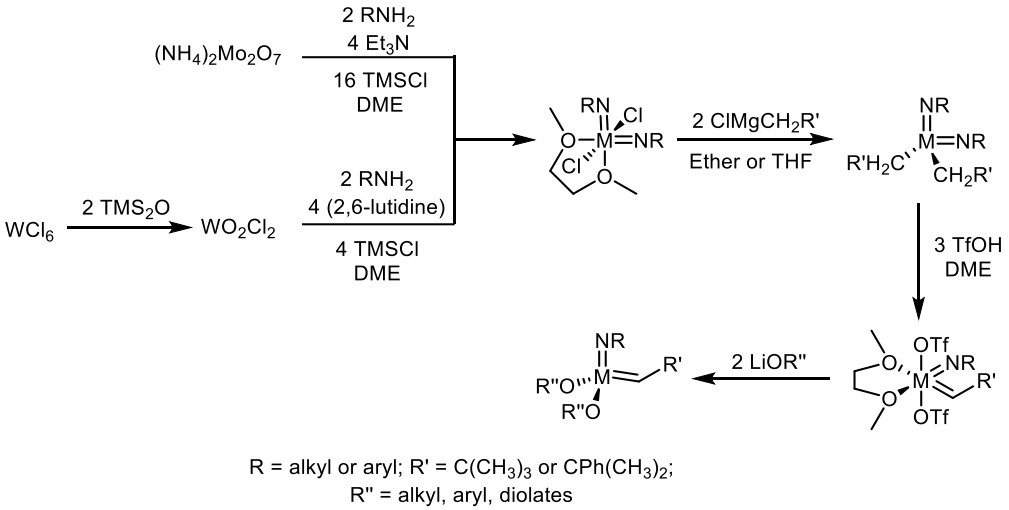

Scheme 13. The most conventional route to *Schrock*-type catalysts.

A general route to *Schrock*-type catalysts starts from the reaction of salts of molybdenum (molybdates) and tungsten (WO_2Cl_2) with two equivalents of alkyl or aryl amine in the presence of four equivalents of triethylamine and 16 equivalents of trimethylsilylchloride in dimethoxyethane (DME) as a solvent to yield bischloro bisimido complex. Further alkylation of $[M(NR)_2Cl_2(DME)]$ with two equivalents of Grignard reagents (neophyl or neopentyl) yields the bisalkyl bisimido complex $[M(NR)_2(CH_2R')_2]$. In the next step, the ‘‘universal precursors’’ of the general formula $[M(NR)(CHR')(OTf)_2(DME)]$ can be obtained after the treatment of Mo bisimido bisalkyl complexes with three equivalents of triflic acid, usually at low temperature. Reaction of the universal precursors with two equivalents of a metal alkoxide results in the *Schrock*-type tetracoordinated imido alkylidene bisalkoxide complexes. The key benefit of the synthetic route described in Scheme 13 is that a broad-spectrum of Mo/W catalysts by varying imido and alkoxide ligands can be accessed with a small change in reaction conditions as temperature or solvent.[70]

Furthermore, the detailed studies unfolded the exciting features of *Schrock*-type metathesis catalysts. The bond between the metal center and the nitrogen atom of the imido ligand can be linear or bent, depending on the utilization of free electron pair of the imido nitrogen towards an empty *d*-orbital of the metal center. In

M(NR)(CHR')(OR'')$_2$ complexes, M=N bond can be considered as a pseudo-triple bond; therefore, the angle of the Mo-N-C is close to the 180°.[71] Another interesting feature is that the orientation of imido ligand and the alkylidene moiety to each other. As the metal center is tetracoordinated and the *d*-orbitals of the metal involved in forming the M=C bond must lie perpendicular to the N-M-C$_{(ipso)}$ plane. Thus, *Schrock*-type catalysts can exist in two stereoisomeric forms; the *syn* isomer and the *anti* isomer. In the *syn* isomer, the R' substituent of the alkylidene points towards the imido ligand, while in the *anti* isomer, it points away from the imido ligand (Figure 10).[72-74] The *syn* isomer is more stable due to the agostic interaction between an empty *d*-orbital and the alkylidene C-H bond. While the *anti* isomer lacks agostic interactions, it increases Lewis acidity at the metal center, making it more reactive. These isomers can be differentiated from ^{1}H NMR spectra by using the alkylidene protons J_{CH} coupling constant. The *syn* isomer displays J_{CH} coupling constant in the range of 110 – 130 Hz, while for the *anti* isomer, it is > 145 Hz. Usually, *anti* isomers are found downfield to the corresponding *syn* isomer in ^{1}H NMR spectra. Apparently, one can get the information about the isomer from the single-crystal X-ray diffraction studies. In general, *syn* and the *anti* isomer can interconvert by simple rotation about the M=C bond. *Schrock* et al.[74] and *Davis* et al.[72] showed that the *syn* and *anti* alkylidenes could be interconverted by irradiation with UV light (preferably 366 nm), and the rate of interconversion can be determined by ^{1}H NMR spectroscopy.

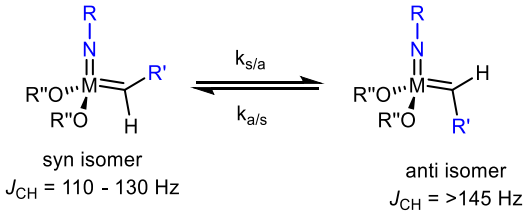

Figure 10. *Syn*/*anti* interconversion in metal alkylidene complexes.

Besides the agostic interactions, steric interactions may also be partially responsible for the lower reactivity of *syn* isomer. It is generally presumed that an alkylidene/olefin complex is a transition state before forming metallacyclobutane intermediate. Therefore, the lower reactivity of syn isomer might result from steric interaction caused between the alkylidene substituent and the aryl imido group (Figure 11).[62, 73]

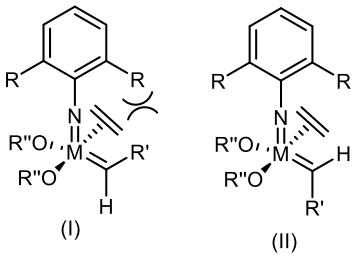

Figure 11. Steric interactions in the square-pyramidal (SP) complex formed upon the olefin coordination may be partly responsible for the lower reactivity of a *syn* alkylidene towards an olefin (here, ethylene used as an example).[62]

In 1993, *Schrock* and coworkers reported on an enantiomerically pure chiral biphenolate Mo complex, which was the first efficient catalyst for enantioselective olefin metathesis (Figure 12).[75] Apart from synthesizing highly tactic polymers, those catalysts were employed in asymmetric RCM (ARCM) reactions of achiral starting materials allowing ee's up to 90%.[76, 77]

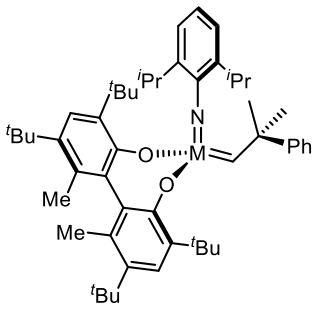

Mo(N-2,6-^{i}Pr-C_6H_3)(CHCMe$_2$Ph)(Biphen)
Biphen = 6,6'-dimethyl-3,3',5,5'-tetra-*tert*-butyl-1,1'-biphenyl-2,2'-diol

Figure 12. First enantioselective Mo-Catalyst (**1993**).[75]

Another significant variation in Mo/W metathesis catalysts entailed the synthesis of monoalkoxide pyrrolide (MAP) type complexes. The MAP type complexes are accessible in two steps from the universal bistriflate precursors. First, the bistriflate can be reacted with two equivalents of lithium pyrrolide to offer bispyrrolide complexes, and further treatment with one equivalent of alcohol yields corresponding MAP-type catalyst.[78, 79] The use of two equivalents of alcohol or one equivalent of diolate offer bisalkoxide complexes. The pyrrolide ligand is isoelectronic to the cyclopentadienyl ligand, and similarly can coordinate either η^1 or η^5 to a metal center. Therefore, bispyrrolide complexes often found as the dimer.[79] The MAP type catalysts are found to be active in RCM as well as enyne metathesis reaction, which were not reported previously.[80]

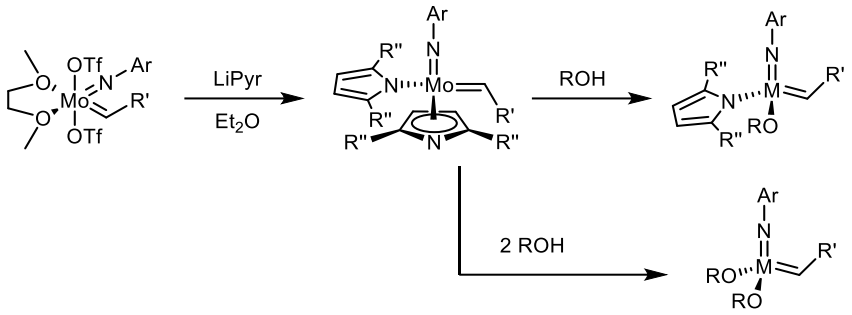

Scheme 14. Synthesis of monoalkoxide pyrrolide (MAP) complexes.

Z-selective olefin metathesis was realized by MAP type catalysts, especially when these contain a 'small' imido ligand and a 'large' aryloxide ligand (Figure 13).[25, 81, 82] *Z*-selectivity becomes possible due to the favored *syn* configuration of the alkylidene and the defined trigonal bipyramidal (TBP) geometry at the metal center. A metallacyclobutane intermediate with all the substituents pointing towards the small imido ligand, due to the large, freely rotating aryloxide ligand promotes the formation of *Z*-alkenes.

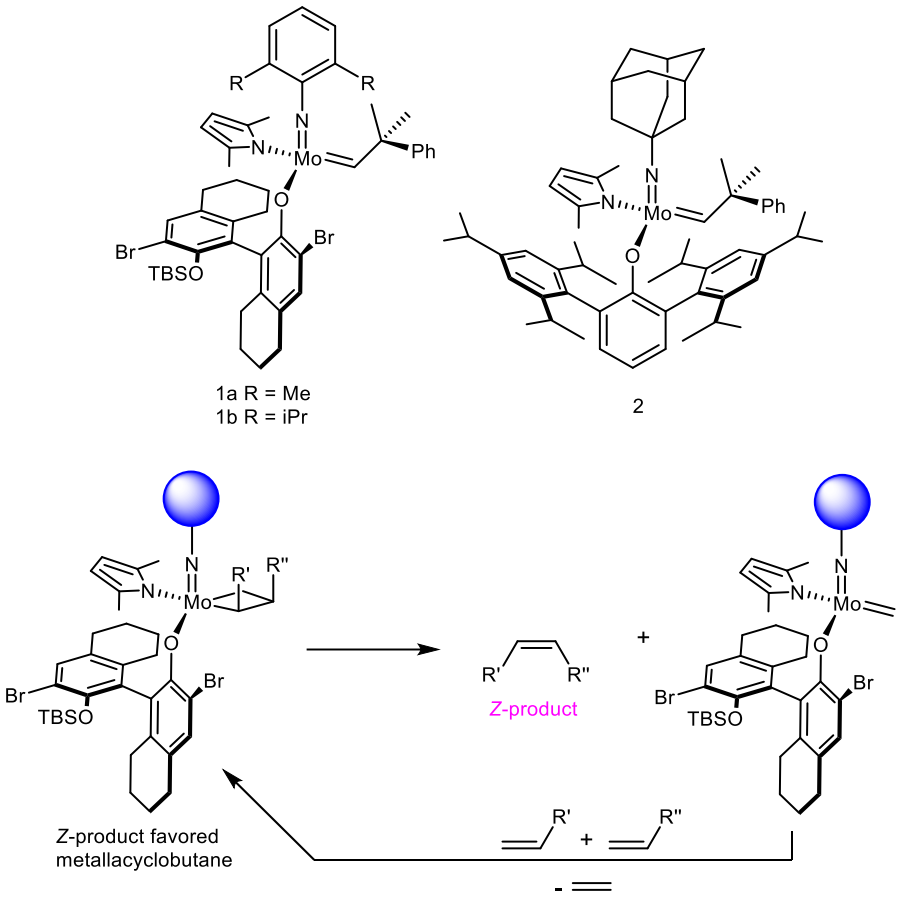

Figure 13. *Z*-selective olefin metathesis catalysts and metallacyclobutane intermediate leading to the favored formation of (*Z*) product

Heterogeneous catalysis has vital importance as it enables faster, large-scale production and selective product formation. In addition to continuous process and ease of handling, recycling, and reuse of catalyst and metal free products are the main reason for the popularity of supported catalysis.[83] The anchoring of a well-defined catalyst on the support is an added advantage in catalysis. In 2002, *Schrock* and coworkers reported the first polymer-supported chiral Mo imido alkylidene catalyst containing the BINOL ligand for enantioselective olefin metathesis reactions.[84] Subsequently, *Buchmeiser* et al. reported a chiral *Schrock* catalyst supported by ROMP-derived polymer and also via the imido ligand.[85, 86] Further, a highly active supported system was achieved by immobilization of a *Schrock* catalyst on partially dehydroxylated silica, which allowed TON's of more than 100,000 with propene as substrate.[87-89]

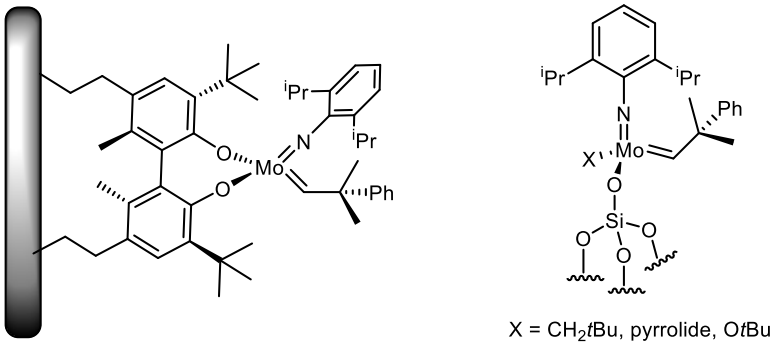

Figure 14. Polymer and silica-supported Mo imido alkylidene catalysts.

1.5.2 *Grubbs* Catalysts

Indeed, the active olefin metathesis catalysts are not only limited to Mo and W metals. Another important class of metathesis-active catalysts is called *Grubbs* catalysts, which contain Ru as the metal center, developed by *Robert H. Grubbs*. They are tolerant towards the air, moisture, and many functionalities of the substrates.[90, 91] However, they are less reactive than the *Schrock*-type catalysts. The most prominent commercially available *Grubbs* catalysts are shown in Figure 13.[92] The 1st-generation *Grubbs* catalyst possesses two phosphine ligands, an alkylidene, and two chloro ligands. In contrast, in the 2nd-generation one of the phosphines is replaced by the NHC, and 3rd-generation Grubbs catalysts contain two pyridine moieties.[92-95] *Grubbs-Hoveyda-type* catalysts bear a chelating alkylidene moiety.[96, 97] Further, the chlorides were exchanged by the other anionic ligands such as the

trifluoroacetate ligand, first reported by *Buchmeiser* et al.[98] They showed enhanced activity without loss of stability.

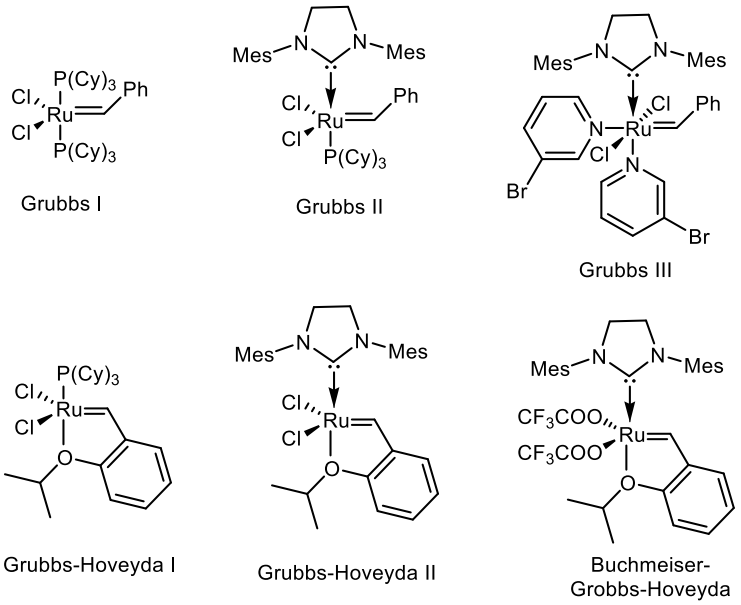

Figure 15. Commercially successful *Grubbs-type* catalysts.

1.5.3 Molybdenum Imido Alkylidene NHC Complexes

The cationic molybdenum and tungsten alkylidene complexes reported by *Schrock* et al. exhibited only low productivities in olefin metathesis. The low reactivity of cationic complexes was attributed to their poor stability.[99, 100] In 2014, *Buchmeiser* and coworkers incorporated *N*-heterocyclic carbenes into *Schrock's* molybdenum imido alkylidene bistriflate complexes, in anticipation of pursuing the synthesis of stable cationic olefin metathesis catalysts.[101] Surprisingly, the neutral pentacoordinated 16-VE complexes of the general formula $Mo(NAr)(CHCMe_2R^1)(NHC)(OTf)_2$ (i.e. Ar = 2,6-Me_2-C_6H_3, R^1 = Ph or Me) were found to be active in olefin metathesis and also showed tolerance towards functional groups. The high activity and functional group tolerance of these complexes was attributed to the stable cationic character of the metal center. ^{19}F NMR experiments showed that one of the triflate ligands dissociates once the substrate approaches or coordinates to the metal center, and thus a metathesis-active, cationic 16-VE complex is formed (Scheme 15). The NHC ligand exerts a strong *trans*-effect on the triflate ligand, thereby facilitating its dissociation. It was presumed that the complexes are stabilized due to the delocalization of the cationic charge between the NHC and metal center. And indeed, DFT calculations confirmed the proposed charge delocalization.[102]

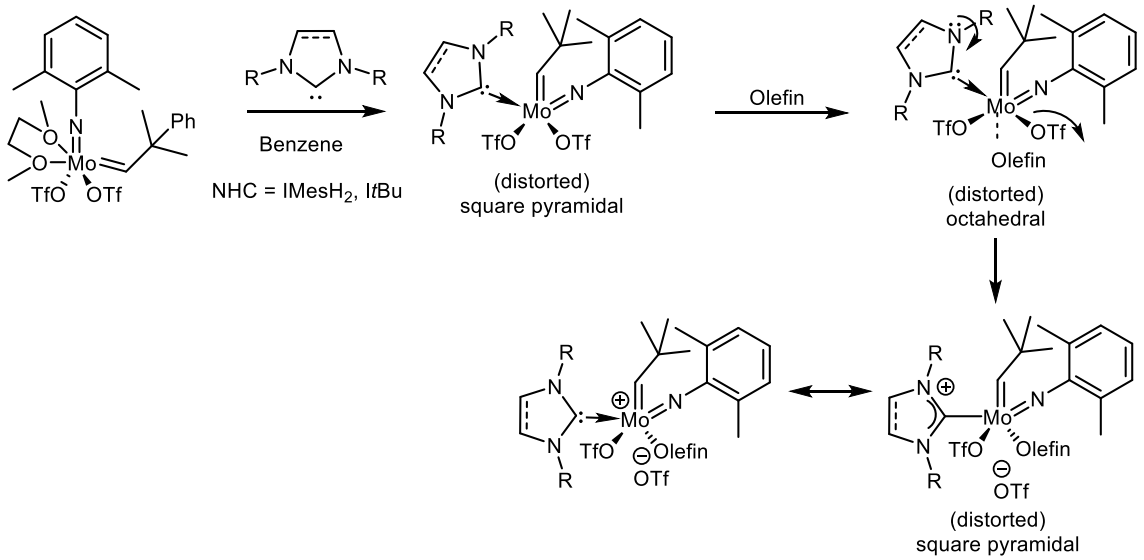

Scheme 15. Synthesis of molybdenum imido alkylidene NHC complexes and formation of cationic species on olefin coordination.[101]

The coalescence temperature T_c for the triflates can be measured for bistriflate as well as monotriflate-monoalkoxide complexes through ^{19}F NMR spectroscopy, at this temperature the triflates exchange on NMR time scale is identical to distinguish the resonance frequency. For monotriflate-monoalkoxide complexes, T_c can be obtained in the presence of additional triflate, e.g. tetrabutylammonium triflate. At this temperature, the triflates appear magnetically equivalent and the complex can be considered cationic. In principle, two possibilities can be conceived for the formation of cationic metathesis active species. The first possibility is the coordination of a substrate molecule to the pentacoordinated metal center and subsequent release of the triflate *trans* to the NHC, i.e. an associative mechanism (Scheme 16). The other possibility is to first form a cationic complex by dissociation of a triflate ligand followed by coordination of the substrate, i.e. a dissociative mechanism (Scheme 16). Recently, mechanistic investigations based on reaction kinetics, single-crystal data, and quantum chemical calculations showed that the reaction follows an associative mechanism for neutral as well as solvent-stabilized cationic 16 VE Mo imido alkylidene NHC complexes, if 2-methoxystyrene is employed as the substrate.[103]

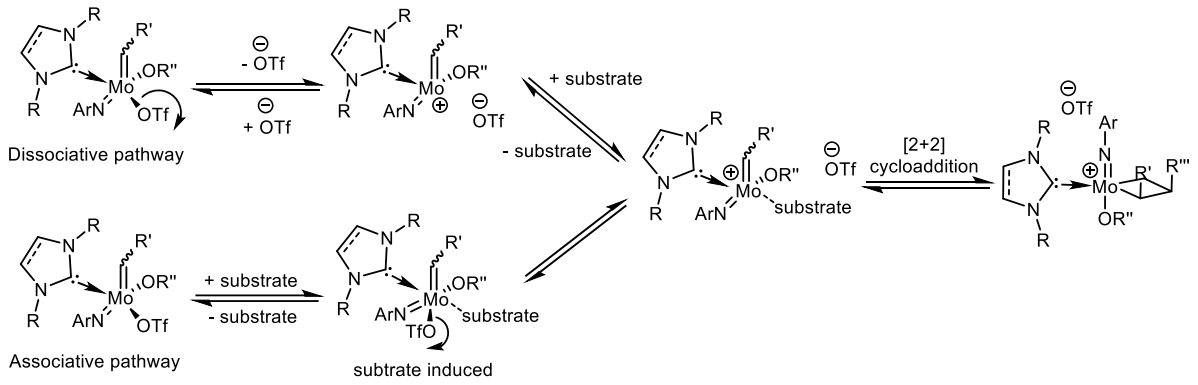

Scheme 16. Associative and dissociative reaction pathways for the formation of a cationic species from Mo imido alkylidene NHC complexes.[103]

Furthermore, the first tetracoordinated cationic Mo imido alkylidene NHC complex was prepared by replacing one triflate ligand in a 16-VE progenitor with the weakly coordinating anion tetrakis[3,5-bis(trifluoromethyl)phenyl]borate (Scheme 17). It displayed high catalytic activity, albeit at the expense of functional group tolerance. It exhibited outstanding productivity with TONs (turnover numbers) in the range of 30000 to 210000 for pure hydrocarbons such as the homometathesis (HM) of 1-hexene, styrene, and 1-octene, as well as the RCM of 1,7-octadiene and ethenolysis of cyclooctene.[104]

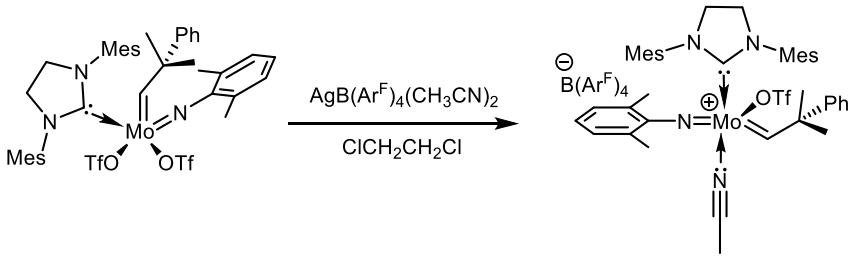

Scheme 17. Synthesis of the first cationic four-coordinate molybdenum imido alkylidene NHC complex.[104]

NHCs with varying σ-donating propensity and steric bulk as well as chelating alkylidene ligands offer access to different tailored penta- and hexacoordinated Mo imido alkylidene NHC complexes, respectively, which were used as latent pre-catalysts for the polymerization of dicyclopentadiene (DCPD).[105, 106] Particularly hexacoordinated 18-VE pre-catalysts containing a chelating alkylidene were found to be air-stable. Complexes bearing *O*-chelating NHCs showed different *cis/trans* selectivities in ROMP, which was mechanistically investigated by determining the *syn/anti* interconversion of these catalysts.[107]

A Mo imido alkylidene NHC complex could be immobilized on silica via the NHC (Scheme 18). This allowed for the synthesis of metal-free olefin metathesis products while maintaining the activity of the homogeneous catalyst.

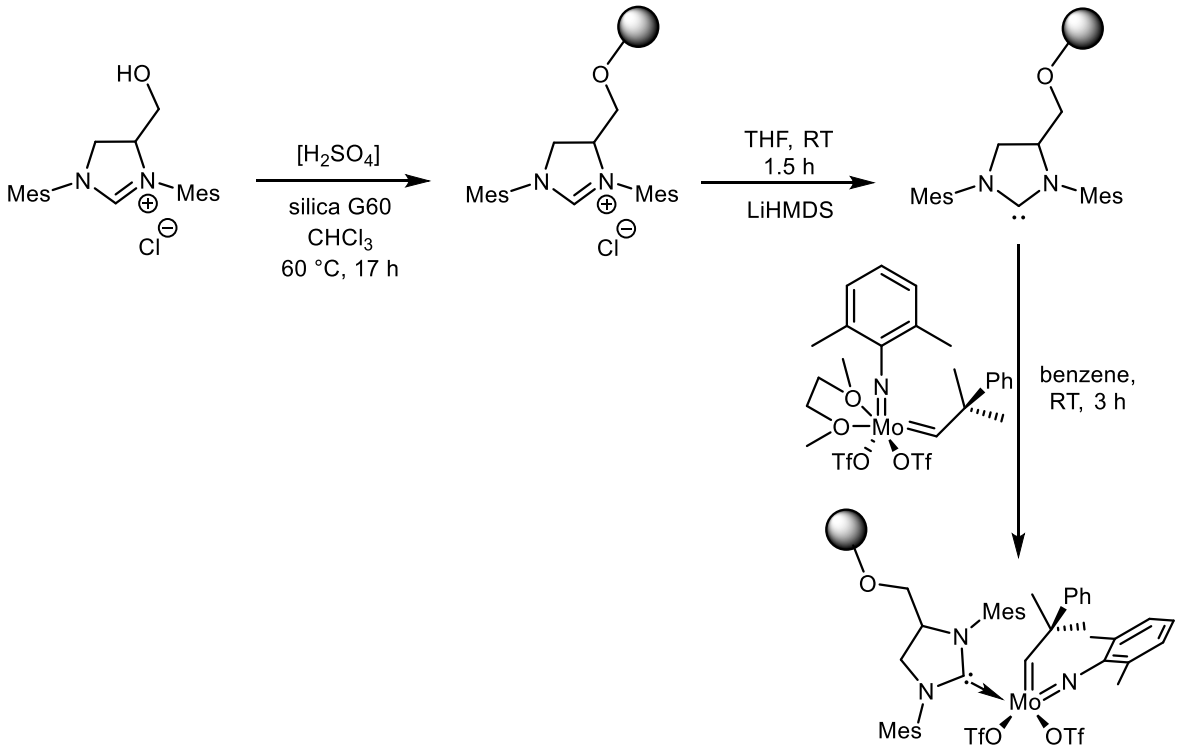

Scheme 18. Immobilization of a Mo imido alkylidene NHC complex via the NHC.[104]

The class of molybdenum imido alkylidene NHC complexes was extended significantly. Various imido ligands such as the 2,6-dimethylphenylimido, 2,6-dichlorophenylimido, 2,6-diisopropylphenylimido, 3,5-dimethylphenylimido, *tert*-butylimido, adamantylimido ligand in combination with different NHCs such as IMes, $IMesH_2$, I*t*Bu, ICy, 4,5-Cl_2-1,3-Me_2-imidazol-2-ylidene and bidentate NHCs allowed for the synthesis of numerous complexes. The replacement of one or both triflate ligands by phenoxide or alkoxide ligands extended the class of complexes further. TONs up to 545 000 were achieved in the homometathesis of 1-octene and 1-nonene with [Mo(*N*-2,6-Me_2-C_6H_3)($CHCMe_2Ph$)(IMes)(OTf)(CH_3CN)$^+$($B(Ar^F)_4$)$^-$].[108]

Chapter 2

Stereoselective Olefin Ring-Opening Cross-Metathesis Catalyzed by Molybdenum Imido Alkylidene *N*-Heterocyclic Carbene Complexes

The content of this chapter appeared in the following publication:

Momin, M.; Nagy, G. M.; Buchmeiser, M. R. Stereoselective Olefin Ring-Opening Cross Metathesis Catalyzed by Molybdenum Imido Alkylidene *N*-Heterocyclic Carbene Complexes. *Adv. Synth. Catal.* **2019**, *361*, 5596–5604.

2.1 Introduction

Olefin ring-opening cross-metathesis (ROCM) is an important synthetic tool. Depending on the bicyclic precursor, it allows for the synthesis of functionalized cycloalkenes.[109] Apart from suppressing undesired competitive and/or parallel reactions (Scheme 19) such as ring-opening metathesis polymerization (ROMP), the ethenolysis of the cyclic olefin, the self-metathesis of the cross partner or the ring-opening double cross-metathesis, stereo- and enantioselective ROCM has moved into the center of interest. In the case of molybdenum and tungsten alkylidenes, i.e. *Schrock*-type catalysts, stereo- and enantioselective ROCM[81, 110-122] has been accomplished by the use of chiral catalysts having a stereogenic metal center, while in the case of ruthenium alkylidene-,[123-125] i.e. *Grubbs*- and *Grubbs-Hoveyda-type* catalyst-triggered ROCM, this was realized by the use of chiral *N*-heterocyclic carbene (NHC) ligands[123-125] or with the aid of a stereogenic metal center.[126] In several reports[123, 127-130] the use of 7-oxa- or 7-azanorbornene compounds has been described, to make use of the heteroatom to increase stereoselectivity. There are also reports, which exclusively use aryl-substituted alkenes i.e. styryl-alkenes, enol ethers or enoates as cross-partners,[58, 131, 132] which are also directing stereoselectivity in ROCM.

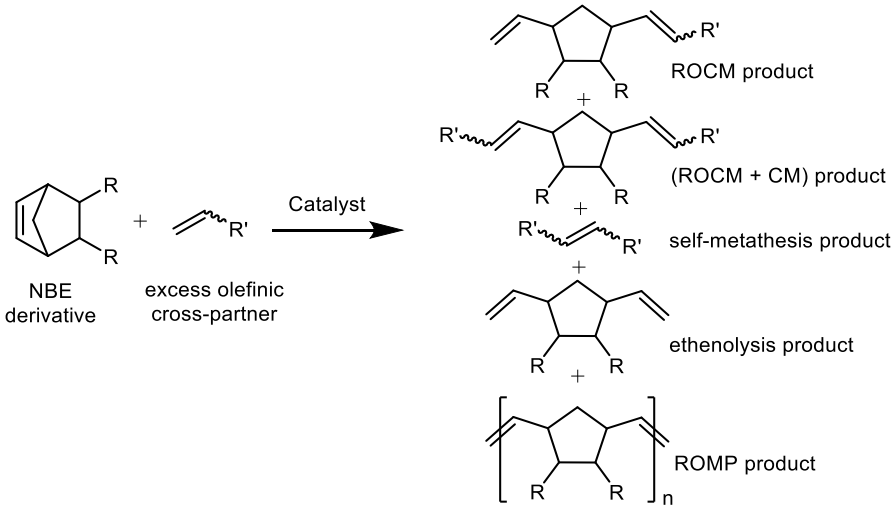

Scheme 19. Ring-opening cross-metathesis (ROCM) and competitive reactions.

Since 2014, *Buchmeiser's* group has developed neutral and cationic molybdenum imido alkylidene NHC complexes and demonstrated their high activity, productivity and functional group tolerance in various olefin metathesis reactions.[104, 133-140] Also, silica-supported versions in cooperation with *Copéret et al.* were reported[104, 141, 142]

and established synthetic routes to anchor sterically demanding alkoxides,[137, 143] which are decisive for the control over stereochemistry.[81, 82] It was confirmed that substrate, i.e. olefin coordination to molybdenum imido alkylidene NHC complexes occurs *trans* to the NHC,[144] which is in full accordance with calculations on olefin coordination in *Schrock-type* catalysts.[145, 146] The studies also revealed that the cationic tetracoordinated 14-VE complexes are indeed the active species to which an olefin approaches *trans* to the NHC followed by metallacyclobutane formation.[144] Recently, the influence of the size of the imido ligand on *E*/*Z*-selectivity in the ROMP of functional norbornenes and 2-azanorborn-5-enes and on the synthesis of all-*trans*, *isotactic* ROMP-derived polymers are reported by Buchmeiser et al.[147] Also, *E*-selectivity was correlated with the buried volume, V_{bur}, of the imido ligand in molybdenum imido alkylidene NHC complexes. Because of these findings, it was at the center of interest, if we could extend this concept to other olefin metathesis reactions such as ROCM. In this regard, molybdenum imido alkylidene NHC complexes bearing the 3,5-dimethyl- and 2-*tert*-butylphenylimido ligand were chosen for further scrutinization, as these complexes display significant differences in their buried volumes (17.4 and 23.2 %, respectively, Figure 16 a). Here, it was hypothesized that the *E* or *Z*-product formation efficiency depends on the sterics of an imido ligand at the metal center (Figure 16 b). As shown in the proposed mechanistic model, the formation of *E* and *Z*-selective metallacylobutane results from the insertion of substrate into the more abundant and stable *syn*-alkylidene.

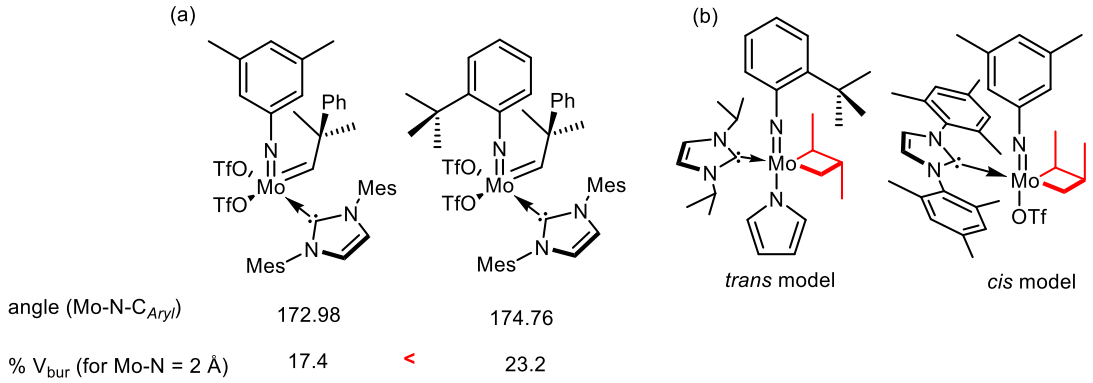

Figure 16. (a) Structure, Mo-N-C$_{aryl}$ angles and buried volumes of bistriflate complexes; (b) mechanistic models for high *E*- and *Z*-selectivity in ROCM metathesis.

Given the limited ROCM activity of cationic, bidentate, *O*-chelated molybdenum imido alkylidene NHC complexes[107] with various substrates in which ROMP dominated, we chose cationic molybdenum imido alkylidene monoalkoxide and monopyrrolide catalysts together with 2,3-disubstituted cyclic olefins.

The ROCM of cyclic olefins, i.e*. endo, endo*-2,3-dicarbomethoxynorborn-5-ene (*endo, endo*-DCMNBE), *exo, exo*-2,3-dicarbomethoxynorborn-5-ene (*exo, exo*-DCMNBE), *endo, exo*-2,3-dicarbomethoxynorborn-5-ene ((+) DCMNBE) and 2*,3-exo,exo-bis*(acetoxymethyl)-7-oxabicyclo[2.2.l] hept-5-ene (7-oxa-NBE derivative) with a variety of terminal olefins are reported. Reactions were carried out on a 1 mol% catalyst loading and were typically completed within 30 min at room temperature. The unusually high catalyst loading was used to address any potential post-metathesis isomerization of the ROCM products by kinetics studies. All ROCM products were isolated by preparative column chromatography. Finally, explored a high *trans*-selective catalyst for self-metathesis (SM) of 1-dodecene and methyl 10-undecenoate.

2.2 Results and Discussion

2.2.1 Structure – Selectivity Correlations

During the initial studies norbornene and styrene were employed, however, which resulted in the substantial amounts of poly(norbornene) even in the presence of twenty-equivalents of styrene. Using *endo, endo*-DCMNBE, predominantly the ROCM products were obtained with various cross-partners including alkyl-, aryl-, silyl-substituted 1-olefins as well as allyl phenyl ether, allyl benzyl ether and ally ethyl ether (Scheme 20). Along with the ROCM products, minor amounts, typically less than 6%, of the ethenolysis product were observed. In some cases, double cross-metathesis led the formation of double-substituted cyclic olefins up to 10 %. Notably, there was no polymer formation in any ROCM reaction.

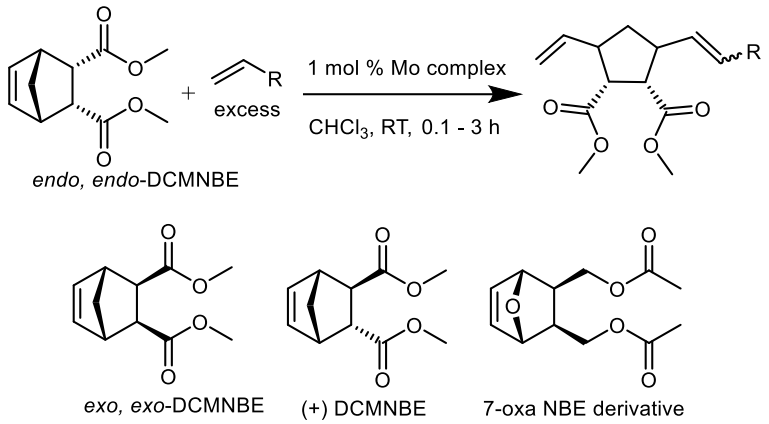

Scheme 20. ROCM of *endo, endo*-DCMNBE and structures of other cyclic olefins.

Taking the values for V_{bur} into account, complexes based on the 2-*tert*-butylphenylimido ligand should favor the formation of an *E*-double bond while those containing the 3,5-dimethylphenylimido ligand should favor the formation of *Z*-double bonds.

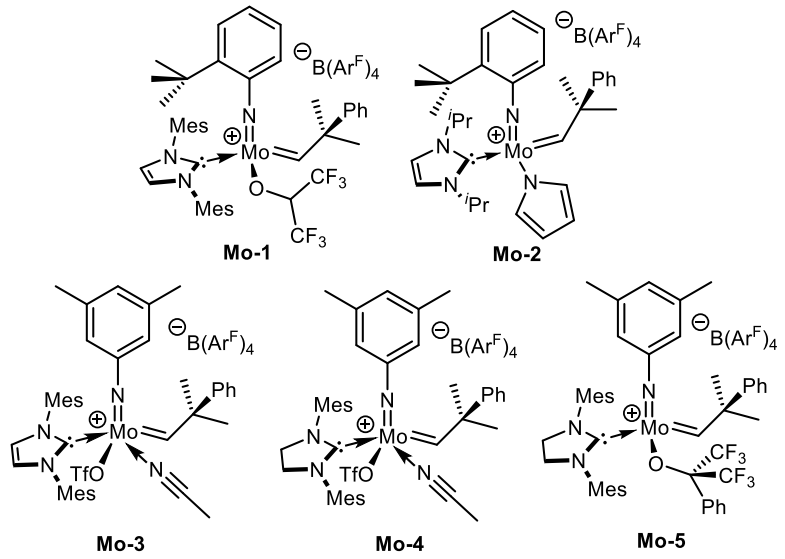

Figure 17. Molybdenum complexes **Mo-1** – **Mo-5** used in the ROCM of cyclic olefins with various 1-alkenes.

Considering the model shown in Figure 16 (b), the complexes **Mo-1** – **Mo-5** (Figure 17) were chosen for the ROCM of cyclic olefins with various 1-alkenes. Notably, complexes **Mo-3** and **Mo-4** are only accessible with coordinating solvents, however, this does not influence the stereoselectivity of the complex,[147] because the solvent dissociates prior to molybdacyclobutane formation from the metal.[144]

E-Selective ROCM

[Mo(*N*-2-*tert*-Bu-C_6H_4)(CHCMe$_2$Ph)(IMes)(OCH(CF$_3$)$_2$)]$^+$ [B(ArF)$_4$]$^-$ (**Mo-1**),[147] and [Mo(N-2-*tert*-Bu-C_6H_4)(CHCMe$_2$Ph)(1,3-bis(*i*Pr)imidazol-2-ylidene)(C_4H_4N)]$^+$ B(ArF)$_4$]$^-$ (**Mo-2**),[137] were prepared according to the literature. In line with the model shown in Figure 1b, both catalysts are indeed found to be *E*-selective in the ROCM of *endo, endo*-DCMNBE with 1-pentene, styrene, allyltrimethylsilane (allyl-TMS), allyl benzyl ether, allyl phenyl ether and allyl ethyl ether as the cross-partner, achieved up to 99% *E*-selectivity. Similar accounts for other cyclic olefins, which except for 7-oxa-NBE all showed high *E*-selectivity with complex **Mo-2**. Results are tabulated in Table 1 and Table 2. Complex **Mo-2** was used to isolate the ROCM products for all cross-partners on a preparative scale since it showed significantly high *E*-selectivity. Column chromatography was used to purify all the crude products. The isolated ROCM products then served as fully characterized standard compounds for the GC-MS-based evaluation of all other catalysts.

Table 1. Stereoselectivity in ROCM[a] of *endo, endo*-DCMNBE catalyzed by **Mo-1** – **Mo-5**.

Sr. No.	Cross partner	*E* (%)		*Z* (%)		
		Mo-1	**Mo-2**	**Mo-3**	**Mo-4**	**Mo-5**
1	1-pentene	79	87	80	90	96
2	styrene	95	97	87	89	59
3	allyl-TMS	92	92	89	93	84
4	allyl benzyl ether	89	95	86	91	89
5	ally phenyl ether	87	>99	<1	35	81
6	allyl ethyl ether	>99	>99	<1	<1	<1

[a]Reaction conditions – cyclic olefin : cross partner = 1 :10, 1 mol% catalyst, room temperature, 3 h, $CHCl_3$ (0.5 M in cyclic olefin), conversion by GC-MS (quantitative conversion in all the catalysts), internal standard : *n*-dodecane.

Table 2. Stereoselectivity in the ROCM[a] of different cyclic olefins with allyl benzyl ether catalyzed by complexes **Mo-2** and **Mo-5**.

Sr. No.	cyclic olefin	*E* (%)	*Z* (%)
		Mo-2	**Mo-5**
1	*exo, exo*-DCMNBE	92	91
2	(+) DCMNBE	91	89
3	7-oxa-NBE	70	60

[a]Reaction conditions – cyclic olefin : cross partner = 1 :10, 1 mol% catalyst, room temperature, 3 h, $CHCl_3$ (0.5 M in cyclic olefin), conversion by GC-MS (quantitative conversion in all the catalysts), internal standard : *n*-dodecane.

E-Selective Self-Metathesis

In view of the high *trans*-selectivity of catalyst **Mo-2** in ROCM, this catalyst was evaluated in the self-metathesis (SM) of 1-dodecene and methyl 10-undecenoate. In accordance with the proposed model, up to 92% *trans*-selectivity (Table 3) was observed. Kinetic studies were carried out to check for any post-metathesis isomerization. Again, no isomerization was observed for any of the substrates (Figures 90 and 91, Appendix).

Table 3. Stereoselectivity in the SM[b] of 1-dodecene and methyl-10-undecenoate by complex **Mo-2**.

Sr.No.	Substrate	TON	*E* (%)
1	1-Dodecene	480	86
2	Methyl 10-undecenoate	500	92

[b]Reaction condition – closed cap vial, catalyst : substrate = 1 : 1000, room temperature, 4 h, $CHCl_3$ (0.5 M in substrate), conversion by GC-MS, internal standard : *n*-dodecane.

Z-Selective ROCM

In line with to the proposed intermediary molybdacyclobutanes (Figure 16 b), [Mo(*N*-3,5-$Me_2C_6H_3$)(CHCMe_2Ph)(IMes)(MeCN)$(OTf)^+$ $B(ArF)_4^-$] (**Mo-3**)[147] and [Mo(*N*-3,5-$Me_2C_6H_3$)(CHCMe_2Ph)(IMesH_2)(MeCN)$(OTf)^+$ $B(ArF)_4^-$] (**Mo-4**) were found to be *Z*-selective in ROCM reactions, showing up to 93 % *Z*-selectivity (Table 1). Notably, catalyst **Mo-4** displayed a significantly higher *Z*-selectivity than catalyst **Mo-3**. **Mo-3** and **Mo-4** differ structurally only in terms of the NHC, complex **Mo-4** having a saturated backbone.

According to *Schrock* and *Hoveyda*, the *Schrock-type* catalysts containing a small imido and a bulky, freely rotating basic alkoxide ligand like *O*-2,6-(2,4,6-Me_3-C_6H_2)$_2$-C_6H_3, (HMTO) or 5,5′,6,6′,7,7′,8,8′-octahydro-3,3′dibromo-2-silyloxy-1,1′-binapth-2′-olate promote *Z*-selective homo- and cross-metathesis.[81] There, the bulkier alkoxide directs the incoming substrate to facilitate *Z*-selective metallacyclobutane formation. Recently, a novel synthetic route to introduce sterically demanding alkoxides into molybdenum imido alkylidene NHC complexes were reported.[137] Despite this progress, it is still challenging to anchor bulky alkoxides, particularly in the case of molybdenum 3,5-dimethylphenylimido alkylidene NHC complexes, for which often decomposition is observed. Therefore, it was aimed to synthesize a molybdenum imido alkylidene NHC alkoxide complex containing a medium-sized, less basic alkoxide ligand such as –OCPh(CF_3)$_2$. Accordingly, **Mo-4** was reacted with one equivalent of LiOCPh(CF_3)$_2$ in CH_2Cl_2 at -35 °C. [Mo(*N*-3,5-$Me_2C_6H_3$)(CHCMe_2Ph)(IMesH_2)(OCPh(CF_3)$_2$)$^+$ B(Ar^F)$_4^-$] (**Mo-5**) was successfully isolated in 55% yield by purification from a mixture of CH_2Cl_2 and *n*-pentane (Scheme 21). In the ^{13}C NMR spectrum, the alkylidene carbon signal is barely visible at δ = 310.7 ppm, suggesting a dynamic species. In line with that, one can see the broad alkylidene proton resonance in the ^{1}H NMR spectrum at δ = 12.50 ppm. The backbone protons (δ = 4.06 – 4.24 ppm, m, 4H) of the NHC show a well-defined splitting pattern, suggesting that the dynamics are restricted to the alkylidene moiety.

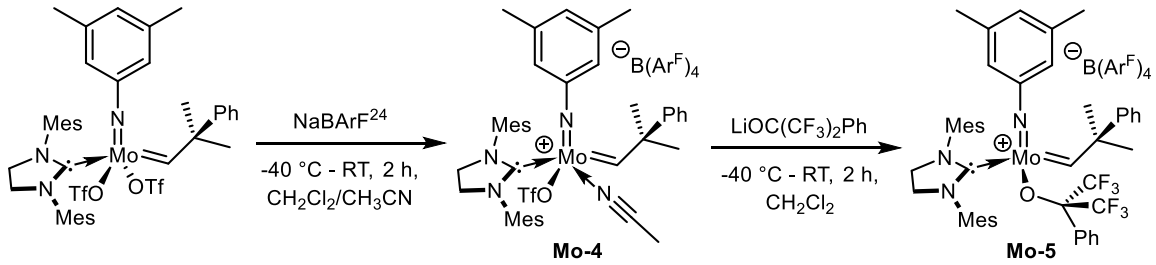

Scheme 21. Synthesis of catalyst **Mo-4** and **Mo-5**.

After several efforts to crystallize complex **Mo-5**, finally the solution was doped with a few acetonitrile drops. Fortunately, the crystals of complex **Mo-5** bearing acetonitrile (**Mo-5-CAN)** were obtained. Complex **Mo-5-ACN** crystallized in the triclinic space group *P-1, a* = 1157.37(4) pm, *b* = 1727.34(6) pm, *c* = 1043.04(7) pm; α = 100.763(2)°, β = 102.462(2)°, γ = 92.2840(10)° and *Z* = 2 (Figure 18). The structure

exhibits a distorted square pyramidal geometry (τ = 0.27), with the alkylidene at the apex. The acetonitrile is coordinated *trans* to the NHC ligand.

Catalyst **Mo-5** displayed high reactivity in the ROCM. The comparably electron-withdrawing alkoxide i.e. -OCPh$(CF_3)_2$ attributes to increased activity. During the kinetics measurements with all six cross partners, there were no residual *endo, endo*-DCMNBE left (Figures 20, 21 and 87-89) in the first sample withdrawn after 30 s. This implies the underlying rate constants for ROCM were all >180 min^{-1}. Except for allyl vinyl ether (*vide infra*) and styrene, *Z*-selectivities with catalyst **Mo-5** were in the range of 81 – 96%.

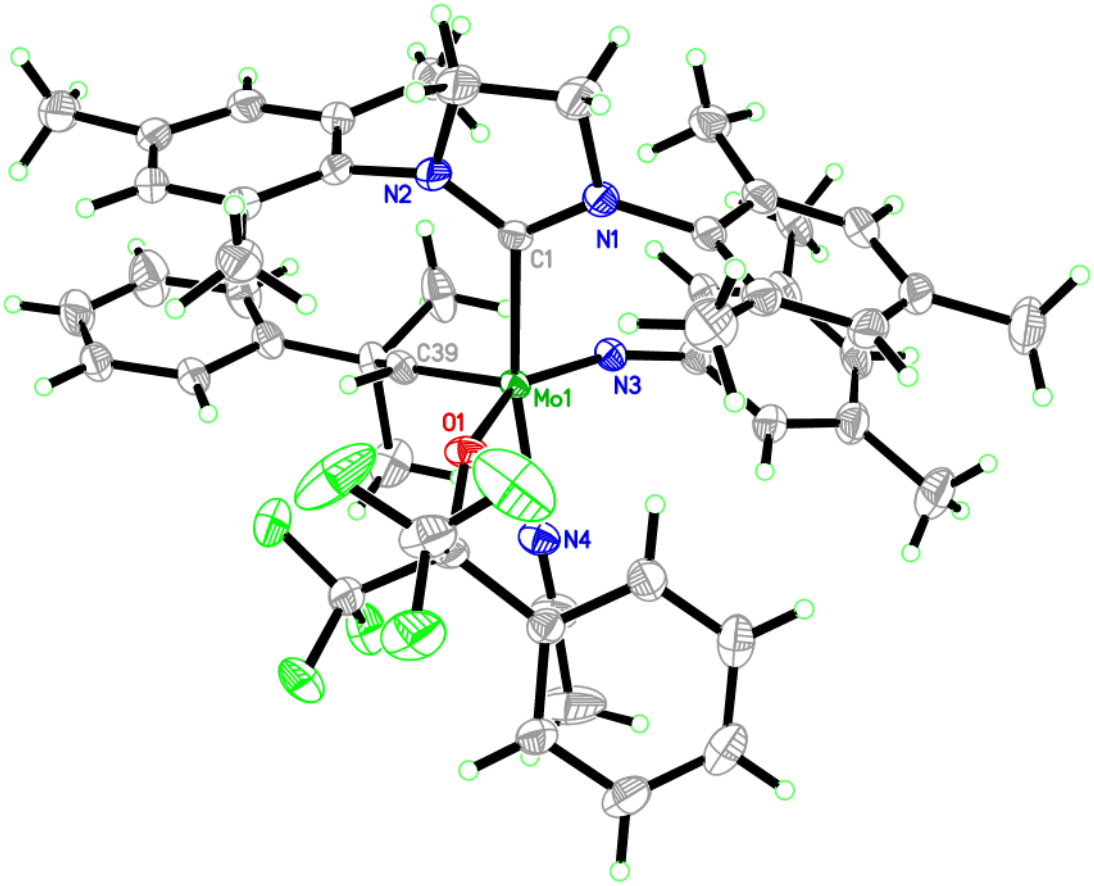

Figure 18. Single-crystal X-ray structure of complex **Mo-5-ACN**. Selected bond lengths [pm] and angles [°]. Mo-N3 173.53(10), Mo-C39 189.25(12), Mo-O1 199.59(8), Mo-N4 221.36(11), Mo-C1 222.80(11); N3-Mo-C39 102.41(5), N3-Mo-O1 149.11(4), C39-Mo-O1 107.20(4), N3-Mo-N4 84.15(4), C39-Mo-N4 92.29(5), O1-Mo-N4 86.06(4), N3-Mo-C1 97.34(4), C39-Mo1-C1 101.73(5), O1-Mo-C1 85.23(4), N4-Mo-C1 165.18(4). The anion has been omitted for clarity.

2.2.2 Role of *O*-Chelation in Metallacyclobutanes

Based on the model (Figure 16 b), one can expect high *E*-selectivity with the *E*-selective catalysts **Mo-1** and **Mo-2**, particularly for the vinyl ethers, as *O*-chelation was expected to further improve stereoselectivity. Indeed, in the ROCM of *endo, endo*-DCMNBE with allyl ethyl ether, complex **Mo-2** containing a small pyrrolide ligand facilitated the expected >99% *E*-selectivity. In comparison, complex **Mo-1** containing a medium-sized alkoxide showed only 87% *E*-selectivity. This demonstrates the synergistic roles in terms of the size of both the alkoxide and the imido ligand. Here, it indirectly reconfirms the trigonal bipyramidal structure of the intermediary molybdacyclobutane with the alkoxide and the imido ligand forming the apexes.

Notably, the ROCM of *endo, endo*-DCMNBE with allyl ethyl ether proceeded highly *E*-selective (>99%) (Table 1), irrespective of the catalyst used. This high *E*-selectivity with any of the catalysts used here is attributed to the strong chelation of the ether-oxygen to the metal center, which directs the cross-partner to proceed in that fashion (Figure 19), resulting in a virtual selective formation of *E*-double bonds.

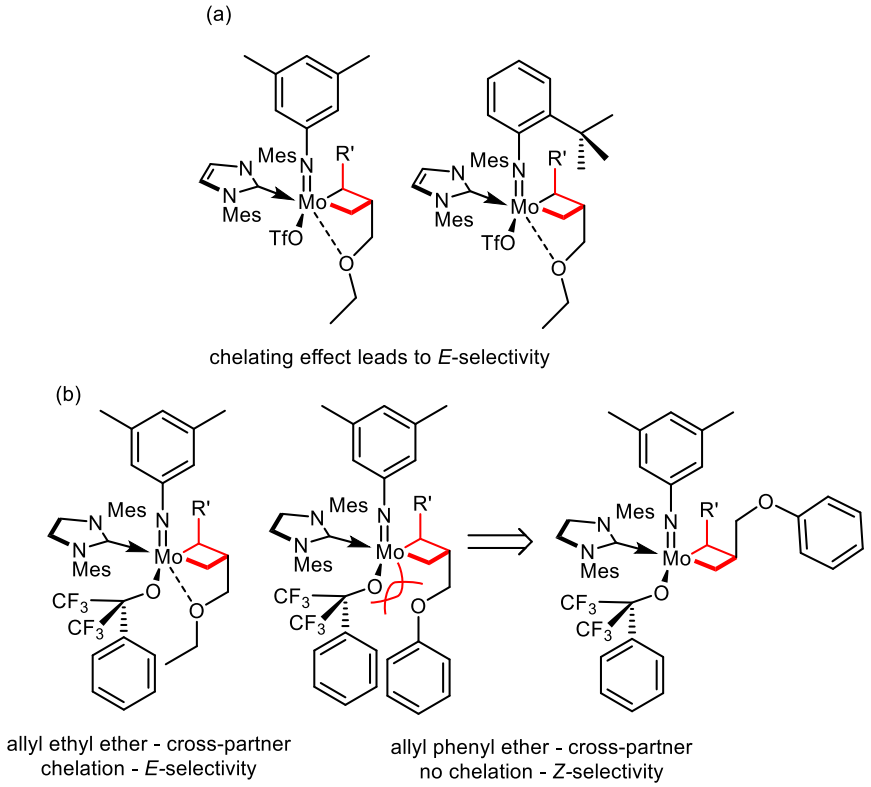

Figure 19. (a) Hypothesis for an *O*-chelation effect of allyl ethyl ether leading to high *E*-selectivity; (b) Influence of sterically demanding alkoxides on incoming cross-partners.

This chelating effect is fully operative with the “small” allyl ethyl ethers. While, chelation with other, larger ether substrates such as allyl phenyl ether and allyl benzyl ether is increasingly impeded through steric interaction with the alkoxide (Figure 19). Thus, the ROCM of *endo, endo*-DCMNBE with allyl phenyl ether by the action of catalysts **Mo-3** – **Mo-5** proceeded with *E*-selectivities between 19 – 99% (Table 1). In line with the underlying models shown in Figure 4, the larger alkoxide present in the *Z*-selective complex **Mo-5** had the most pronounced effect on *E*/*Z* selectivity in the ROCM with allyl *phenyl* ether. In **Mo-5**, the sterically demanding alkoxide and the phenyl group in the allyl phenyl ether can sterically interact and reduce *O*-chelation. Finally, again in line with the underlying model, the ROCM of *endo, endo*-DCMNBE with allyl benzyl ether catalyzed by catalysts **Mo-3** – **Mo-5** generally turned out to be highly *Z*-selective (86 – 91 % *Z*) due to steric interaction with the alkoxide in the metallacyclobutane.

2.2.3 Kinetic Studies

It is generally of enormous advantage to dispose over catalysts that deliver high stereoselectivity under *thermodynamic* but not under *kinetic* control. Only in this case, one can run reactions to completion without the necessity of a tedious control over conversion. Therefore it was important to check, whether the achieved selectivities are obtained through thermodynamic control. This is of particular interest with *Z*-selective catalysts, since *Z*-double bonds are often affected by post-metathesis isomerization. The catalytically active alkylidene species usually reacts faster with the *Z*-alkene than with the *E*-alkene to give the thermodynamically more stable *E*-product.[148] Complex **Mo-5** was used to follow the kinetics of the ROCM reaction of *endo*, *endo*-DCMNBE with all cross-metathesis partners (Figures 20, 21, and 78 – 81). Notably, all ROCM reactions carried out did not show any significant post-metathesis isomerization, except for the one with styrene (Figure 22), for which *Z*-selectivity was significantly reduced from 80 to 59 %.

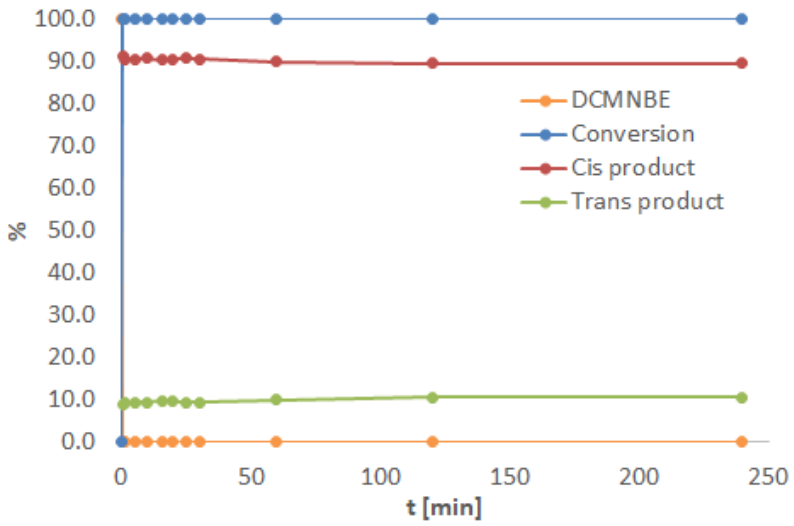

Figure 20. *Z*-selective ROCM kinetics of *endo, endo*-DCMNBE with allyl benzyl ether, complex **Mo-5**.

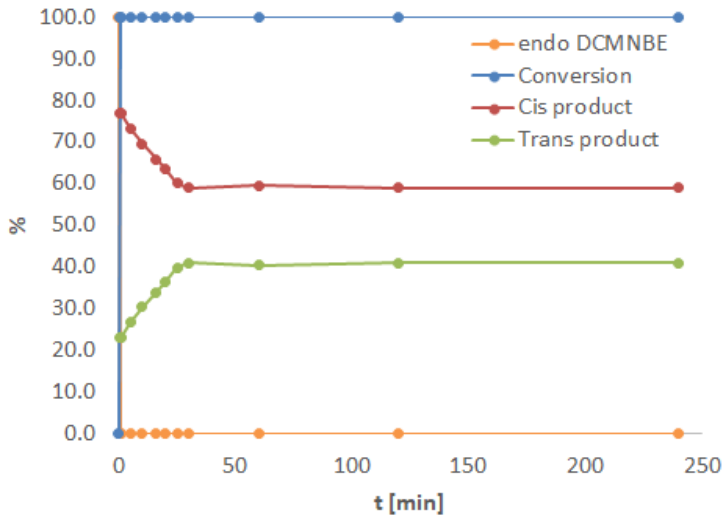

Figure 21. Ring-opening cross-metathesis kinetics of *endo, endo*-DCMNBE with styrene, complex **Mo-5**.

Notably, complex **Mo-2** with styrene as cross-partner did not show any post-metathesis isomerization (Figure 82). Representative *E*-selective ROCM reaction kinetics are shown in Figure 22, and 82 – 83. Equally important, the high *E*-selectivity obtained with complexes **Mo-1** and **Mo-2** is not the result of post-metathesis isomerization, too. Again, ROCM kinetics with complex **Mo-2** (Figure 22, 82 and 83) using styrene, allyl benzyl ether, or allyl phenyl ether as cross-partners did not reveal any post-metathesis isomerization. Also found similar low isomerization propensity for other cyclic olefins such as *exo, exo* DCMNBE, (+) DCMNBE and 7-oxa-NBE, and

did not observe any post-metathesis isomerization, both with complex **Mo-2** and **Mo-5** (Figure 84 – 89).

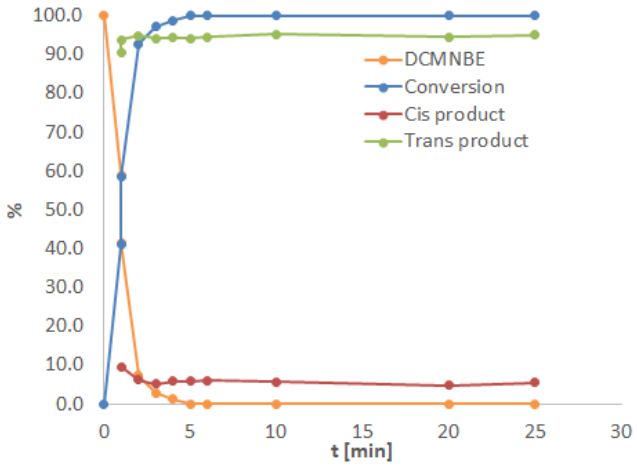

Figure 22. *E*-selective ROCM kinetics of *endo, endo*-DCMNBE with allyl benzyl ether, complex **Mo-2**.

Further, it was checked whether the catalyst was still active after the corresponding metathesis reactions by adding excess substrate and monitoring the reaction by GC-MS. The additionally added substrate quickly gets consumed, which supports the presence of active catalyst. Furthermore, in a separate reaction, norbornene (100 equiv.) was added to the reaction mixtures after two min. i. e. after the complete consumption of DCMNBE and stirred the mixture for two h. The formation of poly(norbornene) also confirmed the presence of active catalyst.

2.3 Conclusions

Ring-opening cross-metathesis of functional norbornenes with 1-alkenes can be accomplished with high *E*- or *Z*-selectivity. The choice of a sizeable imido ligand with a buried volume, V_{bur}, >23%, combined with a small alkoxide or pyrrolide, allows for high *E*-selectivity. In comparison, the use of a small imido ligand with V_{bur} <18% in combination with a comparably large alkoxide allows for high *Z*-selectivity. “Small” allyl ethers experience *O*-chelation to the cationic metal center, which leads to high *E*-selectivity, at least with “small” alkoxides or, generally, anionic ligands. Most important, the cationic molybdenum imido alkylidene NHC catalysts do, with one exception, not show any post-metathesis isomerization activity; products are formed under thermodynamic control. This makes these classes of catalysts attractive candidates for stereoselective organic synthesis.

Chapter 3

Tuning the Latent Behavior of Molybdenum Imido Alkylidene *N*-Heterocyclic Carbene Complexes in Dicyclopentadiene Polymerization

The content of this chapter appeared in the following publication:

Momin, M.; Musso, J. V.; Frey, W.; Buchmeiser, M. R. Tuning the Latent Behavior of Molybdenum Imido Alkylidene *N*-Heterocyclic Carbene Complexes in Dicyclopentadiene Polymerization. *Organometallics,* **2021**, *40*, 253–265.

3.1 Introduction

Poly(dicyclopentadiene), poly(DCPD), is prepared by ring-opening metathesis polymerization (ROMP) and is one of the most influential polymer among the metathesis-derived polymers due to its excellent mechanical properties, outstanding damage tolerance, and corrosion resistance.[149-152] Poly(DCPD) is mainly accessed or processed *via* reaction injection molding (RIM), resin transfer molding (RTM), or vacuum-assisted RTM (VARTM) techniques. A precise processing window or adequate pot time before processing is the critical factor in producing RIM, RTM or VARTM molded parts of good quality, aesthetics, and dimensions. Mostly non-latent catalysts are used, which requires a fast mixing with the monomer. Early 90's reports evidenced that the inhibitor or retarder (Lewis Base) was added along with the catalyst activators (aluminum alkyls) to fill large or complex molds.[149, 153]

Thermally latent pre-catalysts gained a lot of attention. They allow to set-up one-component systems, which substantially simplify both the handling and the necessary equipment. It avoids mixing the catalyst, activator, and monomer for the *in situ* creation of a polymerization-active system. An ideal latent catalyst does not show catalytic activity in the presence of monomer or substrate under the storage conditions; however, the quantitative and fast activation is desired exactly when and where it is needed. Latent catalysts should be tolerant towards all components of the polymerization mixture as well as towards decomposition or thermal degradation.

In general, the light, heat, acids, phosphines, or mechanical force activates the latent catalyst or pre-catalyst for ROMP.[151, 154-158] So far, most of the pre-catalyst for the ROMP of DCPD are based on ruthenium, due to their tolerance towards moisture and protic groups.[151, 159] Latency in the well-defined ruthenium alkylidene catalysts is often achieved by chelating alkylidenes[160, 161] such as *N*-chelating (pyridyl, Schiff base, quinoline, quinoxalines),[162-170] *O*-chelating (ether, carboxylate),[171-175] or *S*-chelating (thio-ether)[161, 169, 176-178] structural motifs.

Control over the onset of polymerization facilitates the proper mixing of reactive components, the preparation of ready-to-use formulations and extends both the pot time and processing window. Therefore, the design of a thermally stable pre-catalyst is highly on demand. In 2005, *Slugovc* and co-workers described the general

approaches toward thermally switchable well-defined ruthenium olefin metathesis initiators, followed by different research groups (Scheme 22).[151, 179] Class A retains the classic *Grubbs* first and second-generation catalyst, while class B represents *Fischer* carbenes, for which no catalytic activity was observed. However, these catalysts can be activated thermally or photochemically. Activated class C catalysts open the coordination site by the dissociation of L_2. Nevertheless, the dangling L_2 ligand is close to the metal, and will therefore compete with the incoming olefin substrate for coordination, which can reduce the propagation rate. There will be no such competition in case one uses class D motifs since the chain propagation takes away L_2 from the metal center.

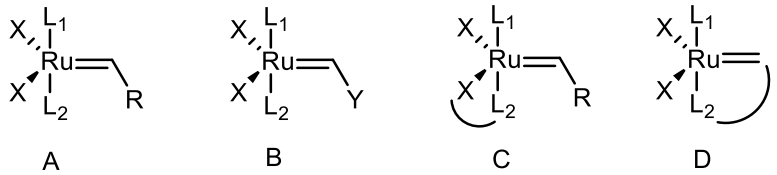

Scheme 22. Different approaches towards the design of well-defined latent catalysts.

In contrast to Ru-alkylidenes, very few reports are available on Mo- and W-based latent olefin metathesis pre-catalysts due to their sensitivity towards air and moisture.[180] Thermally switchable molybdenum initiators comprise chelating alkylidene type,[181-185] chelating alkoxide type,[186] chelating *N*-heterocyclic carbene (NHC) type,[107, 138] and tailored molybdenum imido alkylidene NHC type[187] pre-catalysts as well as photo-induced tungsten pre-catalysts.[188, 189] In particular, finger-countable reports of latent group 6 pre-catalysts for the ROMP of DCPD are available.[185, 187, 189] In 1996, *Mühlebach* et al. reported the first photo-induced ROMP of DCPD using simple tungsten alkyl complexes by *in situ* generations of ROMP active initiator through light irradiation.[189] Further, after almost two decades, in 2017, *Buchmeiser's* group reported the successful ROMP of DCPD by the action of thermally latent molybdenum imido alkylidene NHC complexes[187] in which the combination of NHCs with different σ-donating propensity and different anionic ligands at the molybdenum centre allows to perform latency in *endo*-DCPD curing. The concept was later extended to fully latent, air-stable, penta- and hexacoordinated molybdenum imido alkylidene NHC complexes as pre-catalysts for the ROMP of DCPD,[185] in which the *O*-chelating alkylidene motif provides good control over the latent behavior. So far, however, most of these air-stable pre-catalysts suffered from

a comparatively high onset temperature of polymerization, T_{onset} > 140 °C and a high exotherm maximum, $T_{max,exo}$ > 160 °C,[106] which is close to the cracking temperature of DCPD (170 °C) and thus considerably complicates processing.

Therefore, several new molybdenum(VI) imido alkylidene NHC complexes bearing *O*- and *N*-chelating alkylidene moiety, mostly designed from commercially available, cheap olefins viz. *N*-vinyl-2-pyrrolidone and 2-vinylpyridine were synthesized. These are the first olefin metathesis complexes bearing a four-membered chelating alkylidene obtained from 2-vinylpyridine, which might allow studying the influence of the chelate's ring size on ROMP. These complexes were demonstrated to become thermally activated for the ROMP of dicyclopentadiene. Furthermore, the monotriflate monoalkoxide analogs were synthesized to deliver enhanced activity and a further fine-tuning of the onset of polymerization. Such fine-tuning of the onset temperature of polymerization can avoid overheating of the entire system, typically on an industrial scale, as the ROMP of DCPD is an exothermic reaction. Besides, the first molybdenum η^2-olefin NHC complex through 2-vinylpyridine was prepared.

3.2 Results and Discussion

Pentacoordinated molybdenum imido alkylidene NHC complexes bearing 1,3-dimesitylimidazol-2-ylidene (IMes) as a NHC ligand were used as precursor complexes to obtain the targeted hexacoodinated chelating alkylidene complexes bearing different imido ligands. Cheap, readily available *N*-vinyl-2-pyrrolidone and 2-vinylpyridine were employed to exchange the alkylidene, resulted in *O*- and *N*-chelating alkylidene complexes, respectively.

3.2.1 Pre-Catalysts Bearing an *O*-Chelating Alkylidene

N-vinyl-2-pyrrolidone was explored to offer *O*-chelating alkylidene complexes. Molybdenum imido alkylidene bistriflate NHC complexes were treated with two equivalents of *N*-vinyl-2-pyrrolidone to obtain Mo(*N*-2,6-Me_2-C_6H_3)(CHC_4H_6NO)(IMes)$(OTf)_2$ (**Mo-6**) and Mo(*N*-3,5-Me_2-C_6H_3)(CHC_4H_6NO)(IMes)$(OTf)_2$ (**Mo-7**) in good isolated yield, 78 and 73%, respectively (Scheme 23). The alkylidene exchange worked well; immediate solution color change from yellow to bright orange was observed. Crystals of **Mo-6** suitable for single-crystal X-ray analysis were grown from a mixture of dichloromethane,

diethyl ether and pentane. **Mo-6** crystallizes in the triclinic space group *P-1* with *a* = 1139.65(5) pm, *b* = 1153.25(5) pm, *c* = 1777.35(7) pm; *α* = 76.514(2)°, *β* = 75.379(2)°, *γ* = 84.558(2)° and *Z* = 2 (Figure 23).

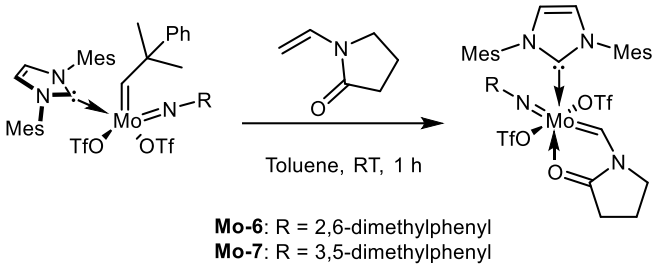

Mo-6: R = 2,6-dimethylphenyl
Mo-7: R = 3,5-dimethylphenyl

Scheme 23. Synthesis of pre-catalysts **Mo-6** and **Mo-7** *via* the exchange of the neophylidene moiety by *N*-vinyl-2-pyrrolidone.

In the solid-state, **Mo-6** adopts a distorted octahedral geometry with the NHC and one of the triflates in the apexes. The O(2)-Mo-C(1) angle is 165.80(8)°. The Mo-O(C=O) bond distance is 221.4(2) pm, which is comparable to the previously reported chelating carboxylate-functionalized alkylidene complex Mo(*N*-3,5-Me_2-C_6H_3)(CHOCOC_3H_7)(IMes)(OTf)(OC_6F_5),[185] Mo-O(C=O), 223.2(2) pm; but almost 14 pm shorter than the previously reported chelating alkoxide-functionalized alkylidene complex Mo(*N*-3,5-Me_2-C_6H_3)(CH(2-OCH_3)C_6H_4)(IMes)$(OTf)_2$,[185] Mo-O(Ar-O-CH_3), 235.2(7) pm. The Mo=C(alkylidene) bond distance 196.4(3) pm, is almost similar to the molybdenum mono alkoxide pyrrolide (MAP) type complex Mo(*N*-2,6-*i*Pr-C_6H_3)(CH(2-O)C_4H_6N)(2,5-Me_2-C_4H_2N)(OTPP) bearing *N*-vinyl-2-pyrrolidone, 195.78(11) pm reported by Schrock and co-workers.[183]

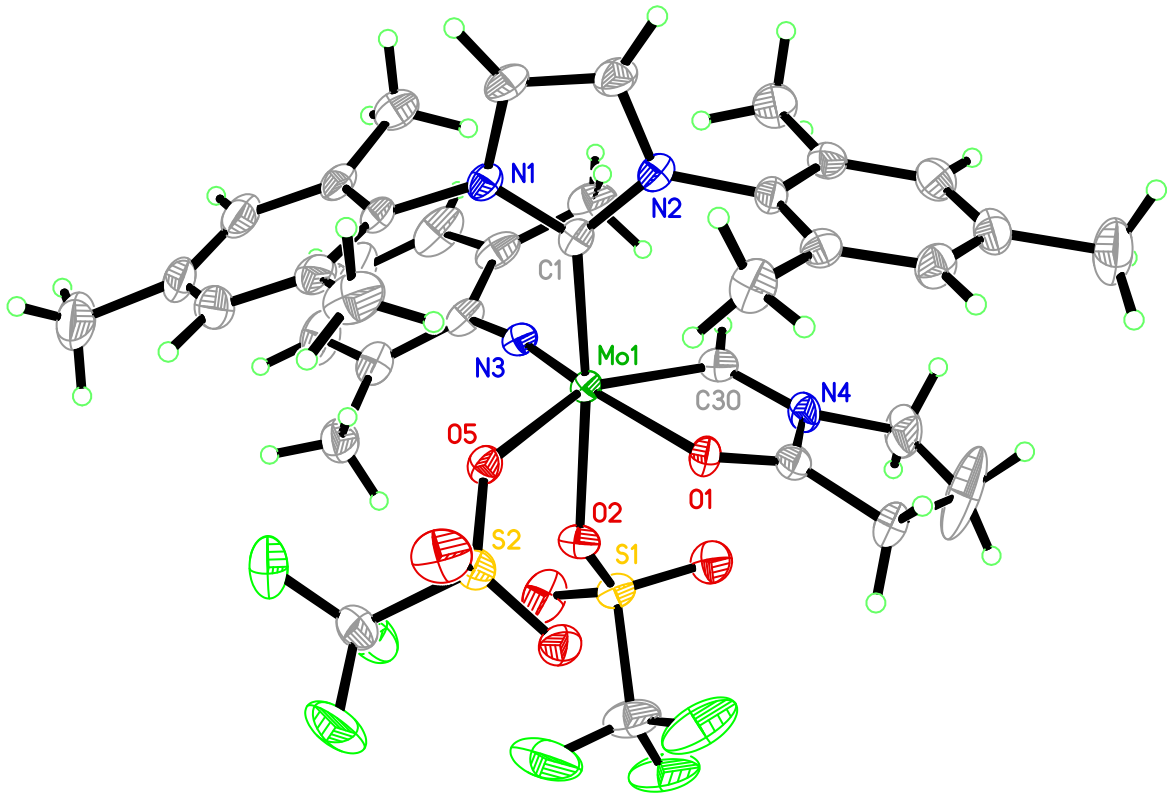

Figure 23. Single-crystal X-ray structure of complex **Mo-6**. Selected bond lengths [pm] and angles [°]. Mo1-N3 173.0(2), Mo-C30 196.4(3), Mo-O2 216.4(2), Mo-O5 218.2(2), Mo-C1 221.2(3), Mo-O1 221.4(2); N3-Mo-C30 93.89(11), N3-Mo-O2 93.89(9), C30-Mo-O2 91.92(10), N3-Mo-O5 113.38(9), C30-Mo-O5 151.06(10), O2-Mo-O5 77.32(7), N3-Mo-C1 94.33(10), C30-Mo-C1 99.04(11), O2-Mo-C1 165.80(8), O5-Mo-C1 88.79(9), N3-Mo-O1 167.69(9), C30-Mo-O1 74.62(10), O2-Mo-O1 82.29(8), O5-Mo-O1 77.33(7), C1-Mo-O1 91.90(9).

Complex **Mo-7,** bearing the 3,5-dimethylphenylimido ligand, was crystallized from a solution in dichloromethane and pentane at - 40 °C. **Mo-7** crystallized in the monoclinic space group $P2_1/c$, a = 1342.76(10) pm, b = 1664.53(13) pm, c = 1873.62(14) pm; $\alpha = \gamma = 90°$, β = 91.984(4)°, and Z = 4 (Figure 24). The Mo-O(C=O) bond distance is 221.3(2) pm, which is virtually identical to the one in **Mo-6** (Mo-O(C=O), 221.4(2) pm). Interestingly, both Mo-OTf bonds are almost identical (Mo-O5(OTf in-plane) 218.0(2) and Mo-O3(OTf-axial) 218.1(2) pm), even though one triflate is *trans* to the NHC and the second *trans* to the alkylidene. In **Mo-6**, as observed in the previously reported *O*-chelating alkylidene complexes,[147, 185] it was observed that, the triflate ligand *trans* to the NHC (Mo-O2, 216.4(2) pm) is about 2 pm shorter than the triflate ligand trans to the alkylidene (Mo-O5, 218.2(2) pm), despite the expected *trans* effect of the NHC.

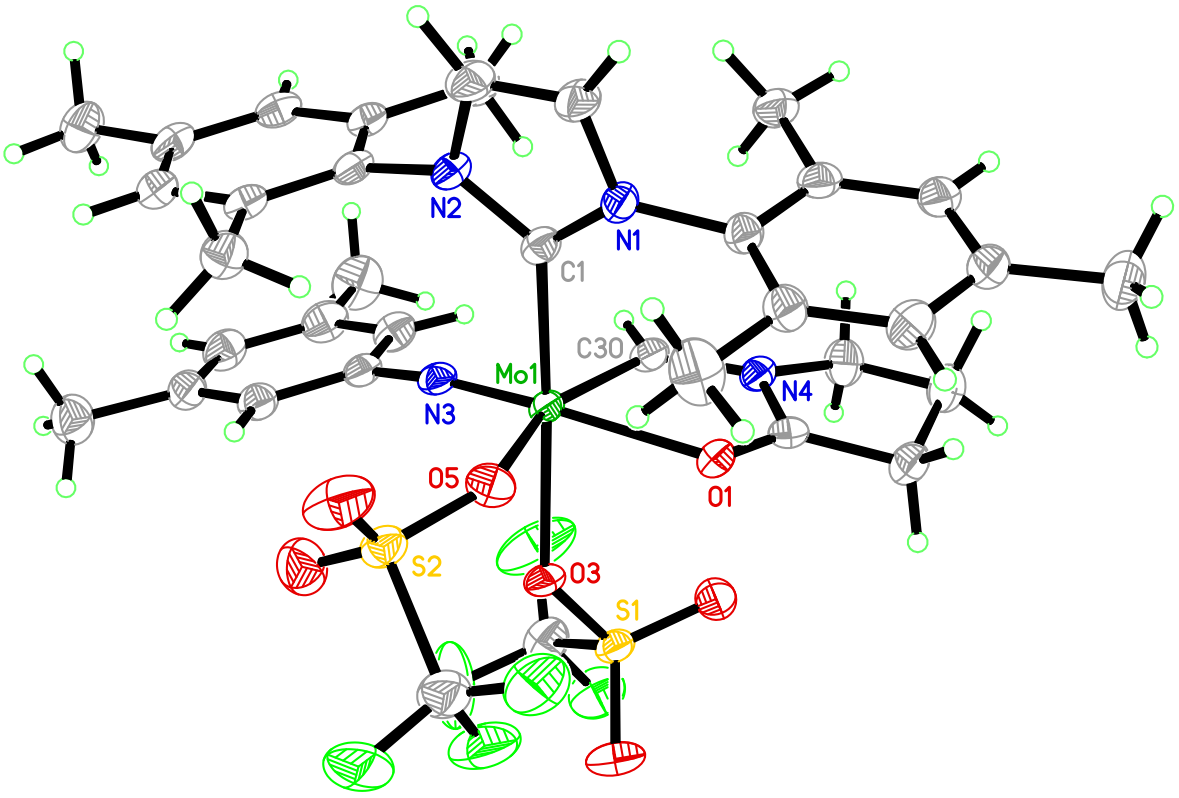

Figure 24. Single-crystal X-ray structure of complex **Mo-7**. Selected bond lengths [pm] and angles [°]. Mo-N3 171.7(3), Mo-C30 197.5(3), Mo-O5 218.0(2), Mo-O3 218.1(2), Mo-C1 219.8(3), Mo-O1 221.3(2); N3-Mo-C30 92.24(13), N3-Mo-O5 110.97(11), C30-Mo-O5 156.73(12), N3-Mo-O3 92.19(11), C30-Mo-O3 98.52(11), O5-Mo-O3 79.55(9), N3-Mo-C1 96.28(12), C30-Mo-C1 95.76(13), O5-Mo-C1 83.76(10), O3-Mo-C1 163.09(10), N3-Mo-O1 163.58(11), C30-Mo-O1 74.77(11), O5-Mo-O1 82.09(9), O3-Mo-O1 80.14(9), C1-Mo-O1 95.00(10).

The $J_{C\text{-}H}$ coupling constants obtained from the ^{1}H NMR spectrum of **Mo-6** and **Mo-7** were found to be $^1J_{CH}$ = 161.2 Hz and $^1J_{CH}$ = 160.3 Hz, respectively; besides the crystal structure, this also supports the existence of the *anti*-isomer and the chelating oxygen being *trans* to the imido ligand.

3.2.2 Pre-Catalysts Bearing a *N*-Chelating Alkylidene

Incorporation of cheap, readily available 2-vinylpyridine in molybdenum imido alkylidene NHC complexes, as the *N*-chelating alkylidene moiety was expected to furnish a four-membered chelate ring at molybdenum. Consequently, this was considered a promising candidate as such, since due to the chelation, it will offer a stable, latent hexacoordinated complex. Simultaneously, the inherent strain in the four-membered chelate ring will make it labile at elevated temperature to yield the active form. Therefore, in principle, the de-chelation at high temperature will open a coordination site for the incoming olefin or substrate. As the growing polymer chain

will take away the chelation site (*N*-) from the metal center. This avoids back-coordination and will not retard the propagation once initiated.

Molybdenum imido alkylidene NHC complexes with various imido ligands such as 2,6-dimethylphenylimido, 3,5-dimethylphenylimido, 2,6-difluorophenylimido and 2-(trifluoromethyl)phenylimido ligands were treated with two equivalents of 2-vinylpyridine to offer Mo(*N*-2,6-Me_2-C_6H_3)(CHC_5H_4N)(IMes)$(OTf)_2$ **(Mo-8),** Mo(*N*-3,5-Me_2-C_6H_3)(CHC_5H_4N)(IMes)$(OTf)_2$ **(Mo-9),** Mo(*N*-2,6-F_2-C_6H_3)(CHC_5H_4N)(IMes)$(OTf)_2$ **(Mo-10)** and Mo(*N*-2-CF_3-C_6H_3)(CHC_5H_4N)(IMes)$(OTf)_2$ **(Mo-11)** in moderate to good yield (55 – 69%) (Scheme 24). Reaction of Mo-*N*-2,6-difluorophenylimido neophylidene IMes bistriflate and Mo-*N*-2-(trifluoromethyl)phenylimido neophylidene IMes bistriflate with 2-vinylpyridine was quite fast, the reaction mixture turned yellow to dark red within 5 min, attributable to the weakly basic imidos. **Mo-8** and **Mo-9** were crystallized from a mixture of dichloromethane, diethyl ether and pentane.

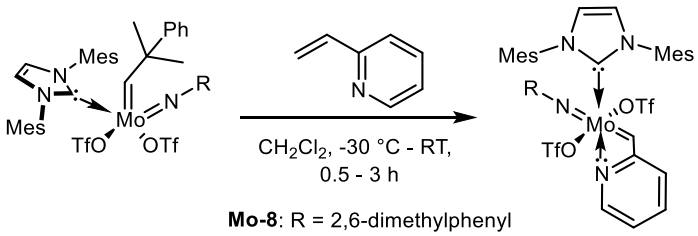

Scheme 24. Synthesis of pre-catalysts **Mo-8** - **Mo-11** *via* the exchange of neophylidene moiety by 2-vinylpyridine.

Mo-8 crystallized in the monoclinic space group *P2₁/c, a* = 1378.67(7) pm, *b* = 1059.84(5) pm, *c* = 2957.38(14) pm; *α* = *γ* = 90°, *β* = 93.105(2)°, and *Z* = 4 (Figure 25). The Mo-N (*N*-pyridine) bond distance is 236.26(14) pm, and unambiguously confirms *N*-chelation furnishing a four-membered chelate ring. Unlike in **Mo-6**, the chelation in **Mo-8** is weaker; in **Mo-6,** the Mo-O (C=O, pyrrolidone) bond length is 221.4(3) pm. **Mo-9** crystallized in the orthorhombic space group *P2(1)2(1)2(1), a* = 1189.55(9) pm, *b* = 1733.38(13) pm, *c* = 2163.89(18) pm; *α* = *β* = *γ* = 90°, and *Z* = 4 (Figure 26). The Mo-N (*N*-pyridine) bond is 229.0(3) pm, and thus about 7 pm shorter than in **Mo-8** and confirms *N*-chelation to furnish a four-membered chelate ring. Also, in the case of **Mo-8** and **Mo-9**, the triflate ligand *trans* to the NHC is about 2 and 4 pm shorter than the other triflate ligand, despite the expected *trans* effect. Unexpectedly,

from the available single-crystal X-ray data, in **Mo-6** to **Mo-9** and in the previously reported, hexacoordinated chelating alkylidene bistriflate NHC complexes, the triflate ligand *trans* to the NHC is about 2 – 8 pm shorter than the second triflate ligand present in the complex. Further, as complex **Mo-6** is analogous to **Mo-8** while **Mo-7** is analogous to **Mo-9**, a vigilant observation reveals that the imido ligands in **Mo-6** (171.8°) and **Mo-7** (169.1°) are slightly more linear than **Mo-8** (167.9°) and **Mo-9** (164.1°), which suggests the π-donor abilities of the lone pair at nitrogen are better utilized in **Mo-6** and **Mo-7**. In the solid-state, both complexes, **Mo-8** and **Mo-9,** exhibit a distorted octahedral geometry with carbene(C1)-Mo-O1/O4(OTf) angles of 164.85(5)° and 165.83(10)°, respectively.

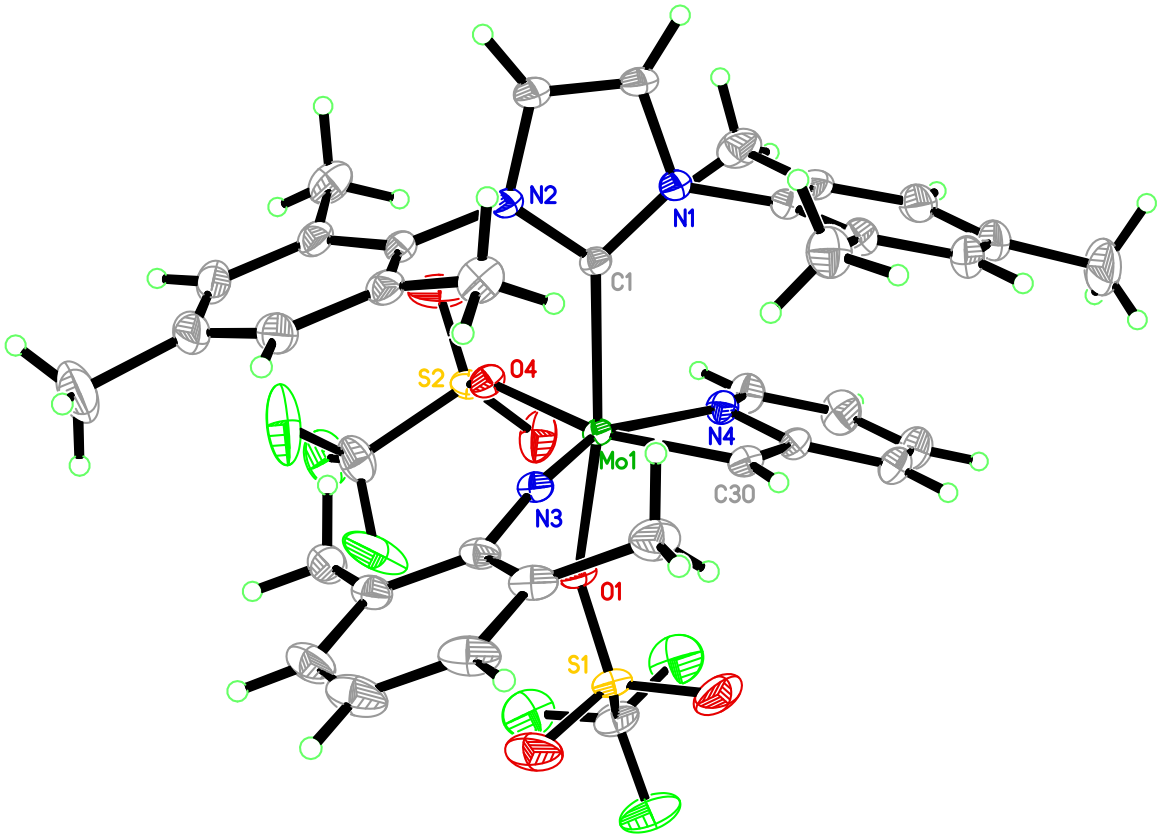

Figure 25. Single-crystal X-ray structure of complex **Mo-8**. Selected bond lengths [pm] and angles [°]. Mo-N3 172.62(14), Mo-C30 193.50(17), Mo-O1 216.56(12), Mo-O4 218.42(12), Mo-C1 222.02(15), Mo-N4 236.26(14); N3-Mo-C30 98.16(7), N3-Mo-O1 92.23(6), C30-Mo-O1 94.92(6), N3-Mo-O4 112.56(6), C30-Mo-O4 148.98(6), O1-Mo-O4 80.17(5), N3-Mo-C1 96.18(6), C30-Mo-C1 96.33(6), O1-Mo-C1 164.85(5), O4-Mo-C1 84.96(5), N3-Mo-N4 158.87(6), C30-Mo-N4 63.08(6), O1-Mo-N4 80.56(5), O4-Mo-N4 85.92(5), C1-Mo-N4 95.56(5).

The $J_{C\text{-}H}$ coupling constants obtained from the ^{1}H NMR spectrum of **Mo-8**, **Mo-9**, **Mo-10,** and **Mo-11** are 167.6 Hz, 167.3 Hz, 170.9 Hz, and 170.8 Hz respectively, this supporting the existence of an *anti* alkylidene. Although single crystal X-ray analysis

could not be accomplished for **Mo-10** and **Mo-11**, it is worth to emphasize that the *anti* alkylidene reaffirms *N*-chelation in those complexes, too.

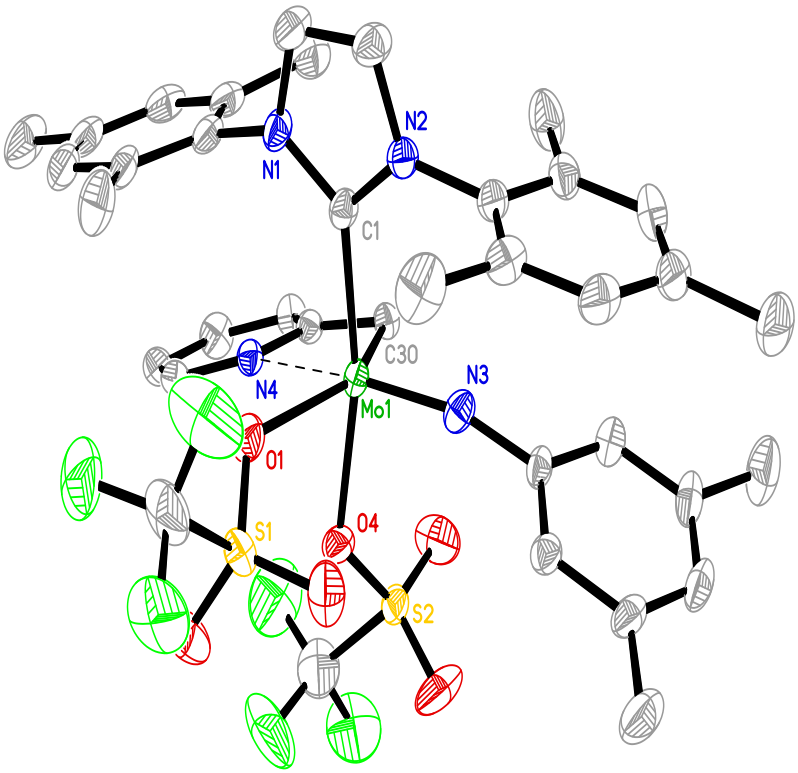

Figure 26. Single-crystal X-ray structure of complex **Mo-9**. Selected bond lengths [pm] and angles [°]. Mo-N3 172.1(3), Mo-C30 194.5(3), Mo-O1 220.4(2), Mo-O4 216.6(3), Mo-C1 220.2(3), Mo-N4 229.0(3); N3-Mo-C30 99.39(13), N3-Mo-O4 91.57(12), C30-Mo-O4 94.10(12), N3-Mo-C1 96.87(12), C30-Mo-C1 95.72(13), O4-Mo-C1 165.83(10), N3-Mo-O1 112.61(12), C30-Mo-O1 147.48(12), O4-Mo-O1 79.85(9), C1-Mo-O1 86.39(11), N3-Mo-N4 158.95(11), C30-Mo-N4 64.02(11), O4-Mo-N4 77.59(9), C1-Mo-N4 97.62(11), O1-Mo-N4 83.50(10). Hydrogen atoms and dichloromethane molecule are omitted for clarity.

Furthermore, the replacement of one of the triflate ligands with a weakly basic alkoxide ligand was expected to facilitate triflate dissociation to obtain more active catalysts without sacrificing the latent behaviour. 2-chlorophenoxide (2-chlorophenol, pK_a – 8.56) was chosen to replace the triflate ligand since the phenoxide (phenol, pK_a – 10) is more basic. As expected, the direct replacement of triflate from the chelated alkylidene complex did not work; may be because of the labile four-membered chelate. Instead, molybdenum imido neophylidene bistriflate NHC complexes were reacted with one equivalent of lithium-2-chlorophenoxide to obtain Mo(*N*-2,6-Me_2-C_6H_3)(CHCPhMe_2)(IMes)(*O*-2-Cl-C_6H_4)(OTf), **Mo-12** and Mo(*N*-3,5-Me_2-C_6H_3)(CHCPhMe_2)(IMes)(*O*-2-Cl-C_6H_4)(OTf) **Mo-13** in good isolated yields of 71 and 61 %, respectively. Subsequently, **Mo-12** and **Mo-13** were reacted with 2-

vinylpyridine to obtain the *N*-chelating alkylidene complexes, but only **Mo-12** furnished the targeted complex, **Mo-14**, while in the case of **Mo-13**, decomposition was observed (Scheme 25).

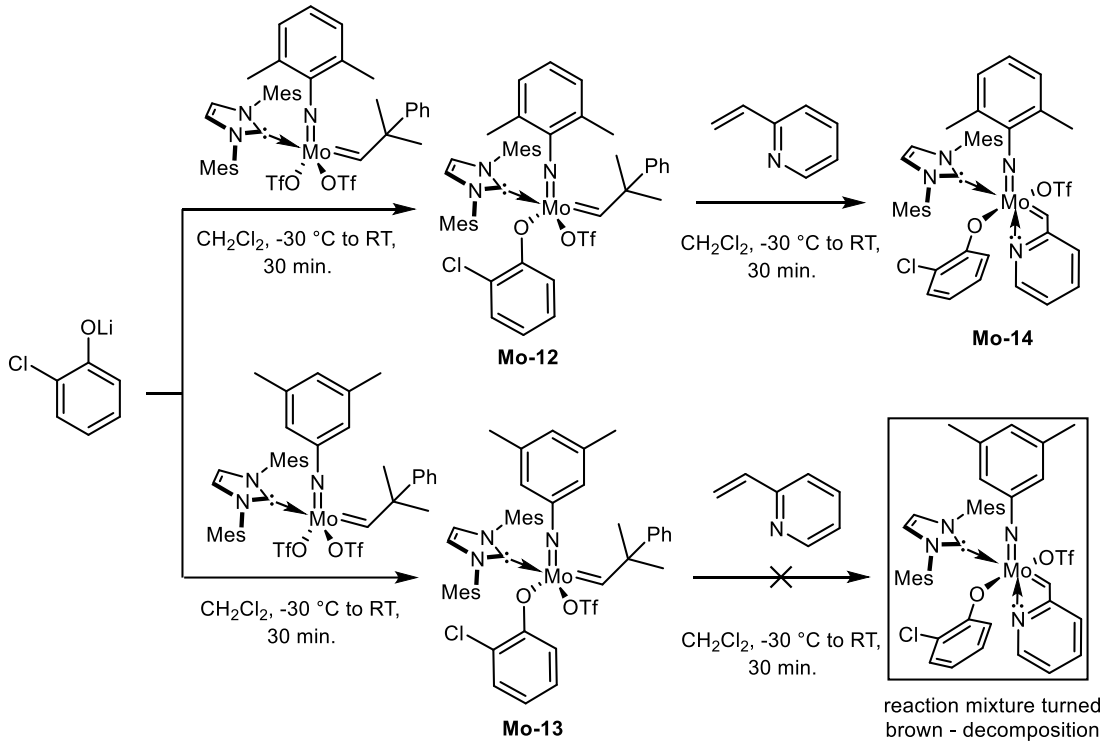

Scheme 25. Synthesis of monotriflate monoalkoxide complexes.

Crystals of **Mo-12** were grown from a mixture of dichloromethane and pentane. **Mo-12** crystallizes in the monoclinic space group *P2₁/c, a* = 1139.95(4) pm, *b* = 1914.76(9) pm, *c* = 2056.76(9) pm; *α* = *γ* = 90°, *β* = 100.502(2)°, and *Z* = 4 (Figure 27). The structure is best described as a distorted trigonal bipyramidal (TBP) geometry (τ = 0.92). The O2-Mo-C1 angle is 164.87°. The NHC and triflate ligands are *trans* to each other and occupy the axial position. The short distance of 328.6 pm, between the chlorine atom of the phenoxide and the molybdenum, within the sum of the van der Waals radii (384 pm) for molybdenum and chlorine, supports the presence of a weak interaction/coordination between them. Simultaneously, we also attempted the synthesis of monotriflate monoalkoxide analogs of **Mo-10** and **Mo-11**. However, the exchange of triflate in molybdenum imido neophylidene NHC bistriflate complexes got obstructed, due to the many alkylidene signals that appeared in reaction mixture.

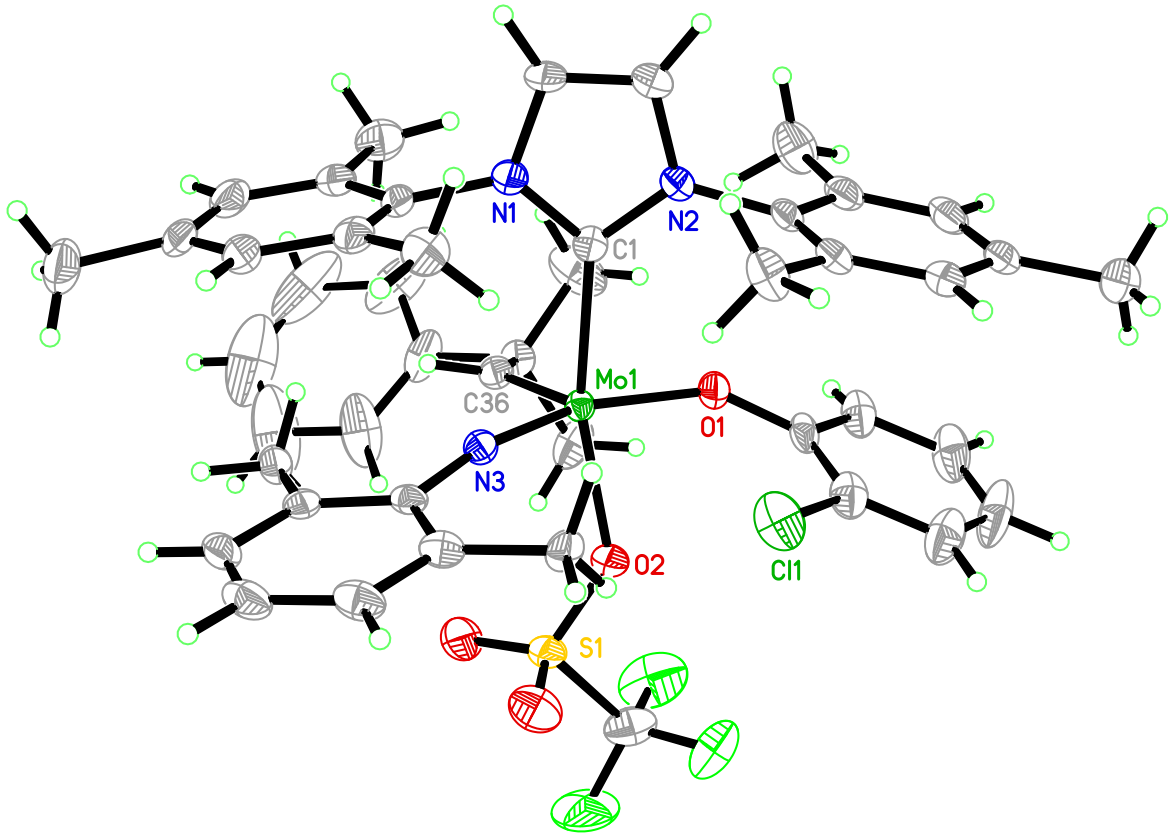

Figure 27. Single-crystal X-ray structure of complex **Mo-12**. Selected bond lengths [pm] and angles [°]. Mo-N3 176.4(2), Mo-C36 190.5(3), Mo-O1 194.65(17), Mo-O2 217.02(18), Mo-C1 222.3(3); N3-Mo-C36 97.77(10), N3-Mo-O1 158.37(9), C36-Mo-O1 102.91(9), N3-Mo-O2 91.32(9), C36-Mo-O2 97.02(9), O1-Mo-O2 80.05(7), N3-Mo-C1 94.96(9), C36-Mo1-C1 95.75(10), O1-Mo-C1 89.22(8), O2-Mo-C1 164.87(8).

Lastly, we aimed on the synthesis of an *N*-chelating alkylidene complex, an analog of the previously reported *O*-chelating alkylidene complex, to quantify the influence of *N*-chelating alkylidene over the *O*-chelating one. Molybdenum 3,5-dimethylphenylimido neophylidene IMes bistriflate was treated with two equivalents of 2-vinyl-*N*,*N*-dimethylaniline in dichloromethane to obtain Mo(*N*-3,5-Me_2-C_6H_3)(CHC_6H_4-2-NMe2)(IMes)$(OTf)_2$ **(Mo-15)** as a light orange solid, in 78% yield (Scheme 26).

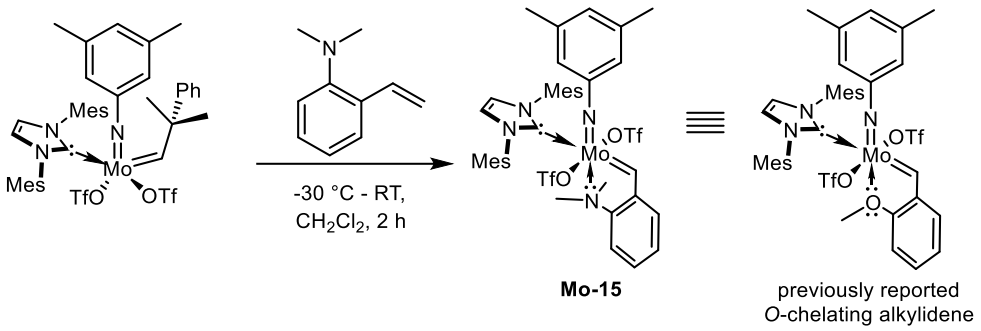

Scheme 26. Synthesis of pre-catalyst **Mo-15**.

The $J_{C\text{-}H}$ coupling constant obtained from the ^{1}H NMR spectrum of **Mo-15** is 151.0 Hz, which shows the presence of an *anti* alkylidene, also indicating that the *N*-chelation is present.

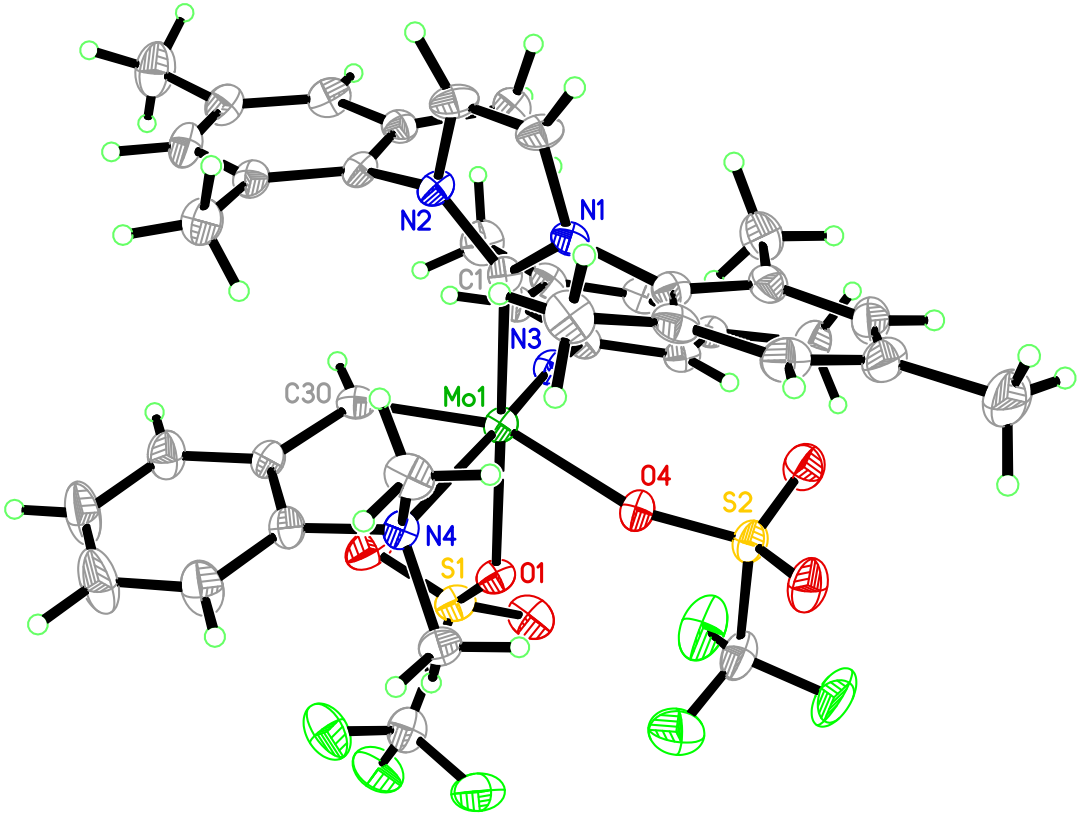

Figure 28. Single-crystal X-ray structure of complex **Mo-15**. Selected bond lengths [pm] and angles [°]. Mo-N3 172.5(2), Mo-C30 193.3(3), Mo-O1 218.5(2), Mo-O4 221.4(2), Mo-C1 223.7(3), Mo-N4 241.2(2); N3-Mo-C30 95.18(13) N3-Mo-O1 92.31(10) C30-Mo-O1 89.58(11), N3-Mo-O4 106.33(10), C30-Mo-O4 155.39(11), O1-Mo-O4 77.95(8), N3-Mo-C1 95.69(11), C30-Mo-C1 92.52(12), O1-Mo-C1 171.51(9), O4-Mo-C1 97.01(9), N3-Mo-N4 168.49(10), C30-Mo-N4 76.89(11), O1-Mo-N4 79.46(8), O4-Mo1-N4 80.00(8), C1-Mo-N4 93.00(9).

Mo-15 crystallizes in the triclinic space group *P-1, a* = 1144.40(5) pm, *b* = 1220.31(6) pm, *c* = 1763.94(8) pm; *α* = 77.638(3)°, *β* = 78.969(3)°, *γ* = 71.747(2)°, and *Z* = 2 (Figure 28). The single-crystal analysis of **Mo-15** reveals that the -*N*-Me$_2$ group is

coordinated to the molybdenum center with a Mo-N bond length of 241.2(2) pm. Weaker coordination may be attributed to the steric bulk caused by two methyl groups present on the nitrogen. In the ^{1}H NMR spectrum of **Mo-15,** two non-equivalent methyl groups on the nitrogen atom are observed (δ 2.88 and 2.78 ppm). This is in accordance with the solid state structure of **Mo-15**, which shows that one methyl group is above and one is below the equatorial plane. As observed for other complexes, the Mo-OTf bond (Mo-O1 218.5 pm) with the OTf *trans* to the NHC is about 3 pm shorter than the second Mo-OTf bond (Mo-O4 221.4 pm). Further, the reaction of 2-vinyl-*N*,*N*-dimethylaniline with molybdenum 2,6-dimethylphenylimido neophylidene IMes bistriflate did not yield any isolable compound.

3.2.3 Molybdenum η^2-Olefin NHC Complex

While purifying **Mo-14**, the second crop obtained was crystalline and thus submitted to single-crystal X-ray analysis. Surprisingly, a molybdenum olefin complex was observed (Scheme 27).

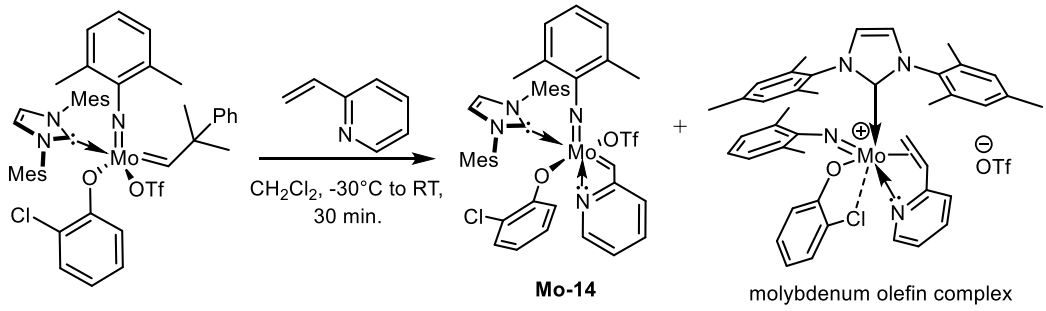

Scheme 27. Synthesis of latent catalyst **Mo-14** and a molybdenum olefin complex (**MOC**).

The molybdenum olefin complex crystallizes in the triclinic space group *P-1, a* = 1025.46(6) pm, *b* = 1951.56(15) pm, *c* = 2372.1(2) pm; *α* = 72.382(6), *β* = 79.241(6)°, *γ* = 75.826(5)°, and *Z* = 4, *R(int)* = 0.20 (Figure 29). The high R-value and standard deviation are a result of the poor crystal quality, despite the sufficiently good geometry parameters. The unexpected free triflate counter ion was severely disordered, and two independent conformers are present in the asymmetric unit cell. The Mo(1A)-N(4A) bond distance of 229.2(7) pm shows that *N*-chelation is sustained. The olefinic C(41A)-C(42A) bond distance is 140.0(11) pm, which indicates a double bond character. The Mo---Cl bond distance of 265.8(9) pm suggests a strong interaction that might facilitate dissociation of the triflate ligand due to the increased electron density at the metal. Comparable molybdenum methylidene and olefin

complexes were reported by *Schrock* and coworkers in previous reports while studying catalyst decomposition pathways.[190-194]

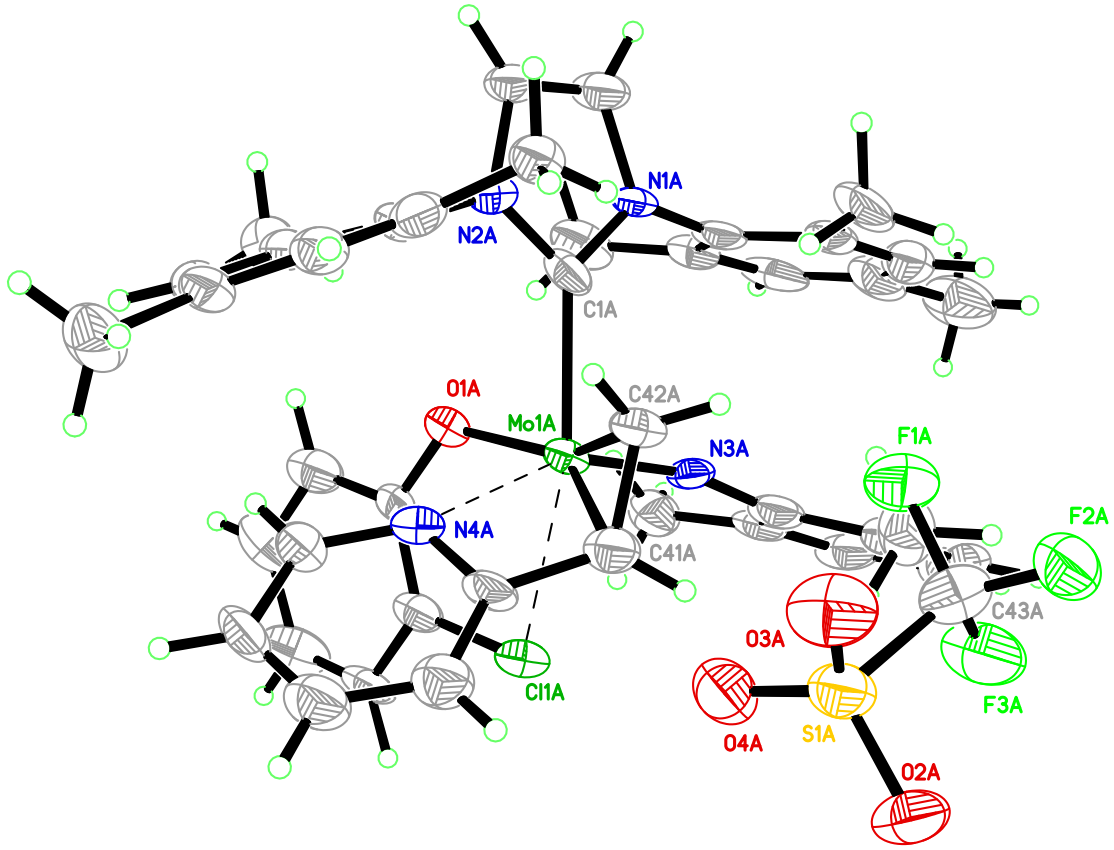

Figure 29. Single-crystal X-ray structure of the molybdenum olefin complex **(MOC)**, Relevant bond lengths [pm] and angles [°]. Mo(1A)-N(3A) 171.8(6), Mo(1A)-O(1A) 200.6(5), Mo(1A)-C(1A) 216.7(8), Mo(1A)-C(42A) 220.6(9), Mo(1A)-C(41A) 222.8(9), Mo(1A)-N(4A) 229.2(7), Mo(1A)-Cl(1A) 265.8(9), C(41A)-C(42A) 140.0(11); N(3A)-Mo(1A)-O(1A) 109.0(3), N(3A)-Mo(1A)-C(1A) 97.7(3), O(1A)-Mo(1A)-C(1A) 81.5(3), N(3A)-Mo(1A)-C(42A) 98.6(3), O(1A)-Mo(1A)-C(42A) 148.2(3), C(1A)-Mo(1A)-C(42A) 79.4(3), N(3A)-Mo(1A)-C(41A) 99.2(3), O(1A)-Mo(1A)-C(41A) 144.9(3), C(1A)-Mo(1A)-C(41A) 115.6(3), C(42A)-Mo(1A)-C(41A) 36.8(3), N(3A)-Mo(1A)-N(4A) 151.7(3), O(1A)-Mo(1A)-N(4A) 85.4(2), C(1A)-Mo(1A)-N(4A) 108.7(3), C(42A)-Mo(1A)-N(4A) 77.1(3), C(41A)-Mo(1A)-N(4A) 60.6(3), N(3A)-Mo(1A)-Cl(1A) 84.0(2), O(1A)-Mo(1A)-Cl(1A) 77.61(15), C(1A)-Mo(1A)-Cl(1A) 158.4(2), C(42A)-Mo(1A)-Cl(1A) 121.8(2), C(41A)-Mo(1A)-Cl(1A) 85.2(2), N(4A)-Mo(1A)-Cl(1A) 75.24(16).

To support this observation of an olefin complex, ^{1}H NMR of the reaction mixture was cross-checked and olefinic protons of δ = 4.67 (t, 1H), 3.21 (dd, 1H) and 3.30 (dd, 1H) ppm were observed (Figure 30). Approximately 25% molybdenum olefin complex is present, according to the peak integral ratio.

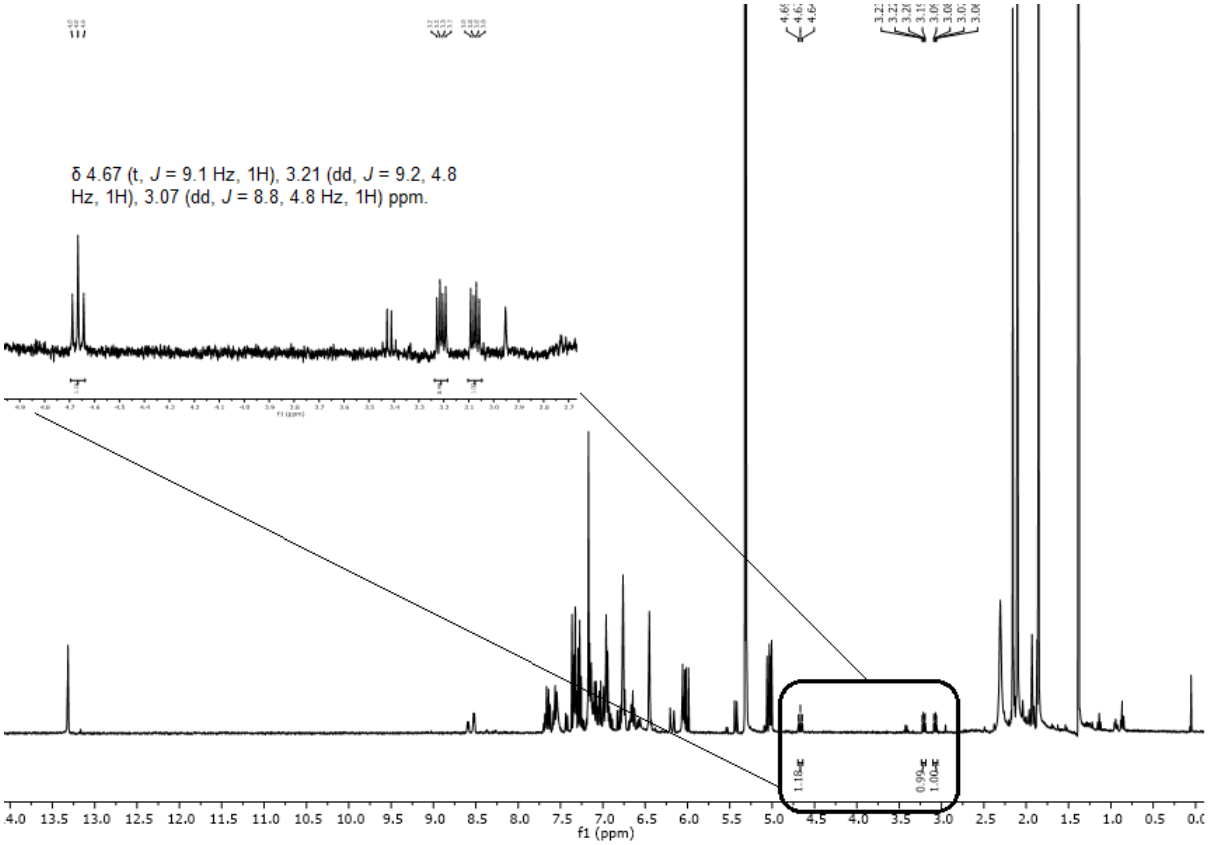

Figure 30. ^{1}H NMR spectrum of the crude reaction mixture showing the olefinic protons of the molybdenum olefin complex (**MOC**) (Scheme 8).

Indeed, similar was observed earlier, when the molybdenum 2,6-dichlorophenylimido neophylidene IMes bistriflate complex was treated with 2-vinylpyridine. There, an inseparable mixture (almost 50:50) of the molybdenum alkylidene complex and molybdenum olefin complex was obtained. Reasonably, neat and clean ^{1}H and ^{19}F NMR spectra (Figure 31 and 32) indicate a mixture of both complexes.

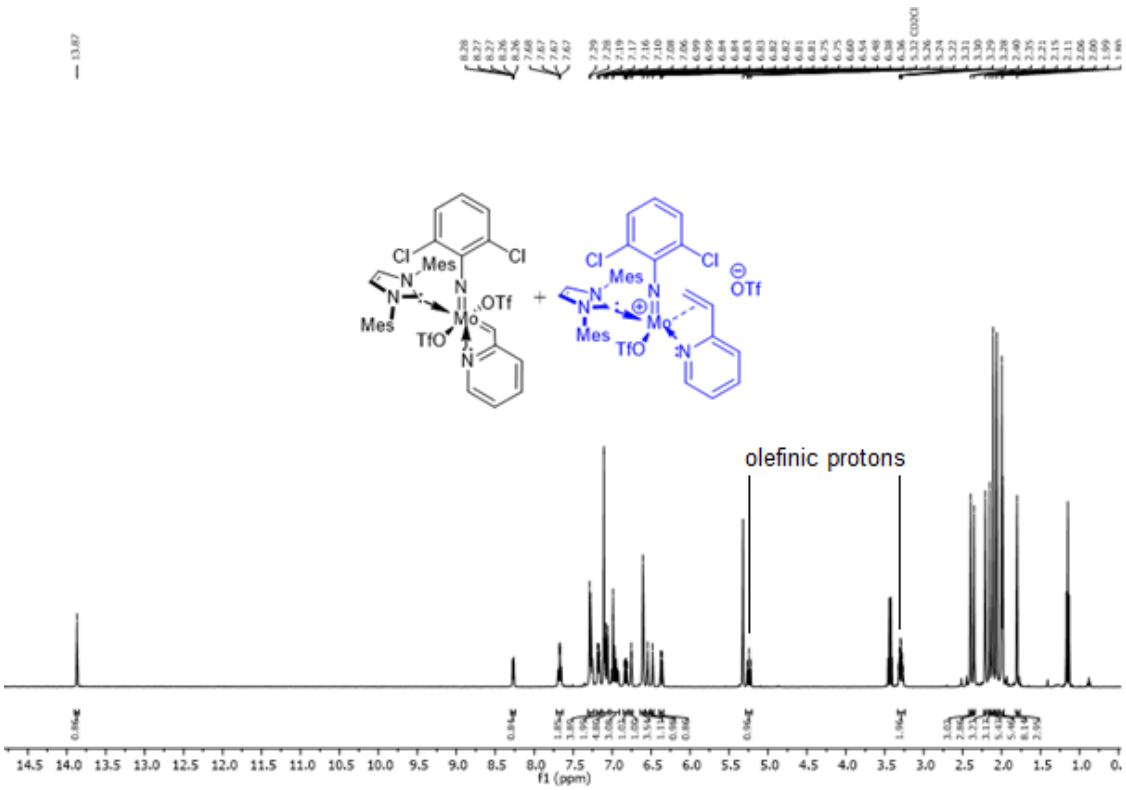

Figure 31. ^{1}H NMR spectrum of the reaction mixture showing a mixture of the alkylidene complex and olefin complex.

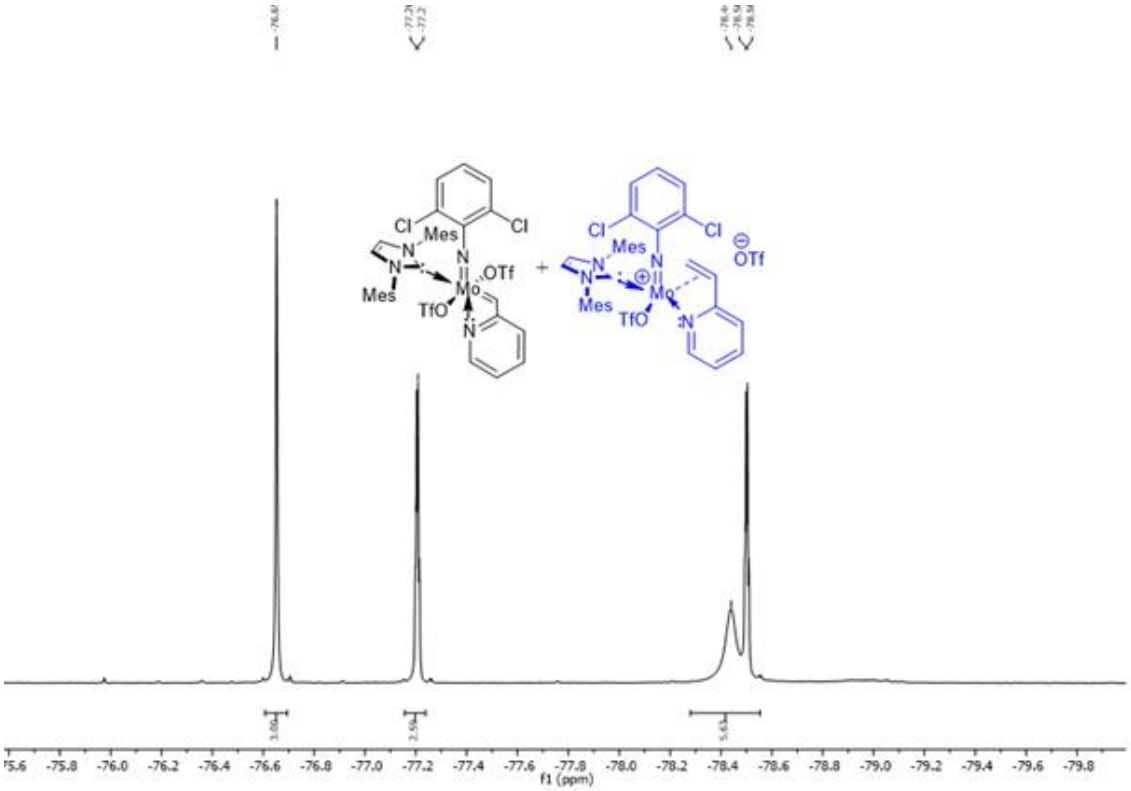

Figure 32. ^{19}F NMR spectrum of the reaction mixture showing a mixture of the alkylidene complex and olefin complex.

3.2.4 Latent Behavior in the Polymerization of Dicyclopentadiene (DCPD)

The activity of the novel molybdenum imido alkylidene NHC complexes in the ROMP of DCPD was evaluated by differential scanning calorimetry (DSC). To comply with the task-specific olefin metathesis catalyst, the onset of polymerization (T_{onset}) is the tool to define a pre-catalyst's latency. T_{onset} is the temperature at which the exotherm of polymerization starts. As a lower onset of polymerization will avoid the potential overheating of the entire polymerization system, one aims at candidates that can furnish an onset temperature between 70 and 80 °C without compromising latency behavior. Pre-catalysts **Mo-6** – **Mo-11** and **Mo-14** – **Mo-15** displayed latency for several hours upon mixing with DCPD at room temperature. However, **Mo-6** and **Mo-7** were found to be inactive owing to the stronger Mo-O(vinylpyrrolidone) bond (221.4 pm, **Mo-6**, and 221.3 pm, **Mo-7**) compared to previously reported *O*-chelating pre-catalyst (Mo-O(chelate), 235.2 pm), which leads to the stable chelate. The DSC thermograms of **Mo-6** and **Mo-7** showed no exothermal curing peak. Instead, an endothermic peak at about 200 °C was observed (Figure 39 and 40, Experimental Section), which can be attributed to the cracking of DCPD.

Further, the pre-catalysts bearing an *N*-chelating alkylidene, **Mo-8** - **Mo-11,** were evaluated for DCPD polymerization and found to be active with acceptable latency. As reported earlier,[185] the effect of a sterically demanding 2,6-dimethylphenylimido ligand **(Mo-8)** compared to 3,5-dimethylphenylimido ligand **(Mo-9)** on T_{onset} can be seen. The lower T_{onset} of **Mo-9** (100 °C) compared to the one of **Mo-8** (140 °C) shows that the 3,5-dimethylphenylimido ligand facilitates the incoming substrate to the metal centre. Subsequently, at identical catalyst loading, one can compare the exothermic reaction enthalpies for **Mo-8** and **Mo-9** obtained from DSC measurements; almost doubled enthalpy was observed for **Mo-9** (Table 4). In the case of **Mo-8**, both endothermic and exothermic peaks were observed (Figure 33), which suggests higher catalyst loading is needed. Pre-catalysts bearing imido ligands substituted with an electron-withdrawing group such as the difluorophenylimido and (trifluoromethyl)phenylimido moiety, **Mo-10** and **Mo-11,** showed a higher T_{onset} (124 °C and 130 °C) and T_{max} (164 °C and 167 °C) than **Mo-9** (T_{onset} 100 °C and T_{max} 158 °C). Furthermore, the other *N*-chelating alkylidene bistriflate pre-catalyst **Mo-15** displayed two exotherms in the DSC thermogram (Figure 42, Experimental Section). The first T_{max} was observed at 140 °C and the second at 216 °C. Out of curiosity, one

sample was cured up to 190 °C and another sample up to 250 °C. The latter one was found to be a charred hard crispy black solid, while the former one was an opaque polymer film. In view of that the second exothermic peak is tentatively assigned to a crosslinking reaction.

Table 4. $T_{exo,max}$, T_{onset}, T_g and reaction enthalpies for pre-catalysts **Mo-8 – Mo-11** and **Mo-14**.

Pre-catalyst	T_{exo} (°C)	T_{onset} (°C)[i]	ΔH (J·g^{-1})[ii]	T_g (°C)[iii]
Mo-8	174	140	-70	124
Mo-9	158	100	-145	133
Mo-10	164	124	-98	152
Mo-11	167	130	-93	141
Mo-14	128	76	-187	149

Pre-catalyst/CH_2Cl_2/DCPD, CH_2Cl_2 – 10 µL, cat. loading – 660 ppm (mol.), Heating program: 0 °C for one minute, 0 °C → 250 °C (10 K·min^{-1}) (i) temperature at which the heat flow begins to drop.; (ii) derived from integration of the area under the curve by Pyris Manager (Perkin Elmer). (iii) midpoint temperature.

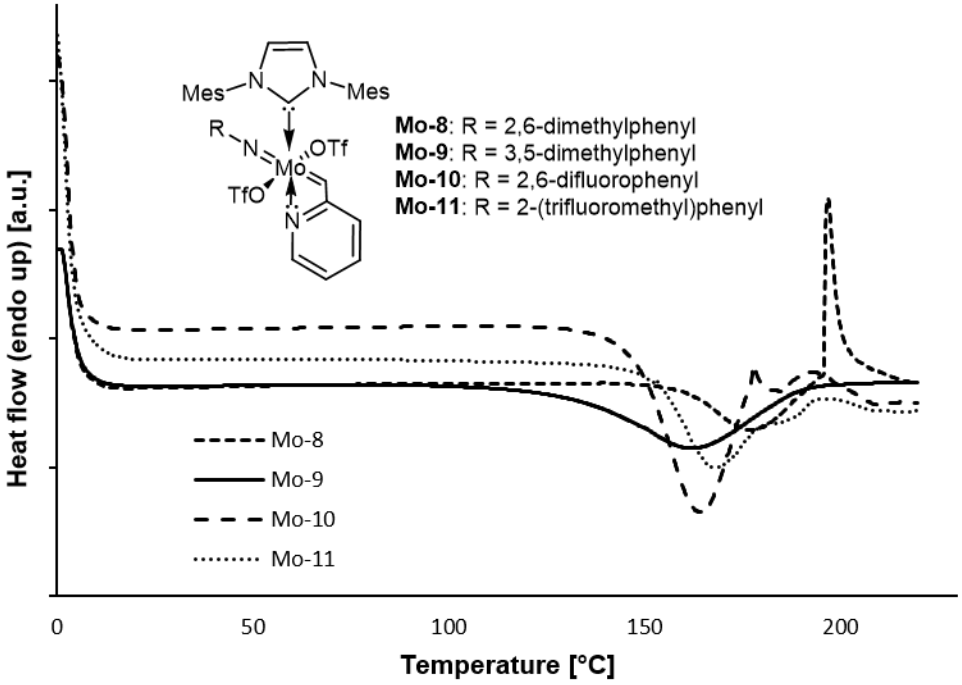

Figure 33. Temperature scan DSC thermograms of chelated hexacoordinated pre-catalysts **Mo-8** – **Mo-11** bearing different imido ligands. Pre-catalyst/CH_2Cl_2/DCPD, CH_2Cl_2 – 10 µL, cat. loading – 660 ppm (mol.), Heating program: 0 °C for one minute, 0 °C → 220 °C (10 K·min^{-1}).

It has been shown that triflate release activates the neutral molybdenum imido alkylidene NHC complexes containing at least one triflate.[103, 195, 196] The second anionic ligand's nature is the driving force for the pre-catalyst to form an olefin metathesis active species. The chlorophenoxy ligand in **Mo-14** exhibited a strong influence on both T_{onset} and T_{max} compared to its bistriflate analog, **Mo-8** (Figure 34), as anticipated. The T_{onset} for **Mo-14** is almost 70 °C lower (76 °C) in comparison to **Mo-8** (140 °C) and the reaction enthalpy found was almost twice as high (-187 $J \cdot g^{-1}$, **Mo-14,** and -70 $J \cdot g^{-1}$, **Mo-8**) at identical catalyst loading. This finding unambiguously demonstrates the influence of a second anionic ligand on the T_{onset} and T_{max} without sacrificing the latency behavior. The high activity of **Mo-14** might be attributed to the cationic character at molybdenum due to the possible free triflate as counter ion. Since the triflate was observed at δ = -78.9 ppm in the ^{19}F NMR spectrum and in the single crystal X-ray structure of the analogous olefin complex (Figure 29), a free triflate counter ion is proposed. The reaction mixture was found thermally latent for a minimum of 12 hours at room temperature. The catalyst loading of 660 ppm (mol.) resulted in a decent reaction enthalpy of -187 $J \cdot g^{-1}$, while at 300 ppm (mol.), it also showed an acceptable reaction enthalpy (164 $J \cdot g^{-1}$) (Table 7 and Figure 41, Experimental Section).

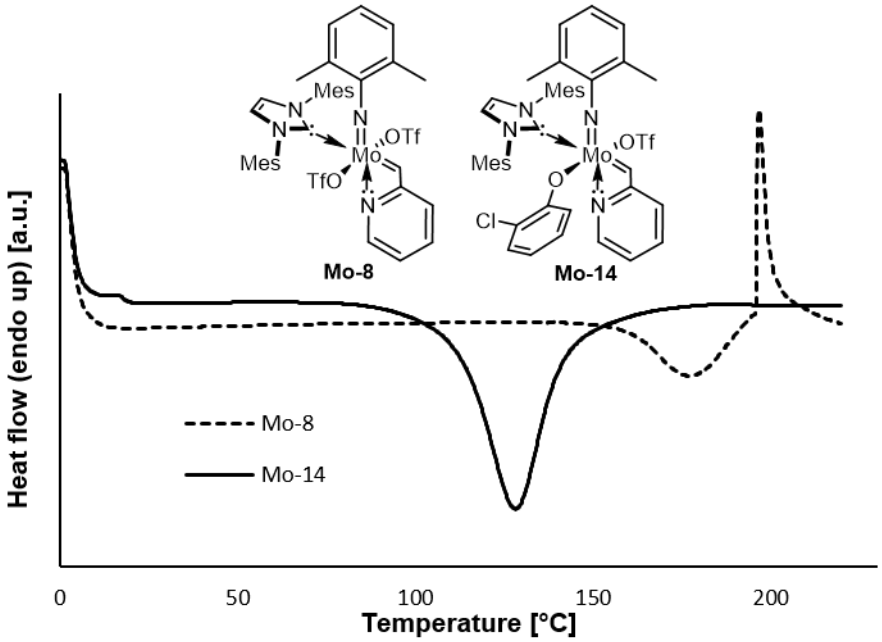

Figure 34. Temperature scan DSC thermograms of chelated hexacoordinated bistriflate pre-catalysts **Mo-8** compared to the chelated hexacoordinated monotriflate monoalkoxide pre-catalyst **Mo-14.** Pre-catalyst/CH_2Cl_2/DCPD, CH_2Cl_2 – 10 µL, cat. loading – 660 ppm (mol.), Heating program: 0 °C for one minute, 0 °C → 220 °C (10 $K \cdot min^{-1}$).

Mo-9 and **Mo-15** showed higher monomer conversion of 94 and 98 %, respectively, while pre-catalysts **Mo-8**, **Mo-10**, **Mo-11** and **Mo-14** showed 60 – 70 % monomer conversion (Table 6, Experimental Section). Here, the pre-catalysts bearing a sterically less bulky 3,5-dimethylphenylimido ligand i.e. **Mo-9** and **Mo-15,** showed the highest monomer conversion. The swelling studies performed in toluene for the poly(DCPD) derived from all the pre-catalysts showed 5 – 75% swelling (Table 6, experimental section). Pre-catalysts **Mo-9** and **Mo-15,** which showed almost complete monomer conversion displayed 15 and 25% swelling. However, pre-catalysts **Mo-10** and **Mo-11** with moderate monomer conversion (60%) revealed only 5 and 15% swelling. The high degree of crosslinking can be explained by the high curing temperature (120 °C).

Noticeably, only pre-catalyst **Mo-8** was air-stable (up to 12 h), according to the ^{1}H NMR spectrum recorded in dry deuterated solvent after storage in air (Figure 121, Appendix). While in the case of its monoalkoxide monotriflate analog, **Mo-14**, exposed to the air under the same condition, showed 50% decomposition (Figure 125, Appendix). The signal at about δ = 9.0 ppm in most of the ^{1}H NMR spectra indicates the catalyst's decomposition through NHC salt formation (Figure 122 – 126, Appendix).

3.3 Conclusions

Molybdenum imido alkylidene NHC complexes with a four-membered chelate ring derived from 2-vinylpyridine were successfully synthesized and structurally characterized by single-crystal X-ray studies. Variations in the alkoxide ligand's electronic properties in molybdenum imido alkylidene NHC monoalkoxide monotriflate complexes finally yielded a thermally latent catalyst with T_{onset} 76 °C and $T_{exo,max}$ 128 °C, which is the excellent candidate for the ROMP of DCPD. The 3,5-dimethylphenylimido ligand is a promising imido ligand, as it offers a low onset temperature, high monomer conversion and highly cross-linked polymer. Notably, the hexacoordinated molybdenum imido alkylidene monotriflate monalkoxide complex (**Mo-14**) showed fairly good solubility in DCPD as compared to other hexacoordinated complexes. This helps in the proper mixing of the catalyst in the monomer.

Chapter 4

2,6-Difluorophenylimido Molybdenum Alkylidene NHC Complexes: Air Stable, Functional Group Tolerant Catalysts

The content of this chapter partially appeared in the following publication:

Schowner, R.; Elser, I.; Benedikter, M. J.; Momin, M.; Frey, W.; Stöhr, L.; Schneck, T.; Buchmeiser, M. R., Origin and Use of Hydroxyl Group Tolerance in Cationic Molybdenum Imido Alkylidene *N*-Heterocyclic Carbene Catalysts. *Angew. Chem. Int. Ed.* **2020**, *59*, 951-958.

4.1 Introduction

In general, ruthenium-based olefin metathesis catalysts are more tolerant towards moisture and many protic functional groups than *Schrock* catalysts; however, they show low activity, selectivity, and productivity. On the other hand, molybdenum-based catalysts have proved to be more selective, active, and productive, although they are sensitive to moisture and protic functional groups.[91, 197]

Recently, *Buchmeiser* and coworkers found that cationic catalysts bearing weakly basic aromatic imido ligands, weakly basic anionic ligands, and the sterically demanding 1,3-dimesitylimidazol-2-ylidene NHC ligand are reactive and robust in the olefin metathesis of substrates containing hydroxyl functionalities.[198] A wide range of complexes with weakly basic aromatic imido ligands such as the 2,6-dichlorophenylimido or the 2-trifluoromethylphenylimido ligand has been prepared and used in hydroxyl group-tolerant olefin metathesis. Certainly, the imido ligands are not only spectator ligands, since both from a steric and electronic perspective, but also play a vital role in the reactivity and selectivity at the metal center.[70, 199] In course of these investigations, the previously not reported 2,6-difluorophenylimido complexes were investigated and the first 2,6-difluorophenylimido molybdenum alkylidene complexes have been prepared.

4.2 Results and Discussion

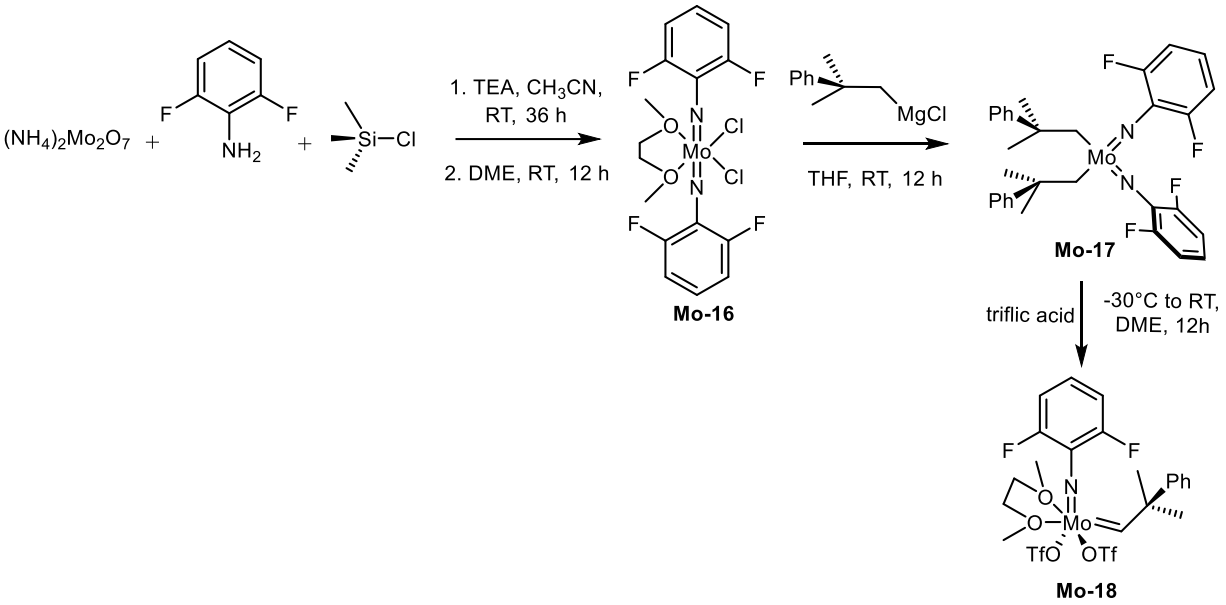

Scheme 28. Synthesis of the universal bistriflate precursor complex **Mo-18**.

In 1993, *Schrock* et al. reported on ligand variations in molybdenum alkylidene complexes with several new imido ligands.[70] Among the reported complexes, the synthesis of a complex bearing the weakly basic imido ligand i.e. the 4-cyano-2,6-diisopropylphenylimido ligand was accomplished by using acetonitrile as the solvent, and the desired DME adduct was prepared by dissolving the crude product in DME and removing salts by filtration. Therefore, similar approach for the weakly basic 2,6-difluorophenylimido ligand by varying the working up procedure was applied. Due to the poor solubility of the 2,6-difluorophenylimido complex (**Mo-16**) in DME, the solids were extracted by soxhlet extraction in DME to yield the first 2,6-difluorophenylimido molybdenum complex, Mo(N-2,6-F_2-C_6H_3)$_2$$Cl_2$(DME), **Mo-16** in moderate yield (47 %). Further, the synthesis of the universal bistriflate precursor, Mo(N-2,6-F_2-C_6H_3)(CHCMe_2Ph)(OTf)$_2$(DME) **Mo-18** involved the dialkylation of **Mo-16** to give Mo(N-2,6-F_2-C_6H_3)$_2$(CH_2CMe_2Ph)$_2$ **Mo-17**, followed by treatment of **Mo-17** with three equivalents of triflic acid in DME (Scheme 28). **Mo-17** was obtained as a bright orange solid in excellent yield, 92%, and **Mo-18** was obtained as a yellow solid in a moderate yield of 64%. Crystals of **Mo-18** were grown from a mixture of CH_2Cl_2/diethyl ether/*n*-pentane. **Mo-18** crystallized in orthorhombic space group *Pbca* with *a* = 1335.48(4) pm, *b* = 1649.16(5) pm, *c* = 2625.01(8) pm, $\alpha = \beta = \gamma = 90°$ and *Z* = 2 (Figure 35). The N1-Mo1-O3 bond angle of 169.95° describes that **Mo-18** exhibits a distorted octahedral geometry. The Mo-N1-C5 bond angle is 174.54° and the Mo-OTf bond in the triflate *trans* to the imido was found to be 10 pm longer than the other triflate bond (Mo-O3 218.3 pm > Mo-O6 208.5 pm).

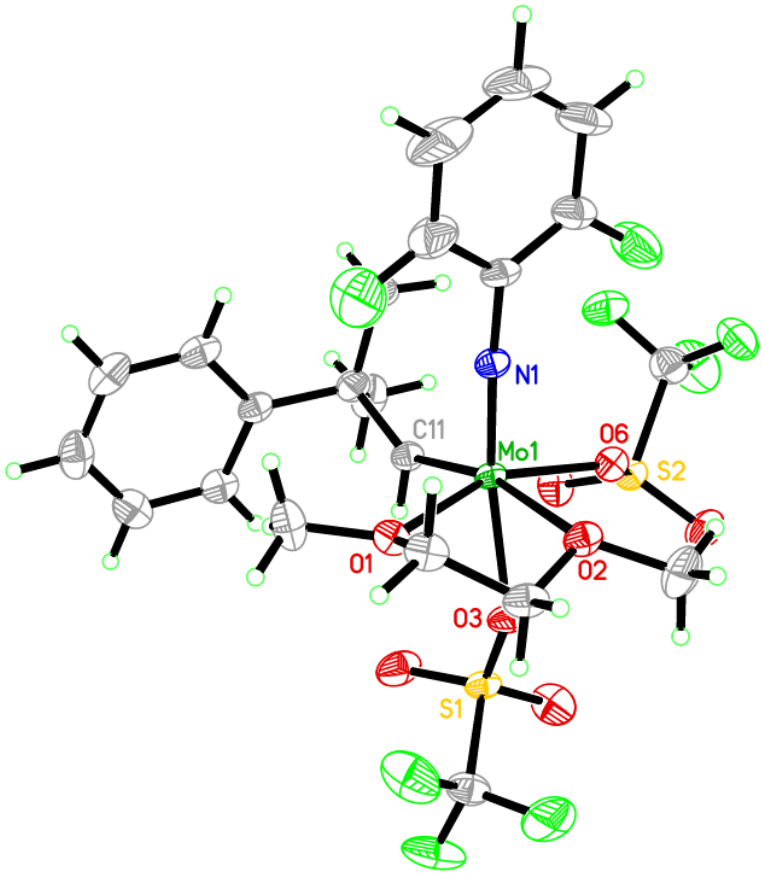

Figure 35. Single crystal X-ray structure of [Mo(N-2,6-F_2-C_6H_3)(CHCMe$_2$Ph)(DME)(OTf)$_2$], **Mo-18**. Relevant bond lengths [pm] and angles [°]. Mo–N1 172.5, Mo–C11 190.8, Mo–O6 208.5, Mo– O1 212.6, Mo–O3 218.3, Mo-O2 231.6; N1-Mo1-C11 98.67, N1-Mo1-O6 95.95, C11-Mo1-O6 99.35, N1-Mo1-O1 98.07, C11-Mo1-O1 96.84, O6-Mo1-O1 156.68, N1-Mo1-O3 169.95, C11-Mo1-O3, 91.29, O6-Mo1-O3 81.05, O1-Mo1-O3 81.93, N1-Mo1-O2 93.11, C11-Mo1-O2 165.97, O6-Mo1-O2 86.90, O1-Mo1-O2 73.85, O3-Mo1-O2 77.20.

Often, bistriflate precursor complexes exist in form of two isomers in solution. According to the spectroscopic data (^{1}H, ^{13}C and ^{19}F NMR) obtained for complex **Mo-18** in solution, a major (δ 14.74 ppm, alkylidene ^{1}H, 67%) and a minor (δ 13.89 ppm, alkylidene ^{1}H, 33%) isomer was observed. Spectroscopic data corresponding to the major isomer describe that the methylene groups in the DME ligand are inequivalent and so are the triflate ligands and the neophylidene methyl groups. In view of these findings the major isomer's structure is depicted in Figure 36 (a). The obtained crystal structure unambiguously supports the illustrated structure. The minor isomer, as described in Figure 36 (b), has a symmetry plane. Hence, NMR spectra do not show any inequivalent signals for the triflate, the neophylidene methyl groups, etc., for the minor isomer. The magnitude of the J_{CH} coupling confirms that both isomers exist in form of the *syn*-alkylidene rotamer (major isomer J_{CH} = 127.5 Hz and minor isomer J_{CH} = 121.2 Hz).

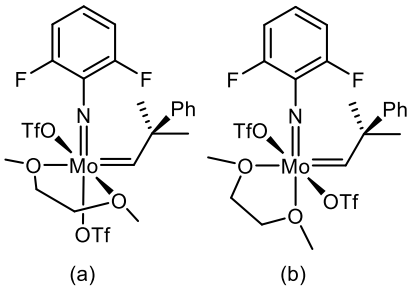

Figure 36. (a) Major isomer of complex **Mo-18**, (b) minor isomer of complex **Mo-18**.

The molybdenum 2,6-difluorophenylimido bistriflate precursor was treated with different NHC ligands such as 1,3-dimesitylimidazol-2-ylidene (IMes), 1,3-dimesitylimidazolin-2ylidene ($IMesH_2$), 1,3-dimesityl-4,5-dichloroimidazol-2-ylidene ($IMesCl_2$), 1,3-diisopropylimidazol-2-ylidene, and the silver(I) salts of 1,3-dimethylimidazol-2-ylidene and 1,3-dimethyl-4,5-dichloroimidazol-2-ylidene etc. The successful synthesis of complexes bearing an NHC ligand was realized with the bulkier NHCs *viz.* IMes, $IMesH_2$, and $IMesCl_2$, while with smaller NHC ligands, syntheses failed (Scheme 29). Instead either abstraction of the alkylidene proton by the NHC and formation of the NHC salt or many alkylidene signals were observed.

Complex **Mo-19** was obtained as a yellow solid in 67% yield; it crystallizes in a mixture of CH_2Cl_2/diethyl ether/*n*-pentane**. Mo-19** crystallizes in the monoclinic space group $P2_1/n$ with a = 1033.21(7) pm, b = 1794.29(12) pm, c = 2181.41(14) pm, $\alpha = \gamma$ = 90°, β = 91.499(3)° and Z = 4 (Figure 36). and exhibits a distorted square pyramidal geometry (τ_5 = 0.37) with the alkylidene at the apex. The Mo-OTf bond with the triflate *trans* to the NHC is 4 pm longer than the other Mo-OTf bond (Mo-O1 214.00 pm > Mo-O4 210.65 pm), experiencing the *trans* influence of the NHC. Similarly, complexes **Mo-20** and **Mo-21** bearing the $IMesH_2$ and $IMesCl_2$, respectively, were obtained in moderate yields of 60% and 67%, respectively. Crystals for structure analysis were obtained for **Mo-21**.

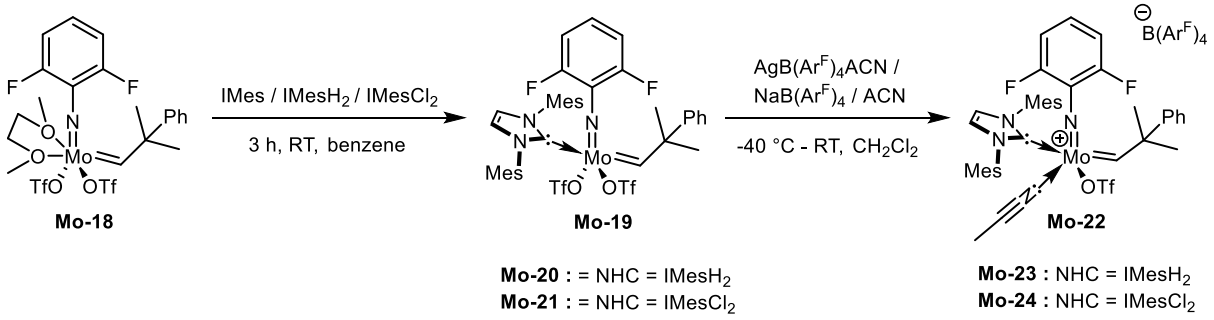

Scheme 29. Anchoring of an NHC followed by the synthesis of cationic complexes.

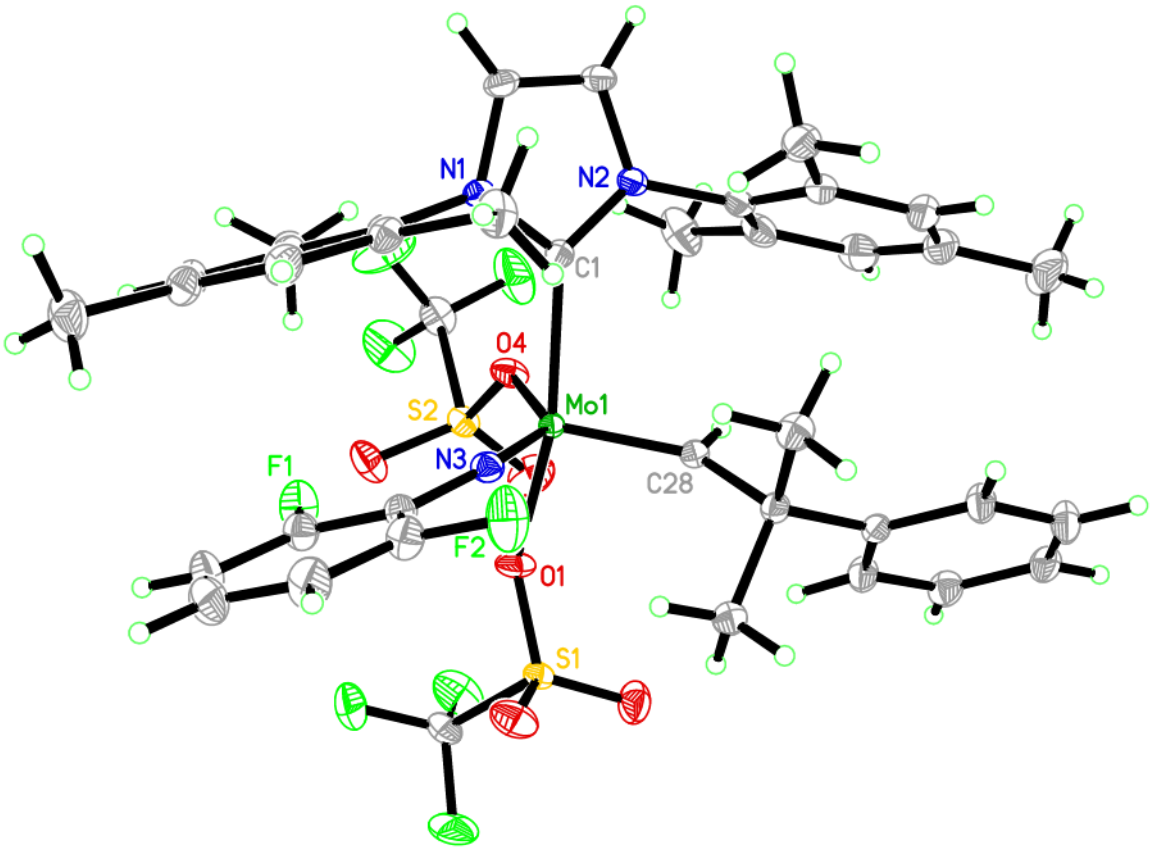

Figure 36. Single crystal X-ray structure of [Mo(N-2,6-F_2-C_6H_3)(CHCMe_2Ph)(IMes)$(OTf)_2$], **Mo-19**. Relevant bond lengths [pm] and angles [°]. Mo–N3 172.3, Mo–C28 187.4, Mo–O4 210.7, Mo– O1 214.0, Mo–C1 220.0; N3-Mo1-C28 102.69, N3-Mo1-O4 137.32, C28-Mo1-O4 119.73, N3-Mo1-O1 92.735, C28-Mo1-O1 98.19, O4-Mo1-O1 77.66, N3-Mo1-C1 98.12, C28-Mo1-C1 96.01, O4-Mo1-C1 82.81, O1-Mo1-C1 159.78.

Complex **Mo-21** crystallizes in the monoclinic space group $P2_1/c$ with a = 1210.04(4) pm, b = 1756.29(7) pm, c = 2188.33(8) pm, $\alpha = \gamma = 90°$, β = 98.083(2)° and Z = 4 (Figure 37). Complex **Mo-21** exhibits a distorted square pyramidal geometry (τ_5 = 0.37) with the alkylidene at the apex. One molecule of dichloromethane was co-crystallized. Surprisingly, both the Mo-OTf bonds are almost the same (Mo-O1 211.3 pm and Mo-O4 211.9 pm).

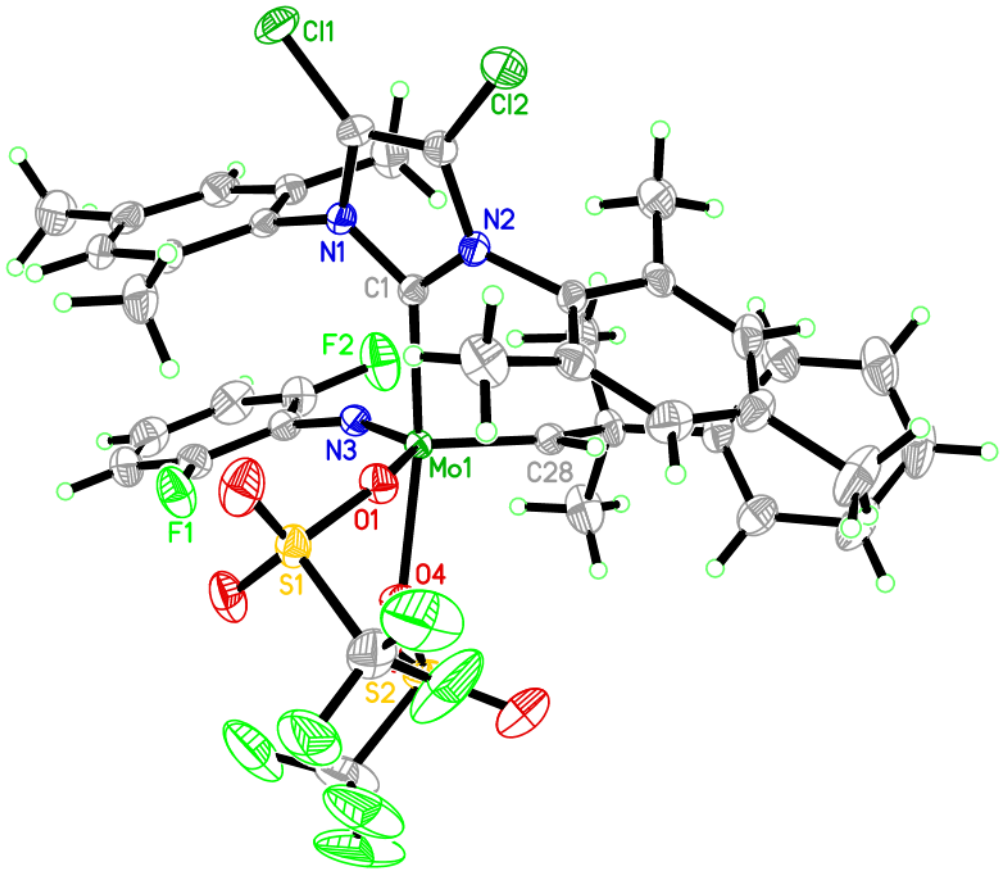

Figure 37. Single crystal X-ray structure of [Mo(N-2,6-F_2-C_6H_3)(CHCMe_2Ph)(IMesCl_2)$(OTf)_2$], **Mo-21**. Relevant bond lengths [pm] and angles [°]. Mo–N3 171.8, Mo–C28 188.4, Mo–O1 211.3, Mo– O4 211.9, Mo–C1 221.2; N3-Mo1-C28 102.69, N3-Mo1-O1 135.19, C28-Mo1-O1 122.05, N3-Mo1-O4 95.48, C28-Mo1-O4 97.38, O1-Mo1-O4 77.59, N3-Mo1-C1 98.29, C28-Mo1-C1 96.93, O1-Mo1-C1 80.04, O4-Mo1-C1 157.43.

Furthermore, the ultimate aim of achieving a cationic complex was accomplished by the reaction of the molybdenum imido alkylidene NHC bistriflate complexes **Mo-19** – **Mo-21** with AgB(Ar^F)$_4$3CH_3CN or NaB(Ar^F)$_4$ to yield the cationic complexes **Mo-22** - **Mo-24** (Scheme 11). The structure of **Mo-22** was unambiguously proven by single-crystal X-ray analysis. **Mo-22** crystallizes in the triclinic space group *P*-1 with *a* = 1279.17(5) pm, *b* = 1815.54(7) pm, *c* = 1860.54(8) pm, α = 64.059(2)°, β = 70.333(2)°, γ = 73.654(2)° (Z=2) (Figure 38). The molybdenum center has a slightly distorted square-pyramidal coordination sphere (τ_5 = 0.14) with the alkylidene in the apex (Figure 38). Coordination of acetonitrile is observed *trans* to the NHC, as it has been seen in general with other cationic monoalkoxide complexes.[200]

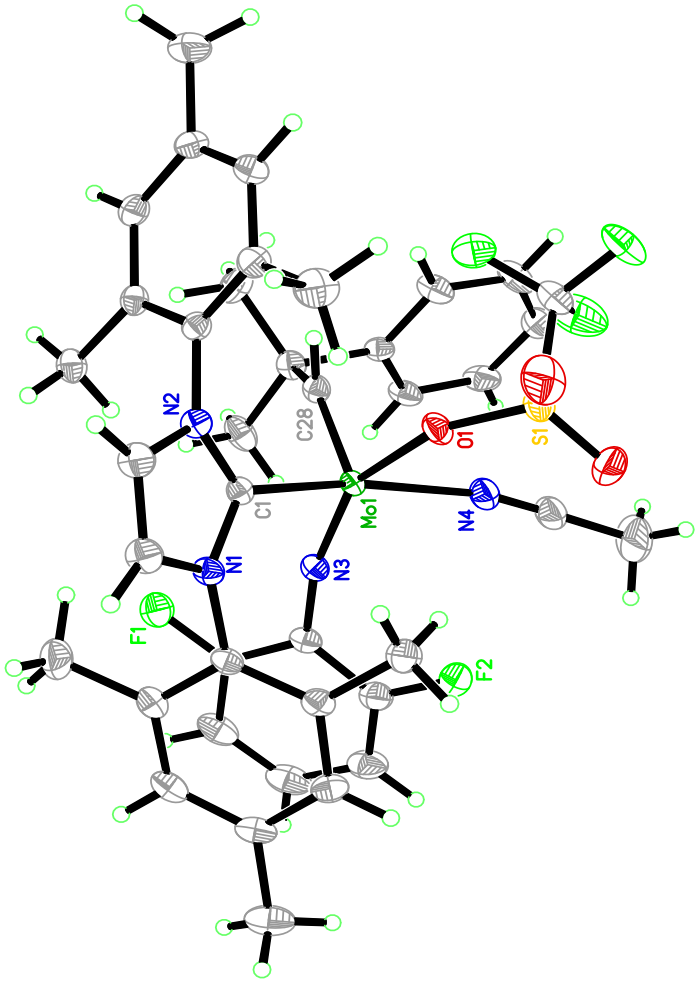

Figure 38. Single crystal X-ray structure of [Mo(N-2,6-F_2-C_6H_3)-(CHCMe_2Ph)(IMes)(OTf)(MeCN)][B(Ar^F)$_4$], **Mo-22**. Relevant bond lengths [pm] and angles [°]. Mo–N3 173.1, Mo–C28 187.1, Mo–O1 208.9, Mo– N4 217.2, Mo–C1 218.3; N3-Mo-C28 102.03, N3-Mo-O1 151.93, C28- Mo-O1 105.03, N3-Mo-C1 97.06, C28-Mo-C1 102.72, N4-Mo-C1 160.29, N3-Mo-O1 151.93, C28-Mo-O1 105.03, N4-Mo-O1 81.88, C1-Mo-O1 84.21, C22-N3-Mo 166.38, C29-C28-Mo 143.56. The anion has been omitted for clarity.

Mo-22 was subjected to benchmark olefin metathesis reactions such as homo-metathesis (HM) and ring-closing metathesis (RCM) of substrates bearing alcohol groups. Turnover numbers (TON) for different substrates are tabulated in Table 5. Comparable results with other analogous complexes were obtained.[198]

Further, we tested the air stability of cationic complexes **Mo-22** – **Mo-24** for a minimum of 12 hours. The ^{1}H NMR spectra remained virtually unchanged after 12 hours (Figures 154 – 156, Appendix).

Table 5. Turnover numbers (TON) for the HM and RCM of hydroxyl-substituted substrates with the cationic NHC-type catalyst **Mo-22**.

Cross partners	TON	
	2 h	**4 h**
4-penten-1-ol	4000	NA
5-hexen-1-ol	1900	2260
7-octen-1-ol	0	0
2-allylphenol	2500	2900
1-octene	2240	1800
1,7-octadiene	4000	NA

Reaction conditions. Catalyst: substrate = 1:4000, room temperature, CH_2Cl_2 (3M wrt. substrate), TON by GC-MS, internal standard: *n*-dodecane, NA = not applicable.

4.3 Conclusions

The previously not reported 2,6-difluorophenylimido molybdenum alkylidene NHC complexes have been accomplished and their activity in the olefin metathesis of hydroxyl-substituted substrates have been demonstrated. Cationic complexes were found to be air stable for at least 12 h.

Chapter 5

Experimental

5.1 General Information

All reactions were carried out in a N_2-filled glovebox (MBraun Labmaster 130) or under the exclusion of air and moisture by standard Schlenk techniques unless stated otherwise. Glassware was stored at 120°C at least for an hour and cooled in an evacuated antechamber.

5.2 Solvents and Chemicals

Starting materials and all reagents were purchased from Sigma-Aldrich, Alfa Aesar, TCI and abcr. All substrates were stirred over CaH_2 for several hours, distilled, degassed by several freeze-pump-thaw cycles and finally stored over 4 Å Linde type molecular sieves. Prior to use, these substrates were passed through activated neutral alumina. Dichloromethane, THF, diethyl ether, toluene, and *n*-pentane were dried using an MBraun SPS-800 solvent purification system with alumina drying columns stored over 4 Å Linde type molecular sieves (THF, toluene, CH_2Cl_2). Deuterated solvents were filtered over activated alumina and stored over 4 Å Linde type molecular sieves inside the glove box.

5.3 Equipment and Analytics

NMR: NMR spectra were recorded on a Bruker Avance III 400 at 400 MHz for ^{1}H, 376 MHz for ^{19}F and 101 MHz for ^{13}C. Chemical shifts are reported in ppm from the residual solvent protons (CD_2Cl_2 5.32 and 53.5 ppm, $CDCl_3$ 7.26 and 77.16 ppm, respectively) as a reference; coupling constants are reported in Hz. ^{1}H spectra were recorded on a Bruker Avance III 400 spectrometer. Data are reported as follows: chemical shift, multiplicity (s = singlet, d = doublet, t = triplet, q = quartet, quint = quintet, sept = septet, br = broad, m = multiplet), coupling constants (Hz) and integration.

GC-MS: GC-MS data were obtained on an Agilent Technologies 5975C inert MSD with triple-axis detector, a 7693 autosampler and a 7890B GC system equipped with an SPB-5 fused silica column (34.13 m×0.25 mm×0.25 µm film thickness). *n*-Dodecane was used as an internal standard. The injection temperature was set to 300 °C. The column temperature ramped from 60 to 320 °C in 28 min and was then held for a further 5 min. The column flow was 1.50 mL min^{-1}.

Elemental Analysis (EA): EA (CHN) was carried out at the Institute of Inorganic Chemistry (University of Stuttgart, Germany) by Barbara Förtsch using a Perkin Elmer Analyzer 240.

Infrared Spectroscopy (IR): IR spectra were measured on an ATR/FT-IR spectrometer Bruker IFS 128 in the range of 4000 - 400 cm^{-1} and analyzed by the OPUS software (Vers. 7.2). Wavenumbers are reported in cm^{-1}, peak intensities are denoted (s = strong, m = medium and w = weak).

High-Resolution Mass Spectrometry (HRMS): Analyses were carried out at the Institute of Organic Chemistry, University of Stuttgart, Germany.

X-Ray Structure Analysis: Single-crystal X-ray structures were measured by Dr. W. Frey at the Institute of Organic Chemistry (University of Stuttgart) using a Bruker Kappa APEX II Duo. Dr. W. Frey also performed the structure determination and refinement with direct methods (*SHELXTL*-+ software suite (G.M. Sheldrick, Program package SHELXTL V.5.1, Bruker Analytical X-Ray Instruments Inc., Madison, USA (1997)).

Differential Scanning Calorimetry (DSC): DSC measurements were performed under nitrogen on a Perkin Elmer DSC 4000; data were analyzed with Pyris and Microsoft Excel.

5.4 Stereoselective Olefin Ring-Opening Cross-Metathesis Catalyzed by Molybdenum Imido Alkylidene *N*-Heterocyclic Carbene Complexes

5.4.1 General: *endo, endo*-DCMNBE,[14] *exo, exo*-DCMNBE,[14] (+) DCMNBE[201] and 2,*3-exo, exo-bis*(acetoxymethyl)-7-oxabicyclo[2.2.l]hept-5-ene[202] were prepared according to the literature. For column chromatography, silica gel (Fluka, 60M, 0.040–0.063 mm grain size, 230–400 mesh ASTM) was used as stationary phase. [Mo(*N*-2-*tert-Bu*-C_6H_4)(CHCMe$_2$Ph)(IMes)(OCH(CF$_3$)$_2$)$^+$ B(Ar^F)$_4^-$] (**Mo-1**),[147] [Mo(N-2-*tert-Bu*-C_6H_4)(CHCMe$_2$Ph)(1,3-bis(*i*Pr)imidazol-2-ylidene)(C_4H_4N)$^+$ B(Ar^F)$_4^-$] (**Mo-2**),[137] [Mo(*N*-3,5-Me$_2$$C_6H_3$)(CHCMe$_2$Ph)(IMes)($CH_3CN$)(OTf)$^+$ B(Ar^F)$_4^-$] (**Mo-3**)[147] and [Mo(*N*-3,5-Me$_2$$C_6H_3$)(CHCMe$_2$Ph)(IMesH$_2$)(OTf)$_2$] (**Mo-4a**)[134] were prepared according to the literature.

5.4.2 General Procedure for ROCM: The catalyst stock solution was prepared in $CHCl_3$ (10 mg/mL). *endo, endo*-DCMNBE (about 50 mg, one equiv.) was weighed in an oven-dried glass vial. The required amount of the cross partner i.e. the terminal olefin (10 equiv.) was weighed into the same vial and 0.25 mL $CHCl_3$ were added. To this mixture, the required amount of a stock solution of the catalyst in $CHCl_3$ (10 mg·mL^{-1}, ca. 300 µL, 0.1 equiv.) was added and the reaction mixture was stirred for 1 hour at room temperature. After completion of the reaction, all volatiles were removed *in vacuo* at room temperature and the residual reaction mixture was subjected to purification by silica gel chromatography (*n*-pentane/diethyl ether).

5.4.3 General Procedure for Recording the ROCM kinetics: In general, kinetics were measured following the above-mentioned ROCM procedure using $CHCl_3$ as solvent, *n*-dodecane as an internal standard and one mol% catalyst unless stated otherwise. Aliquots were withdrawn at regular time intervals and quantified by GC-MS using *n*-dodecane as an internal standard.

5.4.4 General Procedure for SM: The catalyst stock solution was prepared in $CHCl_3$ (10 mg/mL). Substrate (about 40 mg) was weighed in an oven-dried glass vial and 0.35 mL $CHCl_3$ was added. To this solution, the required amount of a stock solution of the catalyst in $CHCl_3$ (10 mg·mL^{-1}, ca. 30 µL) were added and the reaction mixture was stirred for 4 hours at room temperature. After completing the reaction, all

volatiles were removed *in vacuo* at room temperature and the residual reaction mixture was subjected to NMR and GC-MS for characterization.

5.4.5 General Procedure for Recording of the SM Kinetics: Kinetics were measured following the procedure outlined above procedure using CHCl3 as solvent, n-dodecane as an internal standard and 0.1 mol% catalyst unless stated otherwise. Aliquots were withdrawn at regular time intervals and subjected to GC-MS using n-dodecane as an internal standard.

5.4.6 Synthesis of Catalysts:

[Mo(*N*-3,5-$Me_2C_6H_3$)(CHCMe_2Ph)(IMesH_2)(OTf)(MeCN)$^+$B(Ar^F)$_4^-$], (Mo-4)

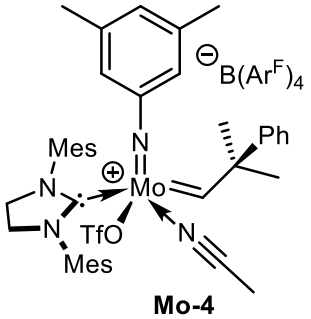

Mo-4

In a 10 mL vial complex **4a** (52.5 mg; 0.057 mmol) were dissolved in 2 mL of CH_2Cl_2 and few drops of CH_3CN was added followed by cooling to -30 °C. Then NaB(Ar^F)$_4$ (48.4 mg, 0.056 mmol, 0.99 eq.) was added in small portions over 15 min and the reaction mixture was stirred for 25 min at -30°C. After the given time the reaction mixture was filtered through a pad of celite, then the CH_2Cl_2 removed in *vacuo* followed by the addition of diethyl ether. The mixture was again filtered through a pad of celite. Then the diethyl ether was removed *in vacuo* followed by trituration with *n*-pentane, which resulted in the formation of a yellow solid (80 mg, 0.047 mmol, 82% yield). **^{1}H NMR** (CD_2Cl_2). *δ* = 13.37 (s, 1H), 7.72 (s, 8H), 7.56 (s, 4H), 7.18 (m, 3H), 7.08 (s, 1H), 7.03 (s, 1H), 7.01 (s, 1H), 6.93 (s, 2H), 6.70 (s, 2H), 6.57 (s, 2H), 4.05 (m, 4H), 2.34 (s, 6H), 2.29 (s, 6H), 2.21 (s, 12H), 1.83 (s, 3H), 1.79 (s, 3H), 1.00 (s, 3H) ppm. **^{19}F NMR** (CD_2Cl_2). δ = 62.9 (s, 24F), 76.1 (s, 3F) ppm. **^{13}C NMR** (CD_2Cl_2). δ = 328.9 (Mo=CH), 207.1 (CN$_{carbene}$), 162.5 (q, $^1J_{BC}$ = 49.9 Hz, B(Ar^F)$_4$), 144.5, 140.8, 139.4, 137.1, 135.9, 135.4, 134.4, 134.1, 130.9, 130.1, 129.4 (qq, J_{CF} = 31.3, J_{CB} = 2.8 Hz, CF_3-B(Ar^F)$_4$), 127.4, 126.6, 126.5, 123.8, 123.1, 117.5 (q, J = 318.7 Hz, CF_3 OTf), 118.0 (sept, J_{CF} = 4.0 Hz, *p*-Ar-B(Ar^F)$_4$), 56.9, 52.7, 29.7, 28.9, 21.4,21.3,

18.7, 18.5, 3.2 ppm. **Elemental analysis** (%) calcd. for $C_{74}H_{62}BF_{27}MoN_4O_3S$: C, 52.07; H, 3.66; N, 3.28; Found: C, 52.08; H, 3.982; N, 3.58.

[Mo(*N*-3,5-$Me_2C_6H_3$)(CHCMe_2Ph)(IMesH_2)(OCPh(CF_3)$_2$)$^+$B(Ar^F)$_4^-$], (Mo-5)

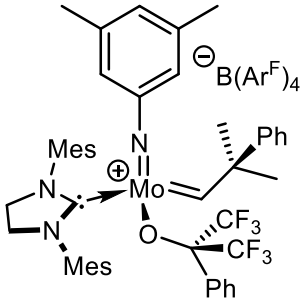

Mo-5

Mo-4 (71 mg, 0.042 mmol) was dissolved in 5 mL of CH_2Cl_2 and the solution was cooled to -35 °C. A cold solution of LiOCPh(CF_3)$_2$ (11.2 mg, 0.0415 mmol) in CH_2Cl_2 was added dropwise and the reaction mixture was stirred at room temperature for 1h. The reaction mixture was then filtered through a pad of celite and all volatiles were removed *in vacuo*. The residue was washed with *n*-pentane, dried, and crystallized from a mixture of CH_2Cl_2 and *n*-pentane to obtain a yellow solid (40 mg, 0.023 mmol, 55% yield). **^{1}H NMR** (400 MHz, CD_2Cl_2) δ 12.51 (broad s, 1H), 7.80 (s, 8H), 7.57 (s, 4H), 7.52 (t, J = 7.4 Hz, 1H), 7.42 (t, J = 7.8 Hz, 2H), 7.30 (d, J = 8 Hz, 2H), 7.22 (m, 3H), 7.06 (dd, J_1 = 8.1, J_2 = 1.7 Hz, 2H), 6.88 (m, 3H), 6.69 (s, 2H), 6.20 (s, 2H), 4.15 (m, 4H), 2.35 (s, 6H), 2.16 (s, 6H), 2.13 (s, 6H), 2.12 (s, 6H), 1.62 (s, 3H), 1.41 (s, 3H) ppm. **^{19}F NMR** (376 MHz, CD_2Cl_2) δ -62.83 (s, 24F), -74.73 (broad s, 3F), 75.02 (broad s, 3F) ppm. **^{13}C NMR** (101 MHz, CD_2Cl_2) δ 310.8 (Mo=CH), 209.0 (CN$_{carbene}$), 162.3 (q, J_{CB} = 49.7 Hz, C_{ipso} B(Ar^F)$_4$), 155.9, 146.9, 141.5, 138.5, 136.3, 135.5, 135.4, 133.9, 133.0, 132.1, 131.3, 131.2, 131.1, 128.9 (qq, J_{CF} = 31.3, J_{CB} = 2.8 Hz, CF_3-B(Ar^F)$_4$), 127.4, 126.9, 126.5, 126.3, 126.1, 123.8, 121.1, 118.0 (sept, J_{CF} = 4.0 Hz, *p*-Ar-B(Ar^F)$_4$), 85.8 (m, OCPh(CF_3)$_2$), 57.0, 52.9, 32.5, 31.1, 21.2, 18.5 and 18.4 ppm; **Elemental analysis** (%) calcd. for $C_{80}H_{64}BF_{30}MoN_3O$: C 54.59, H 3.67, N 2.39; Found: C 54.44, H 3.784, N 2.41.

5.4.7 Isolation of ROCM Products:

Dimethyl (*E*)-3-(pent-1-en-1-yl)-5-vinylcyclopentane-1,2-dicarboxylate, (P1)

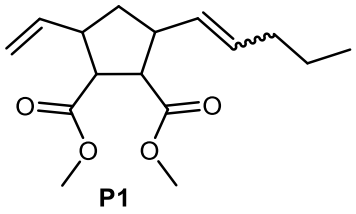

P1

The ROCM product was purified by column chromatography using *n*-pentane : diethyl ether (98 : 2) as mobile phase to give a colorless oil (29.2 mg, yield 44%) with an *E:Z* ratio of 87:13. **^{1}H NMR** (400 MHz, $CDCl_3$) δ 5.94 (m, 1H), 5.48 (m, 2H), 5.00 (m, 2H), 3.65 (s, 3H), 3.64 (s, 3H), 3.16 (m, 2H), 2.91 (m, 2H), 2.05 (m, 2H), 1.95 (m, 2H) 1.35 (m, 2H), 0.86 (t, 3H, *J* = 7.4 Hz) ppm. **^{13}C NMR** (101 MHz, $CDCl_3$, major *E*-isomer) δ 172.7, 172.7, 139.0, 132.3, 130.1, 115.7, 515, 51.45, 51.4, 51.3, 45.8, 45.1, 39.2, 38.1, 37.5, 34.6, 22.7, 13.7 ppm. **IR** (ATR, cm^{-1}). 2692 (m), 2871 (m), 1734 (s), 1639 (w), 1435 (m), 1384 (m), 1196 (s), 1177 (s), 1158 (s), 1105 (w), 973 (m), 798 (m), 664 (w). **HRMS *m/z*** calcd. for $(C_{16}H_{24}O_4Na)^+$: 303.1572, Found: 303.1567.

Dimethyl (*E*)-3-styryl-5-vinylcyclopentane-1,2-dicarboxylate, (P2)

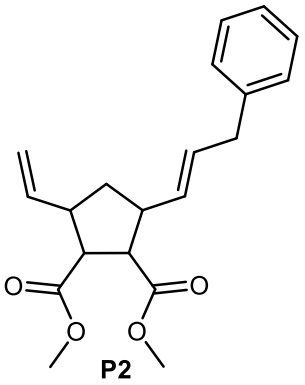

P2

The ROCM product was purified by column chromatography using *n*-pentane : diethyl ether (95:5) as mobile phase to give a colorless oil (41.1 mg, yield 55%) with an *E:Z* ratio of 97:3. The *E*-isomer was collected and characterized. **^{1}H NMR** (400 MHz, $CDCl_3$) δ 7.33 (d, 2H, *J* = 7.2 Hz), 7.26 (t, 2H, *J* = 6.7 Hz), 7.20 (m, 1H), 6.32 (t, *J* = 15.3 Hz, 1H), 6.26 (dd, J_1 = 15.8, J_2 = 8.3 Hz, 1H), 5.94 (m, 1H), 5.04 (m, 2H), 3.69 (s, 3H), 3.65 (s, 3H), 3.26 (m, 2H), 3.23 (m, 1H), 3.13 (m, 1H), 2.15 (m, 2H) ppm. **^{13}C NMR** (101 MHz, $CDCl_3$) δ 172.7, 172.6, 138.5, 137.5, 131.2, 130.59, 128.6, 127.3,

126.4, 116.1, 51.9, 51.6, 51.4, 46.0, 45.2, 37.4 ppm. **IR** (ATR, cm^{-1}). 2949 (m), 1732 (s), 1640 (w), 1492 (w), 1435 (m), 1384 (m), 1197 (s), 1175 (s), 1046 (w), 971 (m), 916 (m), 748 (m), 694 (m). **HRMS *m/z*** calcd. for $(C_{19}H_{22}O_4Na)^+$: 337.1416, Found: 337.1410.

Dimethyl(E)-3-(3-(trimethylsilyl)-prop-1-en-1-yl)-5-vinylcyclopentane-1,2-dicarboxylate, (P3)

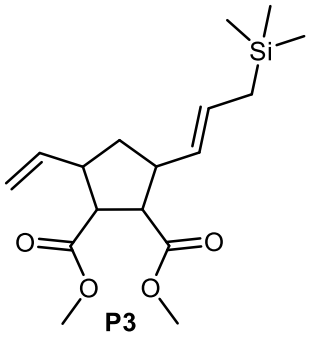

P3

The ROCM product was purified by column chromatography using *n*-pentane : diethyl ether (95:5) as mobile phase to give a colorless oil (35.0 mg, yield 45%) with an *E:Z* ratio of 92:8. The *E*-isomer was collected and characterized. **^{1}H NMR** (400 MHz, $CDCl_3$) δ 5.98 (m, 1H), 5.47 (ddd, J_1 = 8.7, J_2 = 7.9, J_3 = 0.7 Hz, 1H), 5.30 (dd, J_1 = 15.1, J_2 = 8.5 Hz, 1H), 5.00 (m, 2H), 3.63 (s, 6H), 3.19 (m, 2H), 3.07 (m, 1H), 2.01 (m, 2H), 1.40 (dd, 2H, J_1 = 8, J_2 = 1.2 Hz), -0.04 (s, 9H) ppm. **^{13}C NMR** (101 MHz, $CDCl_3$) δ 173.1, 172.5, 139.5, 128.6, 127.9, 115.50, 51.6, 51.7, 51.5, 46.7, 46.5, 38.0, 22.4, -1.9 ppm. **IR** (ATR, cm^{-1}). 2950 (m), 1736 (s), 1639 (w), 1435 (m), 1385 (m), 1247 (m), 1198 (s), 1158 (s), 1103 (w), 967 (m), 914 (w), 854 (s), 733 (m), 698 (w). **HRMS *m/z*** calcd. for $(C_{17}H_{28}O_4SiH)^+$: 325.1835, Found: 325.1830.

Dimethyl(*E*)-3-(3-(benzyloxy)-prop-1-en-1-yl)-5-vinylcyclopentane-1,2dicarboxylate, (P4)

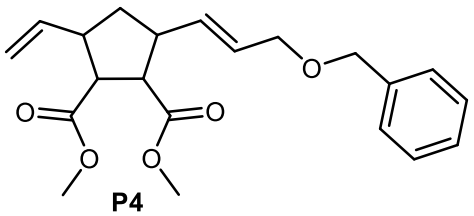

P4

The ROCM product was purified by column chromatography using *n*-pentane : diethyl ether (90:10) as mobile phase to give a colorless oil (55.0 mg, yield 65%) with an *E:Z*

ratio of 95:5. The *E*-isomer was collected and characterized. **^{1}H NMR** (400 MHz, $CDCl_3$) δ 7.34 (m, 4H), 7.28 (m, 1H), 5.90 (m, 1H), 5.84 (dd, J_1 = 15.4, J_2 = 8.6 Hz, 1H), 5.64 (dtd, J_1 = 15.4, J_2 = 6.2, J_3 = 0.7 Hz, 1H), 5.03 (m, 2H), 4.49 (s, 2H), 3.96 (dd, 2H, J_1 = 6.2, J_2 = 1.2 Hz), 3.65 (s, 3H), 3.63 (s, 3H), 3.20 (m, 2H), 2.97 (m, 2H), 2.08 (m, 2H) ppm. **^{13}C NMR** (101 MHz, $CDCl_3$) δ 172.6, 172.5, 138.5, 138.4, 134.3, 128.5, 128.1, 127.9, 127.7, 116.0, 71.9, 70.6, 51.6, 51.5, 51.4, 45.8, 44.5, 37.2 ppm. **IR** (ATR, cm^{-1}). 2948 (m), 2849 (m), 1733 (s), 1639 (w), 1435 (m), 1384 (m), 1197 (s), 1177 (s), 1159 (s), 1107 (w), 1069 (w), 976 (m), 916 (m), 737 (m), 699 (m). **HRMS *m/z*** calcd. for $(C_{21}H_{26}O_5Na)^+$: 381.1678, Found: 381.1672.

Dimethyl (*E*)-3-(3-phenoxyprop-1-en-1-yl)-5-vinylcyclopentane-1,2-dicarboxylate, (P5)

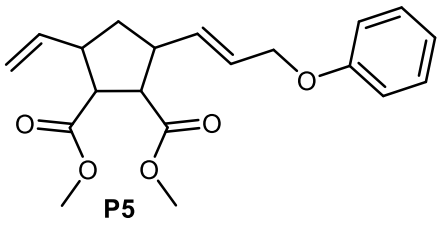

P5

The ROCM product was purified by column chromatography using *n*-pentane : diethyl ether (90:10) as mobile phase to give a colorless oil (50.8 mg, yield 62%) with >99 % *E*-isomer, which was collected and characterized. **^{1}H NMR** (400 MHz, $CDCl_3$) δ 7.26 (dd, 2H, J_1 =8.7, J_2 = 7.4 Hz), 6.92 (t, 1H, J =7.4 Hz), 6.86 (dd, 2H, J_1 =8.8, J_2 = 1.0 Hz), 5.96 (dd, J_1 = 15.3, J_2 = 8.6 Hz, 1H), 5.89 (m, 1H), 5.74 (dtd, J_1 = 15.4, J_2 = 6.0, J_3 = 0.7 Hz, 1H) 5.03 (m, 2H), 4.46 (d, 2H, J = 6.0 Hz), 3.65 (s, 3H), 3.61 (s, 3H), 3.20 (m, 2H), 3.02 (m, 1H), 2.93 (m, 1H), 2.09 (m, 2H) ppm. **^{13}C NMR** (101 MHz, $CDCl_3$) δ 172.7, 172.4, 158.7, 138.3, 135.1, 129.5, 126.8, 120.8, 116.1, 114.8, 68.4, 51.6, 51.4, 51.3, 45.9, 44.3, 37.1 ppm. **IR** (ATR, cm^{-1}). 2949 (m), 1731 (s), 1640 (w), 1598 (m), 1493 (m), 1434 (m), 1383 (m), 1195 (s), 1173 (s), 1157 (s), 1029 (m), 975 (m), 915 (m), 733 (m), 691 (m), 664 (w), 511 (m). **HRMS *m/z*** calcd. for $(C_{20}H_{24}O_5Na)^+$: 367.1521, Found: 367.1524.

Dimethyl (*E*)-3-(3-ethoxyprop-1-en-1-yl)-5-vinylcyclopentane-1,2-dicarboxylate, (P6)

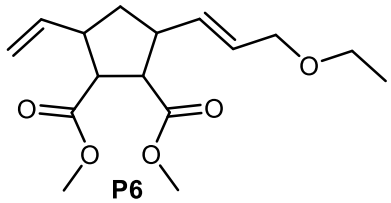

P6

The ROCM product was purified by column chromatography using *n*-pentane : diethyl ether (95:5) as mobile phase to give a colorless oil (35.0 mg, yield 50%) containing >99 % of the *E*-isomer, which was collected and characterized. **^{1}H NMR** (400 MHz, $CDCl_3$) δ 5.90 (m, 1H), 5.78 (dd, J_1 = 15.4, J_2 = 8.6 Hz, 1H), 5.59 (dtd, J_1 = 15.4, J_2 = 6.2, J_3 = 0.7 Hz, 1H), 5.00 (m, 2H), 3.87 (dd, 2H, J_1 = 6.2, J_2 = 1.2 Hz), 3.63 (s, 3H), 3.62 (s, 3H), 3.43 (q, 2H, J = 7.0 Hz), 3.17 (m, 2H), 2.94 (m, 2H), 2.06 (m, 2H), 1.17 (t, 3H, J = 7.0 Hz) ppm. **^{13}C NMR** (101 MHz, $CDCl_3$) δ 172.6, 172.7, 138.5, 133.9, 128.4, 115.9, 71.1, 65.4, 51.5, 51.5, 51.3, 45.8, 44.5, 37.2, 15.3 ppm. **IR** (ATR, cm^{-1}). 2949 (m), 2850 (m), 1733 (s), 1640 (w), 1435 (m), 1383 (m), 1197 (s), 1159 (s), 1100 (w), 977 (m), 917 (m), 811 (m), 733 (w). **HRMS *m/z*** calcd. for $(C_{16}H_{24}O_5Na)^+$: 319.1521, Found: 319.1516.

Dimethyl(*E*)-3-(3-(benzyloxy)-prop-1-en-1-yl)-5-vinylcyclopentane-1,2-dicarboxylate, (P7)

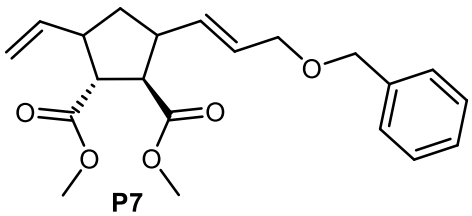

P7

The ROCM product was purified by column chromatography using *n*-pentane : diethyl ether (90:10) as mobile phase to give a colorless oil (42.0 mg, yield 50%) with an *E:Z* ratio of 92:8. The *E*-isomer was collected and characterized. **^{1}H NMR** (400 MHz, $CDCl_3$) δ 7.35 – 7.28 (m, 5H), 5.75 (dd, J_1 = 15.4, J_2 = 7.5 Hz, 1H), 5.67 (m, 2H), 5.03 (m, 2H), 4.50 (s, 2H), 3.99 (d, 2H, J_1 = 5.9, Hz), 3.67 (s, 3H), 3.64 (s, 3H), 3.33 (dd, 1H, J_1 = 9.8, J_2 = 7.9 Hz), 3.07 (m, 2H), 2.81 (m, 1H), 2.08 (m, 1H), 1.65 (m, 1H) ppm. **^{13}C NMR** (101 MHz, $CDCl_3$) δ 174.5, 173.5, 138.4, 137.5, 128.5, 128.0, 127.8, 127.5, 116.4, 72.0, 70.5, 52.3, 52.2, 51.9, 51.8, 46.6, 45.7, 38.4 ppm. **IR** (ATR, cm^{-1}).

2950 (m), 2923 (w), 2851 (m), 1731 (s), 1453 (m), 1435 (m), 1379 (m), 1198 (s), 1169 (s), 1069 (w), 1000 (m), 971 (m), 920 (m), 738 (m), 699 (m). **HRMS *m/z*** calcd. for $(C_{21}H_{26}O_5Na)^+$: 381.1678, Found: 381.1672.

Dimethyl (*E*)-3-(3-(benzyloxy)-prop-1-en-1-yl)-5-vinylcyclopentane-1,2-dicarboxylate, (P8)

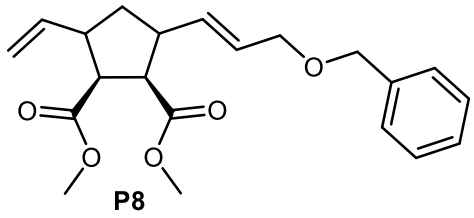

P8

The ROCM product was purified by column chromatography using *n*-pentane : diethyl ether (90.10) as mobile phase to give a colorless oil (47.0 mg, yield 55%) with an *E:Z* ratio of 91:9. The *E*-isomer was collected and characterized. **^{1}H NMR** (400 MHz, $CDCl_3$) δ 7.35 – 7.28 (m, 5H), 5.77 (ddd, J_1 = 17.4, J_2 = 10.3, J_3 = 7.2 Hz, 1H), 5.68 (m, 2H), 5.07 (m, 2H), 4.49 (s, 2H), 3.98 (m, 2H), 3.65 (s, 3H), 3.64 (s, 3H), 3.06 (m, 2H), 2.93 (m, 2H), 2.15 (dt, J_1 = 13.0, J_2 = 6.7 Hz, 1H), 1.43 (m, 1H) ppm. **^{13}C NMR** (101 MHz, $CDCl_3$) δ 173.4, 173.3, 139.5, 138.4, 134.8, 128.5, 128.0, 127.8, 127.3, 115.3, 72.2, 70.6, 52.4, 52.2, 52.0, 46.3, 44.9, 38.7 ppm. **IR** (ATR, cm^{-1}). 2949 (m), 2923 (m), 2852 (m), 1740 (s), 1641 (w), 1453 (m), 1435 (m), 1362 (m), 1274 (m), 1262 (m), 1199 (s), 1065 (w), 971 (m), 917 (m), 740 (m), 699 (m). **HRMS *m/z*** calcd. for $(C_{21}H_{26}O_5Na)^+$: 381.1678, Found: 381.1672.

(*E*)-2-(3-(Benzyloxy)-prop-1-en-1-yl)-5-vinyl-3,4- tetrahydrofurane-3,4-dimethanol diacetate, (P9)

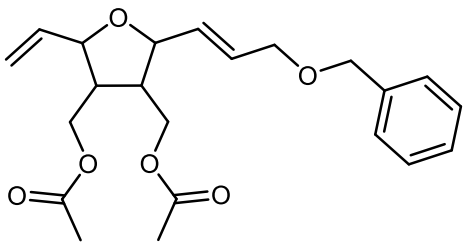

P9

The ROCM product was purified by column chromatography using *n*-pentane : diethyl ether (60:40) as mobile phase to give a colorless oil (40.0 mg, yield 49%) with an *E:Z* ratio of 70:30. The *E*-isomer was collected and characterized. **^{1}H NMR** (400 MHz,

$CDCl_3$) δ 7.34 – 7.28 (m, 5H), 5.87 (m, 2H), 5.77 (dd, J_1 = 15.5, J_2 = 6.6 Hz, 1H), 5.20 (m, 2H), 4.52 (s, 2H), 4.25 (t, J_1 = 6.5 Hz, 1H), 4.18 (m, 5H), 4.04 (dd, J_1 = 5.2, J_2 = 0.6 Hz, 2H), 2.42 (m, 2H), 2.05 (s, 3H), 2.04 (s, 1H) ppm. **^{13}C NMR** (101 MHz, $CDCl_3$) δ 173.4, 173.3, 139.5, 138.4, 134.8, 128.5, 128.0, 127.8, 127.3, 115.3, 72.2, 70.6, 52.4, 52.2, 52.0, 46.3, 44.9, 38.7 ppm. **IR** (ATR, cm^{-1}). 2899 (m), 2851 (m), 1739 (s), 1454 (m), 1388 (m), 1367, 1228 (s), 1113 (m), 1036 (s), 971 (m), 928 (m), 740 (m), 699 (m), 605 (w). **HRMS *m/z*** calcd. for $(C_{22}H_{28}O_6Na)^+$: 411.1784, Found: 411.1778.

5.5 Tuning the Latent Behavior of Molybdenum Imido Alkylidene *N*-Heterocyclic Carbene Complexes in Dicyclopentadiene Polymerization

5.5.1 General: *N*,*N*-Dimethyl-2-vinylaniline,[203] Mo(*N*-2,6-$Me_2C_6H_3$)(CHCMe$_2$Ph)(IMes)(OTf)$_2$,[204] Mo(*N*-3,5-$Me_2C_6H_3$)(CHCMe$_2$Ph)(IMes)(OTf)$_2$[134] and Mo(*N*-2-CF_3-C_6H_4)(CHCMe$_2$Ph)(IMes)(OTf)$_2$[205] were synthesized according to literature known procedure. The synthetic procedure for Mo(*N*-2,6-F_2-C_6H_3)(CHCMe$_2$Ph)(IMes)(OTf)$_2$ is described in chapter 3 of this thesis.

5.5.2 Synthesis of Pre-catalysts:

Mo(*N*-2,6-Me_2-C_6H_3)(CHC_4H_6NO)(IMes)(OTf)$_2$, (Mo-6)

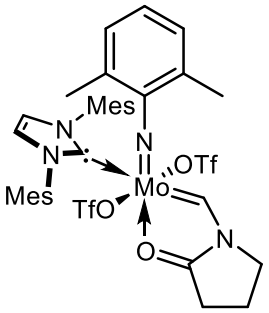

Mo(N-2,6-$Me_2C_6H_3$)(CHCMe$_2$Ph)(IMes)(OTf)$_2$ (0.100 g, 0.105 mmol) was suspended in 6 mL toluene and *N*-vinyl-2-pyrrolidone (0.023 g, 0.210 mmol) in 1 mL toluene was added. After 5 min. reaction solution turned deep orange, further solution stirred for one hour at room temperature. Then, the solution was filtered to obtain bright orange solids as a product. The product was purified by crystallization from a mixture of CH_2Cl_2/*n*-pentane to obtain bright crystalline orange solid (0.075 g, 0.082 mmol, 78% yield).

^{1}H NMR (400 MHz, CD_2Cl_2) δ = 11.95 (s, $^1J_{CH}$ = 161.2 Hz, 1H, Mo=CH), 7.09 (s, 2H, Ar), 7.03 (t, ^2J = 7.5 Hz, 1H, Ar), 6.97(s, 2H, CH=CH-NHC), 7.00 – 6.75 (br s, 2H, *m*-Ar-Mes), 6.62 (s, 2H, *m*-Ar-Mes), 3.65 (m, 1H, $\underline{CH_2}$-pyrrolidone), 3.33 (m, 1H, $\underline{CH_2}$-pyrrolidone), 2.73 (br s, 3H, $\underline{CH_3}$-Ar), 2.60 (m, 1H, $\underline{CH_2}$-pyrrolidone), 2.28 (m, 1H, $\underline{CH_2}$-pyrrolidone), 2.25 (s, 3H, $\underline{CH_3}$-Mes), 2.20 (m, 1H, $\underline{CH_2}$-pyrrolidone), 2.08 (s, 3H, $\underline{CH_3}$-Mes), 1.98 (s, 3H, $\underline{CH_3}$-Mes), 1.93 (m, 1H, $\underline{CH_2}$-pyrrolidone), 1.92 (br s, 3H, $\underline{CH_3}$-Ar). **^{13}C NMR** (101 MHz, CD_2Cl_2) δ = 283.9 (Mo=CH), 185.7 (NCN-NHC), 185.0 (C=O), 154.4, 140.2, 136.9, 136.1, 136.0, 129.5, 129.3, 129.0, 127.9, 125.9 (CH=CH-

NHC), 119.8 (q, $^{1}J_{CF}$ = 318.5 Hz, CF_3 OTf), 120.0 (q, $^{2}J_{CF}$ = 318.5 Hz, CF_3 OTf), 49.1, 27.8, 21.4 (Me-Mes), 20.8 (br, Me-Ar), 19.2 (br, Me-Ar), 18.5 (Me-Mes). **^{19}F NMR** (376 MHz, CD_2Cl_2) δ = -77.66 (br s, 3F, OTf), -78.22 (br s, 3F, OTf). **Elemental analysis** (%) calcd. for $C_{36}H_{40}F_6MoN_4O_7S_2$: C, 45.27; H, 4.41; N, 6.12. Found: C, 45.33; H, 4.43; N, 6.05.

Mo(*N*-3,5-Me$_2$-C$_6$H$_3$)(CHC$_4$H$_6$NO)(IMes)(OTf)$_2$, (Mo-7)

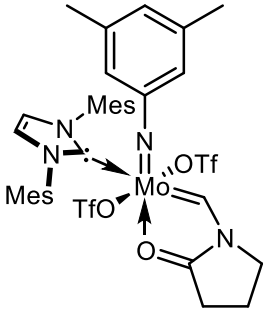

Mo(N-,5-Me$_2$C$_6$H$_3$)(CHCMe$_2$Ph)(IMes)(OTf)$_2$ (0.100 g, 0.105 mmol) was suspended in 6 mL toluene and *N*-vinyl-2-pyrrolidone (0.023 g, 0.210 mmol) in 1 mL toluene was added. The reaction solution immediately turned deep orange, further the solution stirred for one hour at room temperature. Then, the solution was filtered to obtain bright orange solids as a product. The product was purified by crystallization from a mixture of CH_2Cl_2/*n*-pentane to obtain bright crystalline orange solid (0.070 g, 0.077 mmol, 73% yield).

^{1}H NMR (400 MHz, CD_2Cl_2) δ = 11.90 (s, $^{1}J_{CH}$ = 160.3 Hz, 1H, Mo=CH), 7.08 (s, 2H, Ar), 6.90 (s, 2H, CH=CH-NHC), 6.88 (s, 1H, Ar), 6.82 (s, 2H, *m*-Ar-Mes), 6.67 (s, 2H, *m*-Ar-Mes), 3.73 (m, 1H, $\underline{CH_2}$-pyrrolidone), 3.56 (m, 1H, $\underline{CH_2}$-pyrrolidone), 2.57 (m, 1H, $\underline{CH_2}$-pyrrolidone), 2.32 (m, 1H, $\underline{CH_2}$-pyrrolidone), 2.26 (s, 3H, $\underline{CH_3}$-Mes), 2.20 (m, 1H, $\underline{CH_2}$-pyrrolidone), 2.16 (s, 6H, $\underline{CH_3}$-Ar), 2.09 (s, 3H, $\underline{CH_3}$-Mes), 2.05 (s, 3H, $\underline{CH_3}$-Mes), 2.00 (m, 1H, $\underline{CH_2}$-pyrrolidone). **^{13}C NMR** (101 MHz, CD_2Cl_2) δ = 281.4 (Mo=CH), 188.0 (NCN-NHC), 184.9 (C=O), 154.3, 140.0, 137.7, 136.9, 136.3, 135.6, 131.5, 129.7, 129.0, 125.9, 124.5 (CH=CH-NHC), 120.1 (q, $^{1}J_{CF}$ = 319.3 Hz, OTf), 119.7 (q, $^{2}J_{CF}$ = 318.6 Hz, OTf), 49.2, 28.0, 22.1, 21.3 (Me-Mes), 21.2 (Me-Ar), 18.4 (Me-Mes), 18.1 (Me-Mes). **^{19}F NMR** (376 MHz, CD_2Cl_2) δ = -77.10 (s, 3F, OTf), -78.18 (s, 3F, OTf). **Elemental analysis** (%) calcd. for $C_{36}H_{40}F_6MoN_4O_7S_2$: C, 45.27; H, 4.41; N, 6.12. Found: C, 47.16; H, 4.393; N, 6.01.

Mo(*N*-2,6-Me_2-C_6H_3)(CHC_5H_4N)(IMes)($OTf)_2$, (Mo-8)

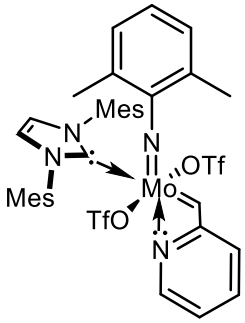

Mo(N-2,6-$Me_2C_6H_3$)($CHCMe_2Ph$)(IMes)($OTf)_2$ (0.075 g, 0.079 mmol) was dissolved in 6 mL dichloromethane and 2-vinylpyridine (0.017 g, 0.158 mmol) in 1 mL dichloromethane was added. The reaction mixture was stirred for 3 hours at room temperature. Then, all volatiles were removed under vacuum and the resulting residue was washed with pentane until it solidifies. The product was crystallized from a mixture of CH_2Cl_2/diethyl ether/*n*-pentane to obtain a crystalline yellow solid (0.050 g, 0.055 mmol, 69% yield).

^{1}H NMR (400 MHz, $CDCl_3$) δ = 13.16 (s, $^1J_{CH}$ = 167.6 Hz, 1H, Mo=CH), 8.61 (d, ^1J = 5.2 Hz, 1H, *o*-N-pyr), 7.57 (td, *J* = 7.8, 1.7 Hz, 1H, *p*-vinylpyr), 7.04 (s, 2H), 6.96 (m, 2H), 6.92 (m, 1H), 6.83 (m, 1H), 6.74 (s, 2H), 6.37 (s, 2H), 6.14 (d, *J* = 7.7 Hz, 1H, *o*-vinylpyr), 2.97 (s, 3H, Me-Ar), 2.13 (s, 6H, Me-Mes), 2.07 (s, 6H, Me-Mes), 1.97 (s, 3H, Me-Ar), 1.92 (s, 6H, Me-Mes). **^{13}C NMR** (101 MHz, $CDCl_3$) δ 294.7 (d, Mo=CH, *J* = 7.0 Hz), 185.2 (NCN-NHC), 160.5, 154.7, 146.5, 143.4, 140.1, 140.1, 138.3, 135.77, 135.3, 135.1, 129.9, 129.5, 129.3, 127.2, 127.1, 125.1, 124.9, 119.57 (q, $^1J_{CF}$ = 318.7 Hz, CF_3 OTf), 118.9 (q, $^2J_{CF}$ = 318.3 Hz, CF_3 OTf), 114.4, 21.1 (Me-Mes), 20.3 (Me-Ar), 18.6 (Me-Ar), 18.2 (Me-Mes). **^{19}F NMR** (376 MHz, $CDCl_3$) δ = -78.32 (s, 3F, OTf), -76.99 (s, 3F, OTf). **Elemental analysis** (%) calcd. for $C_{37}H_{38}F_6MoN_4O_6S_2$: C, 48.90; H, 4.21; N, 6.17. Found: C, 48.86; H, 4.37; N, 6.28.

Mo(*N*-3,5-Me_2-C_6H_3)(CHC_5H_4N)(IMes)($OTf)_2$, (Mo-9)

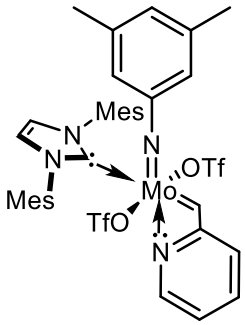

Mo(N-3,5-$Me_2C_6H_3$)($CHCMe_2Ph$)(IMes)($OTf)_2$ (0.100 g, 0.105 mmol) was dissolved in 6 mL dichloromethane and 2-vinylpyridine (0.022 g, 0.210 mmol) in 1 mL dichloromethane was added. The reaction mixture was stirred for 12 h at room temperature. Then, all volatiles were removed under vacuum and the resulting residue was washed with pentane until it solidified. The product was crystallized from a mixture of CH_2Cl_2/diethyl ether/*n*-pentane to obtain a crystalline yellow solid (0.060 g, 0.058 mmol, 55% yield).

^{1}H NMR (400 MHz, $CDCl_3$) δ = (s, $^1J_{CH}$ = 167.3 Hz, 1H, Mo=CH), 7.72 (d, ^1J = 4.9 Hz, 1H, *o*-N-pyr), 7.62 (td, *J* = 7.9, 1.7 Hz, 1H, *p*-vinylpyr), 7.02 (s, 2H), 6.91 (m, 2H), 6.82 (m, 1H), 6.80 (m, 1H), 6.63 (s, 2H), 6.48 (s, 2H), 6.40 (d, *J* = 7.8 Hz, 1H, *o*-vinyl pyr), 2.23 (s, 6H, Me-Mes), 2.17 (s, 6H, Me-Mes), 2.06 (s, 6H, Me-Ar), 1.95 (s, 6H, Me-Mes). **^{13}C NMR** (101 MHz, CD_2Cl_2) δ 293.3 (d, Mo=CH, *J* = 5.9 Hz), 186.3, 160.6, 154.3, 144.6, 140.2, 139.5, 137.3, 136.2, 135.6, 135.5, 132.5, 129.8, 129.6, 126.7, 125.9, 125.6, 120.2 (q, $^1J_{CF}$ = 319.1 Hz, CF_3 OTf), 119.4 (q, $^2J_{CF}$ = 318.7 Hz, CF_3 OTf), 114.5, 21.4, 21.3, 2.16, 2.1, 18.2. **^{19}F NMR** (376 MHz, $CDCl_3$) δ = -78.23 (q, ^1J = 3.3 Hz, 3F, OTf), -76.43 (q, ^2J = 3.3 Hz, 3F, OTf). **Elemental analysis** (%) calcd. for $C_{37}H_{38}F_6MoN_4O_6S_2$: C, 48.90; H, 4.21; N, 6.17. Found: C, 48.71; H, 4.27; N, 6.24.

Mo(*N*-2,6-F_2-C_6H_3)($CH(C_5H_4N)$)(IMes)($OTf)_2$, (Mo-10)

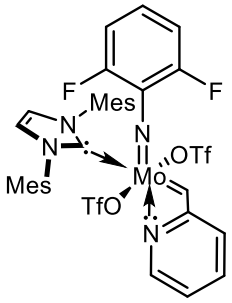

Mo(N-2,6-F_2-C_6H_3)(CHCMe_2Ph)(IMes)(OTf)$_2$ (0.050 g, 0.052 mmol) was dissolved in 4 mL dichloromethane and the solution was cooled to – 40 °C for an hour. The solution of 2-vinylpyridine (0.011 g, 0.104 mmol) in 1 mL dichloromethane was added dropwise to the educt solution. The reaction mixture was stirred for 10 min. at room temperature. Then, all volatiles were removed under vacuum and the resulting residue was washed with pentane until it solidifies. The product was crystallized from a mixture of CH_2Cl_2/diethyl ether/*n*-pentane to obtain light crystalline orange solid (0.032 g, 0.035 mmol, 67% yield).

^{1}H NMR (400 MHz, CD_2Cl_2) δ 13.67 (s, $^1J_{CH}$ = 170.9 Hz, 1H, Mo=CH), 7.83 (d, ^1J = 5.1 Hz, 1H, *o*-N-pyr), 7.70 (td, *J* = 7.9, 1.7 Hz, 1H, *p*-vinylpyr), 7.24 - 7.11 (m, 1H), 6.90 (ddd, *J* = 7.9, 5.0, 1.0 Hz, 1H), 6.81 (t, *J* = 8.3 Hz, 2H), 6.71 (s, 2H), 6.53 (s, 2H), 6.46 (d, *J* = 7.8 Hz, 1H, *o*-vinylpyr), 2.16 (s, 6H, Me-Mes), 2.05 (s, 6H, Me-Mes), 1.93 (s, 6H, Me-Mes). **^{19}F NMR** (376 MHz, CD_2Cl_2) δ = -77.12 (d, *J* = 2.8 Hz, 3F, OTf), -78.61 (d, *J* = 2.4 Hz, 3F, OTf), -112.62 (s, 2F, Imido). **Elemental analysis** (%) calcd. for $C_{35}H_{32}F_8MoN_4O_6S_2$: C, 45.86; H, 3.52; N, 6.11. Found: C, 45.84; H, 3.62; N, 6.13. We could not record the **^{13}C NMR**, as it got decomposed over the recording of spectrum.

Mo(*N*-2-CF_3-C_6H_4)(CH(C_5H_4N))(IMes)(OTf)$_2$, (Mo-11)

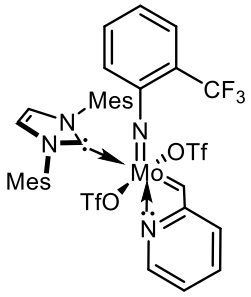

Mo(N-2-CF_3-C_6H_4)(CHCMe_2Ph)(IMes)(OTf)$_2$ (0.050 g, 0.051 mmol) was dissolved in 4 mL dichloromethane and the solution was cooled to – 40 °C for an hour. The solution of 2-vinylpyridine (0.011 g, 0.102 mmol) in 1 mL dichloromethane was added dropwise to the educt solution. The reaction mixture was stirred for 30 min. at room temperature. Then, all volatiles were removed under vacuum and resulting residue was washed with pentane until it solidifies. The product was crystallized from mixture of CH_2Cl_2/diethyl ether/*n*-pentane to obtain crystalline orange solid (0.030 g, 0.032 mmol, 62% yield).

^{1}H NMR (400 MHz, CD_2Cl_2) δ 13.47 (s, $^{1}J_{CH}$ = 170.8 Hz, 1H, Mo=CH), 7.96 (d, ^{1}J = 5.0 Hz, 1H, *o*-N-pyr), 7.69 (td, *J* = 7.9, 1.7 Hz, 1H, *p*-vinylpyr), 7.48 (m, 3H), 7.36 (m, 1H), 7.10 (m, 2H), 6.60 (s, 2H), 6.92 (ddd, *J* = 8.0, 5.0, 1.1 Hz, 1H), 6.53 (s, 2H), 6.41 (d, *J* = 7.7 Hz, 1H, *o*-vinylpyr), 2.07 (s, 6H, Me-Mes), 2.04 (s, 6H, Me-Mes), 1.98 (s, 6H, Me-Mes). **^{13}C NMR** (101 MHz, CD_2Cl_2) δ 297.1 (Mo=CH), 185.8 (NCN-NHC), 159.8, 150.2, 145.2, 140.3, 139.4, 136.1, 135.8, 135.6, 131.9, 130.3, 130.0, 129.7, 126.1, 126.0, 120.0 (q, $^{1}J_{CF}$ = 318.8 Hz, CF_3 OTf), 119.8 (q, $^{2}J_{CF}$ = 318.8 Hz, CF_3 OTf), 115.2, 21.2, 18.3, 18.2. **^{19}F NMR** (376 MHz, CD_2Cl_2) δ = -58.88 (s, 3F, CF_3), -76.90 (s, 3F, OTf), -78.65 (s, 3F, OTf). **Elemental analysis** (%) calcd. for $C_{36}H_{33}F_9MoN_4O_6S_2$: C, 45.58; H, 3.51; N, 5.91. Found: C, 45.60; H, 3.71; N, 6.07.

Mo(N-2,6-F_2-C_6H_3)(CHCMe_2Ph)(OTf)(*O*-2-Cl-C_6H_4)(IMes), (Mo-12)

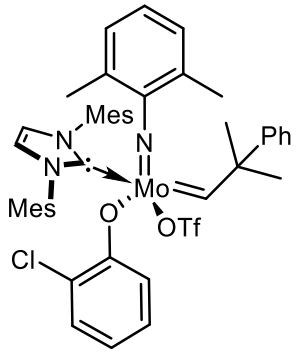

In the separate glass vials, Mo(N-2,6-$Me_2C_6H_3$)(CHCMe_2Ph)(IMes)$(OTf)_2$ (0.050 g, 0.053 mmol) in 4 mL dichloromethane and lithium-2-chlorophenoxide (0.0071 g, 0.053 mmol) in 1 mL dichloromethane were dissolved and both the solutions cooled to -30 °C for 30 min. Then, the lithium-2-chlorophenoxide solution was added dropwise to the educt solution. The reaction mixture was stirred for 6 h at room temperature. It was then filtered through celite and the filtrate was evaporated under vacuum and the resulting residue was washed with pentane until it solidifies. The product was crystallized from mixture of CH_2Cl_2/diethyl ether/*n*-pentane to obtain crystalline yellow solid (0.035 g, 0.038 mmol, 71% yield).

^{1}H NMR (400 MHz, CD_2Cl_2) δ 14.91 (s, 1H, Mo=CH, minor isomer), 13.81 (s, 1H, Mo=CH, major isomer), 7.33 – 7.17 (m, 6H), 7.12 (s, 2H), 7.07 – 6.98 (m, 2H), 6.88 (m, 3H), 6.71 (td, *J* = 7.6, 1.5 Hz, 1H), 6.58 (m, 2H), 6.50 – 6.39 (m, 3H), 2.38 (s, 6H), 2.05 (s, 6H), 2.01 (s, 9H), 1.84 (s, 9H). **^{13}C NMR** (101 MHz, CD_2Cl_2, only major isomer signals reported) δ 318.9 (Mo=CH), 186.0 (NCN-NHC), 160.5, 154.5, 150.9,

140.2, 136.0, 135.8, 134.3, 129.9, 129.8, 129.7, 129.4, 128.7, 128.6, 128.4, 127.7, 127.4, 126.6, 126.1, 125.2, 121.6, 120.3, 119.69 (q, J_{CF} = 318.9 Hz, CF_3 OTf), 55.7, 36.7, 29.9, 21.4, 18.9, 18.8. **^{19}F NMR** (376 MHz, CD_2Cl_2) δ -78.76 (s, 3F, OTf). **Elemental analysis** (%) calcd. for $C_{46}H_{49}ClF_3MoN_3O_4S$: C, 59.51; H, 5.32; N, 4.53. Found: C, 59.60; H, 5.40; N, 4.57.

Mo(N-3,5-F_2-C_6H_3)(CHCMe_2Ph)(OTf)(*O*-2-Cl-C_6H_4)(IMes), (Mo-13)

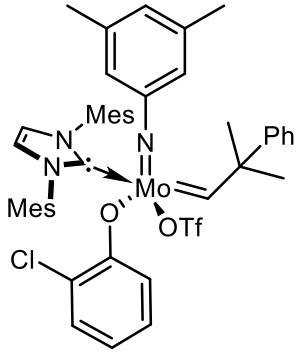

In two separate glass vials, Mo(N-3,5-$Me_2C_6H_3$)(CHCMe_2Ph)(IMes)$(OTf)_2$ (0.050 g, 0.053 mmol) and lithium-2-chlorophenoxide (0.0071 g, 0.053 mmol) were dissolved in 4 and 1 mL dichloromethane, respectively and both solutions were cooled to -30 °C. Next, the lithium-2-chlorophenoxide solution was added dropwise to the educt solution. The reaction mixture was stirred for 3 h at room temperature. It was then filtered through celite and the filterate was evaporated under vacuum and resulting residue was washed with pentane until it solidifies. The product was crystallized from mixture of CH_2Cl_2/diethyl ether/*n*-pentane to obtain crystalline yellow solid (0.030 g, 0.032 mmol, 61% yield).

^{1}H NMR (400 MHz, $CDCl_3$) δ 14.19 (s, 1H, Mo=CH), 7.36 - 7.30 (m, 4H), 7.27 - 7.21 (m, 2H), 7.07 - 7.02 (m, 1H), 6.99 (s, 2H), 6.72 - 6.66 (m, 6H), 6.47 - 6.43 (m, 3H), 2.22 (d, *J* = 0.7 Hz, 6H), 2.18 (s, 6H), 2.16 (s, 3H), 1.93 (s, 6H), 1.68 (s, 6H), 1.58 (s, 3H). **^{13}C NMR** (101 MHz, $CDCl_3$) δ 320.4 (Mo=CH), 186.8 (NCN-NHC), 159.9, 154.0, 149.5, 139.2, 136.5, 135.8, 135.4, 133.9, 129.4, 129.1, 129.1, 128.3, 128.3, 127.1, 126.2, 126.2, 125.7, 124.7, 123.5, 120.6, 119.1, 54.6, 34.0, 30.5, 21.3, 21.1, 18.2, 18.1. $^1J_{CF}$ coupling in ^{13}C NMR could not be determined due to overlap of signals. **^{19}F NMR** (376 MHz, $CDCl_3$) δ -78.13 (s, 3F, OTf). **Elemental analysis** (%) calcd. for $C_{46}H_{49}ClF_3MoN_3O_4S$: C, 59.51; H, 5.32; N, 4.53. Found: C, 59.37; H, 5.26; N, 4.55.

Mo(*N*-2,6-Me_2-C_6H_3)(CH(C_5H_4N))(IMes)(OTf)(*O*-2-Cl-C_6H_4), (Mo-14)

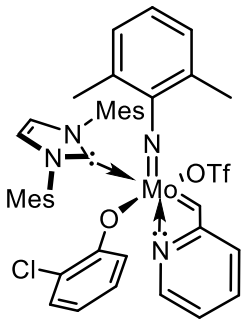

Mo(*N*-2,6-Me_2-C_6H_3)(CHCMe_2Ph)(IMes)(OTf)(*O*-2-Cl-C_6H_4) (0.050 g, 0.054 mmol) was dissolved in 4 mL dichloromethane and the solution was cooled to – 40 °C. A solution of 2-vinylpyridine (0.011 g, 0.108 mmol) in 1 mL dichloromethane was added was added dropwise to the educt solution. The reaction mixture was stirred for 30 min at room temperature. Then, all volatiles were removed under vacuum and resulting residue was washed with pentane until it solidifies. The product was crystallized from mixture of CH_2Cl_2/*n*-pentane to obtain crystalline orange solid (0.031 g, 0.035 mmol, 65% yield).

^{1}H NMR (400 MHz, CD_2Cl_2) δ 13.33 (s, $^1J_{CH}$ = 160.8 Hz, 1H, Mo=CH), 7.64 – 7.48 (m, 2H), 7.18 (s, 2H), 7.16 – 7.03 (m, 3H), 7.02 – 6.95 (m, 3H), 6.78 (s, 3H), 6.69 – 6.61 (m, 1H), 6.47 (d, 2H), 6.07 (d, *J* = 7.7 Hz, 1H), 2.32 (s, 6H), 2.17 (s, 6H), 2.12 (s, 6H), 1.87 (s, 6H). **^{13}C NMR** (101 MHz, CD_2Cl_2) δ 292.7 (Mo=*C*H), 184.7 (N*C*N-NHC), 162.6, 162.3, 155.8, 144.9, 140.9, 140.6, 139.5, 136.0, 135.7, 135.6, 130.4, 129.8, 129.7, 129.2, 127.8, 127.7, 125.7, 124.3, 121.5, 118.8, 114.4, 21.3, 21.2, 19.4, 18.5, 18.5, 18.3. $^1J_{CF}$ coupling in ^{13}C NMR could not be determined due to overlap of signals. **^{19}F NMR** (376 MHz, CD_2Cl_2) δ -78.88 (s, 3F, OTf) **Elemental analysis** (%) calcd. for $C_{42}H_{42}ClF_3MoN_4O_4S$: C, 56.85; H, 4.77; N, 6.31. Found: C, 57.22; H, 4.888; N, 6.21.

Mo(*N*-3,5-Me$_2$-C$_6$H$_3$)(CH(-2-*N*(Me$_2$)-C$_6$H$_4$)(IMes)(OTf)$_2$, (Mo-15)

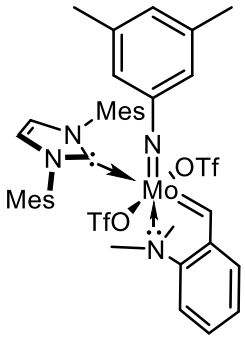

Mo(N-3,5-Me$_2$C$_6$H$_3$)(CHCMe$_2$Ph)(IMes)(OTf)$_2$ (0.100 g, 0.105 mmol) was dissolved in 5 mL dichloromethane and the solution was cooled in at -40 °C. A cold solution of 2-vinyl-*N*,*N*-dimethylaniline (0.031 g, 0.210 mmol) in 1 mL dichloromethane was added dropwise to the educt solution. The reaction mixture was stirred for 2 h at room temperature. Then, all volatiles were removed under vacuum and the resulting residue was washed with pentane until it solidifies. The product was crystallized from mixture of CH_2Cl_2/diethyl ether/*n*-pentane to obtain light orange solid (0.081 g, 0.085 mmol, 81% yield).

^{1}H NMR (400 MHz, CD_2Cl_2) δ 13.28 (s, $^1J_{CH}$ = 150.5 Hz, 1H, Mo=CH), 7.42 (s, 2H), 7.38 (m, 1H), 7.21 (m, 2H), 7.06 (s, 2H), 7.02 (s, 3H), 6.76 (s, 2H), 6.02 (m, 1H), 2.88 (s, 3H, N-*Me*), 2.78 (s, 3H, N-*Me*), 2.41 (s, 6H, *Me*-Mes), 2.37 (s, 6H, *Me*-Mes), 2.02 (s, 6H, *Me*-Ar), 1.66 (s, 6H, *Me*-Mes). **^{13}C NMR** (101 MHz, CD_2Cl_2) δ 307.9 (d, *J* = 5.8 Hz, Mo=*C*H), 186.3 (N*C*N-NHC), 156.4, 155.2, 142.7, 140.4, 138.3, 136.8, 135.4, 134.8, 132.4, 131.8, 130.8, 130.6, 127.5, 126.8, 126.0, 123.6, 120.5, 120.0 (q, $^1J_{CF}$ = 320.3 Hz, CF_3 OTf), 119.5 (q, $^2J_{CF}$ = 318.5 Hz, CF_3 OTf), 53.0, 51.2, 21.5, 21.5, 21.4, 21.4, 19.2, 18.8. **^{19}F NMR** (376 MHz, CD_2Cl_2) δ -75.56, -78.25. **Elemental analysis** (%) calcd. for $C_{40}H_{44}F_6MoN_4O_6S_2$: C, 50.53; H, 4.66; N, 5.89. Found: C, 50.86; H, 4.87; N, 5.99.

5.5.3 Swelling Studies

Determination of the degree of swelling for catalysts Mo-8 – Mo-11 and Mo-14 – Mo-15: The reaction was carried out in a glass vial. The catalyst (660 mol-ppm w.r.t. DCPD) was suspended in CH_2Cl_2 (10 µL) and DCPD (approx. 300 mg) was added. The mixture was stirred at indicated temperature (Table 6) for about 1 hour. The polymer was dried under vacuum for overnight. The mass of the polymer was noted (m_0). Subsequently, 3 mL toluene was added and the mixture was stored at room temperature for two days. Further, the toluene was decanted and the weight of the swollen polymer was determined (m_t).

Table 6. Monomer conversion and degree of swelling (*Q*) of poly(DCPD) obtained from the polymerization of DCPD with pre-catalysts **Mo-8 – Mo-11** and **Mo-14 – Mo-15.**

Pre-catalyst	Reaction Temp. (°C)	Monomer Conversion(i) (%)	*Q* (%)
Mo-8	120	68	75
Mo-9	80	94	15
Mo-10	120	61	15
Mo-11	120	58	5
Mo-14	80	62	75
Mo-15	80	98	25

(i) In the separate reaction, residual monomer extracted in toluene and conversion was determined by the GC-MS using *n*-dodecane as an internal standard; Degree of swelling, $Q = \frac{(m_q - m_0)}{m_o}$ with m_q = mass of swollen polymer and m_0 = initial mass of polymer.

5.5.4 DSC Measurements

Determination of T_{onset} and $T_{exo,max}$ for pre-catalysts Mo-8 – Mo-11 and Mo-14 – Mo-15: The pre-catalyst (660 ppm(mol.) w.r.t. DCPD) was weighed in a glass vial and CH_2Cl_2 (10 µL) was added to suspend the catalyst and DCPD (500 mg) was added. The mixture was stirred at room temperature for five minutes and sample for DSC measurement was withdrawn (2-4 mg) in a pre-heated DSC pan. The DSC pans were pressed inside the glove box. Then, sample was subjected to DSC measurements. T_{onset} was defined as the temperature where polymerization starts and $T_{exo,max}$ was defined as the minimum of DSC curve.

Table 7. $T_{exo,max}$ and reaction enthalpies for pre-catalysts **Mo-14** at different catalyst loadings.

Loading ppm (mol.)	T_{exo} (°C)	T_{onset} (°C)[i]	ΔH (J·g^{-1})[ii]
660	128	76	-187
300	144	91	-164
150	154	95	-115

Pre-catalyst/CH_2Cl_2/DCPD, CH_2Cl_2 - 10 µL, Heating program: 0 °C for one minute, 0 °C → 250 °C (10 K·min^{-1}) (i) temperature at which the heat flow begins to drop.; (ii) derived from integration of the area under the curve by Pyris Manager (Perkin Elmer).

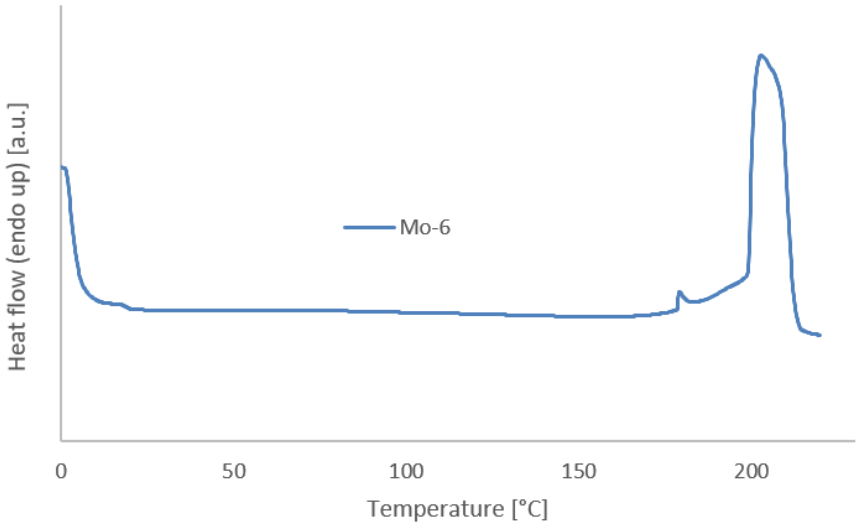

Figure 39. Temperature scan DSC thermogram of a sample of **Mo-6**/CH_2Cl_2/DCPD, CH_2Cl_2 – 10 µL, Cat. Loading – 660 ppm (mol.) Heating program: 0 °C for one minute, 0 °C → 220 °C (10 K·min^{-1}).

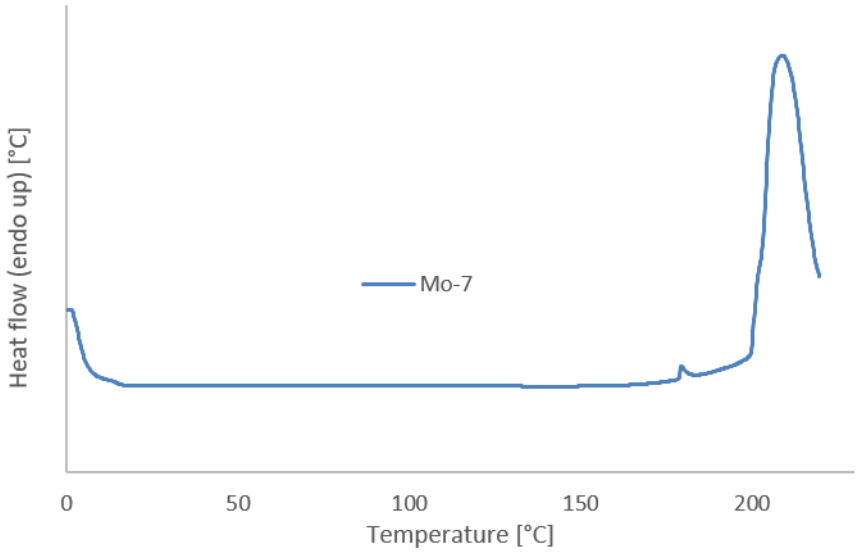

Figure 40. Temperature scan DSC thermogram of a sample of **Mo-7**/CH_2Cl_2/DCPD, CH_2Cl_2 – 10 µL, Cat. Loading – 660 ppm (mol.) Heating program: 0 °C for one minute, 0 °C → 220 °C (10 $K \cdot min^{-1}$).

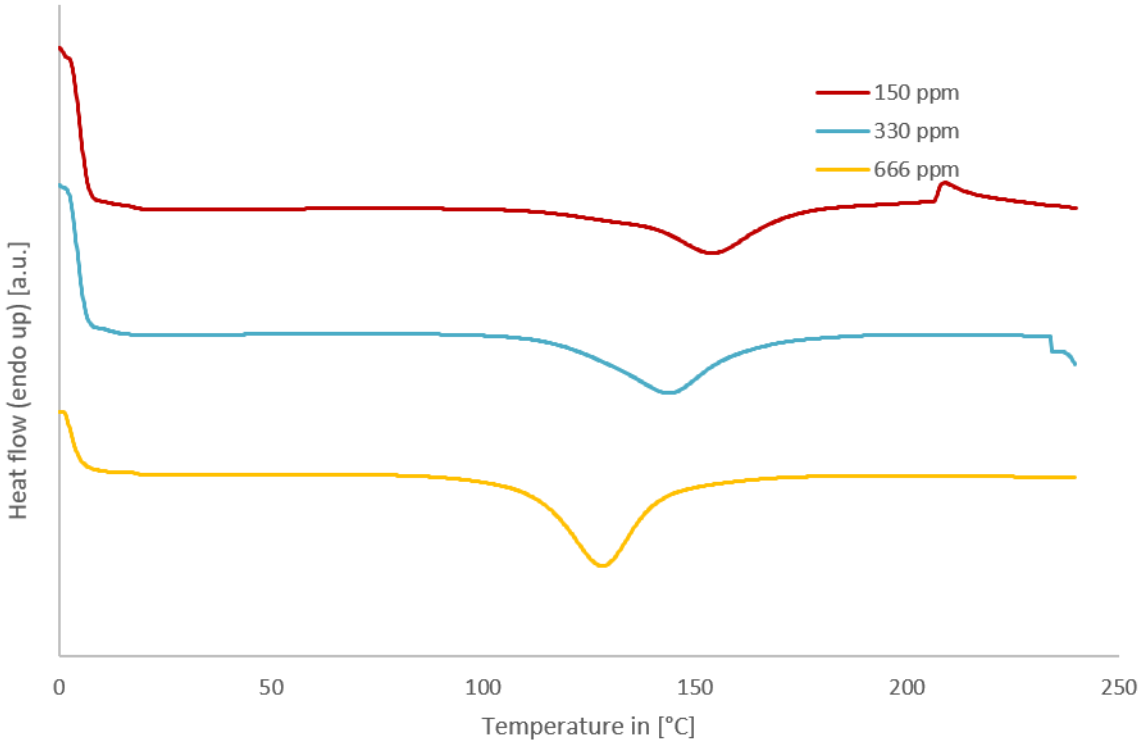

Figure 41. Temperature scan DSC thermogram of chelated hexa-coordinated pre-catalysts **Mo-14** at different catalyst loading. Pre-catalyst/CH_2Cl_2/DCPD, CH_2Cl_2 – 10 µlit., Cat. Loading – 660 ppm (mol.) Heating program: 0 °C for one minute, 0 °C → 250 °C (10 $K \cdot min^{-1}$).

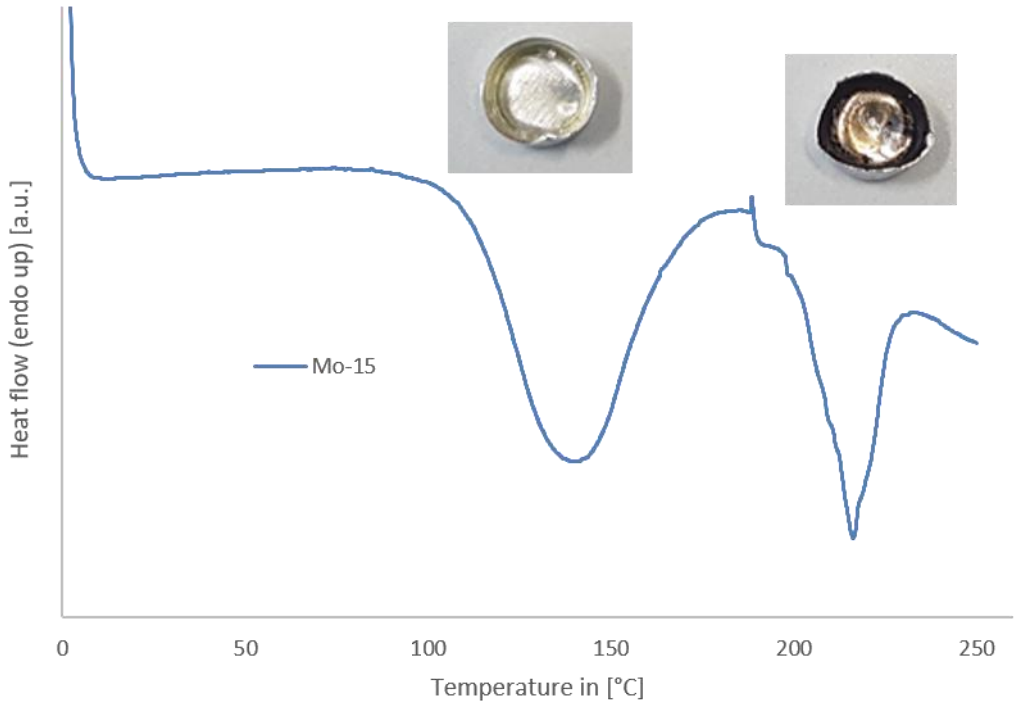

Figure 42. Temperature scan DSC thermogram of **Mo-15.** Pre-catalyst/CH_2Cl_2/DCPD, CH_2Cl_2 – 10 µlL, cat. loading – 660 ppm (mol.) Heating program. 0°C for one minute, 0°C → 250°C (5 $K \cdot min^{-1}$).

5.6 2,6-Difluorophenylimido Molybdenum Alkylidene NHC Complexes: Air Stable, Functional Group Tolerant Catalysts

5.6.1 Synthesis of Catalysts:

Mo(*N*-2,6-F_2-C_6H_3)$_2$(Cl)$_2$(DME), (Mo-16)

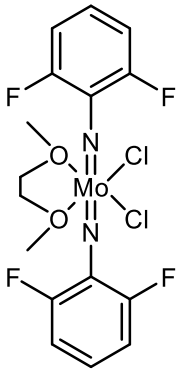

Ammonium dimolybdate (1.00 g, 2.94 mmol) was suspended in 30 mL acetonitrile and triethylamine (2.38 g, 23.52 mmol), chlorotrimethysilane (5.45 g, 50.17 mmol), 2,6-difluoroaniline (1.52 g, 11.77 mmol) were added sequentially under stirring. The reaction mixture was stirred at room temperature for 36 h to afford dark red solution with some precipitate. The solvent was removed in *vacuo* and all solids were stirred with a minimum amount of 1,2-dimethoxyethane (DME) for 12 hours. The solvent was removed in *vacuo* and co-evaporated with *n*-pentane. The resulting black-red solid was extracted with a Soxhlet apparatus using DME as a solvent. The DME was removed in *vacuo* and a minimum amount of CH_2Cl_2 was added to the obtained black-red solid and stirred for 1 hour and crystalline red solid was filtered as a product. The product was washed with cold CH_2Cl_2 and recrystallized from mixture of CH_2Cl_2/diethyl ether to get crystalline bright orange solid (0.72 g, 1.38 mmol, 47% yield).

^{1}H NMR (400 MHz, CD_2Cl_2) δ = 7.11 (m, 2H), 6.92 (m, 4H), 4.01 (s, 4H), 3.99 (s, 6H) ppm. **^{13}C NMR** (101 MHz, CD_2Cl_2) δ = 158.3 (d, $^1J_{CF}$ = 256.6 Hz), 135.5, 129.2, 112.0, 72.0, 64.7 ppm. **^{19}F NMR** (376 MHz, CD_2Cl_2) δ = -117.37 (m, 4F) ppm. **Elemental analysis** (%) calcd. for $C_{16}H_{16}F_4MoN_2O_2$: C, 37.60; H, 3.16; N, 5.48. Found: C, 37.48; H, 3.45; N, 5.59.

Mo(*N*-2,6-F_2-C_6H_3)$_2$($CHCMe_2Ph$)$_2$, (Mo-17)

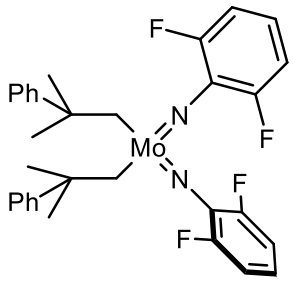

Mo(N-2,6-$F_2C_6H_3$)$_2Cl_2$(DME) (0.131 g, 0.25 mmol) was dissolved in 15 mL THF and cooled to -30 °C. Neophyl magnesium chloride (1.21 M in ether, 0.4 mL, 0.50 mmol) was added dropwise to the solution. The reaction mixture was stirred overnight at 25 – 30 °C and filtered through celite. The solvent was removed in *vacuo* and the red-orange solid was recrystallized from *n*-pentane (0.14 g, 0.23 mmol, 92% yield).

^{1}H NMR (400 MHz, CD_2Cl_2) δ = 7.38 (m, 4H) 7.22 (m, 4H), 7.08 (m, 2H), 6.97 (m, 2H), 6.82 (m, 4H), 1.97 (s, 4H), 1.40 (s, 12H) ppm. **^{13}C NMR** (101 MHz, CD_2Cl_2) δ = 156.6 (d, $^1J_{CF}$ = 252.1 Hz) 151.2, 135.2, 128.7, 126.3, 126.3, 125.1, 111.4, 83.4, 41.2, 32.2 ppm. **^{19}F NMR** (376 MHz, CD_2Cl_2) δ = -119.52 (m, 4F, Imido) ppm. **Elemental analysis** (%) calcd. for $C_{32}H_{32}F_4MoN_2$: C, 62.34; H, 5.23; N, 4.54. Found: C, 62.37; H, 5.39; N, 4.44.

Mo(*N*-2,6-F_2-C_6H_3)($CHCMe_2Ph$)(OTf)$_2$DME, (Mo-18)

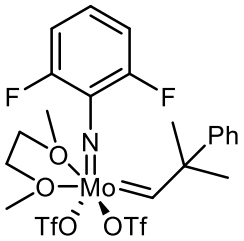

Mo(N-2,6-$F_2C_6H_3$)$_2$(CH_2CMe_2Ph)$_2$ (0.140 g, 0.23 mmol) was dissolved in 20 mL 1,2-dimethoxyethane (DME) and cooled to -30°C. Triflic acid (0.10 g, 0.69 mmol) in 1 mL of 1,2-dimethoxyethane was cooled to -30 °C. After an hour, the cooled triflic acid solution was added dropwise to the solution of adduct. The reaction mixture was stirred overnight and DME was evaporated in *vacuo*. To the residue, benzene was added and stirred for 15 min., subsequently, the reaction mixture was filtered through celite to remove the precipitate. The benzene was removed in *vacuo* and diethyl ether was added. The yellow precipitate was filtered and washed with cold diethyl

ether. Product was recrystallized from mixture of CH_2Cl_2/diethyl ether/*n*-pentane to obtain yellow crystalline solid (0.11 g, 0.15 mmol, 64% yield).

^{1}H NMR (400 MHz, CD_2Cl_2) δ = 14.74 (s, $^1J_{CH}$ = 127.5 Hz, 1H, Mo=CH, major isomer), 13.89 (s, J_{CH} = 121.2 Hz, 1H, Mo=CH, minor isomer), 7.47, 7.30, 7.19, 7.08, 6.98, 6.87, 6.82, 4.19, 4.11, 4.00, 3.88, 3.67, 3.60, 3.56, 1.83, 1.62, 1.50 ppm. It is difficult to assign the peaks as there is mixture of isomers. **^{13}C NMR** (101 MHz, CD_2Cl_2) δ = 335.5 (d, *J* = 32.8 Hz, Mo=CH, major isomer), 327.1 (d, *J* = 11.7 Hz, Mo=CH, minor isomer), 161.3 (dd, *J* = 260.9, 2.4 Hz), 160.9 (dd, *J* = 257.9, 2.6 Hz), 148.5, 147.0, 133.3 (t, *J* = 16.6 Hz), 131.3 (t, *J* = 9.6 Hz), 131.0 (t, *J* = 9.7 Hz), 129.0, 128.5, 127.7, 127.31, 127.30, 126.9, 120.1 (q, $^1J_{CF}$ = 317.6, OTf), 119.8 (qd, $^1J_{CF}$ = 317.7, 5.6 Hz, OTf), 112.7, 112.4, 79.0, 77.1, 75.0, 70.9, 65.7, 63.2, 61.7, 58.8, 58.8, 29.9, 29.6, 29.2 ppm. **^{19}F NMR** (376 MHz, CD_2Cl_2) δ = -77.31, -77.35, -78.24, -111.85, -114.36 ppm. **Elemental analysis** (%) calcd. for $C_{22}H_{25}F_8MoNO_8S_2$: C, 35.54; H, 3.39; N, 1.88. Found: C, 35.50; H, 3.56; N, 1.90.

Mo(*N*-2,6-F_2-C_6H_3)(CHCMe$_2$Ph)(IMes)(OTf)$_2$, (Mo-19)

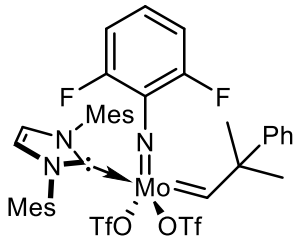

Mo(N-2,6-$F_2C_6H_3$)(CHCMe$_2$Ph)(OTf)$_2$(DME) (0.080 g, 0.11 mmol) was dissolved in 5 mL benzene and solution of 1,3-bis(2,4,6-trimethylphenyl)imidazol-2-ylidene (0.043 g, 0.11 mmol) in 1 mL benzene was added dropwise. The reaction mixture was stirred for 3 h at room temperature. The solvent was removed in *vacuo* and yellow solid was crystallized from mixture of CH_2Cl_2/n-pentane to obtain yellow crystalline solid (0.070 g, 0.07 mmol, 67% yield).

^{1}H NMR (400 MHz, CD_2Cl_2) δ = 13.32 (s, $^1J_{CH}$ = 123.4 Hz, 1H, Mo=*C*H), 7.26 (m, 3H), 7.22 (m, 1H), 7.21 (s, 2H), 7.09 (m, 2H), 6.83 (m, 2H), 6.73 (br s, 2H), 6.63 (br s, 2H), 2.15 (s, 6H), 2.03 (s, 6H), 2.00 (s, 6H), 1.71 (s, 3H), 1.69 (s, 3H) ppm. **^{13}C NMR** (101 MHz, CD_2Cl_2) δ = 320.4 (Mo=*C*H), 184.0 (NC*N*-NHC), 160.2 (d, $^1J_{CF}$ = 258.8 Hz), 148.1, 141.0, 136.0, 135.3, 135.1, 134.0, 131.2, 130.4, 129.7, 128.8, 127.0, 126.0, 126.0, 119.9 (q, $^1J_{CF}$ = 318.8 Hz, OTf), 118.8 (qd, $^1J_{CF}$ = 317.8 Hz, OTf), 111.8

(m, *m*-Ar-Imido), 56.5, 35.1, 27.9, 21.4, 18.49, 18.44 ppm. **^{19}F NMR** (376 MHz, CD_2Cl_2) δ = -75.77 (br s, 3F, OTf), -77.02 (br s, 3F, OTf), -109.53 (br s, 2F, Imido) ppm. **Elemental analysis** (%) calcd. for $C_{39}H_{39}F_8MoN_3O_6S_2$: C, 48.91; H, 4.10; N, 4.39. Found: C, 48.65; H, 4.21; N, 4.41.

[Mo(*N*-2,6-F_2-C_6H_3)(CHCMe$_2$Ph)(IMes)(OTf)(MeCN)][B(Ar^F)$_4$], (Mo-20)

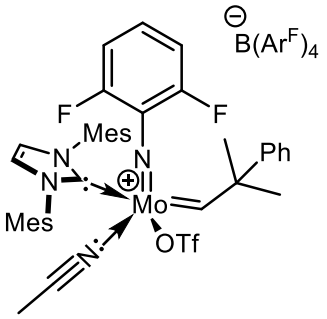

Mo(N-2,6-$F_2C_6H_3$)(CHCMe$_2$Ph)(OTf)$_2$(IMes) (0.050 g, 0.052 mmol) was dissolved in 4 ml dichloromethane and cooled to -30 °C. Then, AgB(Ar^F)$_4$·3CH_3CN (0.057 g, 0.052 mmol) was added in small portions and the reaction mixture was stirred for 2 h at room temperature. The reaction mixture was filtered through a pad of celite and CH_2Cl_2 was removed in *vacuo*. The residue was co-evaporated with pentane to yield yellow solid. The product was crystallized from a mixture of CH_2Cl_2/diethyl ether/n-pentane to obtain crystalline yellow solid (0.080 g, 0.045 mmol, 89% yield).

^{1}H NMR (400 MHz, CD_2Cl_2) δ = 13.26 (s, $^1J_{CH}$ = 124.0 Hz, 1H, Mo=CH), 7.73 (br m, 8H, *o*-Ar-B(Ar^F)$_4$), 7.56 (br s, 4H, *p*-Ar-B(Ar^F)$_4$), 7.33 (s, 2H), 7.30 (m, 1H), 7.22 (m, 2H), 7.15 (m, 1H), 7.07 (m, 2H), 6.95 (s, 2H), 6.88 (br m), 7.00 – 6.35 (br s, 2H), 2.22 (s, 6H), 2.05 (br s, 12H), 1.87 (s, 3H), 1.78 (s, 3H), 1.10 (s, 3H) ppm. **^{13}C NMR** (101 MHz, CD_2Cl_2) δ = 328.6 (Mo=*C*H), 182.8 (N*C*N-NHC), 162.1 (q, $^1J_{CB}$ = 50.0 Hz), 144.2, 141.5, 135.9, 135.2, 134.8, 134.4, 132.7, 130.6, 130.1, 129.8, 129.2 (qq, $^2J_{CF}$ = 31.2 Hz, $^3J_{CB}$ = 2.9 Hz, *m*-Ar-B(Ar^F)$_4$), 129.0, 127.5, 126.4, 125.8, 125.0 (q, $^1J_{CF}$ = 272.4 Hz, CF_3-B(Ar^F)$_4$), 119.5 (q, $^1J_{CF}$ = 318.5 Hz, OTf), 117.9 (sept, $^3J_{CF}$ = 3.6 Hz, *p*-Ar-B(Ar^F)$_4$), 112.3 (dd, J_{CF} = 19.5, 3.1 Hz, *m*-Ar-Imido), 56.5, 28.5, 27.8, 21.3, 18.1, 3.0 (*Me*CN) ppm. **^{19}F NMR** (376 MHz, CD_2Cl_2) δ = -62.76 (s, 24F, B(Ar^F)$_4$), -76.28 (s, 3F, OTf), -111.14 (br s, 2F, Imido) ppm. **Elemental analysis** (%) calcd. for $C_{72}H_{54}BF_{29}MoN_4O_3S$: C, 50.48; H, 3.18; N, 3.27. Found: C, 50.52; H, 3.23; N, 3.32.

Mo(*N*-2,6-F_2-C_6H_3)(CHCMe_2Ph)(IMesH_2)(OTf)$_2$, (Mo-21)

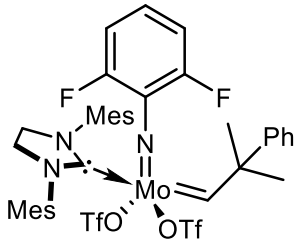

Mo(N-2,6-$F_2C_6H_3$)(CHCMe_2Ph)(OTf)$_2$(DME) (0.103 g, 0.14 mmol) was dissolved in 6 mL benzene and a solution of 1,3-bis(2,4,6-trimethylphenyl)-4,5-dihydroimidazol-2-ylidene (0.043 g, 0.14 mmol) in 1 mL benzene was added dropwise. The reaction mixture was stirred for 3 h at room temperature. The solvent was removed in *vacuo* and the yellow solid was crystallized from a mixture of CH_2Cl_2/*n*-pentane to obtain a yellow crystalline solid (0.081 g, 0.084 mmol, 60% yield).

^{1}H NMR (400 MHz, CD_2Cl_2) δ = 13.27 (s, $^1J_{CH}$ = 123.6 Hz, 1H, Mo=CH), 7.23 (m, 4H), 7.05 (m, 2H), 6.83 (m, 2H), 6.71 (br s, 2H), 6.58 (s, 2H), 4.00 (m, 4H), 2.27 (s, 12H), 2.11 (s, 6H), 1.65 (s, 3H), 1.64 (s, 3H) ppm. **^{13}C NMR** (101 MHz, CD_2Cl_2) δ = 321.5 (Mo=*C*H), 208.2 (N*C*N-NHC), 160.3 (d, $^1J_{CF}$ = 259.7 Hz), 148.1, 140.2, 136.7, 136.1, 135.1, 134.0, 131.3, 130.7, 130.1, 128.8, 127.0, 126.0, 120.0 (q, $^1J_{CF}$ = 318.4 Hz, OTf), 111.6 (dd, J_{CF} = 19.9, 3.1 Hz, *m*-Ar-Imido), 56.6, 52.8, 34.8, 27.9, 21.3, 18.8, 18.6 ppm. **^{19}F NMR** (376 MHz, CD_2Cl_2) δ = -75.55 (s, 3F, OTf), -77.06 (s, 3F, OTf), -109.15 (s, 2F, Imido) ppm. Despite numerous efforts, only inconsistent elemental analysis data were obtained.

[Mo(*N*-2,6-F_2-C_6H_3)(CHCMe_2Ph)(IMesH_2)(OTf)(MeCN)][B(Ar^F)$_4$], (Mo-22)

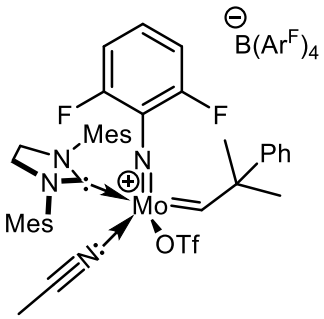

Mo(N-2,6-$F_2C_6H_3$)(CHCMe_2Ph)(OTf)$_2$(IMesH_2) (0.050 g, 0.052 mmol) was dissolved in 4 ml dichloromethane and cooled to -30 °C for about 30 min. Then AgB(Ar^F)$_4$·3CH_3CN (0.057 g, 0.052 mmol) was added in small portions and the

reaction mixture was stirred for 2 h at room temperature. The reaction mixture was filtered through a pad of celite and CH_2Cl_2 was removed in *vacuo*. The residue was co-evaporated with pentane to yield a yellow solid. The product was crystallized from a mixture of CH_2Cl_2/diethyl ether/*n*-pentane to obtain a crystalline yellow solid (0.070 g, 0.041 mmol, 78% yield).

^{1}H NMR (400 MHz, CD_2Cl_2) δ = 13.29 (s, $^1J_{CH}$ = 125.3 Hz, 1H, Mo=CH), 7.73 (br m, 8H, *o*-Ar-B(Ar^F)$_4$), 7.57 (br s, 4H, *p*-Ar-B(Ar^F)$_4$), 7.33 (tt, *J* = 8.5, 6.2 Hz, 1H), 7.19 (m, 2H), 7.13 (m, 1H), 7.03 (m, 2H), 6.93 (s, 2H), 6.90 (br m, 2H), 7.00 – 6.35 (br s, 2H), 4.09 (m, 4H), 2.32 (s, 6H), 2.20 (br s, 12H), 1.87 (s, 3H), 1.74 (s, 3H), 0.98 (s, 3H) ppm. **^{13}C NMR** (101 MHz, CD_2Cl_2) δ = 330.1 (Mo=*C*H), 206.4 (N*C*N-NHC), 162.3 (q, $^1J_{CB}$ = 50.0 Hz, *ipso*-Ar-B(Ar^F)$_4$), 144.5, 141.0, 136.9, 135.4 (br), 133.0, 132.7, 131.1, 130.5, 130.4 (br), 129.4 (dd, $^2J_{CF}$ = 31.6 Hz, $^3J_{CB}$ = 3.3 Hz, *m*-Ar-B(Ar^F)$_4$), 129.0, 127.6, 126.5, 125.5, 122.9 (q, $^1J_{CF}$ = 318.7 Hz, OTf), 118.0 (sept, $^3J_{CF}$ = 3.6 Hz, *p*-Ar-B(Ar^F)$_4$), 112.5 (dd, *J* = 19.5, 3.3 Hz), 56.9, 52.6, 28.6, 27.6, 21.3, 18.3, 3.0 (MeCN) ppm. **^{19}F NMR** (376 MHz, CD_2Cl_2) δ = -62.84 (s, 24F, B(Ar^F)$_4$), -75.90 (s, 3F, OTf), -110.26 (br s, 2F, Imido) ppm. **Elemental analysis** (%) calcd. for $C_{72}H_{56}BF_{29}MoN_4O_3S$: C, 50.42; H, 3.29; N, 3.27. Found: C, 50.52; H, 3.259; N, 3.22.

Mo(*N*-2,6-F_2-C_6H_3)(CHCMe_2Ph)(IMesCl_2)(OTf)$_2$, (Mo-23)

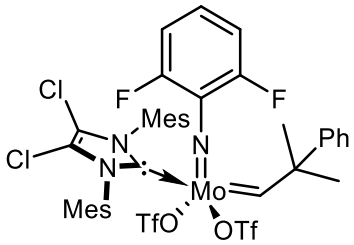

Mo(N-2,6-$F_2C_6H_3$)(CHCMe_2Ph)(OTf)$_2$(DME) (0.065 g, 0.088 mmol) was dissolved in 6 mL benzene and a solution of 1,3-dimesityl-4,5-dichloroimidazol-2-ylidene (0.033 g, 0.088 mmol) in 1 mL benzene was added dropwise. The reaction mixture was stirred for 3 h at room temperature. The solvent was removed in *vacuo* and a yellow solid was crystallized from mixture of CH_2Cl_2/n-pentane to obtain a yellow crystalline solid (0.060 g, 0.058 mmol, 66% yield).

^{1}H NMR (400 MHz, $CDCl_3$) δ = 13.35 (s, $^1J_{CH}$ = 122.8 Hz, 1H, Mo=CH), 7.26 (m, 2H), 7.21 (m, 2H), 7.11 (m, 2H), 6.79 (t, *J* = 8.3 Hz, 1H), 6.70 (br s, 2H), 6.65 (br s, 2H), 2.14 (s, 6H), 2.05 (s, 6H), 2.01 (s, 6H), 1.78 (s, 3H), 1.72 (s, 3H) ppm. **^{13}C NMR** (101

MHz, CD_2Cl_2) δ = 322.4 (Mo=CH), 184.6 (NCN-NHC), 159.8 (d, $^1J_{CF}$ = 260.4 Hz, *o*-Ar-Imido), 147.6, 141.6, 136.3, 135.5, 133.7, 131.8, 130.9, 130.2, 129.5, 128.5, 126.7, 125.6, 121.5, 119.3 (q, $^1J_{CF}$ = 318.7 Hz, OTf), 111.3 (dd, J_{CF} = 19.9, 3.4 Hz, *m*-Ar-Imido), 56.5, 35.4, 27.4, 21.3, 18.3, 18.1 ppm. J_{CF} coupling for second triflate in ^{13}C NMR could not be determined. **^{19}F NMR** (376 MHz, $CDCl_3$) δ = -75.14 (br s, 3F, OTf), -76.53 (br s, 3F, OTf), -108.75 (s, 2F, Imido) ppm. **Elemental analysis** (%) calcd. for $C_{39}H_{37}Cl_2F_8MoN_3O_6S_2$ + CH_2Cl_2: C, 43.22; H, 3.54; N, 3.78. Found: C, 43.30; H, 3.83; N, 3.94.

[Mo(*N*-2,6-F_2-C_6H_3)(CHCMe$_2$Ph)(IMesCl$_2$)(OTf)(MeCN)][B(Ar^F)$_4$], (Mo-24)

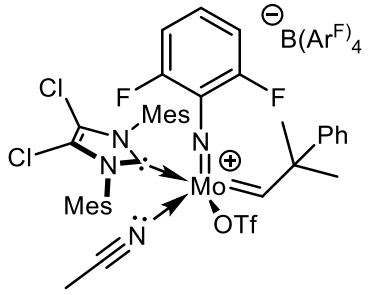

Mo(N-2,6-$F_2C_6H_3$)(CHCMe$_2$Ph)(OTf)$_2$(IMesCl$_2$) (0.056 g, 0.055 mmol) was dissolved in mixture of 4 ml dichloromethane containing a few drops of acetonitrile. Then, the mixture was cooled to -30 °C NaB(Ar^F)$_4$ (0.048 g, 0.055 mmol) was added in small portions and the reaction mixture was stirred for 2 h at room temperature. The reaction mixture was filtered through a pad of celite and CH_2Cl_2 was removed in *vacuo*. The residue was co-evaporated with pentane to yield a yellow solid. The product was crystallized from a mixture of CH_2Cl_2/*n*-pentane to obtain a crystalline yellow solid (0.088 g, 0.050 mmol, 90% yield).

^{1}H NMR (400 MHz, CD_2Cl_2) δ = 13.40 (s, $^1J_{CH}$ = 124.3 Hz, 1H, Mo=CH), 7.74 (br m, 8H, *o*-Ar-B(Ar^F)$_4$), 7.57 (br s, 4H, *p*-Ar-B(Ar^F)$_4$), 7.36 (tt, *J* = 8.6, 6.3 Hz, 1H), 7.20 (m, 3H), 7.07 (m, 2H), 7.02 (s, 2H), 6.92 (t, *J* = 8.5 Hz, 2H), 6.80 (br s, 2H), 2.26 (s, 6H), 2.08 (s, 6H), 2.04 (br s, 6H), 1.88 (s, 3H), 1.79 (s, 3H), 1.08 (s, 3H) ppm. **^{13}C NMR** (101 MHz, CD_2Cl_2) δ = 331.3 (Mo=*C*H), 182.9 (N*C*N-NHC), 162.3 (dd, $^1J_{CB}$ = 99.6, 49.8 Hz, *ipso*-Ar-B(Ar^F)$_4$), 144.3, 143.0, 136.8, 135.8, 135.4, 133.4, 132.8, 131.1, 130.3, 129.4 (dd, $^2J_{CF}$ = 31.6 Hz, $^3J_{CB}$ = 3.3 Hz, *m*-Ar-B(Ar^F)$_4$), 129.2, 127.8, 126.5, 123.8, 121.1, 118.0 (p, $^3J_{CF}$ = 4.0 Hz, *p*-Ar-B(Ar^F)$_4$), 112.5 (dd, *J* = 19.8, 3.3 Hz), 57.0, 28.6, 28.0, 21.4, 18.2, 3.0 (MeCN) ppm. J_{CF} coupling for triflate in ^{13}C NMR

could not be determined. **^{19}F NMR** (376 MHz, CD_2Cl_2) δ = -62.84 (s, 24F, $B(Ar^F)_4$), -76.00 (s, 3F, OTf), -110.77 (br s, 2F, Imido) ppm. **Elemental analysis** (%) calcd. for $C_{72}H_{52}BCl_2F_{29}MoN_4O_3S$: C, 48.53; H, 2.94; N, 3.14. Found: C, 48.64; H, 3.169; N, 3.04.

6. Literature

[1] J. Clayden, N. Greeves, S. Warren, P. Wothers, *Organic Chemistry, Oxford University Press* **2001**.

[2] D. Bourissou, O. Guerret, F. P. Gabbaï, G. Bertrand, *Chem. Rev.* **2000**, *100*, 39-92.

[3] P. de Frémont, N. Marion, S. P. Nolan, *Coord. Chem. Rev.* **2009**, *253*, 862-892.

[4] M. N. Hopkinson, C. Richter, M. Schedler, F. Glorius, *Nature* **2014**, *510*, 485-496.

[5] W. A. Herrmann, *Angew. Chem. Int. Ed.* **2002**, *41*, 1290-1309.

[6] X. Hu, Y. Tang, P. Gantzel, K. Meyer, *Organometallics* **2003**, *22*, 612-614.

[7] A. J. Arduengo, R. L. Harlow, M. Kline, *J. Am. Chem. Soc.* **1991**, *113*, 363-365.

[8] G. M. Weeresakare, Z. Liu, J. D. Rainier, *Org. Lett.* **2004**, *6*, 1625-1627.

[9] H. W. Wanzlick, E. Schikora, *Angew. Chem.* **1960**, *72*, 494.

[10] H. W. Wanzlick, *Angew. Chem. Int. Ed.* **1962**, *1*, 75-80.

[11] H. W. Wanzlick, H. J. Schonherr, *Angew. Chem. Int. Ed.* **1968**, *7*, 141-142.

[12] K. Öfele, *J. Organomet. Chem.* **1968**, *12*, 42-43.

[13] Z. Liu, J. D. Rainier, *Org. Lett.* **2005**, *7*, 131-133.

[14] A. J. Arduengo, J. R. Goerlich, W. J. Marshall, *J. Am. Chem. Soc.* **1995**, *117*, 11027-11028.

[15] M. Alcarazo, S. J. Roseblade, E. Alonso, R. Fernández, E. Alvarez, F. J. Lahoz, J. M. Lassaletta, *J. Am. Chem. Soc.* **2004**, *126*, 13242-13243.

[16] S. Saba, A. Brescia, M. K. Kaloustian, *Tetrahedron Lett.* **1991**, *32*, 5031-5034.

[17] D. Enders, H. Gielen, *J. Organomet. Chem.* **2001**, *617-618*, 70-80.

[18] W. A. Herrmann, L. J. Goossen, G. R. J. Artus, C. Köcher, *Organometallics* **1997**, *16*, 2472-2477.

[19] D. J. D. Wilson, S. A. Couchman, J. L. Dutton, *Inorg. Chem.* **2012**, *51*, 7657-7668.

[20] L. Cavallo, A. Correa, C. Costabile, H. Jacobsen, *J. Organomet. Chem.* **2005**, *690*, 5407-5413.

[21] D. J. Nelson, S. P. Nolan, *Chem. Soc. Rev.* **2013**, *42*, 6723-6753.

[22] C. A. Tolman, *Chem. Rev.* **1977**, *77*, 313-348.

[23] A. C. Hillier, W. J. Sommer, B. S. Yong, J. L. Petersen, L. Cavallo, S. P. Nolan, *Organometallics* **2003**, *22*, 4322-4326.

[24] A. Poater, B. Cosenza, A. Correa, S. Giudice, F. Ragone, V. Scarano, L. Cavallo, *Eur. J. Inorg. Chem.* **2009**, 1759-1766.

[25] H. Clavier, S. P. Nolan, *Chem. Commun.* **2010**, *46*, 841-861.

[26] E. O. Fischer, A. Maasböl, *Angew. Chem. Int. Ed.* **1964**, *3*, 580-581.

[27] D. J. Cardin, B. Cetinkaya, M. F. Lappert, *Chem. Rev.* **1972**, *72*, 545-574.

[28] E. O. Fischer, *Pure Appl. Chem.* **1972**, *30*, 353-372.

[29] E. O. Fischer, in *Adv. Organomet. Chem., Vol. 14* (Eds.: F. G. A. Stone, R. West), Academic Press, **1976**, pp. 1-32.

[30] S. F. Vyboishchikov, G. Frenking, *Chem. Eur. J.* **1998**, *4*, 1428-1438.
[31] R. R. Schrock, *J. Am. Chem. Soc.* **1974**, *96*, 6796-6797.
[32] N. Calderon, *Acc. Chem. Res.* **1972**, *5*, 127-132.
[33] H. S. Eleuterio, *US Patent no. US3074918* **1966**.
[34] H. S. Eleuterio, *J. Mol. Catal.* **1991**, *65*, 55-61.
[35] R. L. Banks, G. C. Bailey, *Ind. Eng. Chem. Res.* **1964**, *3*, 170-173.
[36] L. F. Heckelsberg, R. L. Banks, G. C. Bailey, *Ind. Eng. Chem. Prod. Res. Dev.* **1969**, *8*, 259-261.
[37] N. Calderon, H. Y. Chen, K. W. Scott, *Tetrahedron Lett.* **1967**, *8*, 3327-3329.
[38] Y. Chauvin, *Angew. Chem. Int. Ed.* **2006**, *45*, 3740-3747.
[39] R. H. Grubbs, *Angew. Chem. Int. Ed.* **2006**, *45*, 3760-3765.
[40] R. R. Schrock, *Angew. Chem. Int. Ed.* **2006**, *45*, 3748-3759.
[41] P. Jean-Louis Hérisson, Y. Chauvin, *Die Makromol. Chemie* **1971**, *141*, 161-176.
[42] F. N. Tebbe, G. W. Parshall, G. S. Reddy, *J. Am. Chem. Soc.* **1978**, *100*, 3611-3613.
[43] F. N. Tebbe, G. W. Parshall, D. W. Ovenall, *J. Am. Chem. Soc.* **1979**, *101*, 5074-5075.
[44] F. N. Tebbe, R. L. Harlow, *J. Am. Chem. Soc.* **1980**, *102*, 6149-6151.
[45] T. R. Howard, J. B. Lee, R. H. Grubbs, *J. Am. Chem. Soc.* **1980**, *102*, 6876-6878.
[46] J. B. Lee, K. C. Ott, R. H. Grubbs, *J. Am. Chem. Soc.* **1982**, *104*, 7491-7496.
[47] D. A. Straus, R. H. Grubbs, *Organometallics* **1982**, *1*, 1658-1661.
[48] R. Schrock, S. Rocklage, J. Wengrovius, G. Rupprecht, J. Fellmann, *J. Mol. Catal.* **1980**, *8*, 73-83.
[49] R. R. Schrock, *Dalton Trans.* **2011**, *40*, 7484-7495.
[50] M. M. Flook, J. Börner, S. M. Kilyanek, L. C. H. Gerber, R. R. Schrock, *Organometallics* **2012**, *31*, 6231-6243.
[51] G. S. Weatherhead, J. G. Ford, E. J. Alexanian, R. R. Schrock, A. H. Hoveyda, *J. Am. Chem. Soc.* **2000**, *122*, 1828-1829.
[52] M. F. Schneider, S. Blechert, *Angew. Chem. Int. Ed.* **1996**, *35*, 411-412.
[53] M. M. Faul, B. E. Huff, *Chem. Rev.* **2000**, *100*, 2407-2474.
[54] J. P. Wolfe, M. B. Hay, *Tetrahedron* **2007**, *63*, 261-290.
[55] D. G. Gillingham, A. H. Hoveyda, *Angew. Chem. Int. Ed.* **2007**, *46*, 3860-3864.
[56] P. Walejko, M. Dabrowski, L. Szczepaniak, J. W. Morzycki, S. Witkowski, *Beilstein J. Org. Chem.* **2015**, *11*, 1893-1901.
[57] M. J. Koh, R. K. Khan, S. Torker, A. H. Hoveyda, *Angew. Chem. Int. Ed.* **2014**, *53*, 1968-1972.
[58] R. E. Giudici, A. H. Hoveyda, *J. Am. Chem. Soc.* **2007**, *129*, 3824-3825.
[59] R. R. Schrock, J. S. Murdzek, G. C. Bazan, J. Robbins, M. DiMare, M. O'Regan, *J. Am. Chem. Soc.* **1990**, *112*, 3875-3886.
[60] P. Schwab, M. B. France, J. W. Ziller, R. H. Grubbs, *Angew. Chem. Int. Ed.* **1995**, *34*, 2039-2041.

[61] M. R. Buchmeiser, *Chem. Rev.* **2000**, *100*, 1565-1604.
[62] R. R. Schrock, A. H. Hoveyda, *Angew. Chem. Int. Ed.* **2003**, *42*, 4592-4633.
[63] O. M. Ogba, N. C. Warner, D. J. O'Leary, R. H. Grubbs, *Chem. Soc. Rev.* **2018**, *47*, 4510-4544.
[64] R. R. Schrock, *Acc. Chem. Res.* **1979**, *12*, 98-104.
[65] J. Feldman, R. R. Schrock, in *Prog. Inorg. Chem.*, **1991**, pp. 1-74.
[66] R. R. Schrock, R. T. DePue, J. Feldman, C. J. Schaverien, J. C. Dewan, A. H. Liu, *J. Am. Chem. Soc.* **1988**, *110*, 1423-1435.
[67] R. R. Schrock, R. T. DePue, J. Feldman, K. B. Yap, D. C. Yang, W. M. Davis, L. Park, M. DiMare, M. Schofield, *Organometallics* **1990**, *9*, 2262-2275.
[68] D. L. Morrison, D. E. Wigley, *Inorg. Chem.* **1995**, *34*, 2610-2616.
[69] H. H. Fox, K. B. Yap, J. Robbins, S. Cai, R. R. Schrock, *Inorg. Chem.* **1992**, *31*, 2287-2289.
[70] J. H. Oskam, H. H. Fox, K. B. Yap, D. H. McConville, R. O`Dell, B. J. Lichtenstein, R. R. Schrock, *J. Organomet. Chem.* **1993**, *459*, 185-198.
[71] P. Barrie, T. A. Coffey, G. D. Forster, G. Hogarth, *Dalton Trans.* **1999**, 4519-4528.
[72] R. Toreki, R. R. Schrock, W. M. Davis, *J. Am. Chem. Soc.* **1992**, *114*, 3367-3380.
[73] J. H. Oskam, R. R. Schrock, *J. Am. Chem. Soc.* **1993**, *115*, 11831-11845.
[74] J. H. Oskam, R. R. Schrock, *J. Am. Chem. Soc.* **1992**, *114*, 7588-7590.
[75] D. H. McConville, J. R. Wolf, R. R. Schrock, *J. Am. Chem. Soc.* **1993**, *115*, 4413-4414.
[76] J. B. Alexander, D. S. La, D. R. Cefalo, A. H. Hoveyda, R. R. Schrock, *J. Am. Chem. Soc.* **1998**, *120*, 4041-4042.
[77] D. S. La, J. B. Alexander, D. R. Cefalo, D. D. Graf, A. H. Hoveyda, R. R. Schrock, *J. Am. Chem. Soc.* **1998**, *120*, 9720-9721.
[78] S. C. Marinescu, R. Singh, A. S. Hock, K. M. Wampler, R. R. Schrock, P. Müller, *Organometallics* **2008**, *27*, 6570-6578.
[79] A. S. Hock, R. R. Schrock, A. H. Hoveyda, *J. Am. Chem. Soc.* **2006**, *128*, 16373-16375.
[80] R. Singh, R. R. Schrock, P. Müller, A. H. Hoveyda, *J. Am. Chem. Soc.* **2007**, *129*, 12654-12655.
[81] S. J. Meek, R. V. O'Brien, J. Llaveria, R. R. Schrock, A. H. Hoveyda, *Nature* **2011**, *471*, 461-466.
[82] A. Cordova, R. Rios, *Angew. Chem. Int. Ed.* **2009**, *48*, 8827-8831.
[83] Z. Ma, F. Zaera, in *Encycl. Inorg. Bioinorg. Chem.*, **2014**, pp. 1-16.
[84] K. C. Hultzsch, J. A. Jernelius, A. H. Hoveyda, R. R. Schrock, *Angew. Chem. Int. Ed.* **2002**, *41*, 589-593.
[85] R. M. Kröll, N. Schuler, S. Lubbad, M. R. Buchmeiser, *Chem. Commun.* **2003**, 2742-2743.
[86] D. Wang, R. Kröll, M. Mayr, K. Wurst, M. R. Buchmeiser, *Adv. Synth. Catal.* **2006**, *348*, 1567-1579.

[87] F. Blanc, J. Thivolle-Cazat, J.-M. Basset, C. Copéret, A. S. Hock, Z. J. Tonzetich, R. R. Schrock, *J. Am. Chem. Soc.* **2007**, *129*, 1044-1045.
[88] C. Copéret, *Dalton Trans.* **2007**, 5498-5504.
[89] M. P. Conley, W. P. Forrest, V. Mougel, C. Copéret, R. R. Schrock, *Angew. Chem. Int. Ed.* **2014**, *53*, 14221-14224.
[90] S. T. Nguyen, L. K. Johnson, R. H. Grubbs, J. W. Ziller, *J. Am. Chem. Soc.* **1992**, *114*, 3974-3975.
[91] T. M. Trnka, R. H. Grubbs, *Acc. Chem. Res.* **2001**, *34*, 18-29.
[92] P. Schwab, R. H. Grubbs, J. W. Ziller, *J. Am. Chem. Soc.* **1996**, *118*, 100-110.
[93] M. Scholl, S. Ding, C. W. Lee, R. H. Grubbs, *Org. Lett.* **1999**, *1*, 953-956.
[94] J. Huang, E. D. Stevens, S. P. Nolan, J. L. Petersen, *J. Am. Chem. Soc.* **1999**, *121*, 2674-2678.
[95] T. Weskamp, W. C. Schattenmann, M. Spiegler, W. A. Herrmann, *Angew. Chem. Int. Ed.* **1998**, *37*, 2490-2493.
[96] J. S. Kingsbury, J. P. A. Harrity, P. J. Bonitatebus, A. H. Hoveyda, *J. Am. Chem. Soc.* **1999**, *121*, 791-799.
[97] S. B. Garber, J. S. Kingsbury, B. L. Gray, A. H. Hoveyda, *J. Am. Chem. Soc.* **2000**, *122*, 8168-8179.
[98] J. O. Krause, O. Nuyken, K. Wurst, M. R. Buchmeiser, *Chem. Eur. J.* **2004**, *10*, 777-784.
[99] A. J. Jiang, R. R. Schrock, P. Müller, *Organometallics* **2008**, *27*, 4428-4438.
[100] Z. J. Tonzetich, A. J. Jiang, R. R. Schrock, P. Müller, *Organometallics* **2006**, *25*, 4725-4727.
[101] M. R. Buchmeiser, S. Sen, J. Unold, W. Frey, *Angew.Chem. Int. Ed.* **2014**, *53*, 9384-9388.
[102] M. Benedikter, J. Musso, M. K. Kesharwani, K. L. Sterz, I. Elser, F. Ziegler, F. Fischer, B. Plietker, W. Frey, J. Kästner, M. Winkler, J. van Slageren, M. Nowakowski, M. Bauer, M. R. Buchmeiser, *ACS Catalysis* **2020**, *10*, 14810-14823.
[103] K. Herz, M. Podewitz, L. Stohr, D. Wang, W. Frey, K. R. Liedl, S. Sen, M. R. Buchmeiser, *J. Am. Chem. Soc.* **2019**, *141*, 8264-8276.
[104] S. Sen, R. Schowner, D. A. Imbrich, W. Frey, M. Hunger, M. R. Buchmeiser, *Chem. Eur. J.* **2015**, *21*, 13778-13787.
[105] J. Beerhues, S. Sen, R. Schowner, G. Mate Nagy, D. Wang, M. R. Buchmeiser, *J. Polym. Sci. A Polym. Chem.* **2017**, *55*, 3028-3033.
[106] I. Elser, B. R. Kordes, W. Frey, K. Herz, R. Schowner, L. Stöhr, H. J. Altmann, M. R. Buchmeiser, *Chem. Eur. J.* **2018**, *24*, 12652-12659.
[107] C. Lienert, W. Frey, M. R. Buchmeiser, *Macromolecules* **2017**, *50*, 5701-5710.
[108] M. R. Buchmeiser, S. Sen, C. Lienert, Widmann Laura, R. Schowner, K. Herz, Hauser P., W. Frey, D. Wang, *ChemCatChem* **2016**, 2710-2723.
[109] M. L. Snapper, J. A. Tallarico, M. L. Randall, *J. Am. Chem. Soc.* **1997**, *119*, 1478-1479.

[110] D. S. La, E. S. Sattely, J. G. Ford, R. R. Schrock, A. H. Hoveyda, *J. Am. Chem. Soc.* **2001**, *123*, 7767-7778.
[111] I. Ibrahem, M. Yu, R. R. Schrock, A. H. Hoveyda, *J. Am. Chem. Soc.* **2009**, *131*, 3844–3845.
[112] A. J. Jiang, Y. Zhao, R. R. Schrock, A. H. Hoveyda, *J. Am. Chem. Soc.* **2009**, *131*, 16630-16631.
[113] T. J. Mann, A. W. Speed, R. R. Schrock, A. H. Hoveyda, *Angew. Chem. Int. Ed.* **2013**, *125*, 8553-8558.
[114] S. C. Marinescu, R. R. Schrock, P. Müller, M. K. Takase, A. H. Hoveyda, *Organometallics* **2011**, *30*, 1780-1782.
[115] D. V. Peryshkov, R. R. Schrock, M. K. Takase, P. Müller, A. H. Hoveyda, *J. Am. Chem. Soc.* **2011**, *133*, 20754–20757.
[116] X. Shen, T. T. Nguyen, M. J. Koh, D. Xu, A. W. H. Speed, R. R. Schrock, A. H. Hoveyda, *Nature* **2017**, *541*, 380-387.
[117] A. W. H. Speed, T. J. Mann, R. V. O'Brien, R. R. Schrock, A. H. Hoveyda, *J. Am. Chem. Soc.* **2014**, *136*, 16136-16139.
[118] E. M. Townsend, R. R. Schrock, A. H. Hoveyda, *J. Am. Chem. Soc.* **2012**, *134*, 11334-11337.
[119] C. Wang, F. Haeffner, R. R. Schrock, A. H. Hoveyda, *Angew. Chem. Int. Ed.* **2013**, *52*, 1939-1943.
[120] C. Wang, M. Yu, A. F. Kyle, P. Jakubec, D. J. Dixon, R. R. Schrock, A. H. Hoveyda, *Chem. Eur. J.* **2013**, *19*, 2726–2740.
[121] M. Yu, I. Ibrahem, M. Hasegawa, R. R. Schrock, A. H. Hoveyda, *J. Am. Chem. Soc.* **2012**, *134*, 2788-2799.
[122] H. Zhang, E. C. Yu, S. Torker, R. R. Schrock, A. H. Hoveyda, *J. Am. Chem. Soc.* **2014**, *136*, 16493–16496.
[123] D. G. Gillingham, O. Kataoka, S. B. Garber, A. H. Hoveyda, *J. Am. Chem. Soc.* **2004**, *126*, 12288-12290.
[124] J. M. Berlin, S. D. Goldberg, R. H. Grubbs, *Angew. Chem. Int. Ed.* **2006**, *45*, 7591-7595, *118*, 7753-7757.
[125] A. Kannenberg, D. Rost, S. Eibauer, S. Tiede, S. Blechert, *Angew. Chem. Int. Ed.* **2011**, *50*, 3299-3302.
[126] R. K. Khan, R. V. O'Brien, S. Torker, B. Li, A. H. Hoveyda, *J. Am. Chem. Soc.* **2012**, *134*, 12774-12779.
[127] G. A. Cortez, C. A. Baxter, R. R. Schrock, A. H. Hoveyda, *Org. Lett.* **2007**, *9*, 2871-2874.
[128] G. A. Cortez, R. R. Schrock, A. H. Hoveyda, *Angew. Chem. Int. Ed.* **2007**, *46*, 4534-4538.
[129] G. M. Weeresakare, Z. Liu, J. D. Rainier, *Org. Lett.* **2004**, *6*, 1625-1627.
[130] Z. Liu, J. D. Rainier, *Org. Lett.* **2005**, *7*, 131-133.
[131] M. Yu, I. Ibrahem, M. Hasegawa, R. R. Schrock, A. H. Hoveyda, *J. Am. Chem. Soc.* **2012**, *134*, 2788-2799.

[132] R. K. Khan, R. V. O'Brien, S. Torker, B. Li, A. H. Hoveyda, *J. Am. Chem. Soc.* **2012**, *134*, 12774-12779.
[133] M. R. Buchmeiser, S. Sen, J. Unold, W. Frey, *Angew. Chem. Int. Ed.* **2014**, *53*, 9384-9388.
[134] M. R. Buchmeiser, S. Sen, C. Lienert, W. Laura, R. Schowner, K. Herz, H. P., W. Frey, D. Wang, *ChemCatChem* **2016**, 2710-2723.
[135] J. Beerhues, S. Sen, R. Schowner, G. M. Nagy, D. Wang, M. R. Buchmeiser, *J. Polym. Sci. A: Polym. Chem.* **2017**, *55*, 3028-3033.
[136] M. R. Buchmeiser, *Chem. Eur. J.* **2018**, *24*, 14295-14301.
[137] I. Elser, M. J. Benedikter, R. Schowner, W. Frey, D. Wang, M. R. Buchmeiser, *Organometallics* **2019**, *38*, 2461-2471.
[138] I. Elser, W. Frey, K. Wurst, M. R. Buchmeiser, *Organometallics* **2016**, *35*, 4106-4111.
[139] I. Elser, B. R. Kordes, W. Frey, K. Herz, R. Schowner, L. Stöhr, H. J. Altmann, M. R. Buchmeiser, *Chem. Eur. J.* **2018**, *24*, 12652-12659.
[140] I. Elser, R. Schowner, W. Frey, M. R. Buchmeiser, *Chem. Eur. J.* **2017**, *23*, 6398-6405.
[141] M. Pucino, M. Inoue, C. P. Gordon, R. Schowner, L. Stöhr, S. Sen, C. Hegedüs, E. Robé, F. Tóth, M. R. Buchmeiser, C. Copéret, *Angew. Chem. Int. Ed.* **2018**, *130*, 14774-14777.
[142] M. Pucino, V. Mougel, R. Schowner, A. Fedorov, M. R. Buchmeiser, C. Copéret, *Angew. Chem. Int. Ed.* **2016**, *128*, 4372-4374.
[143] R. Schowner, W. Frey, M. R. Buchmeiser, *Eur. J. Inorg. Chem.* **2019**, *2019*, 1911-1922.
[144] K. Herz, M. Podewitz, L. Stöhr, D. Wang, S. Sen, W. Frey, K. R. Liedl, M. R. Buchmeiser, *J. Am. Chem. Soc.* **2019**, *141*, 8264-8276.
[145] A. Poater, X. Solans-Monfort, E. Clot, C. Coperet, O. Eisenstein, *Dalton Trans.* **2006**, 3077-3087.
[146] A. Poater, X. Solans-Monfort, E. Clot, C. Coperet, O. Eisenstein, *J. Am. Chem. Soc.* **2007**, *129*, 8207-8216.
[147] M. J. Benedikter, R. Schowner, I. Elser, P. Werner, K. Herz, L. Stöhr, D. A. Imbrich, G. M. Nagy, D. Wang, M. R. Buchmeiser, *Macromolecules* **2019**, *52*, 4059-4066.
[148] T. J. Mann, A. W. Speed, R. R. Schrock, A. H. Hoveyda, *Angew. Chem. Int. Ed. Engl.* **2013**, *52*, 8395-8400.
[149] D. S. Breslow, *Prog. Poly. Sci.* **1993**, *18*, 1141 - 1195.
[150] S. Naumann, M. R. Buchmeiser, *Macromol. Rapid. Commun.* **2014**, *35*, 682-701.
[151] S. Monsaert, A. Lozano Vila, R. Drozdzak, P. Van Der Voort, F. Verpoort, *Chem. Soc. Rev.* **2009**, *38*, 3360-3372.
[152] S. Kovačič, C. Slugovc, *Mater. Chem. Front.* **2020**, *4*, 2235-2255.
[153] R. Streck, *J. Mol. Catal.* **1982**, *15*, 3 - 19.

[154] A. Dumas, D. S. Müller, I. Curbet, L. Toupet, M. Rouen, O. Baslé, M. Mauduit, *organometallics* **2018**, *37*, 829-834.
[155] A. Cordova, R. Rios, *Angew. Chem. Int. Ed. Engl.* **2009**, *48*, 8827-8831.
[156] W. S. Andreas, E. Saive, A. Demonceau, A. F. Noels, *J. Chem. Sci., Chem. Comm.* **1995**, 1127-1128.
[157] L. Delaude, A. Demonceau, A. F. Noels, *Chem. Commun.* **2001**, 986-987.
[158] M. R. Buchmeiser, D. Wang, Y. Zhang, S. Naumov, K. Wurst, *Eur. J. Inorg. Chem.* **2007**, *2007*, 3988-4000.
[159] K. M. Engle, G. Lu, S. X. Luo, L. M. Henling, M. K. Takase, P. Liu, K. N. Houk, R. H. Grubbs, *J. Am. Chem. Soc.* **2015**, *137*, 5782-5792.
[160] Y. Vidavsky, A. Anaby, N. G. Lemcoff, *Dalton Trans.* **2012**, *41*, 32-43.
[161] E. Tzur, A. Szadkowska, A. Ben-Asuly, A. Makal, I. Goldberg, K. Wozniak, K. Grela, N. G. Lemcoff, *Chem. Eur. J.* **2010**, *16*, 8726-8737.
[162] P. A. van der Schaaf , R. Kolly, H.-J. Kirner, F. Rime, A. Mühlebach, A. Hafner, *J. Organomet. Chem.* **2000**, *606*, 65 - 74.
[163] T. Ung, A. Hejl, R. H. Grubbs, Y. Schrodi, *Organometallics* **2004**, *23*, 5399 - 5401.
[164] D. Benitez, W. A. Goddard, *J. Am. Chem. Soc.* **2005**, *127*, 12218 - 12219.
[165] C. Slugovc, D. Burtscher, F. Stelzer, K. Mereiter, *Organometallics* **2005**, *24*, 2255 - 2258.
[166] M. Barbasiewicz, A. Szadkowska, R. Bujok, K. Grela, *Organometallics* **2006**, *25*, 3599 - 3604.
[167] A. Hejl, M. W. Day, R. H. Grubbs, *Organometallics* **2006**, *25*, 6149 - 6154.
[168] E. Pump, A. Leitgeb, A. Kozłowska, A. Torvisco, L. Falivene, L. Cavallo, K. Grela, C. Slugovc, *Organometallics* **2015**, *34*, 5383-5392.
[169] N. M. Shcheglova, V. D. Kolesnik, R. V. Ashirov, E. A. Krasnokutskaya, *Russ. Chem. Bull.* **2016**, *65*, 490-497.
[170] S. J. Czarnocki, I. Czeluśniak, T. K. Olszewski, M. Malinska, K. Woźniak, K. Grela, *ACS Catalysis* **2017**, *7*, 4115-4121.
[171] R. Gawin, A. Makal, K. Wozniak, M. Mauduit, K. Grela, *Angew. Chem. Int. Ed.* **2007**, *46*, 7206-7209.
[172] R. Gawin, A. Makal, K. Woźniak, M. Mauduit, K. Grela, *Angew. Chem. Int. Ed.* **2007**, *119*, 7344-7347.
[173] Ł. Gułajski, A. Michrowska, R. Bujok, K. Grela, *J. Mol. Catal. A Chem.* **2006**, *254*, 118-123.
[174] Y. Xie, Y. Yuan, B. Mousavi, Y. Cai, C. Kai, Y. Lu, M. Yusubov, F. Verpoort, *Appl. Organomet. Chem.* **2015**, *29*, 573-579.
[175] K. M. Engle, G. Lu, S. X. Luo, L. M. Henling, M. K. Takase, P. Liu, K. N. Houk, R. H. Grubbs, *J Am Chem Soc* **2015**, *137*, 5782-5792; **May 6**.
[176] T. Kost, M. Sigalov, I. Goldberg, A. Ben-Asuly, N. G. Lemcoff, *J. Organomet. Chem.* **2008**, *693*, 2200-2203.
[177] A. Ben-Asuly, E. Tzur, C. E. Diesendruck, M. Sigalov, I. Goldberg, N. G. Lemcoff, *Organometallics* **2008**, *27*.

[178] Y. Ginzburg, A. Anaby, Y. Vidavsky, C. E. Diesendruck, A. Ben-Asuly, I. Goldberg, N. G. Lemcoff, *Organometallics* **2011**, *30*, 3430-3437.
[179] G. C. Bazan, J. H. Oskam, H.-N. Cho, L. Y. Park, R. R. Schrock, *J. Am. Chem. Soc.* **1991**, *113*, 6899-6907.
[180] L. Piola, F. Nahra, S. P. Nolan, *Beilstein J. Org. Chem.* **2015**, *11*, 2038-2056.
[181] H. H. Fox, J.-K. Lee, L. Y. Park, R. R. Schrock, *Organometallics* **1993**, *12*, 759 - 768.
[182] J. T. Ciszewski, B. Xie, C. Cao, A. L. Odom, *Dalton Trans.* **2003**, 4226 - 4227.
[183] E. M. Townsend, S. M. Kilyanek, R. R. Schrock, P. Muller, S. J. Smith, A. H. Hoveyda, *Organometallics* **2013**, *32*, 4612-4617.
[184] H. Jeong, R. R. Schrock, P. Müller, *Organometallics* **2015**, *34*, 4408-4418.
[185] I. Elser, B. R. Kordes, W. Frey, K. Herz, R. Schowner, L. Stohr, H. J. Altmann, M. R. Buchmeiser, *Chem. Eur. J.* **2018**, *24*, 12652-12659.
[186] P. E. Sues, J. M. John, K. V. Bukhryakov, R. R. Schrock, P. Müller, *Organometallics* **2016**, *35*, 3587-3593.
[187] J. Beerhues, S. Sen, R. Schowner, G. Mate Nagy, D. Wang, M. R. Buchmeiser, *J. Polym. Sci. A: Polym. Chem.* **2017**, *55*, 3028-3033.
[188] P. A. van der Schaar, A. Hafner, A. Mühlebach, *Angew. Chemie* **1996**, *108*, 1974 - 1977.
[189] P. A. van der Schaar, A. Hafner, A. Mühlebach, *Angew. Chem. Int. Ed.* **1996**, *35*, 1845 - 1847.
[190] W. C. P. Tsang, J. Y. Jamieson, S. L. Aeilts, K. C. Hultzsch, R. R. Schrock, A. H. Hoveyda, *Organometallics* **2004**, *23*, 1997-2007.
[191] S. C. Marinescu, A. J. King, R. R. Schrock, R. Singh, P. Müller, M. K. Takase, *Organometallics* **2010**, *29*, 6816-6828.
[192] T. M. Cameron, C. G. Ortiz, I. Ghiviriga, K. A. Abboud, J. M. Boncella, *Organometallics* **2001**, *20*, 2032 - 2039.
[193] W. C. P. Tsang, R. R. Schrock, A. H. Hoveyda, *Organometallics* **2001**, *20*, 5658 - 5669.
[194] W. C. P. Tsang, K. C. Hultzsch, J. B. Alexander, P. J. Bonitatebus Jr., R. R. Schrock, A. H. Hoveyda, *J. Am. Chem. Soc.* **2003**, *125*, 2652 - 2666.
[195] M. R. Buchmeiser, S. Sen, J. Unold, W. Frey, *Angew. Chem. Int. Ed.* **2014**, *53*, 9384-9388.
[196] M. R. Buchmeiser, S. Sen, C. Lienert, L. Widmann, R. Schowner, K. Herz, P. Hauser, W. Frey, D. Wang, *ChemCatChem* **2016**, *8*, 2710-2723.
[197] R. R. Schrock, *Adv. Synth. Catal.* **2007**, *349*, 25-25.
[198] R. Schowner, I. Elser, M. Benedikter, M. Momin, W. Frey, T. Schneck, L. Stöhr, M. R. Buchmeiser, *Angew. Chem. Int. Ed.* **2020**, *59*, 951-958.
[199] A. K. Rappe, W. A. Goddard, *J. Am. Chem. Soc.* **1982**, *104*, 3287-3294.
[200] R. Schowner, W. Frey, M. R. Buchmeiser, *Eur. J. Inorg. Chem.* **2019**, *2019*, 1911-1922.
[201] R. O'Dell, D. H. McConville, G. E. Hofmeister, R. R. Schrock, *J. Am. Chem. Soc.* **1994**, *116*, 3414-3423.

[202] S. Y. Lu, J. M. Amass, N. Majid, D. Glennon, A. Byerley, F. Heatley, P. Quayle, C. Booth, *Macromol. Chem. Phys.* **1994**, *195*, 1273-1288.

[203] Q.-Y. Lin, X.-H. Xu, F.-L. Qing, *J. Org. Chem.* **2014**, *79*, 10434-10446.

[204] M. R. Buchmeiser, S. Sen, J. Unold, W. Frey, *Angew. Chem. Int. Ed.* **2014**, *53*, 9384-9388.

[205] M. Pucino, M. Inoue, C. P. Gordon, R. Schowner, L. Stöhr, S. Sen, C. Hegedüs, E. Robé, F. Tóth, M. R. Buchmeiser, C. Copéret, *Angew. Chem. Int. Ed.* **2018**, *57*, 14566-14569.

7. Appendix

7.1 Stereoselective Olefin Ring-Opening Cross-Metathesis Catalyzed by Molybdenum Imido Alkylidene *N*-Heterocyclic Carbene Complexes

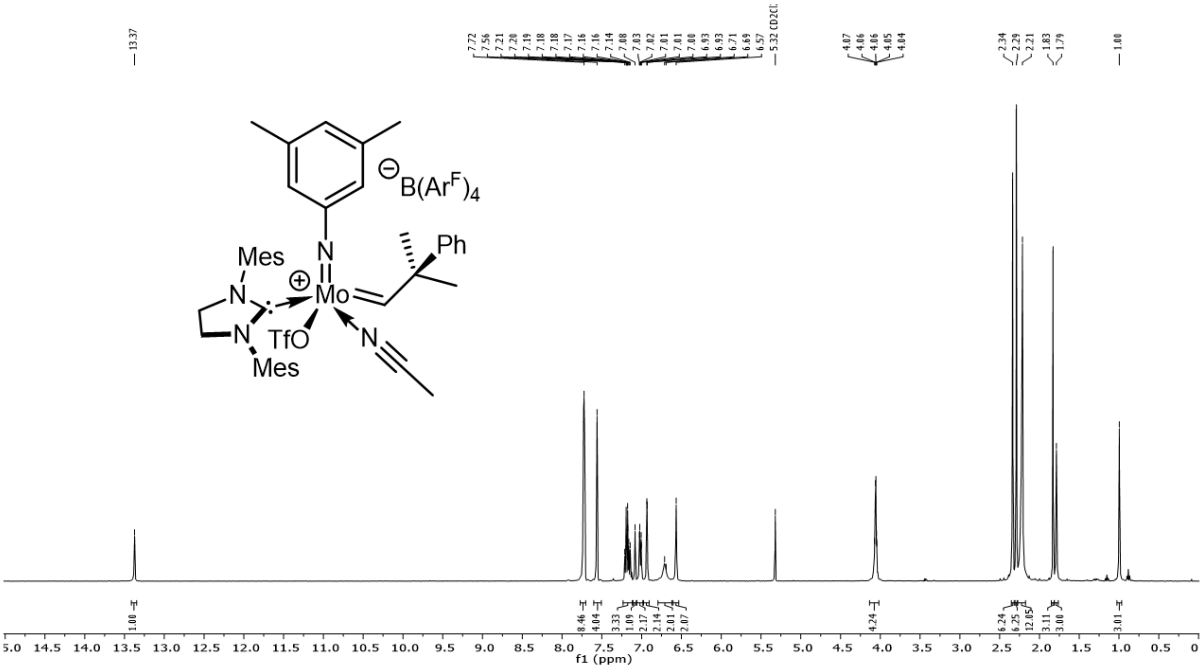

Figure 43. ^{1}H NMR spectrum of **Mo-4** (400 MHz, CD_2Cl_2).

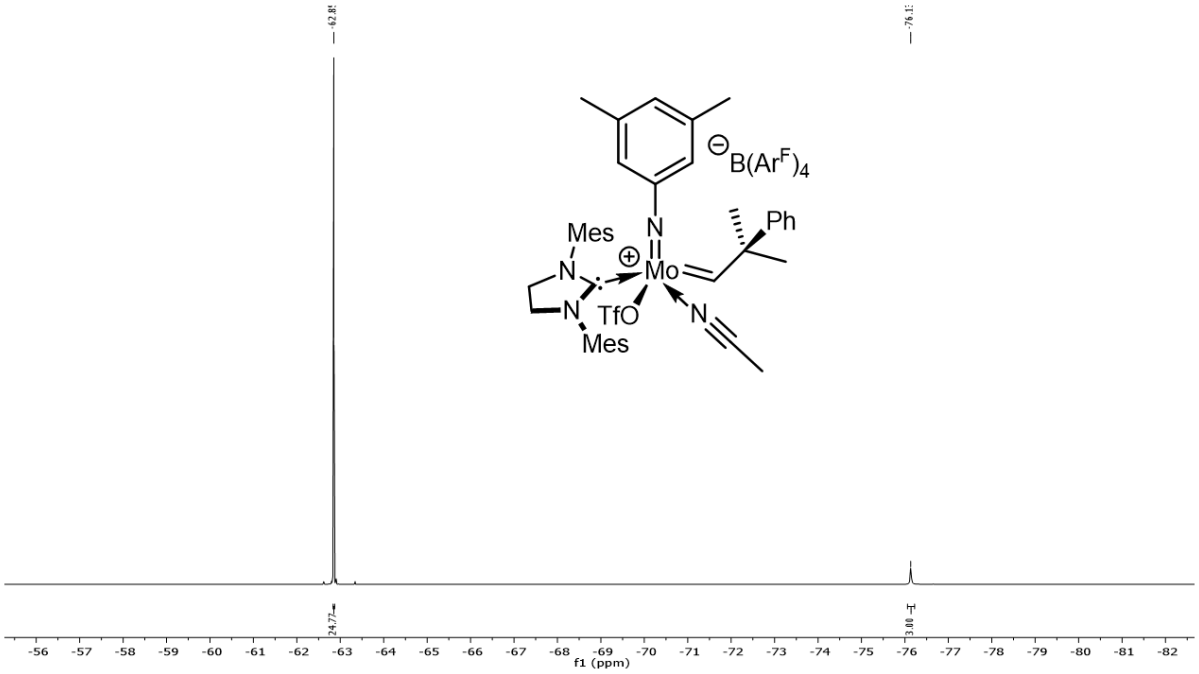

Figure 44. ^{19}F NMR spectrum of **Mo-4** (376 MHz, CD_2Cl_2).

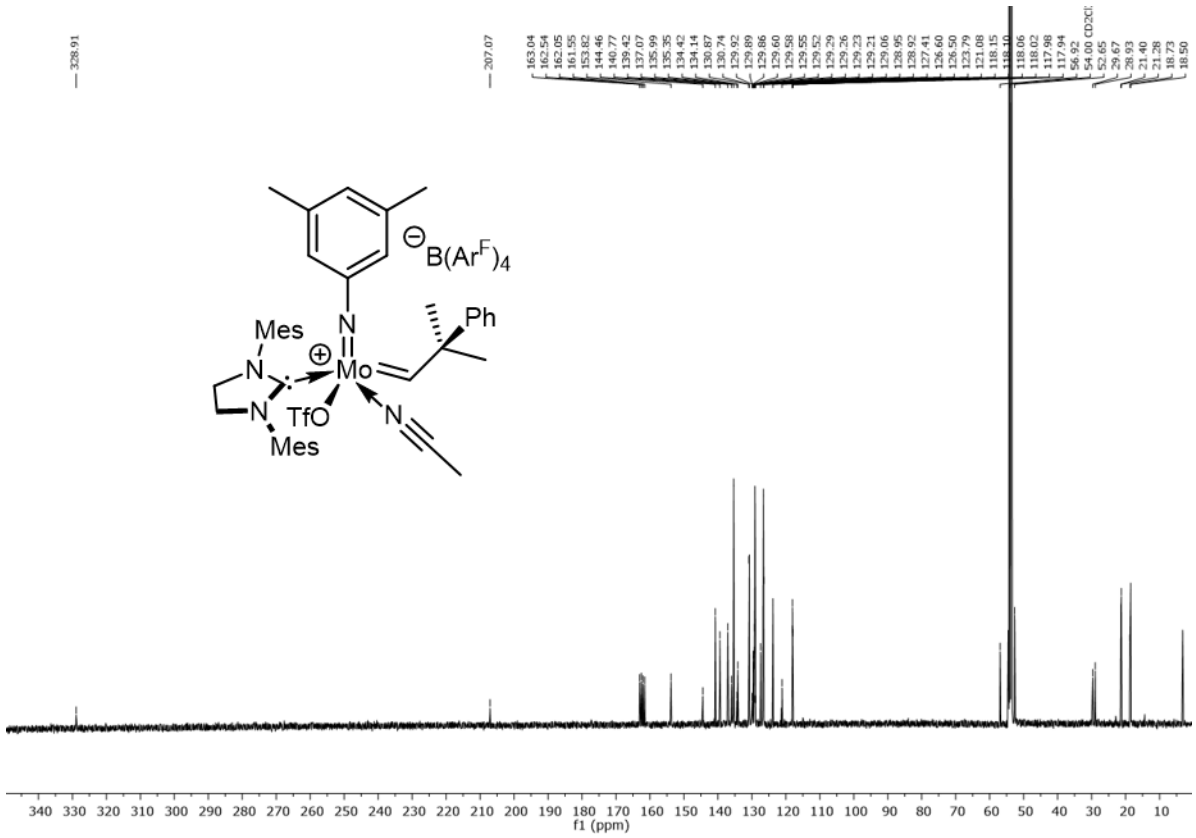

Figure 45. ^{13}C NMR spectrum of **Mo-4** (101 MHz, CD_2Cl_2).

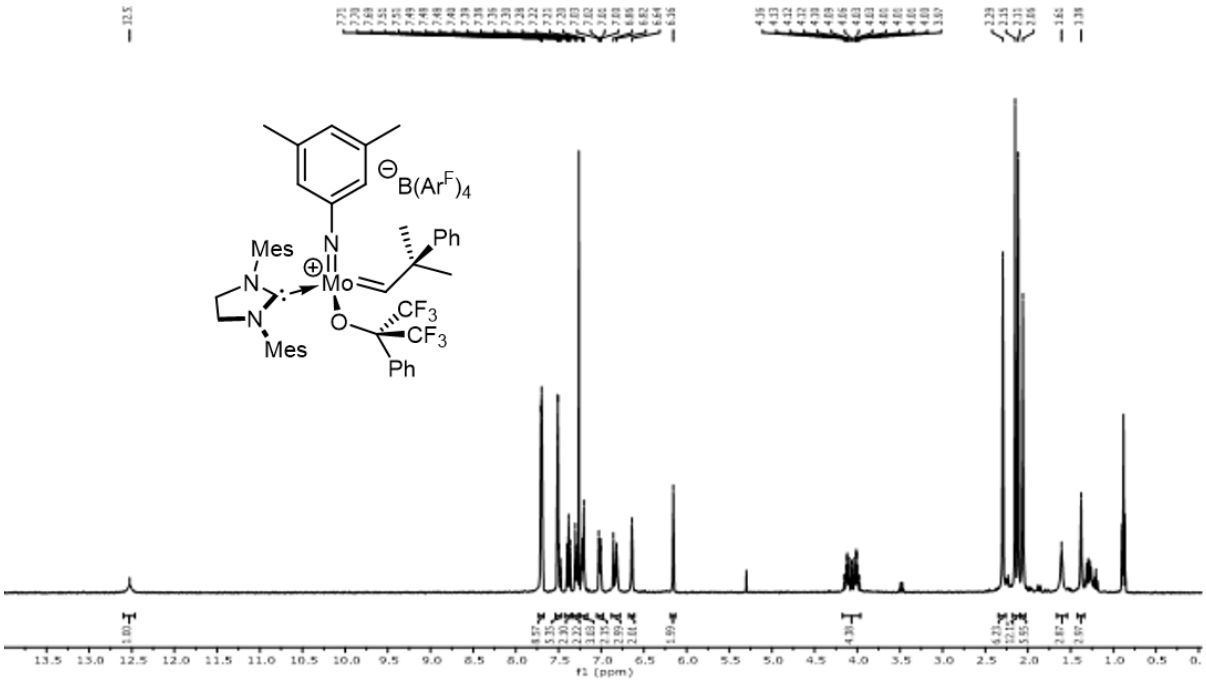

Figure 46. ^{1}H NMR spectrum of **Mo-5** (400 MHz, CD_2Cl_2).

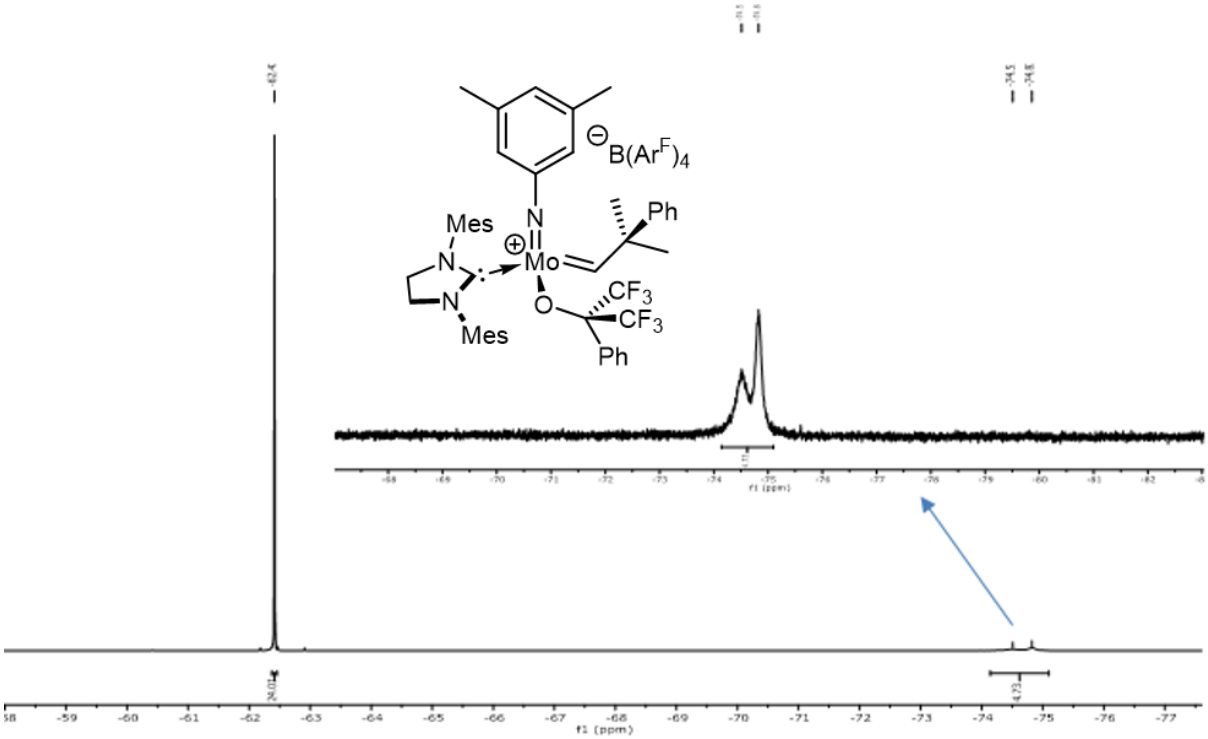

Figure 47. ^{19}F NMR spectrum of **Mo-5** (376 MHz, CD_2Cl_2).

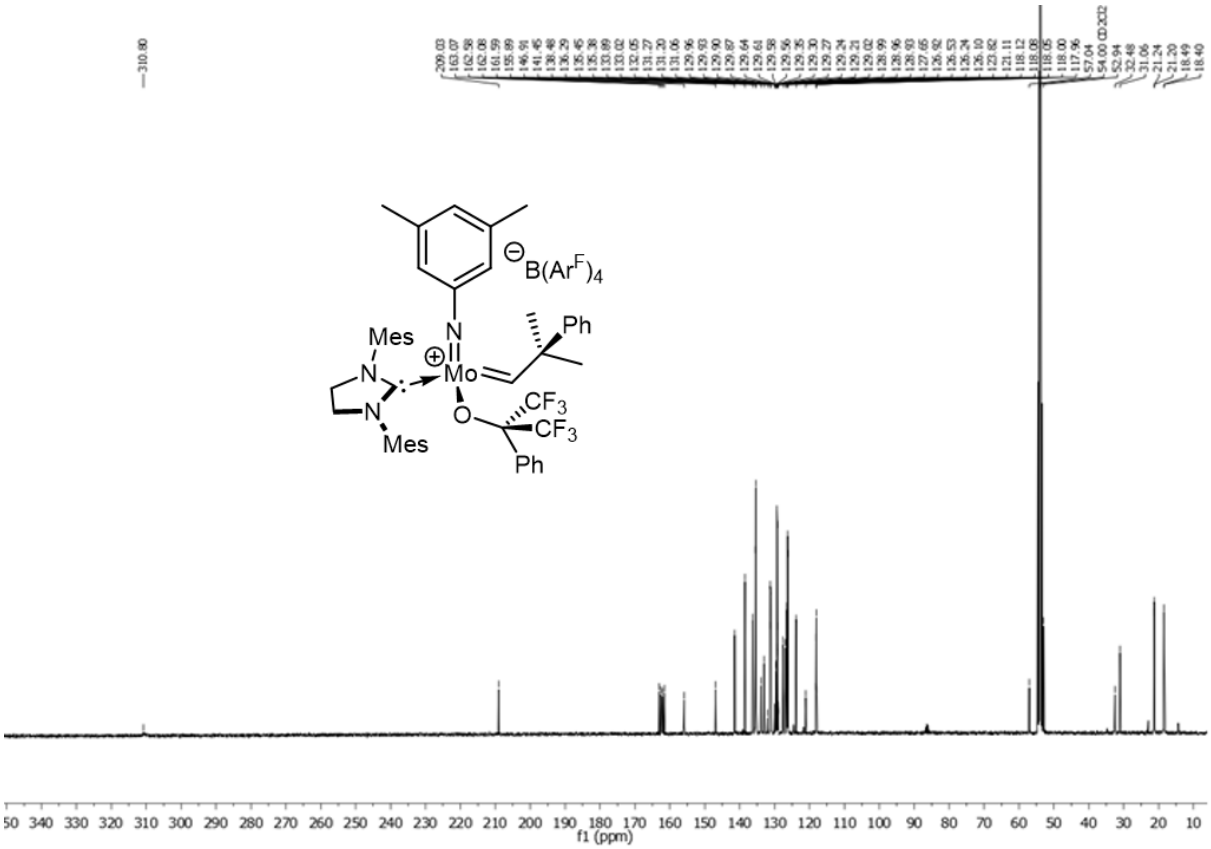

Figure 48. ^{13}C NMR spectrum of **Mo-5** (101 MHz, CD_2Cl_2).

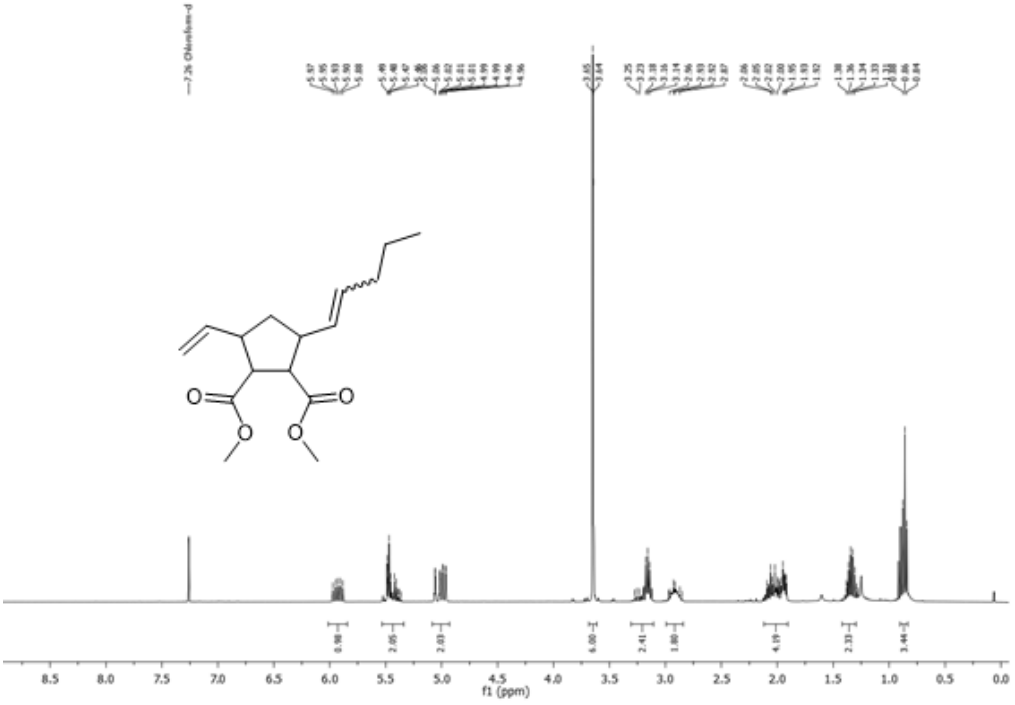

Figure 49. ^{1}H NMR spectrum of **P1** (400 MHz, CD_2Cl_2).

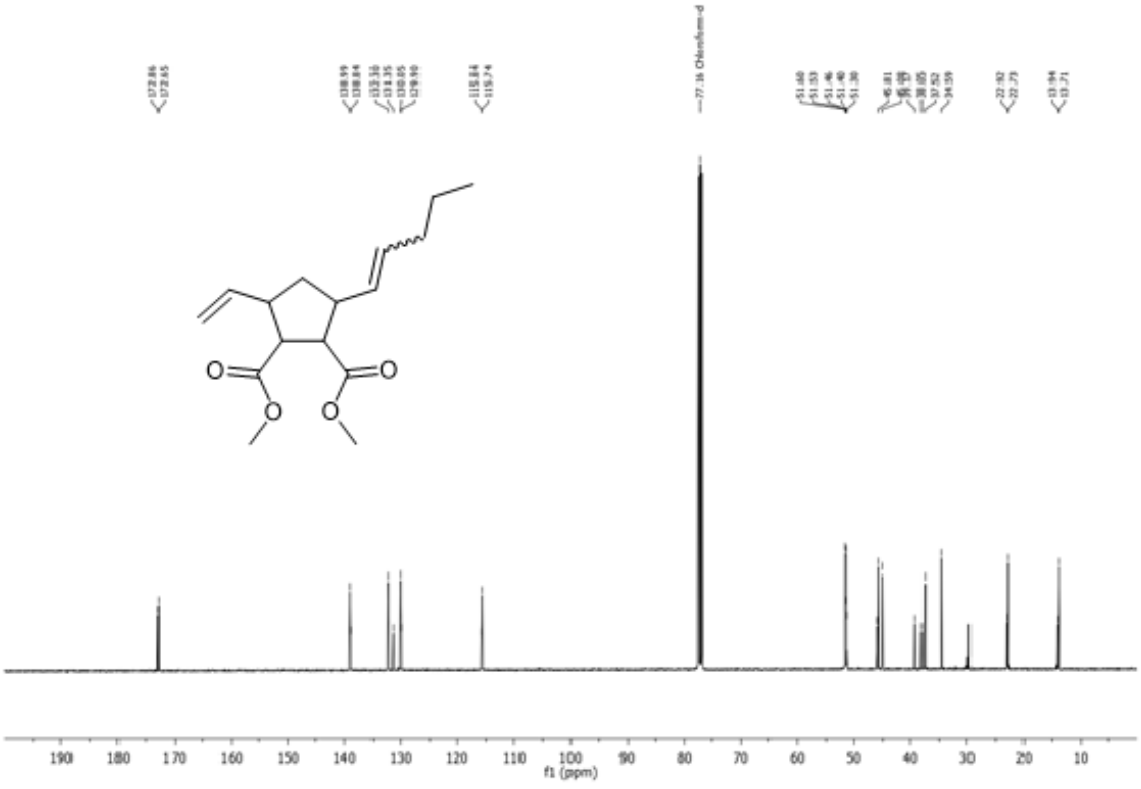

Figure 50. ^{13}C NMR spectrum of **P1** (101 MHz, $CDCl_3$).

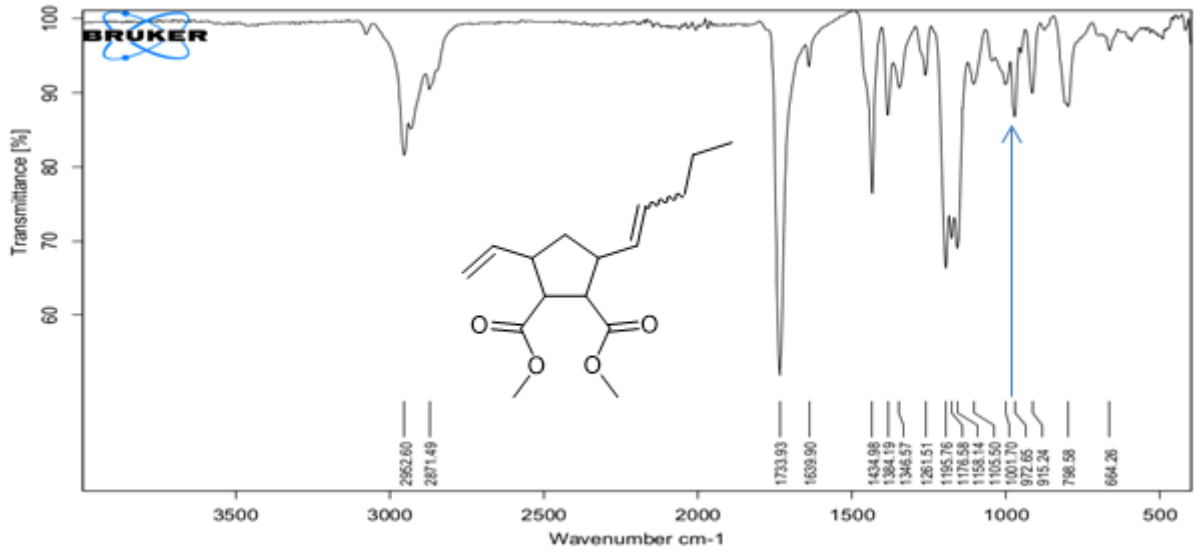

Figure 51. IR-spectrum of **P1**. The characteristic sharp peak for the *trans*-isomer are observed at 972.7 cm^{-1} along with a small peak for the *cis*-isomer at 664.3 cm^{-1}.

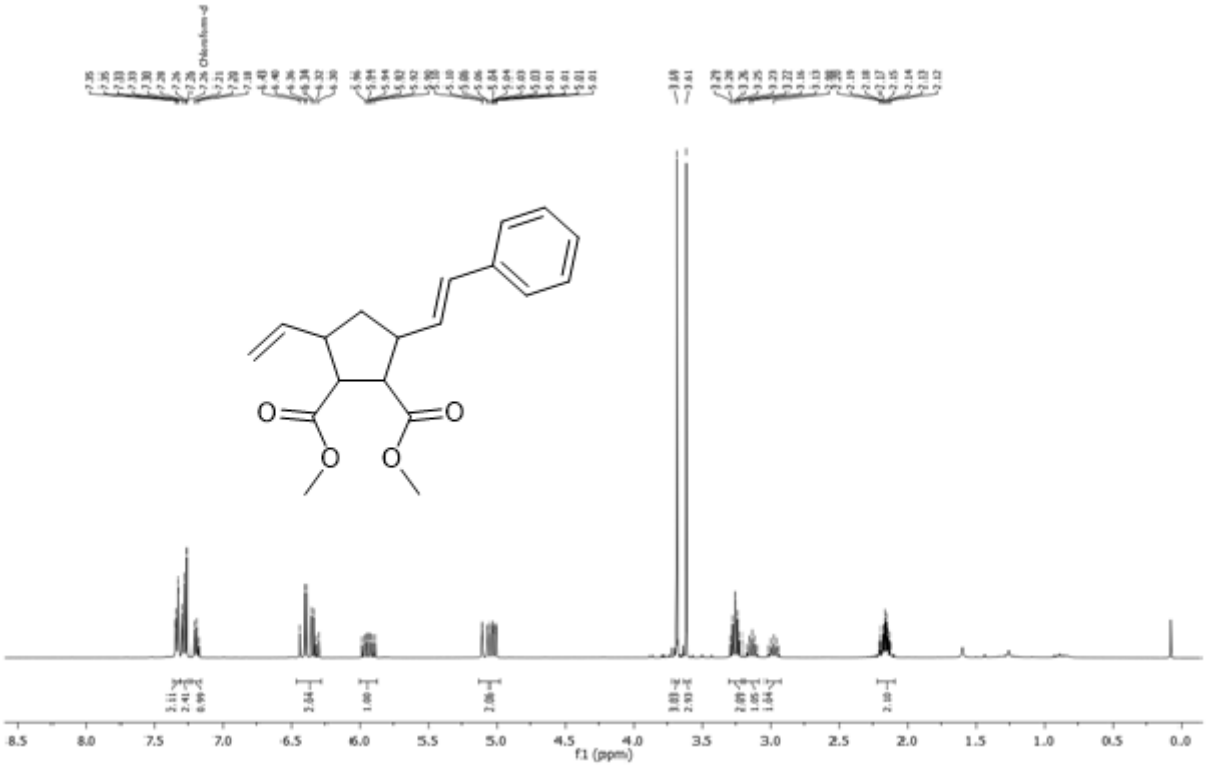

Figure 52. ^{1}H NMR spectrum of **P2** (400 MHz, $CDCl_3$).

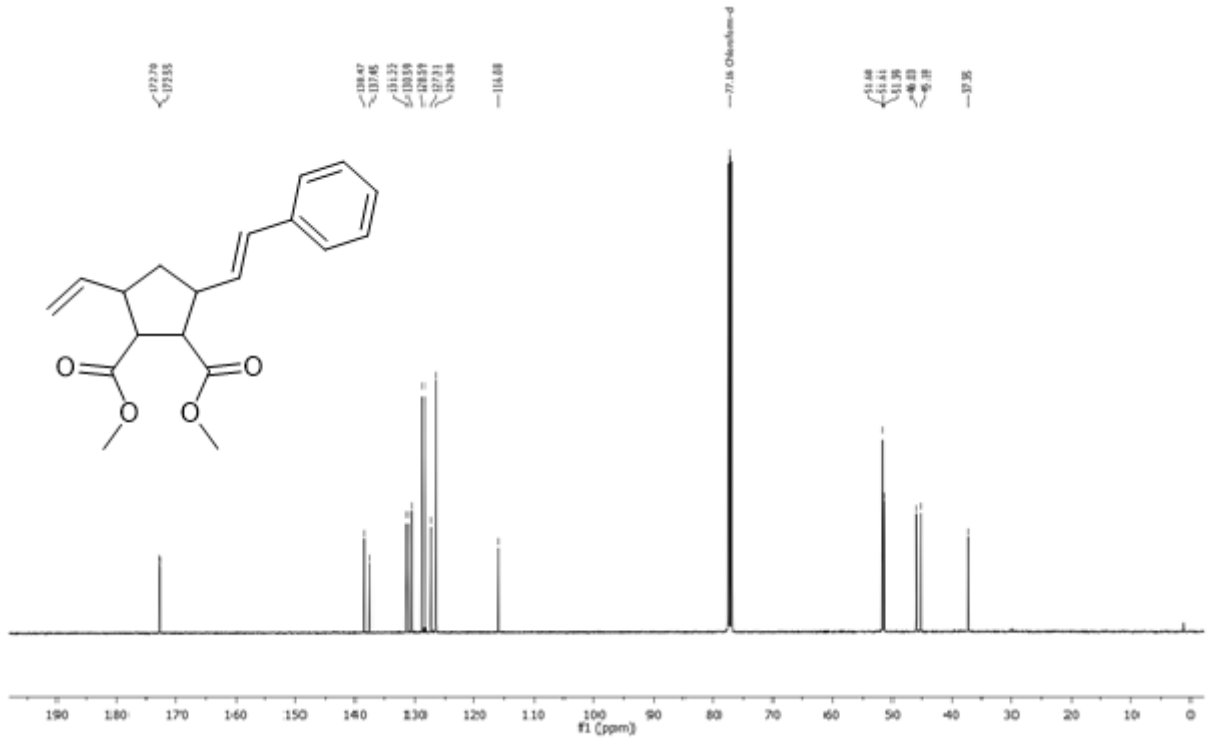

Figure 53. ^{13}C NMR spectrum of **P2** (101 MHz, $CDCl_3$).

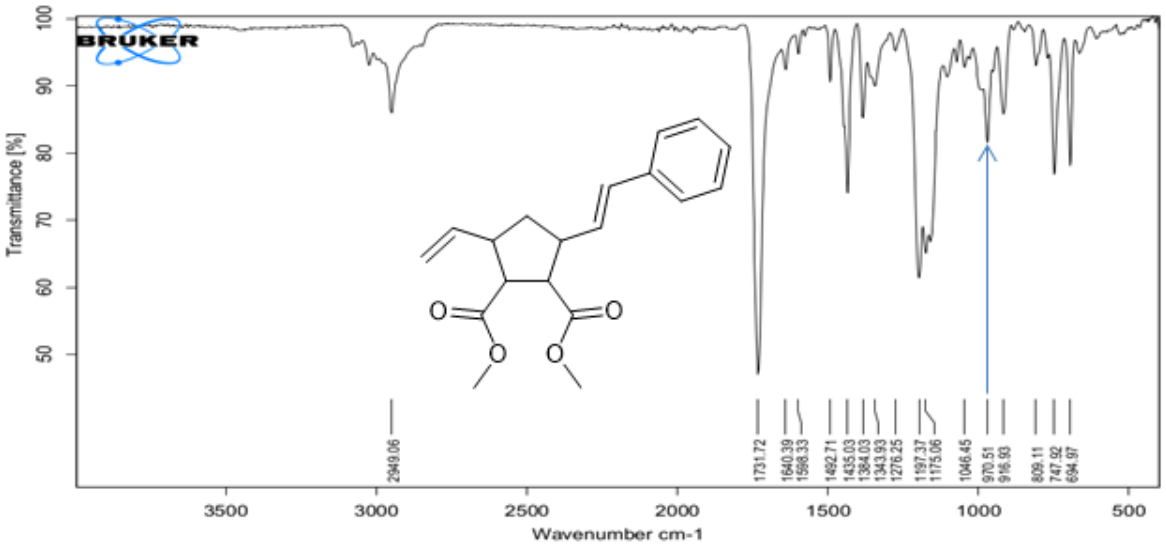

Figure 54. Infrared spectrum of **P2**. The characteristic peak the peak for the *trans*-isomer is observed at 970.5 cm^{-1}.

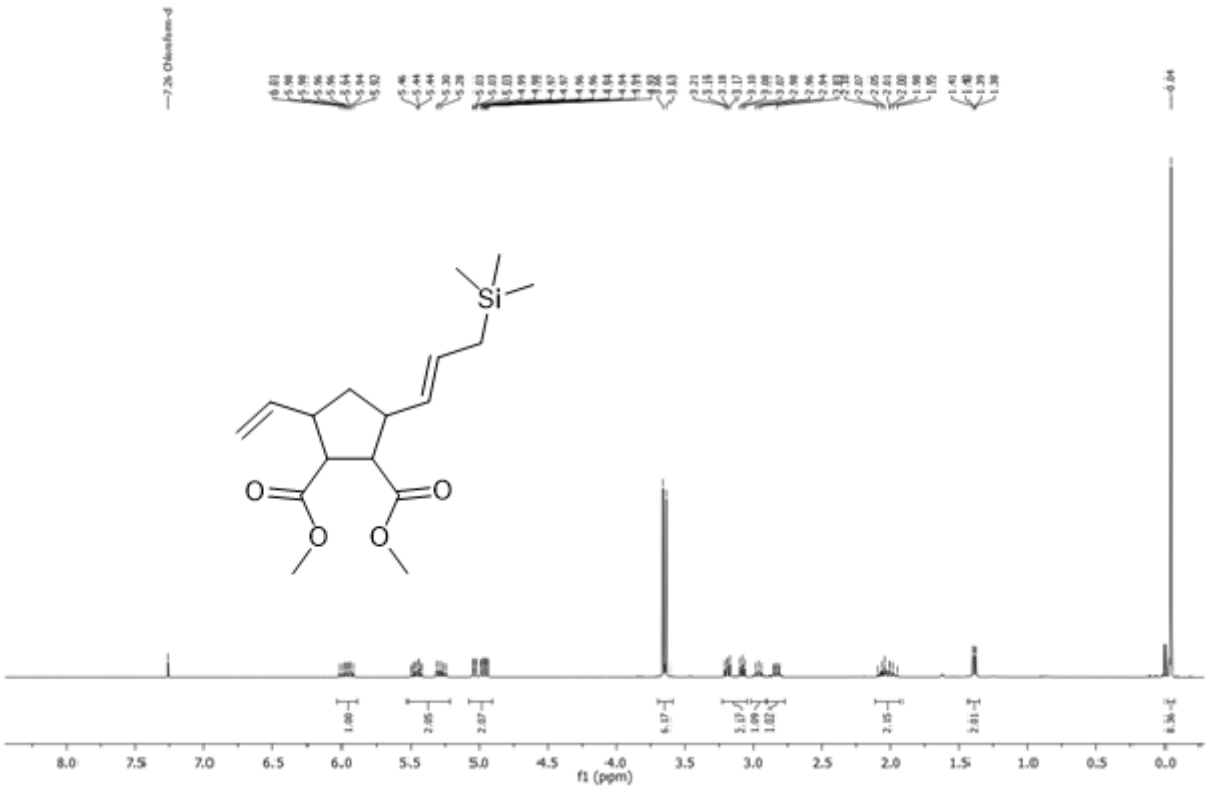

Figure 55. ^{1}H NMR spectrum of **P3** (400 MHz, $CDCl_3$).

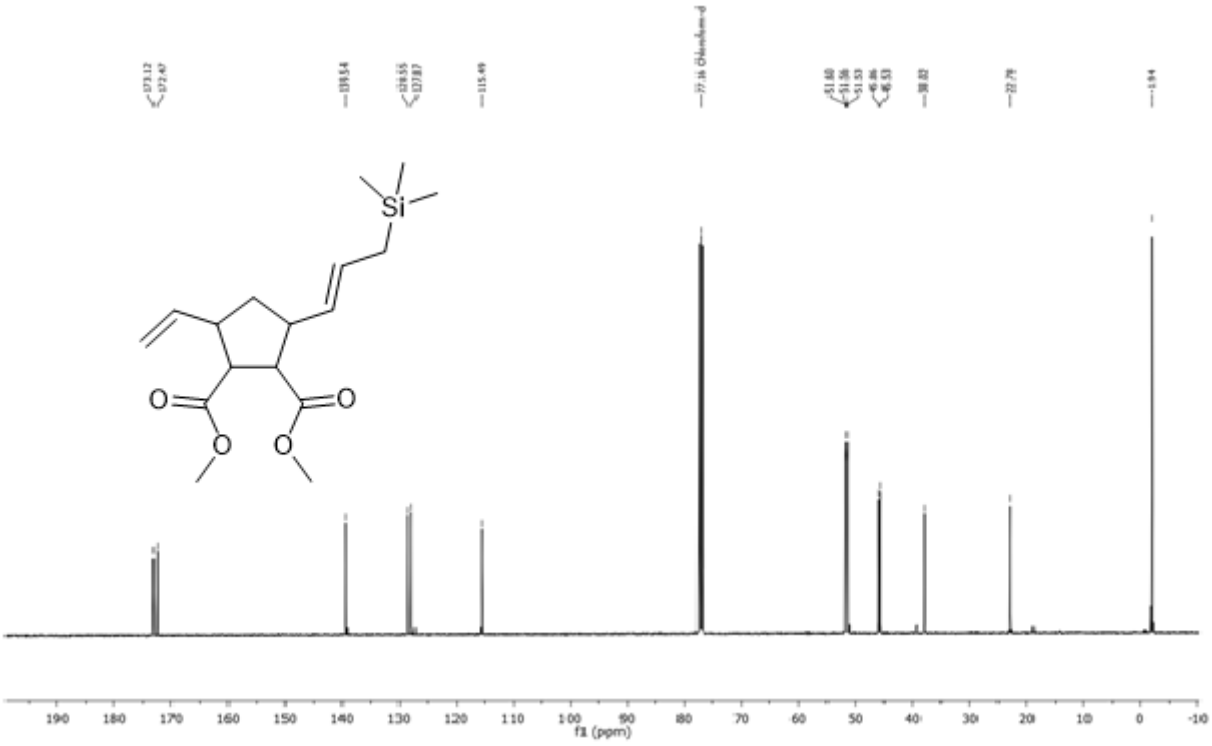

Figure 56. ^{13}C NMR spectrum of **P3** (101 MHz, $CDCl_3$).

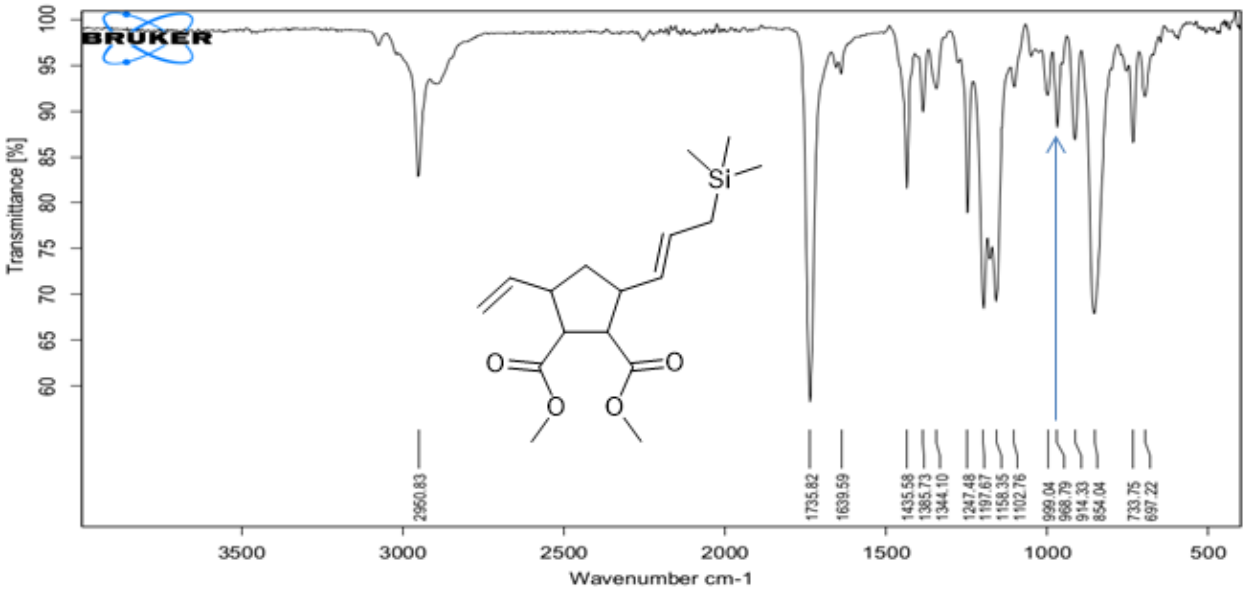

Figure 57. IR-spectrum of **P3**. The characteristic peak for the *trans*-isomer is observed at 968.8 cm^{-1}.

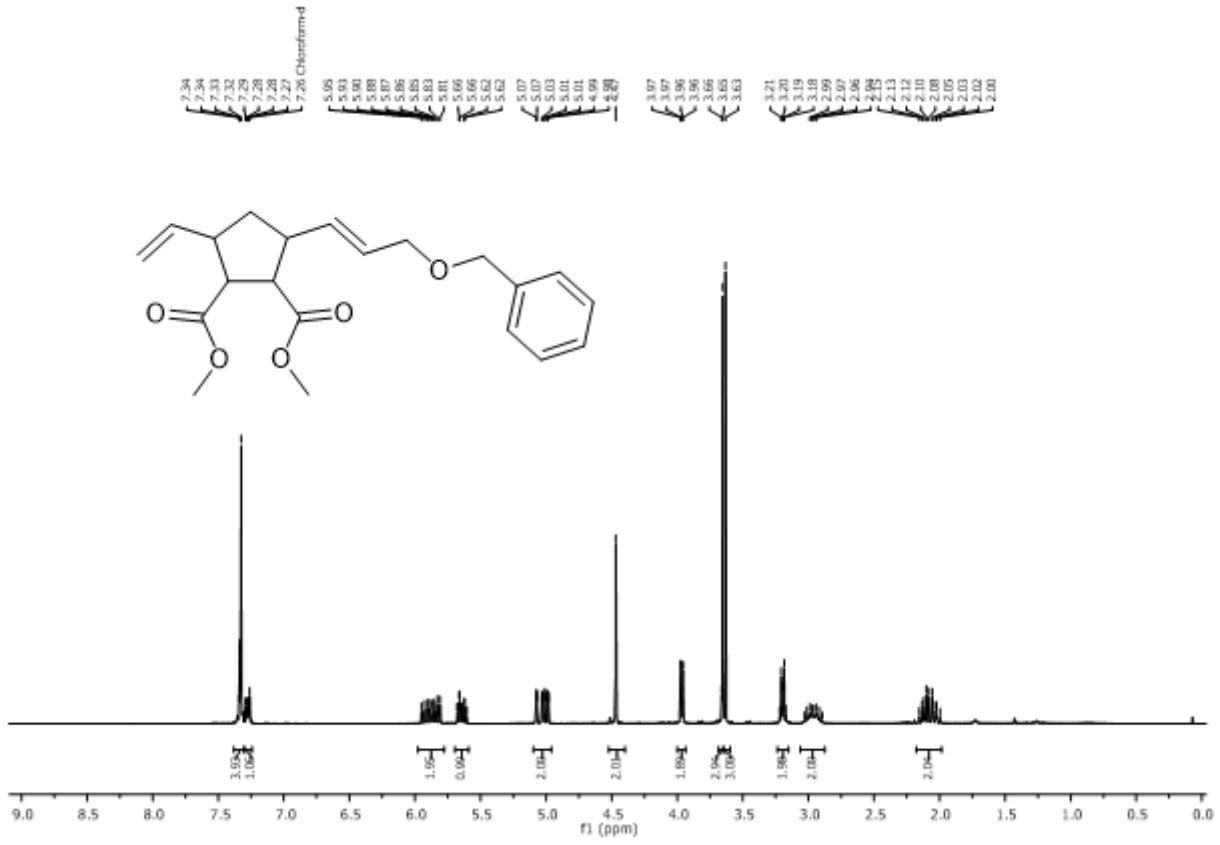

Figure 58. ^{1}H NMR spectrum of **P4** (400 MHz, $CDCl_3$).

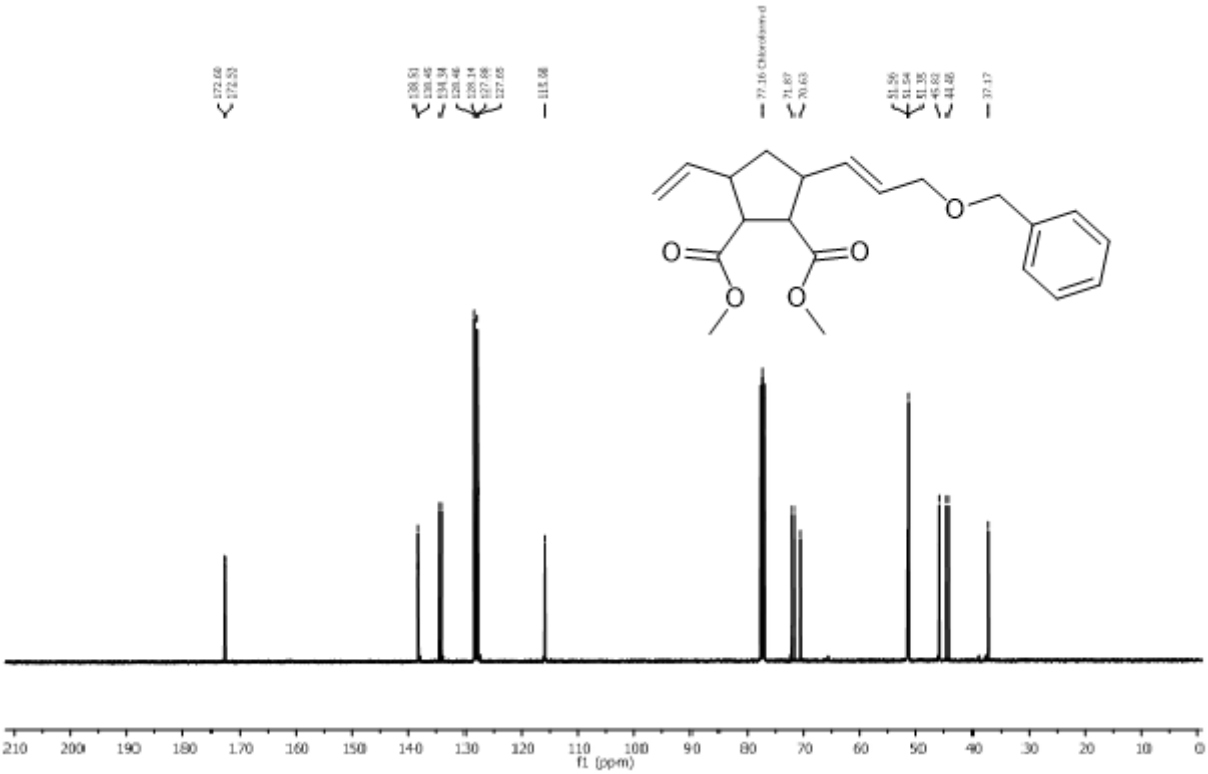

Figure 59. ^{13}C NMR spectrum of **P4** (101 MHz, $CDCl_3$).

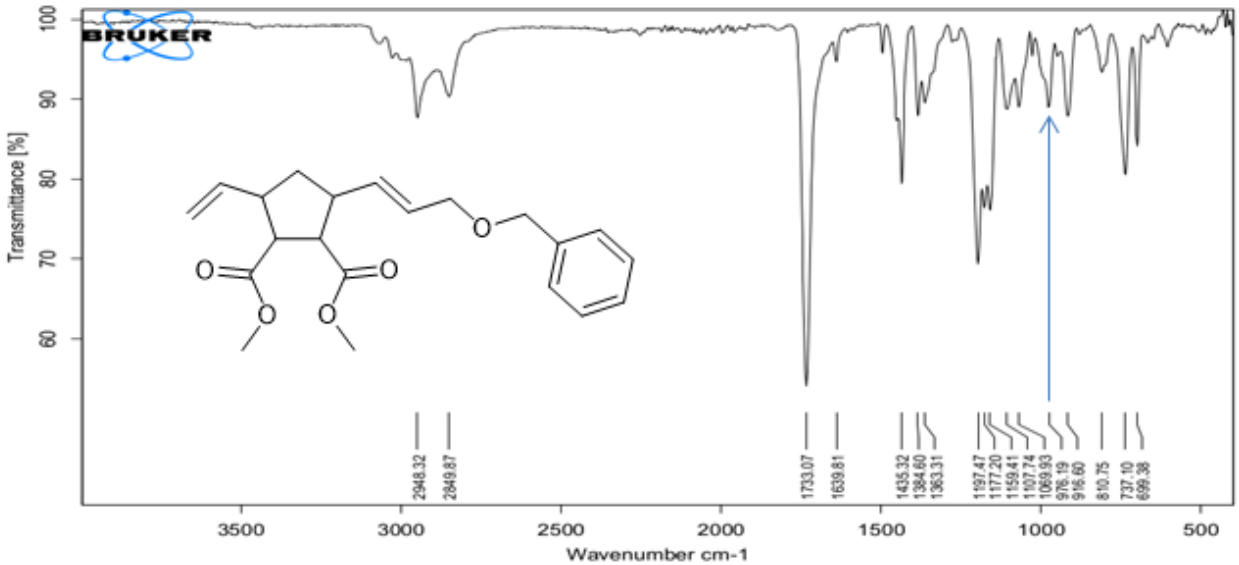

Figure 60. IR-spectrum of **P4**. The characteristic peak for the *trans*-isomer is observed at 976.2 cm^{-1}.

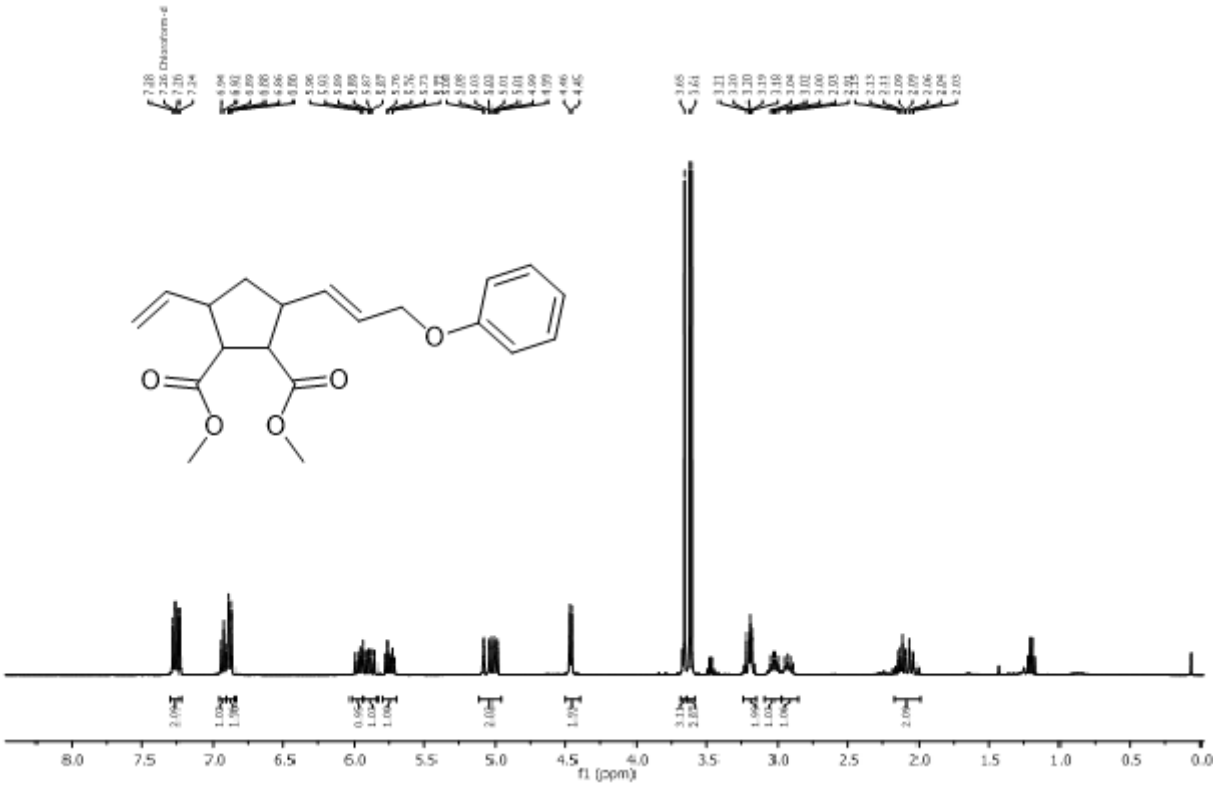

Figure 61. ^{1}H NMR spectrum of **P5** (400 MHz, $CDCl_3$).

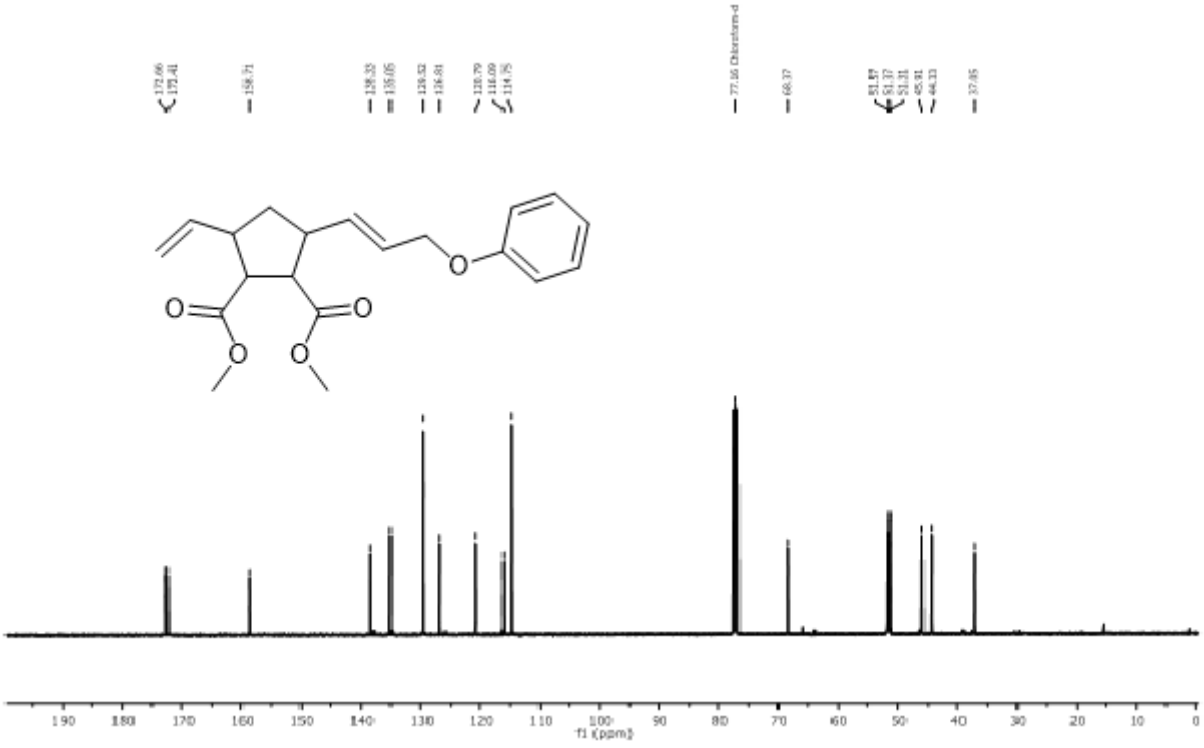

Figure 62. ^{13}C NMR spectrum of **P5** (101 MHz, $CDCl_3$).

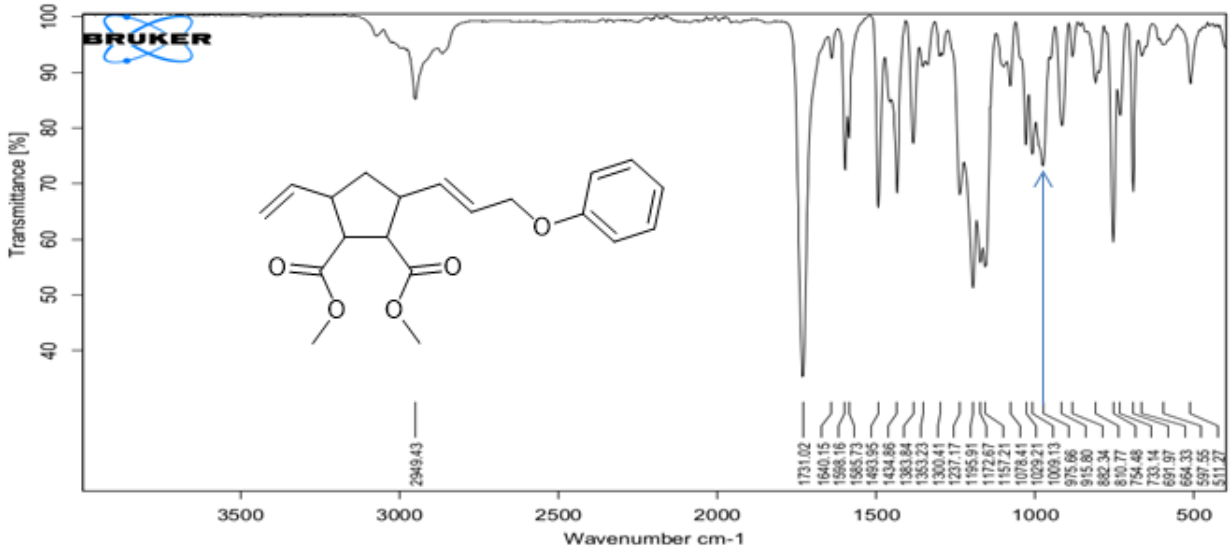

Figure 63. IR-spectrum of **P5**. The characteristic peak for the *trans*-isomer is observed at 975.7 cm^{-1}.

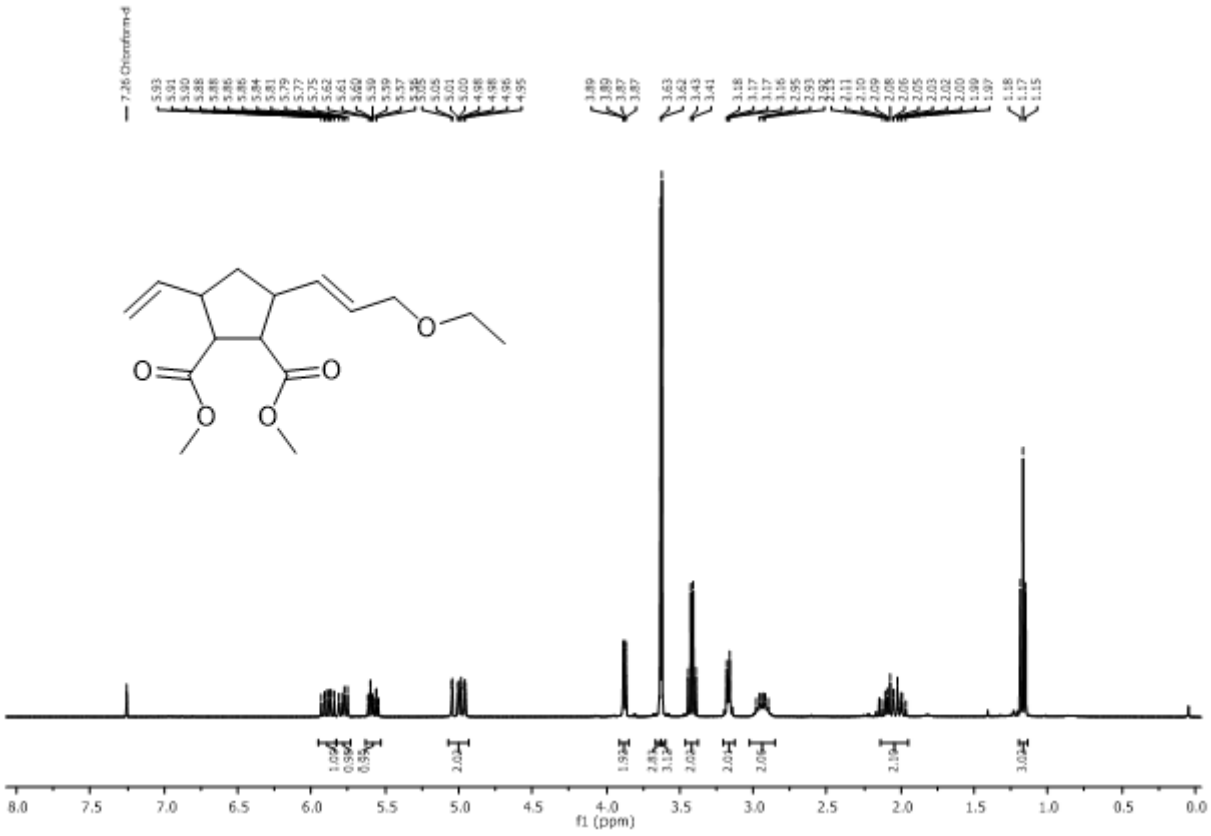

Figure 64. ^{1}H NMR spectrum of **P6** (400 MHz, $CDCl_3$).

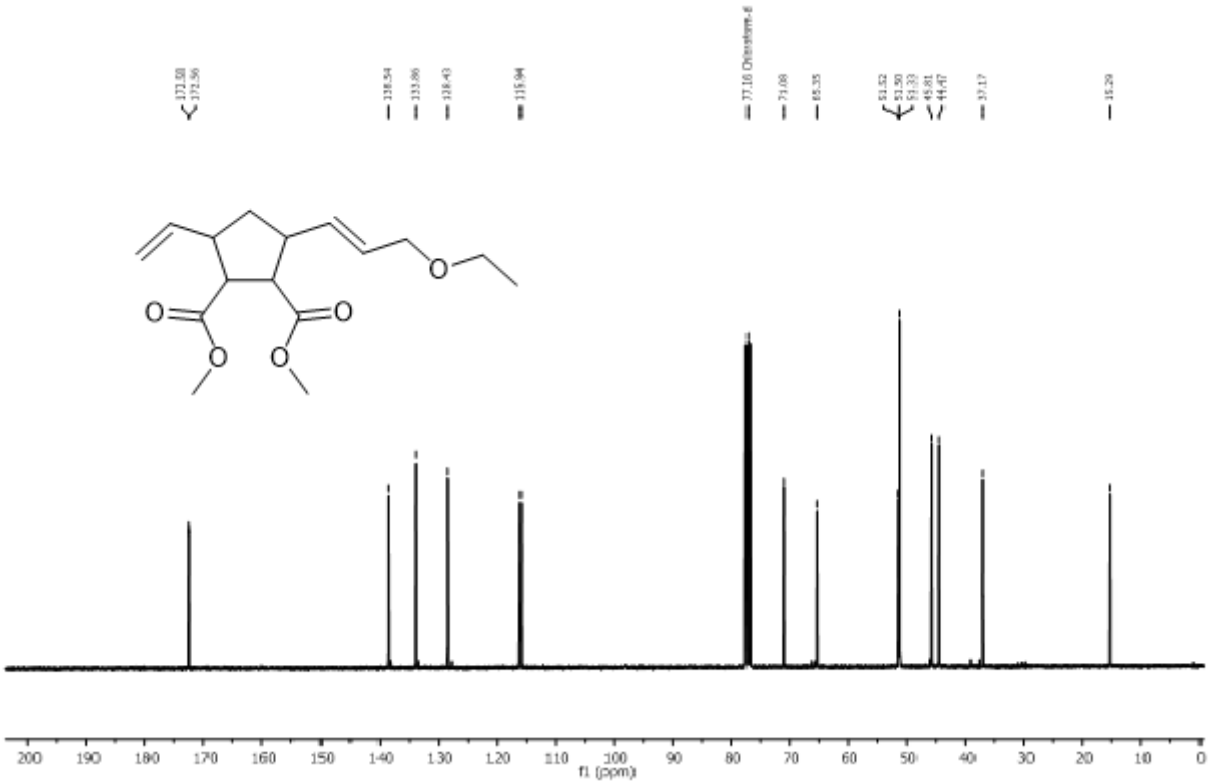

Figure 65. ^{13}C NMR spectrum of **P6** (101 MHz, $CDCl_3$).

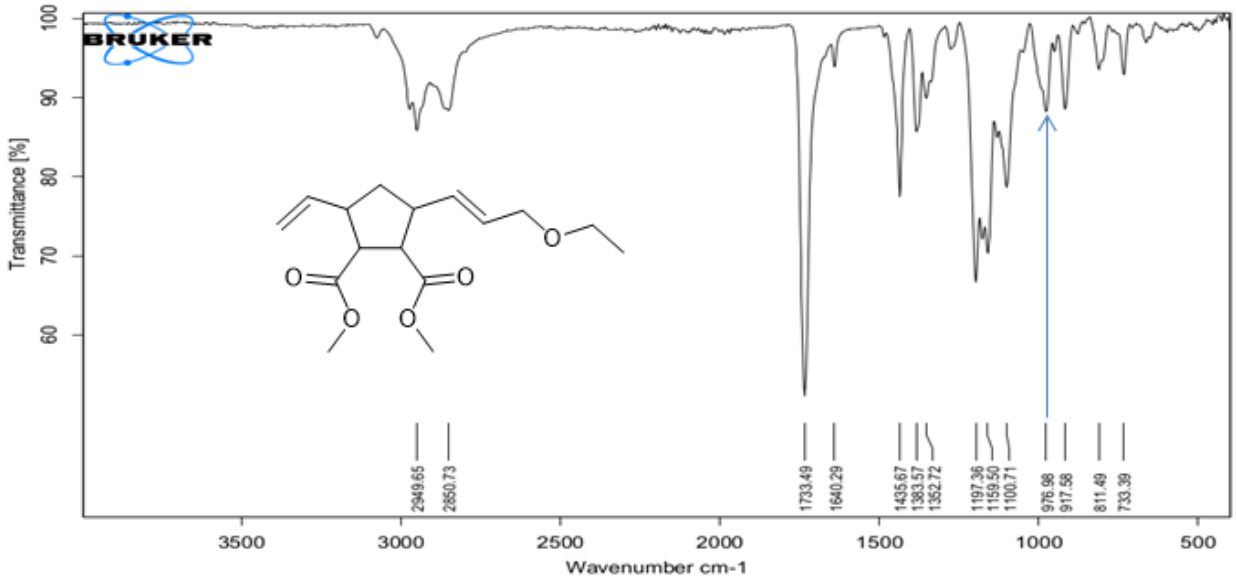

Figure 66. IR-spectrum of **P6**. The characteristic peak for the *trans*-isomer is observed at 977.0 cm^{-1}.

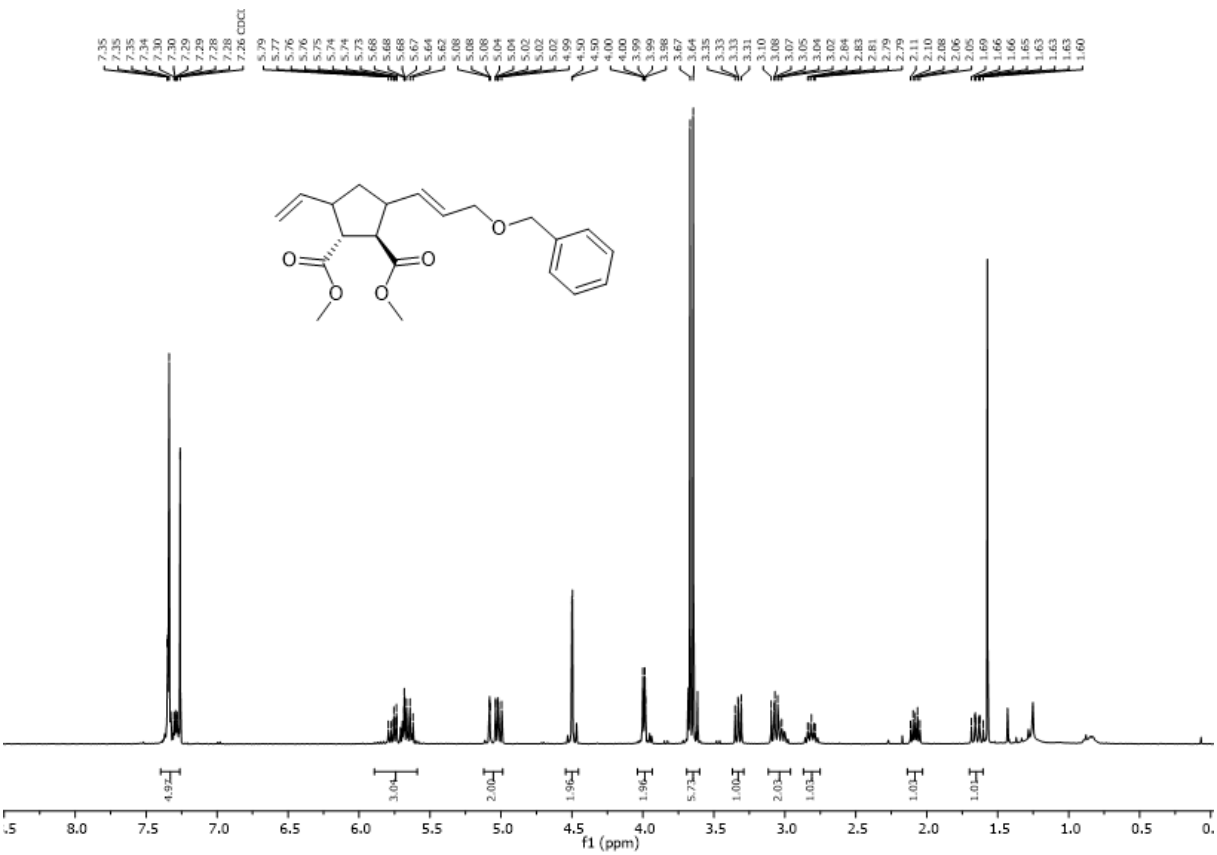

Figure 67. ^{1}H NMR spectrum of **P7** (400 MHz, $CDCl_3$).

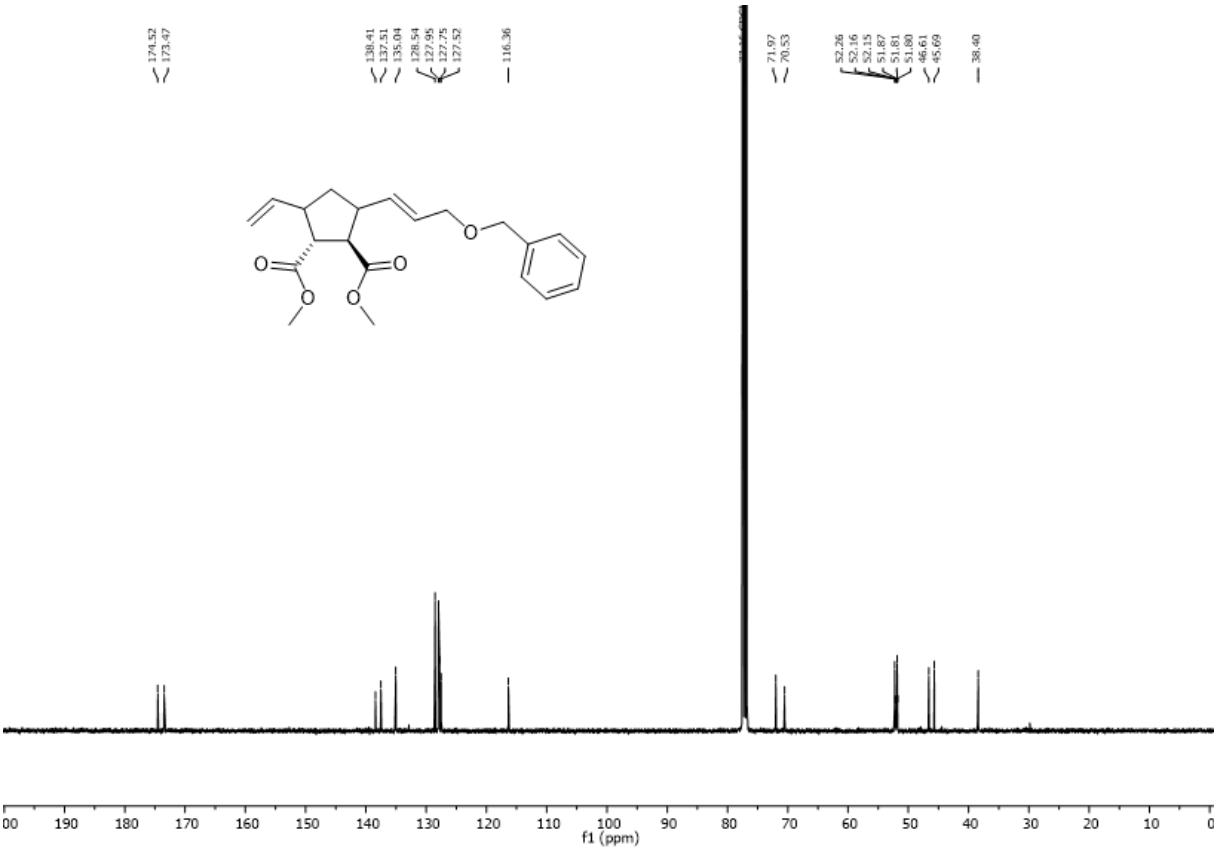

Figure 68. ^{13}C NMR spectrum of **P7** (101 MHz, $CDCl_3$).

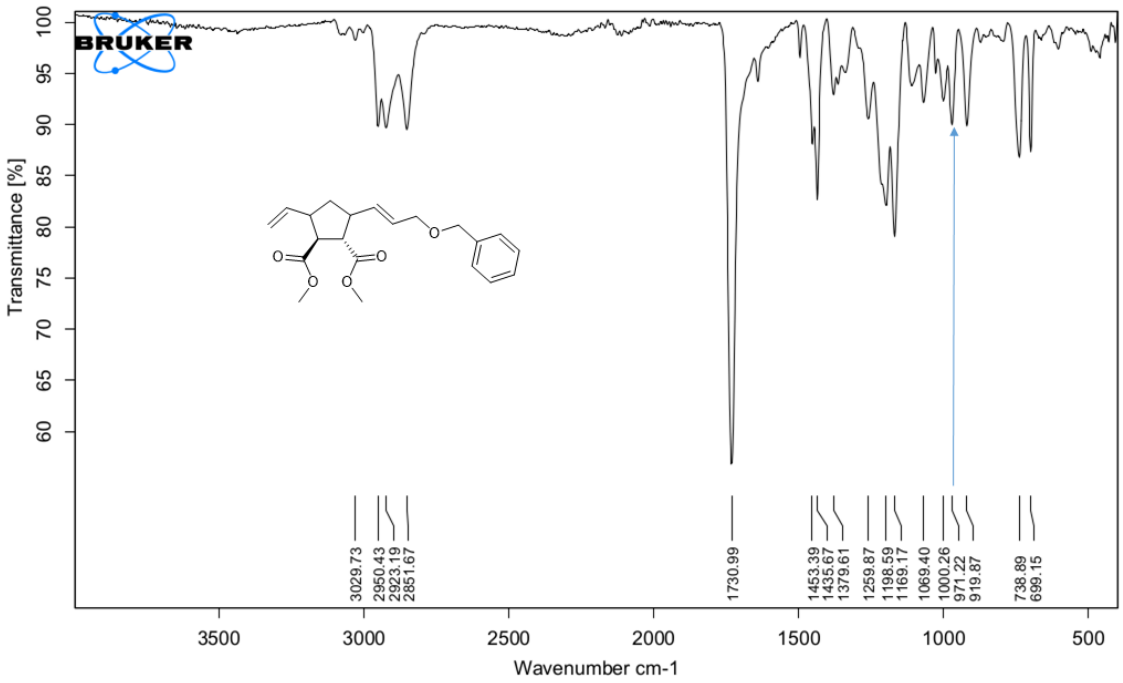

Figure 69. IR-spectrum of **P7**. The characteristic peak for the *trans*-isomer is observed at 971.2 cm^{-1}.

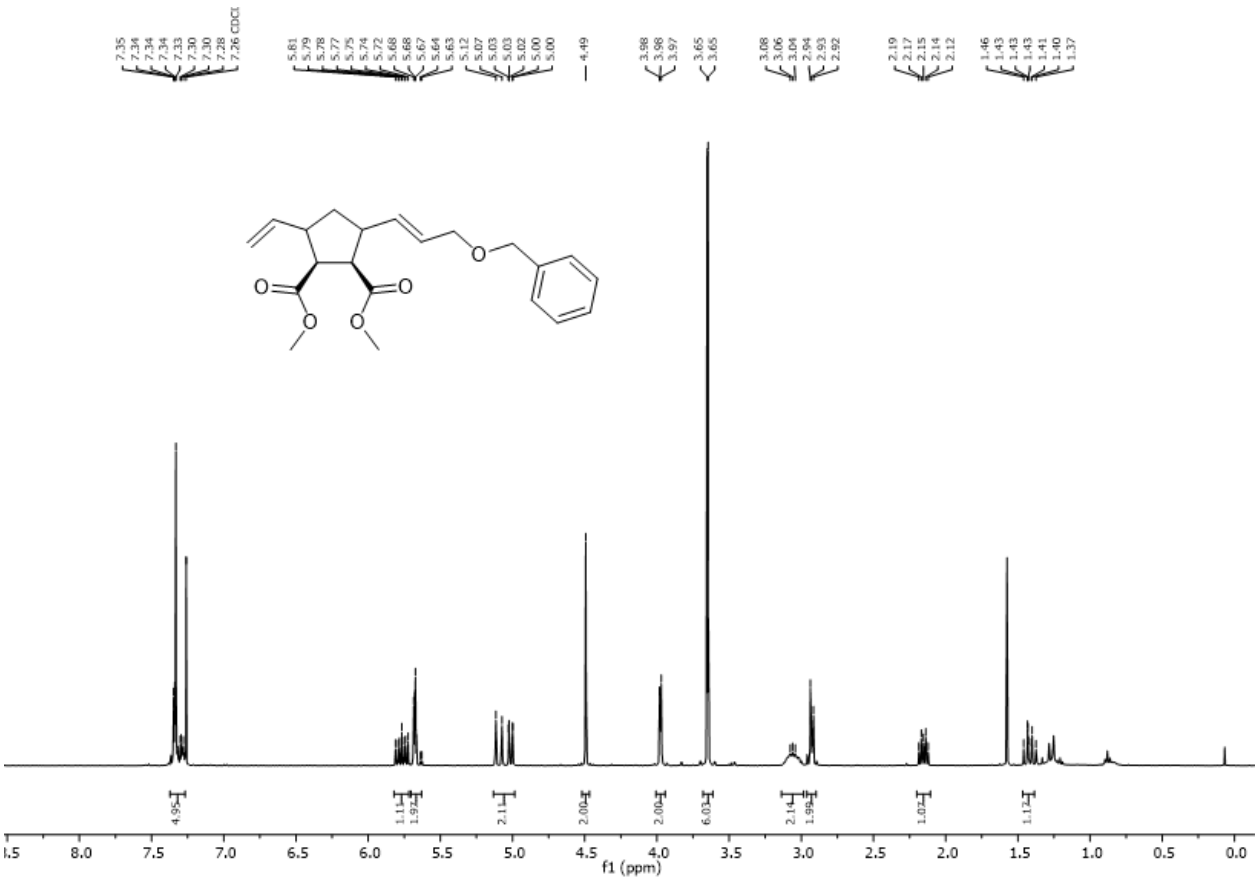

Figure 70. ^{1}H NMR spectrum of **P8** (400 MHz, $CDCl_3$).

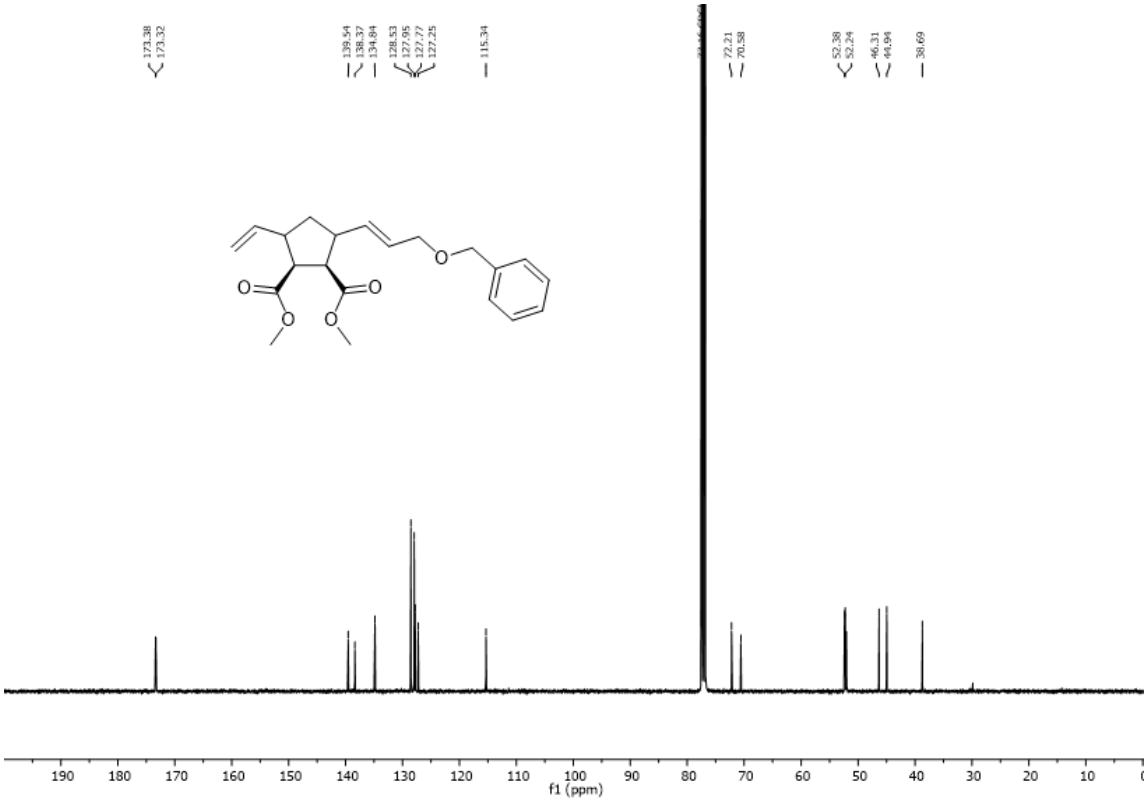

Figure 71. ^{13}C NMR spectrum of **P8** (101 MHz, $CDCl_3$).

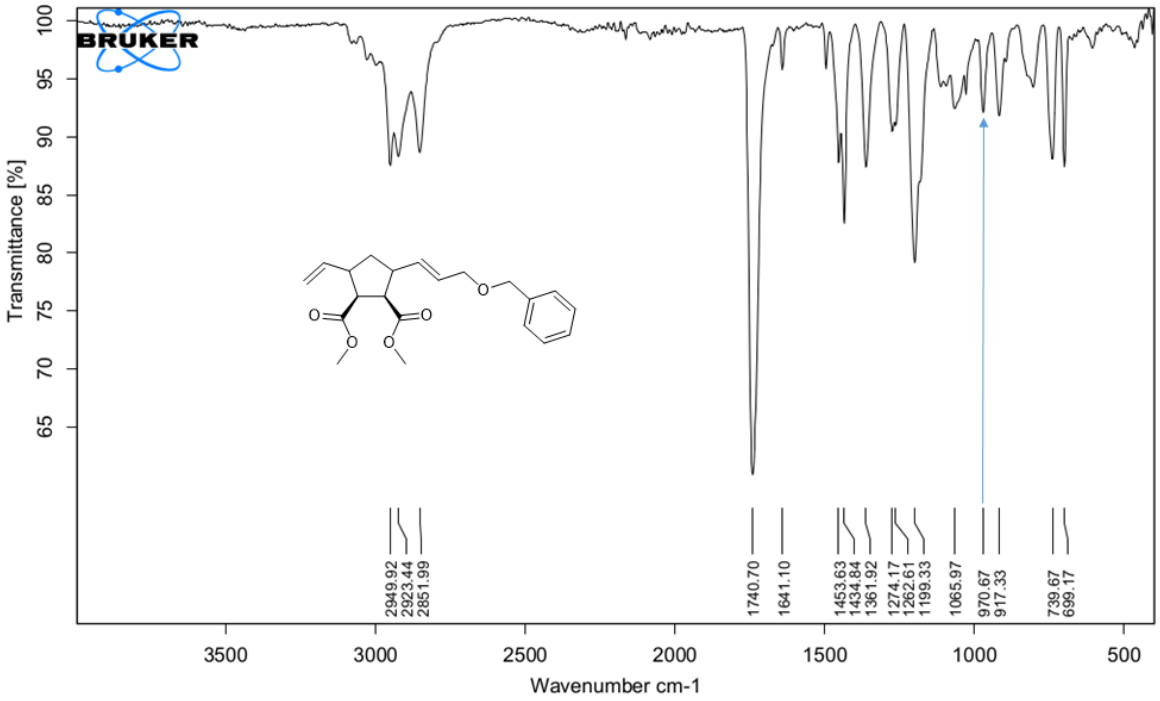

Figure 72. IR-spectrum of **P8**. The characteristic peak for the *trans*-isomer is observed at 970.7 cm^{-1}.

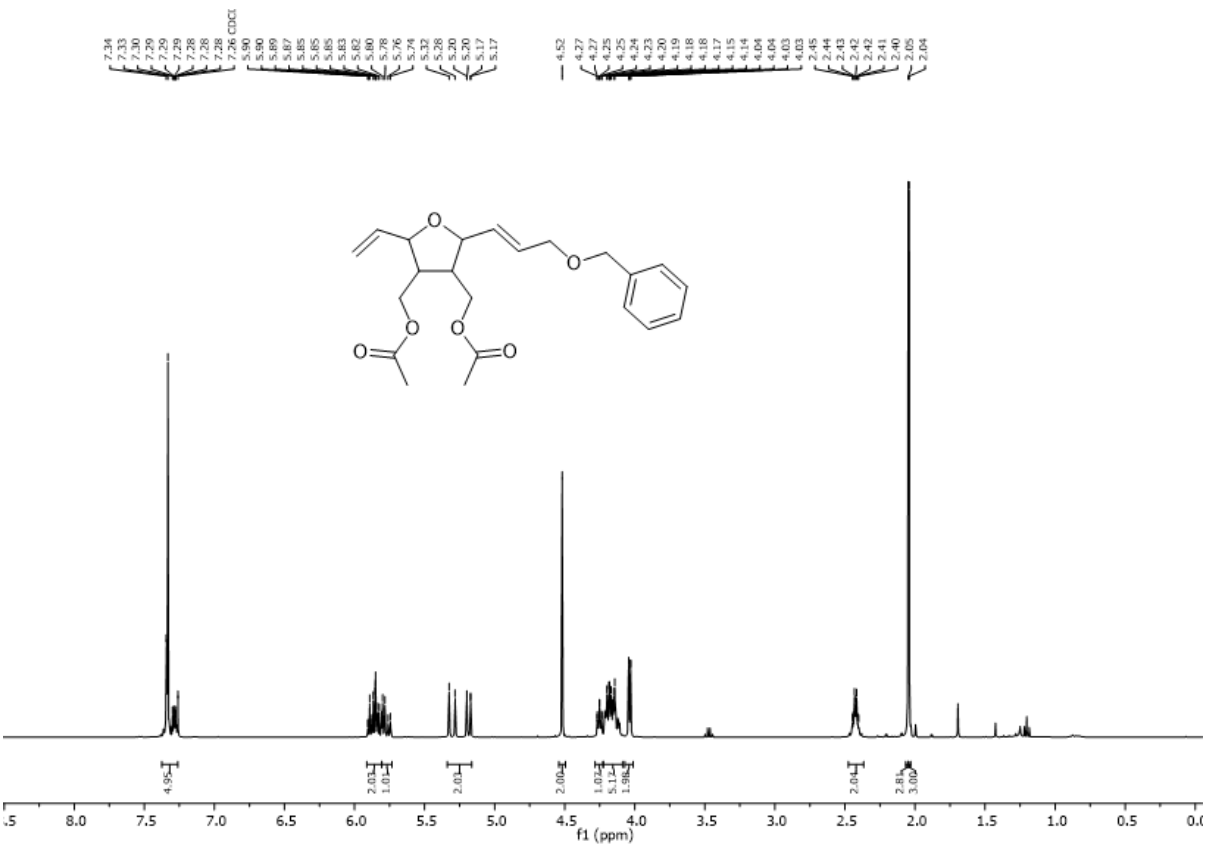

Figure 73. ^{1}H NMR spectrum of **P9** (400 MHz, $CDCl_3$).

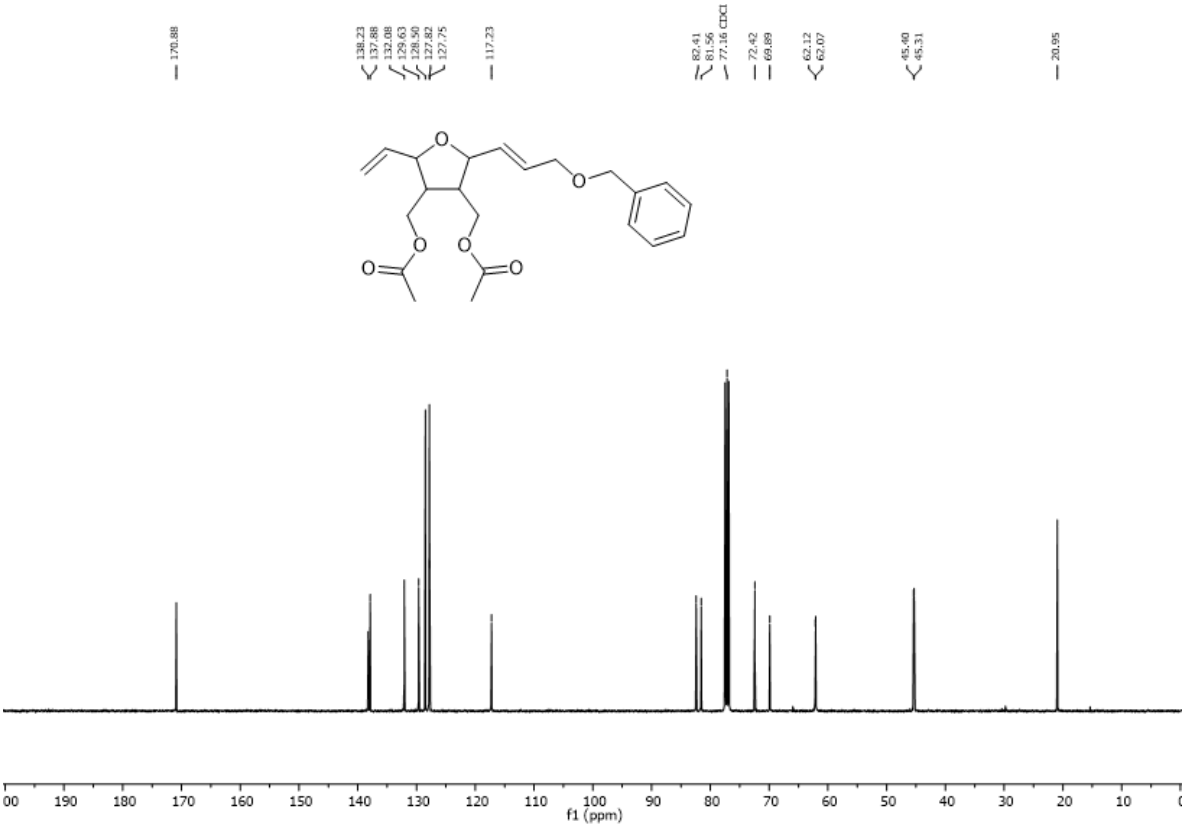

Figure 74. ^{13}C NMR spectrum of **P9** (101 MHz, $CDCl_3$).

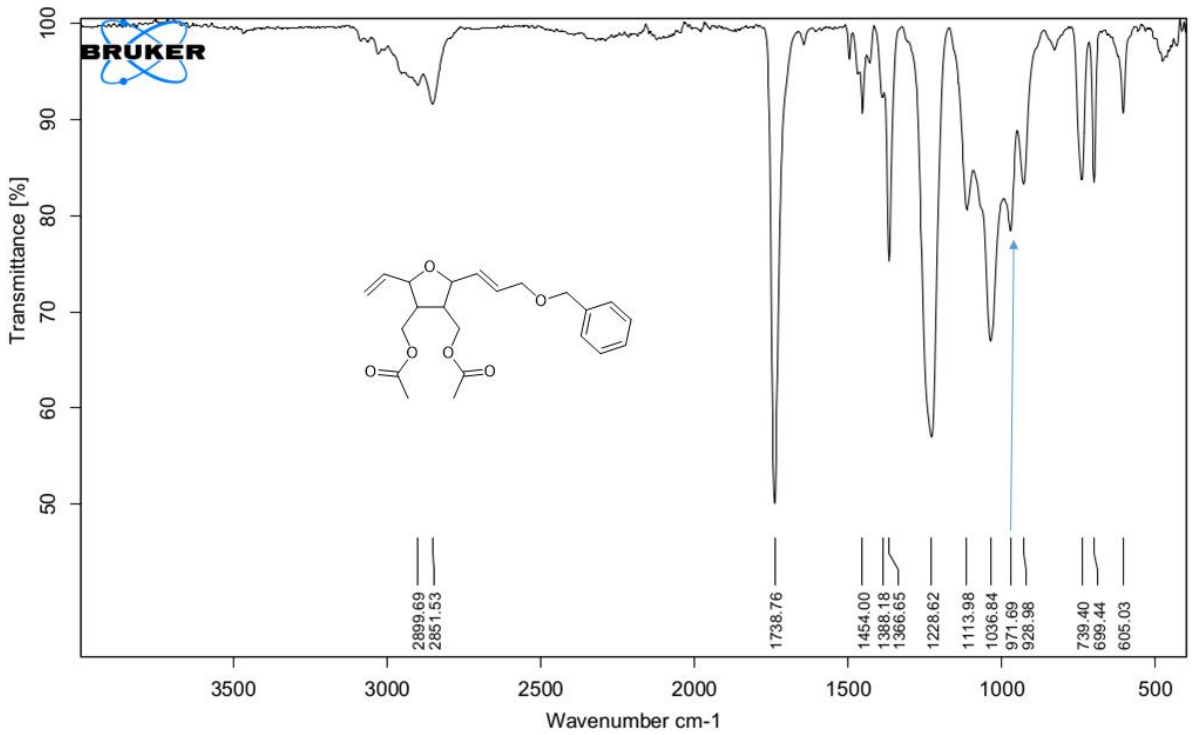

Figure 75. IR-spectrum of **P9**. The characteristic peak for the *trans*-isomer is observed at 971.7 cm^{-1}.

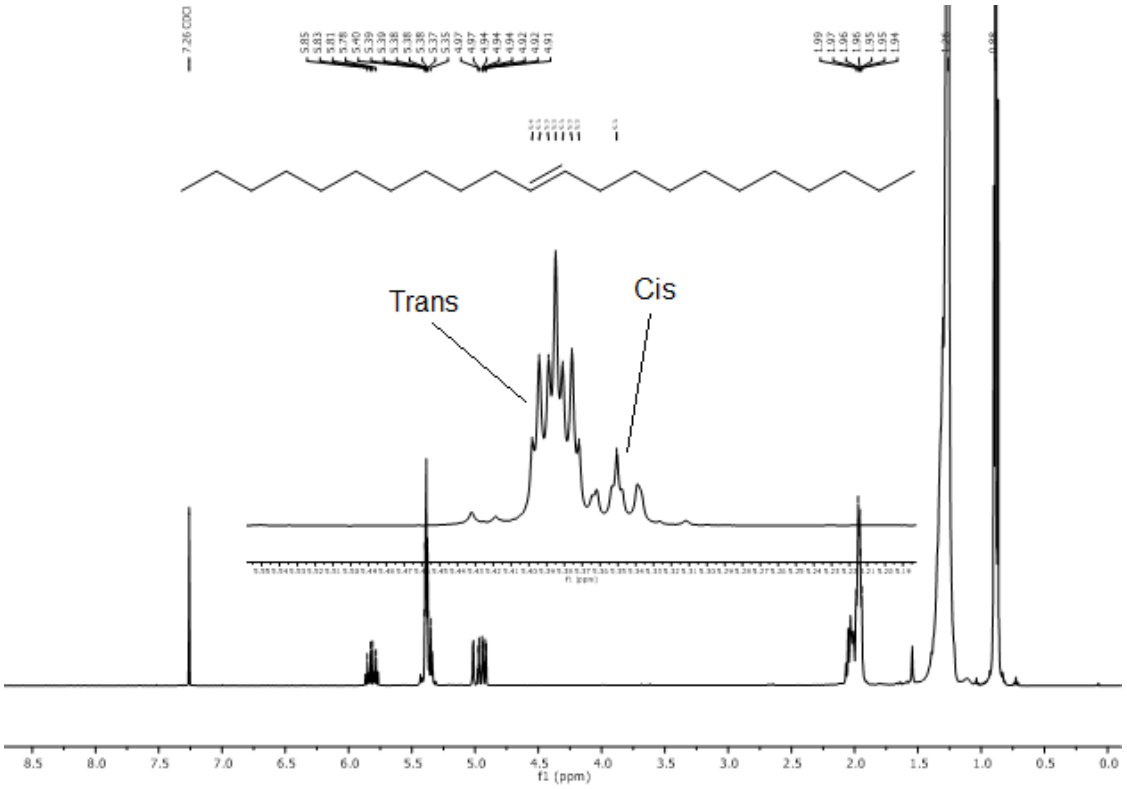

Figure 76. ^{1}H NMR spectrum of a mixture of product from the SM of 1-dodecene and the unreacted 1-dodecene ($CDCl_3$, 400 MHz).

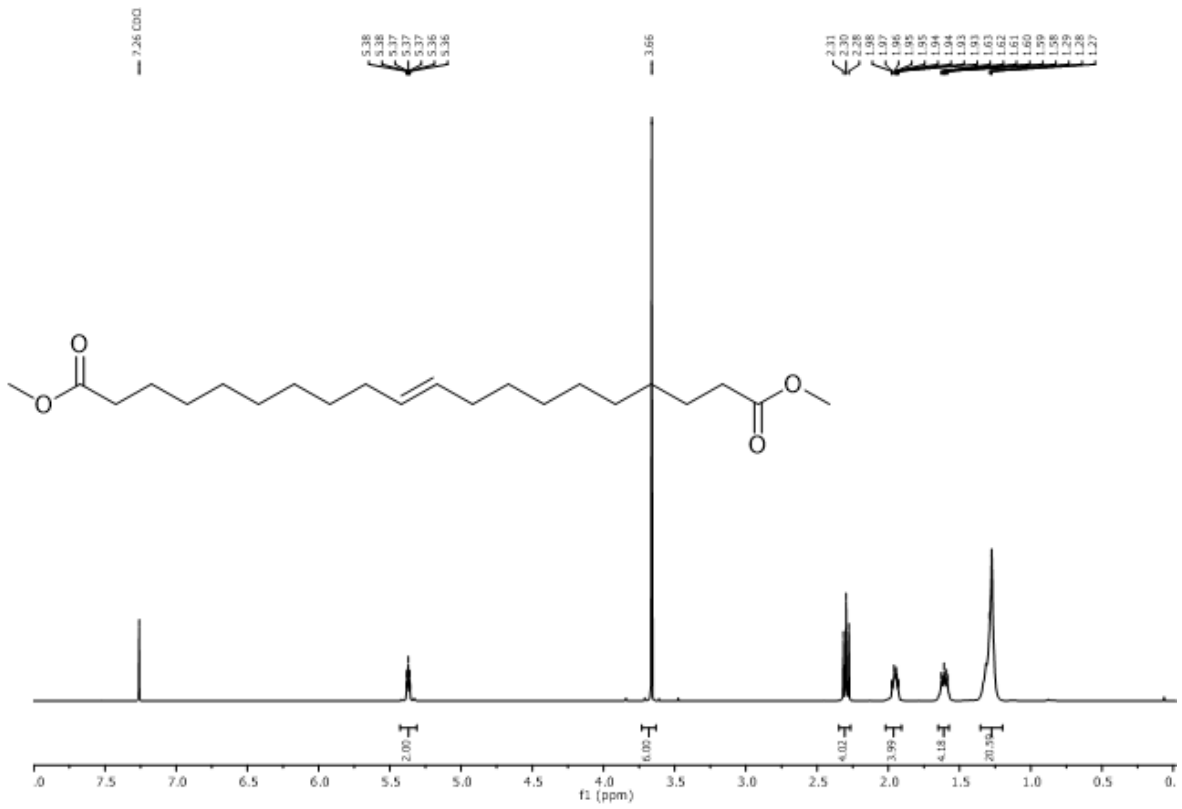

Figure 77. ^{1}H NMR spectrum of the SM product of methyl 10-undecenoate ($CDCl_3$, 400 MHz).

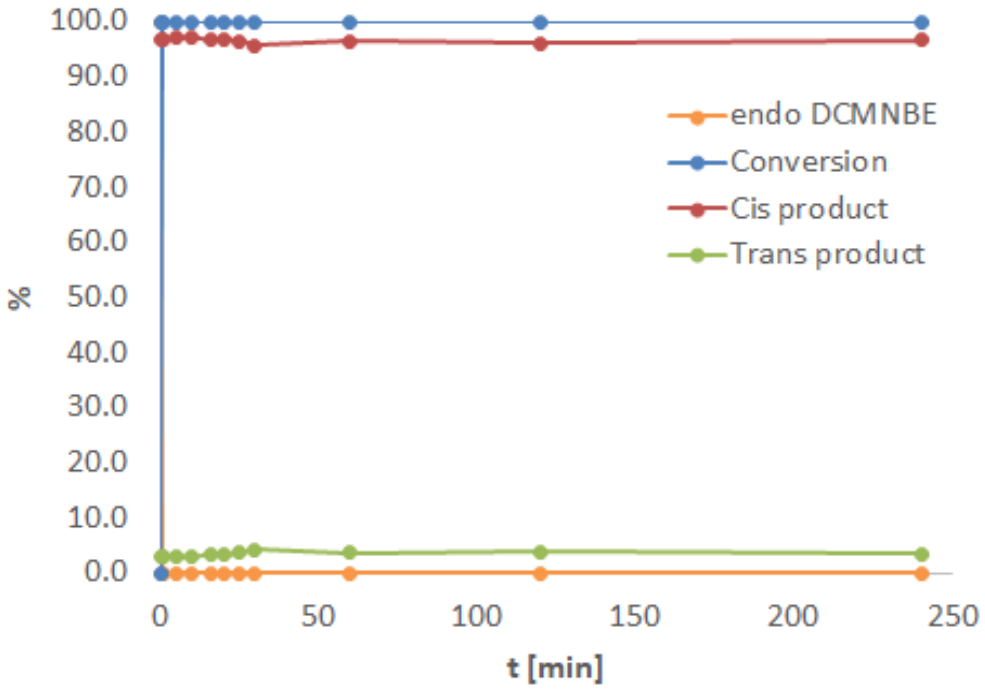

Figure 78. Ring-opening cross-metathesis kinetics of *endo, endo*-DCMNBE with 1-pentene, complex **Mo-5**.

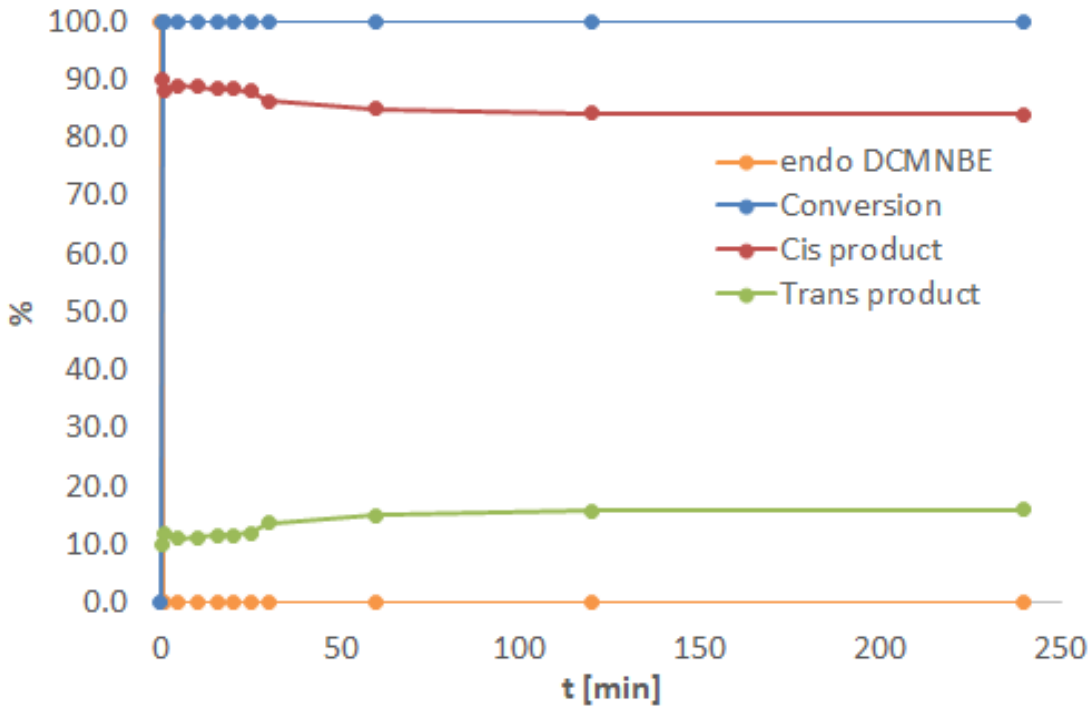

Figure 79. Ring-opening cross-metathesis kinetics of *endo, endo*-DCMNBE with allytrimethylsilane, complex **Mo-5**.

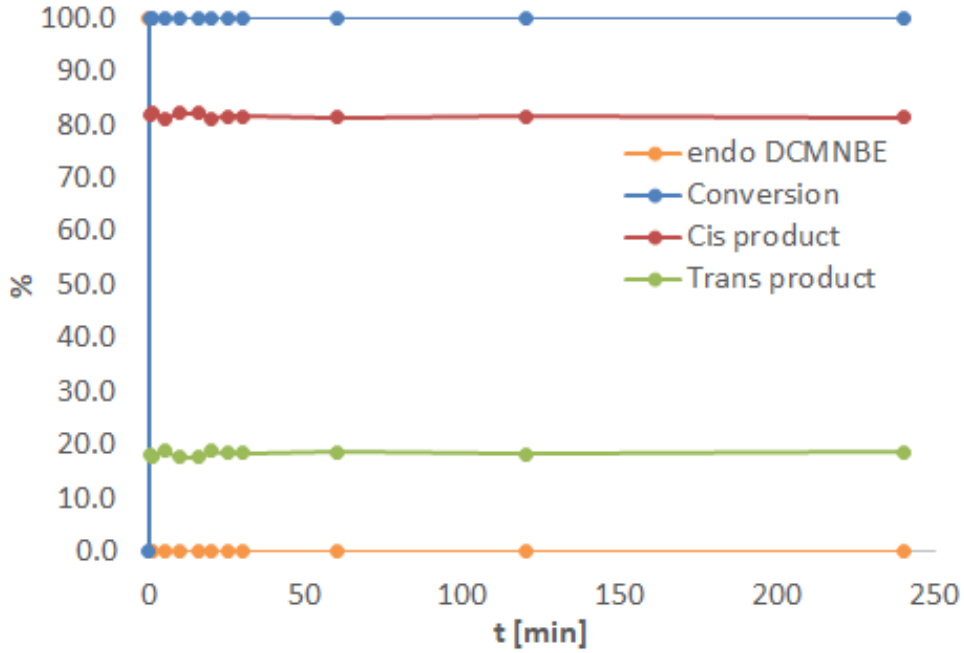

Figure 80. Ring-opening cross-metathesis kinetics of *endo, endo*-DCMNBE with allyl phenyl ether, complex **Mo-5**.

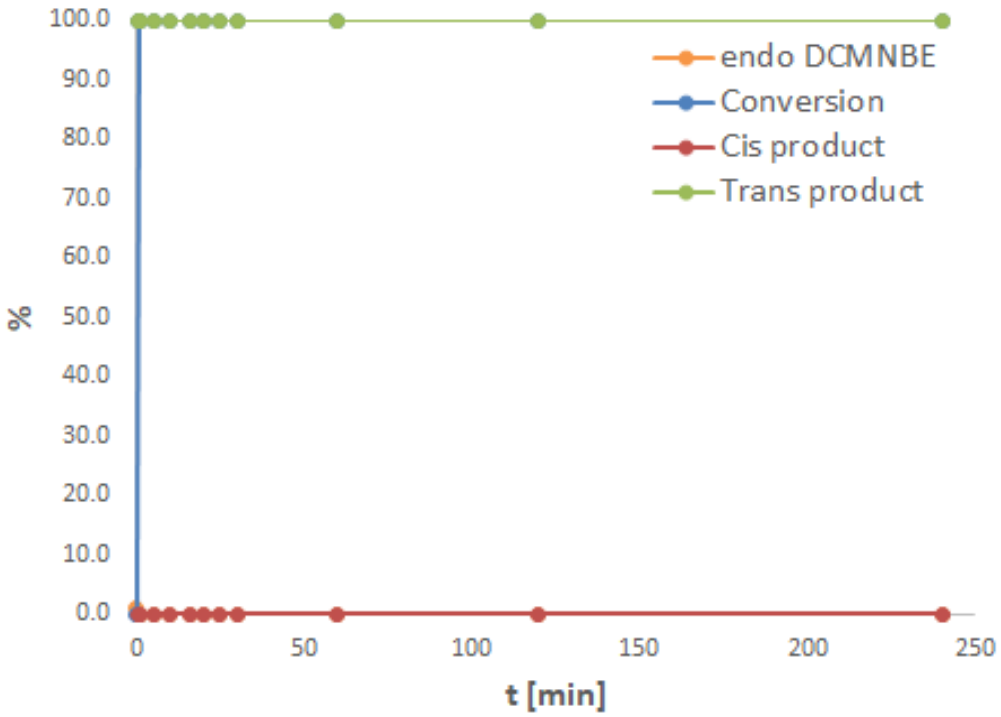

Figure 81. Ring-opening cross-metathesis kinetics of *endo*, *endo*-DCMNBE with allyl ethyl ether, complex **Mo-5**.

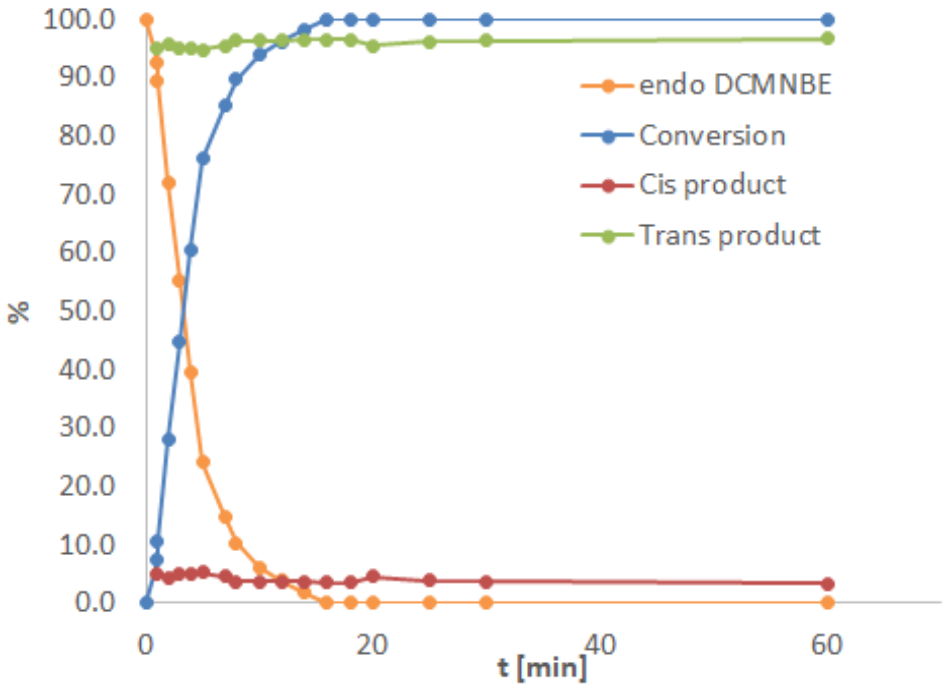

Figure 82. Ring-opening cross-metathesis kinetics of *endo, endo*-DCMNBE with styrene, complex **Mo-2**.

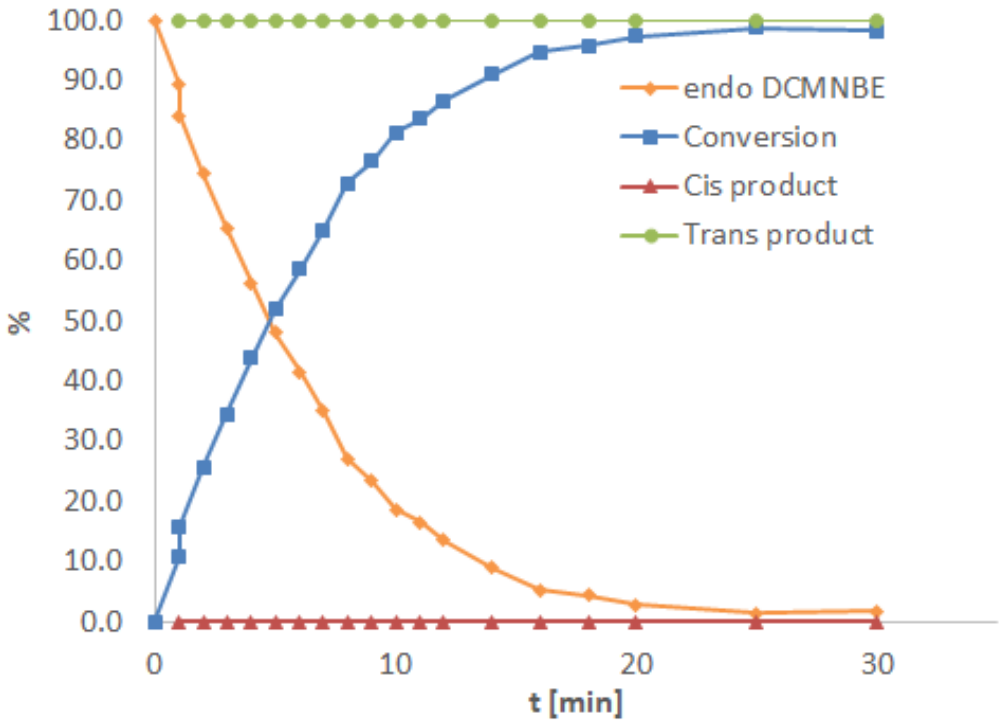

Figure 83. Ring-opening cross-metathesis kinetics of *endo* DCMNBE with allyl phenyl ether, complex **Mo-2**.

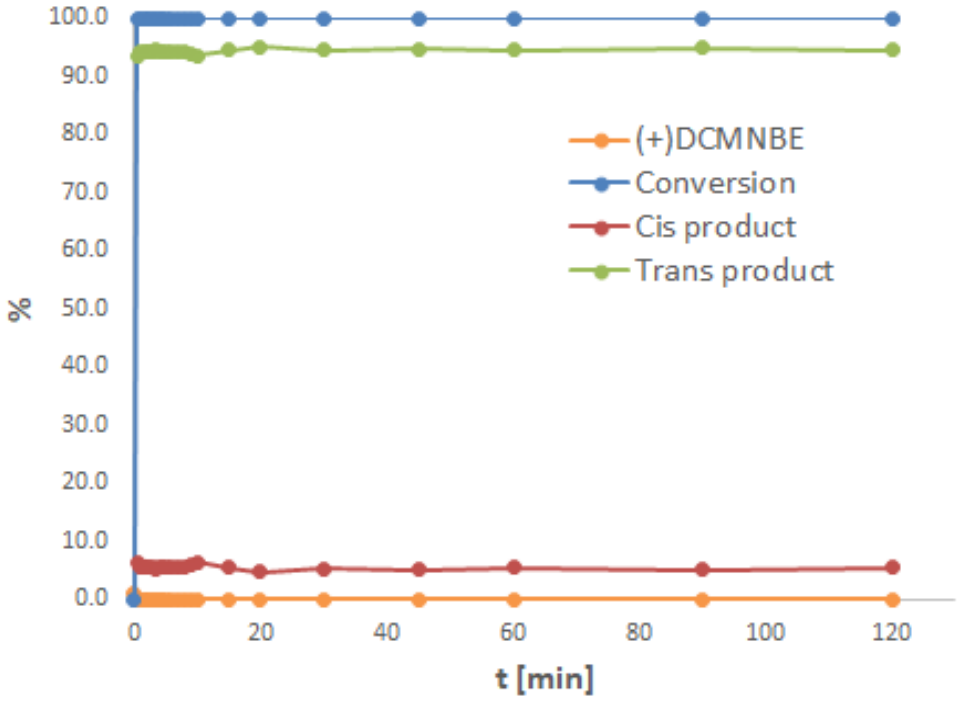

Figure 84. Ring-opening cross-metathesis kinetics of (+) DCMNBE with allyl benzyl ether, complex **Mo-2**.

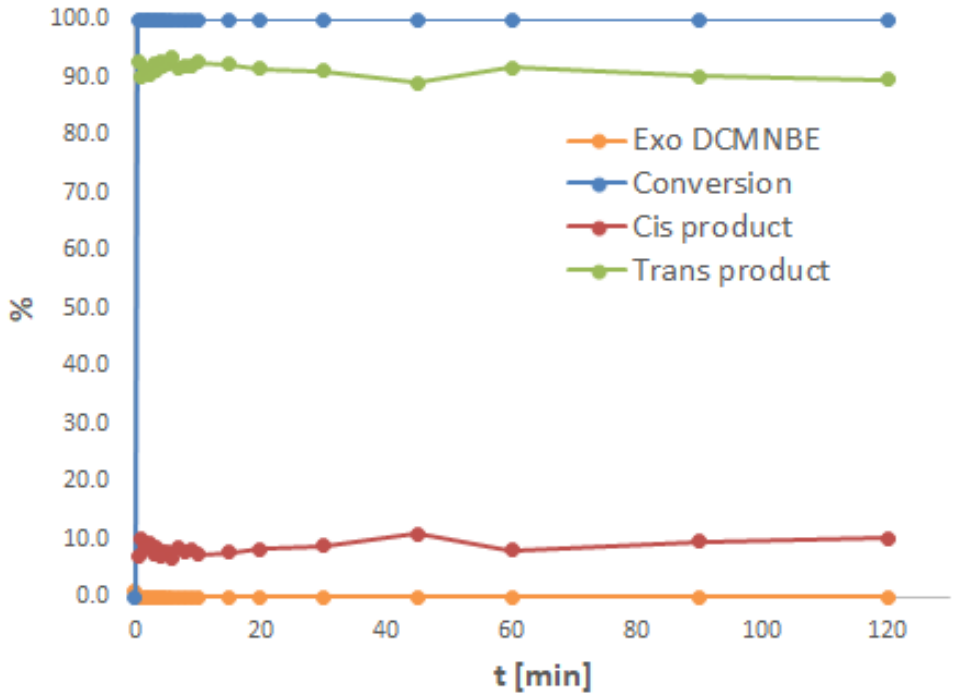

Figure 85. Ring-opening cross-metathesis kinetics of *exo, exo*-DCMNBE with allyl benzyl ether, complex **Mo-2**.

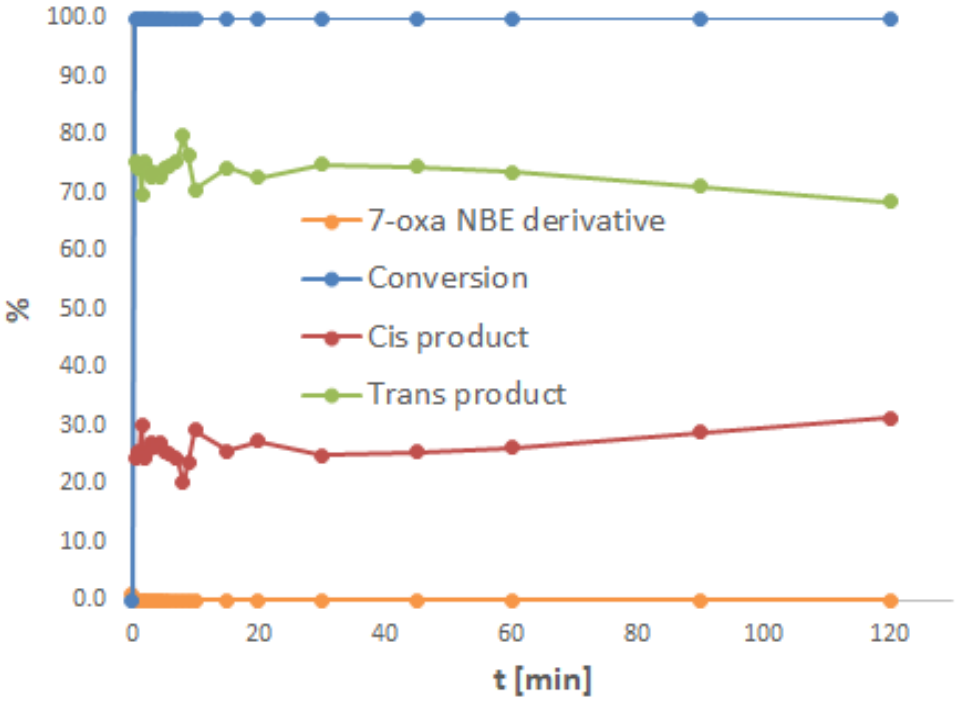

Figure 86. Ring-opening cross-metathesis kinetics of 7-oxa-NBE with allyl benzyl ether, complex **Mo-2**.

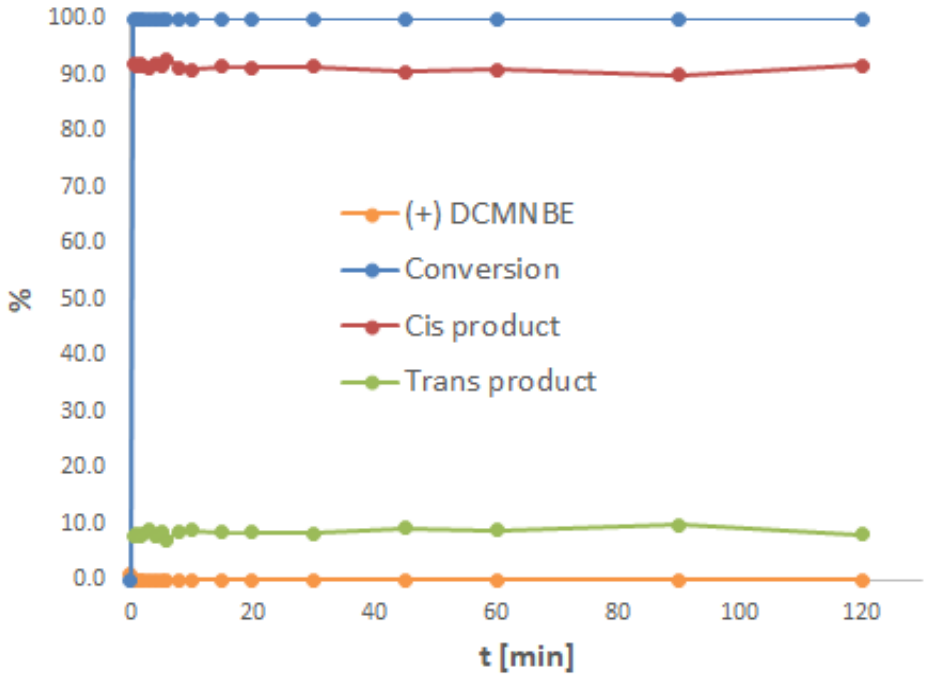

Figure 87. Ring-opening cross-metathesis kinetics of (+) DCMNBE with allyl benzyl ether, complex **Mo-5**.

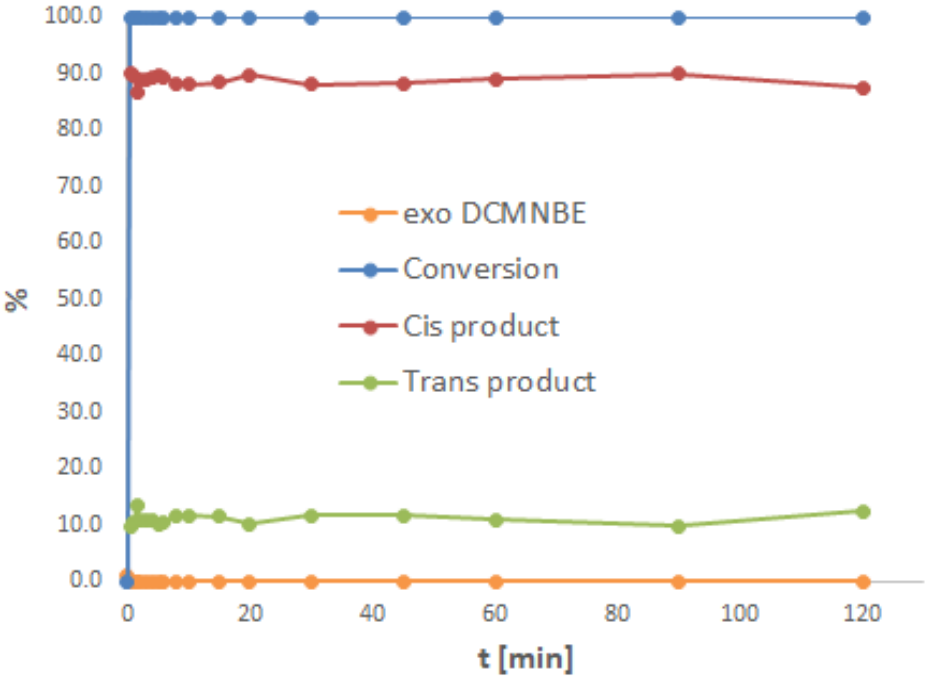

Figure 88. Ring-opening cross-metathesis kinetics of *exo, exo*-DCMNBE with allyl benzyl ether, complex **Mo-5**.

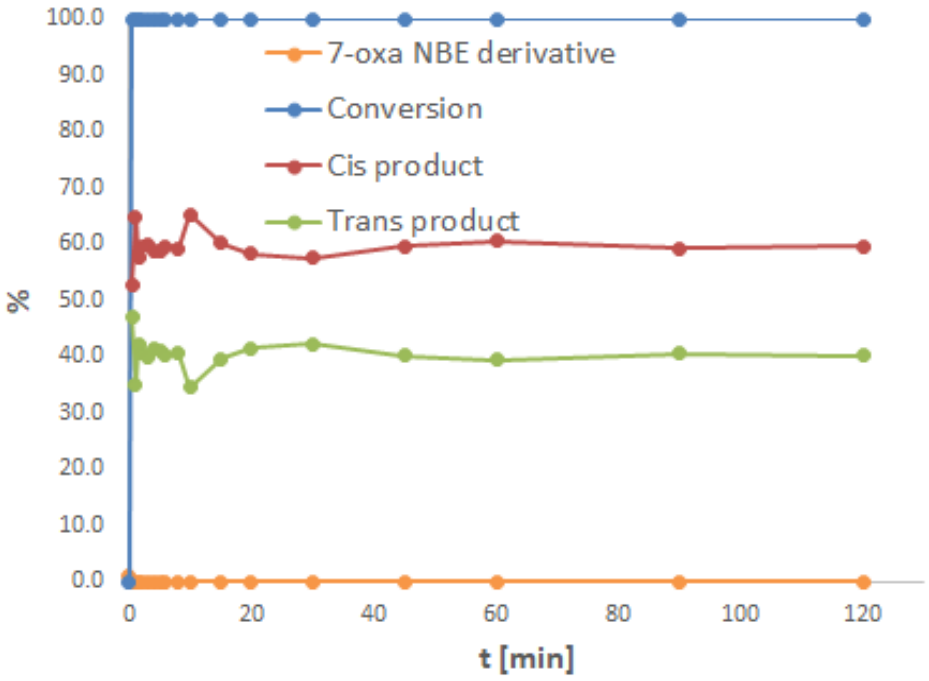

Figure 89. Ring-opening cross-metathesis kinetics of 7-oxa-NBE with allyl benzyl ether, complex **Mo-5**.

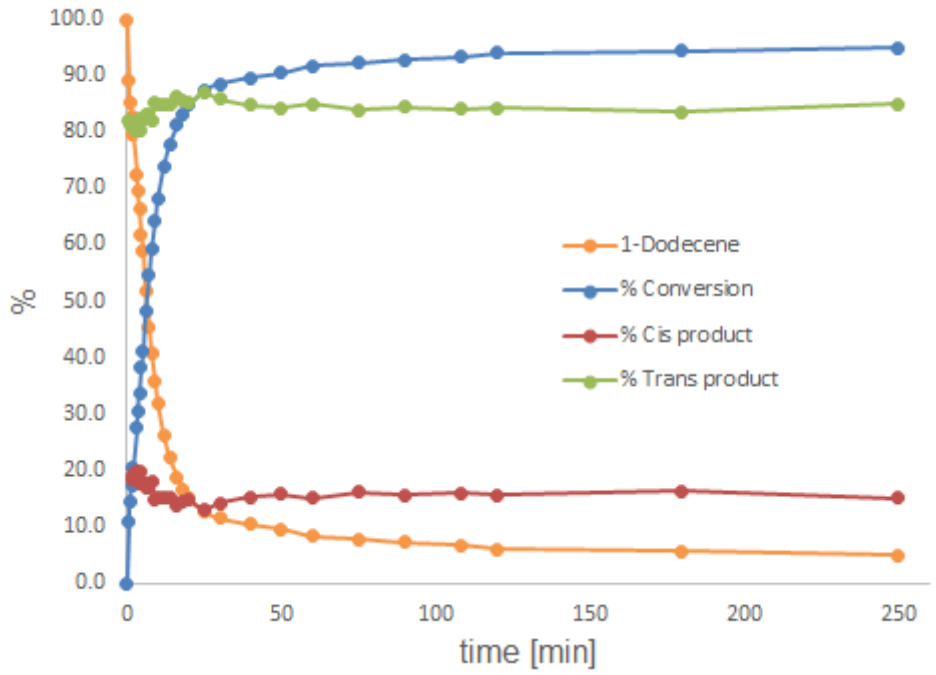

Figure 90. Self-metathesis kinetics of 1-dodecene, complex **Mo-2**.

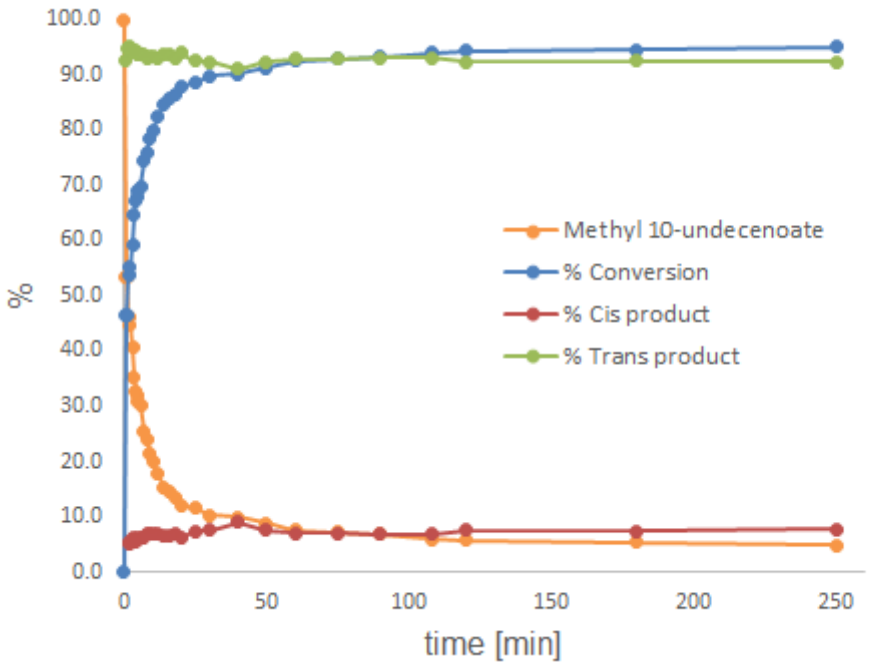

Figure 91. Self-metathesis kinetics of methyl 10-undecenoate, complex **Mo-2**.

7.2 Tuning the Latent Behavior of Molybdenum Imido Alkylidene *N*-Heterocyclic Carbene Complexes in Dicyclopentadiene Polymerization

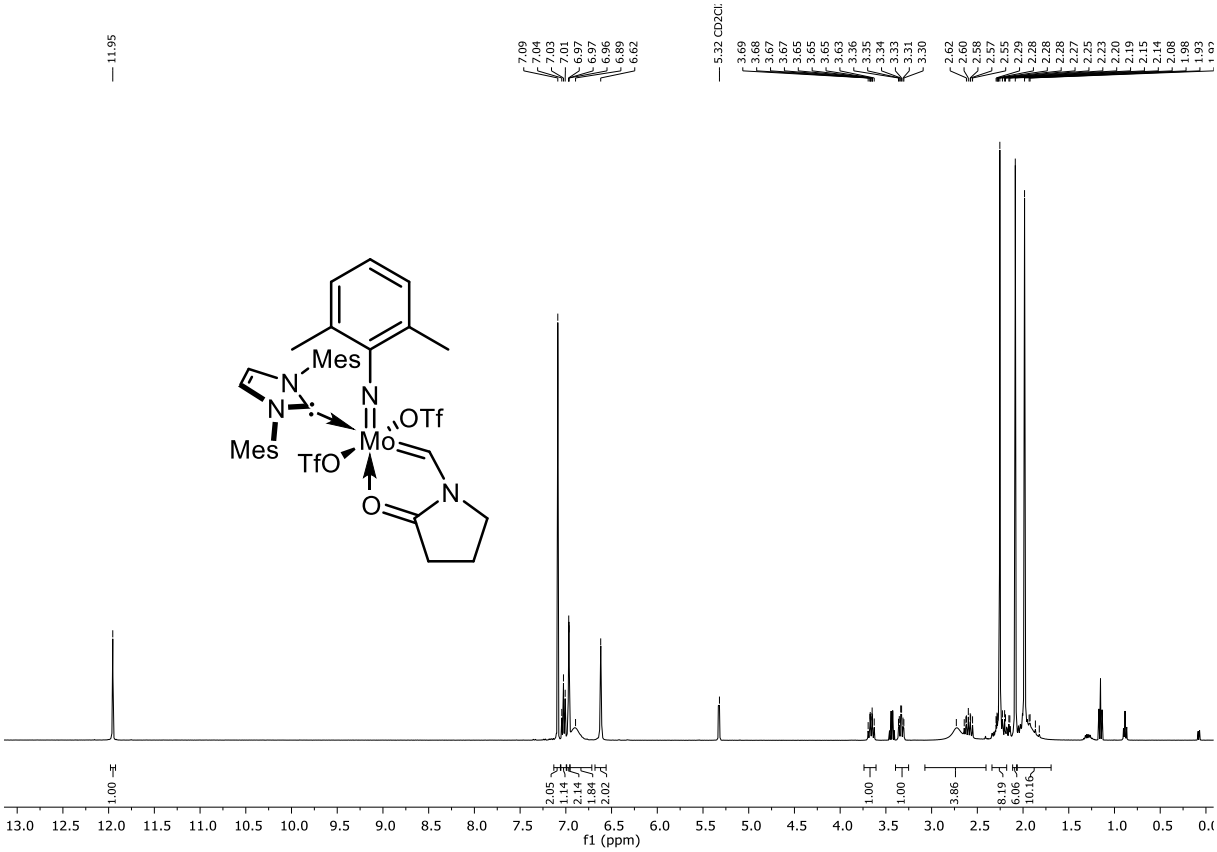

Figure 92. ^{1}H NMR spectrum of **Mo-6** (400 MHz, CD_2Cl_2).

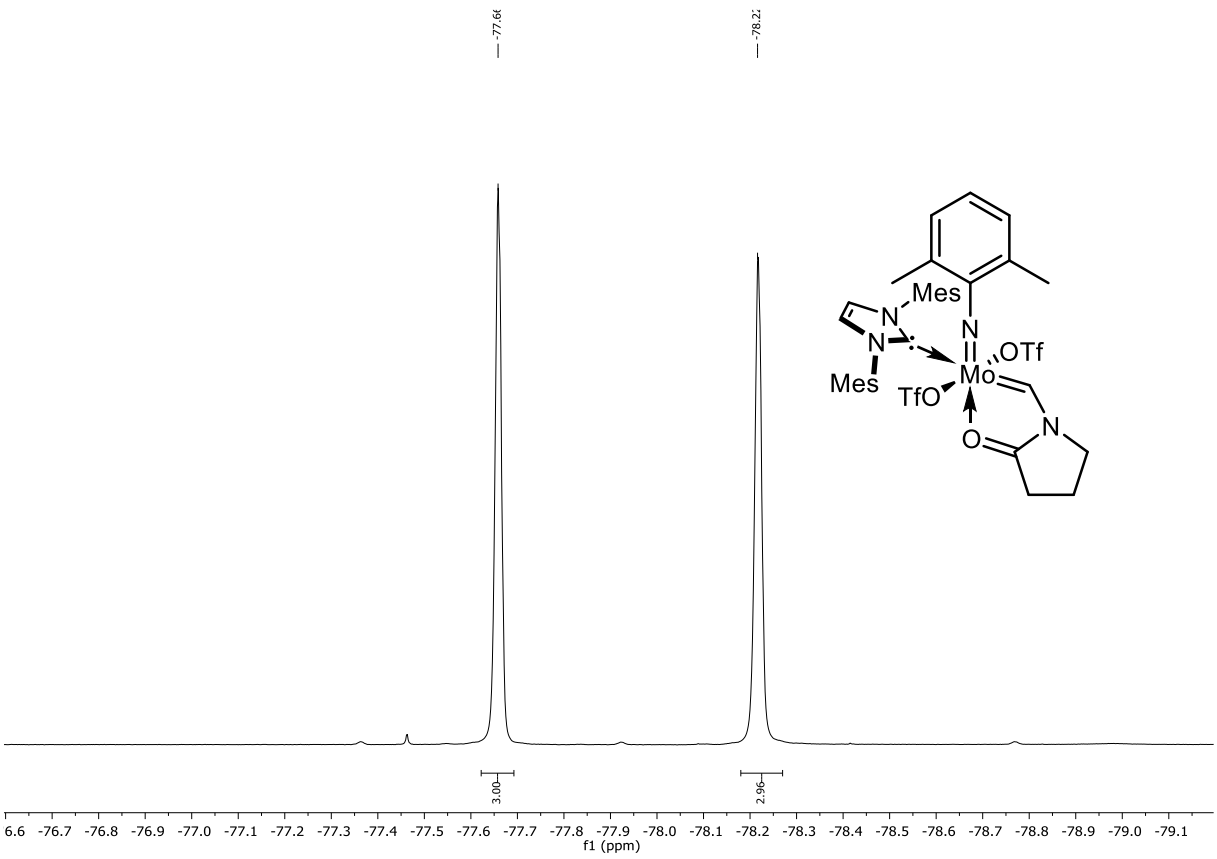

Figure 93. ^{19}F NMR spectrum of **Mo-6** (376 MHz, CD_2Cl_2).

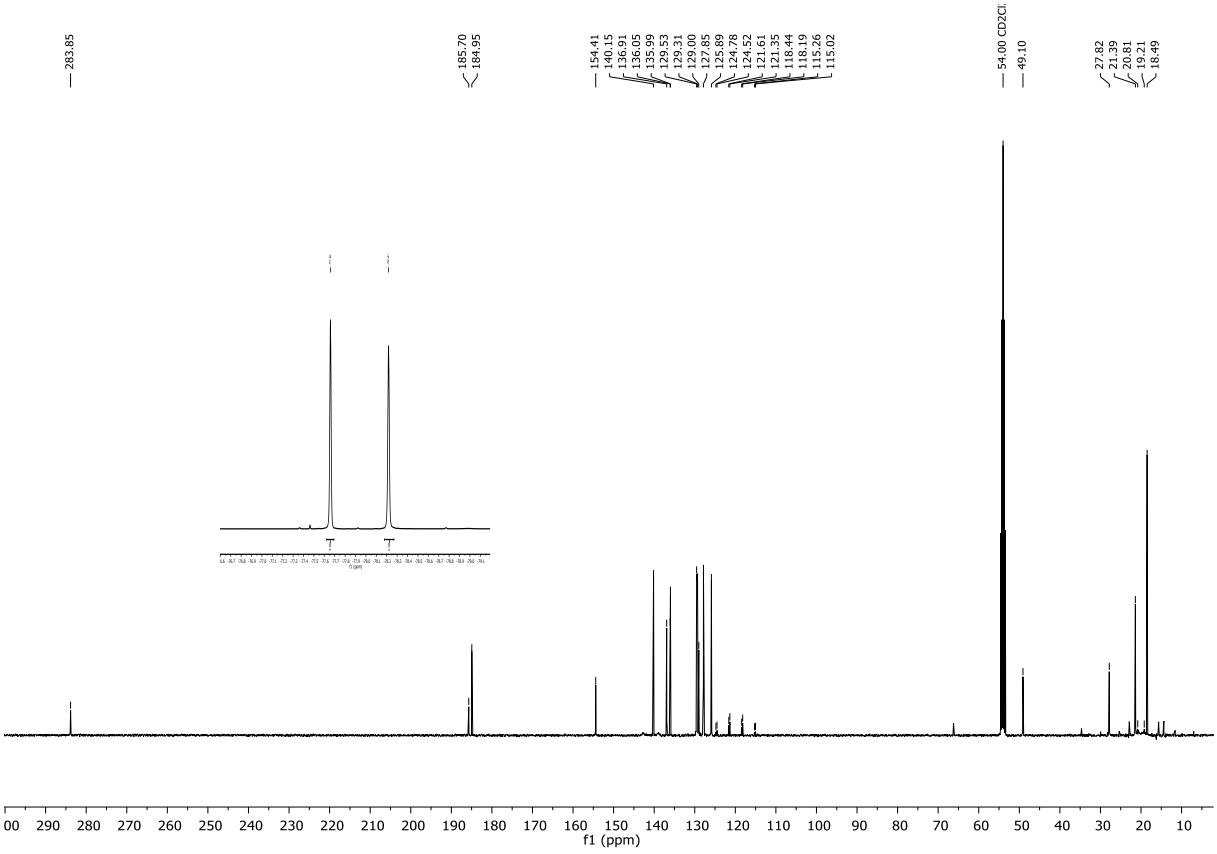

Figure 94. ^{13}C NMR spectrum of **Mo-6** (101 MHz, CD_2Cl_2).

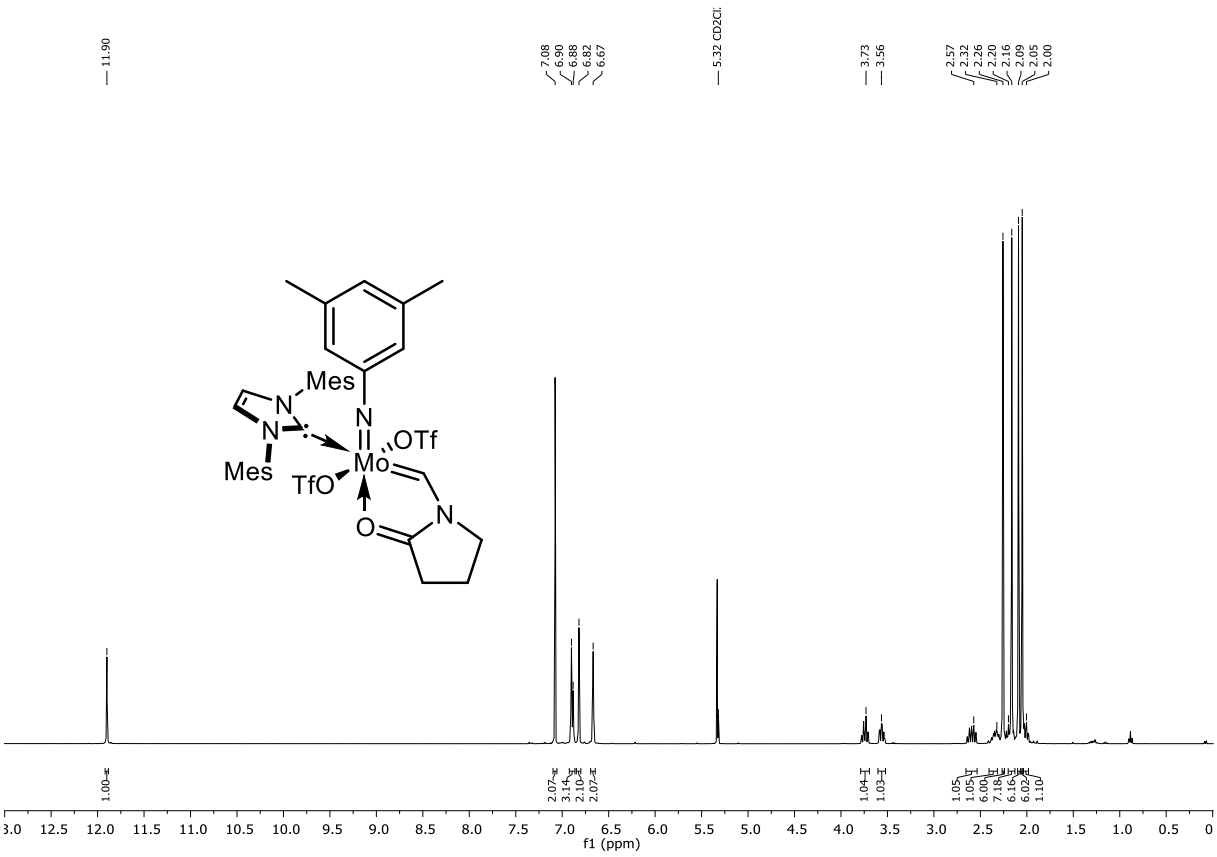

Figure 95. ^{1}H NMR spectrum of **Mo-7** (400 MHz, CD_2Cl_2).

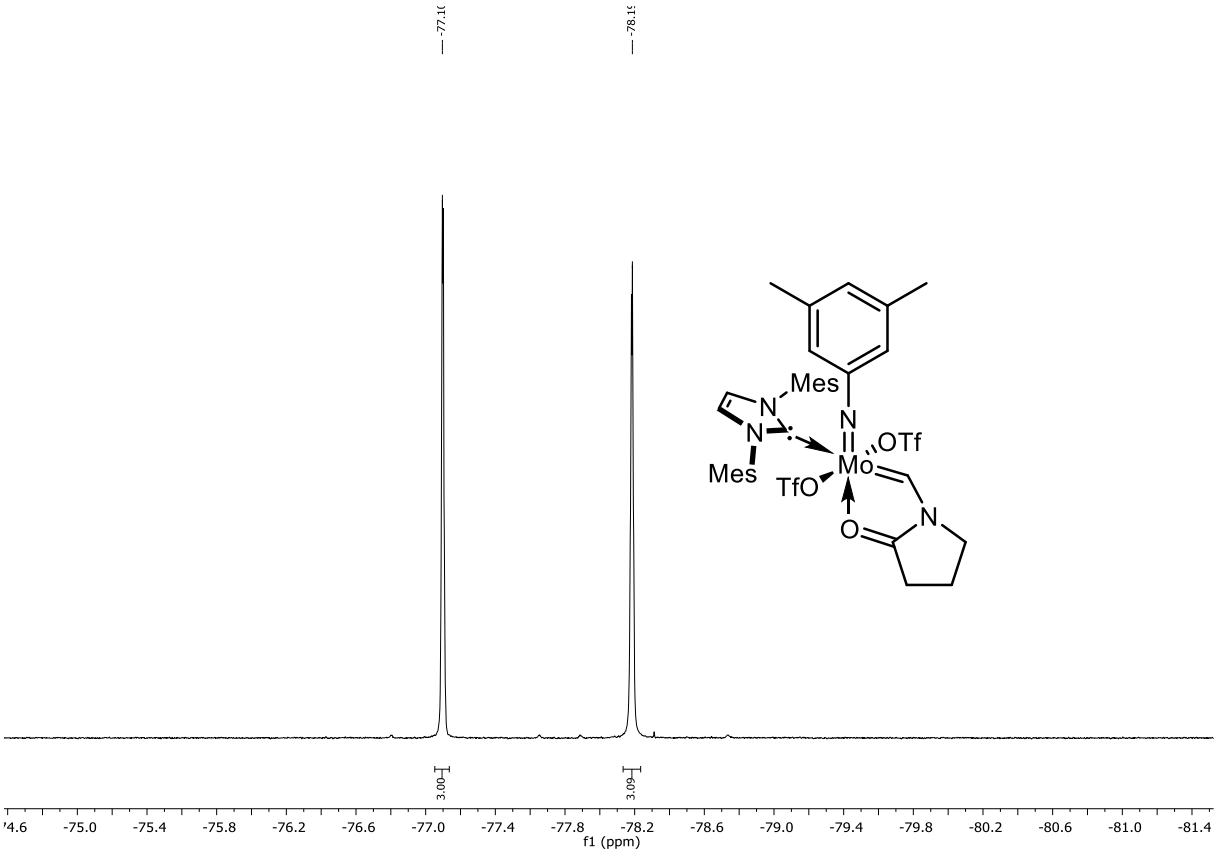

Figure 96. ^{19}F NMR spectrum of **Mo-7** (376 MHz, CD_2Cl_2).

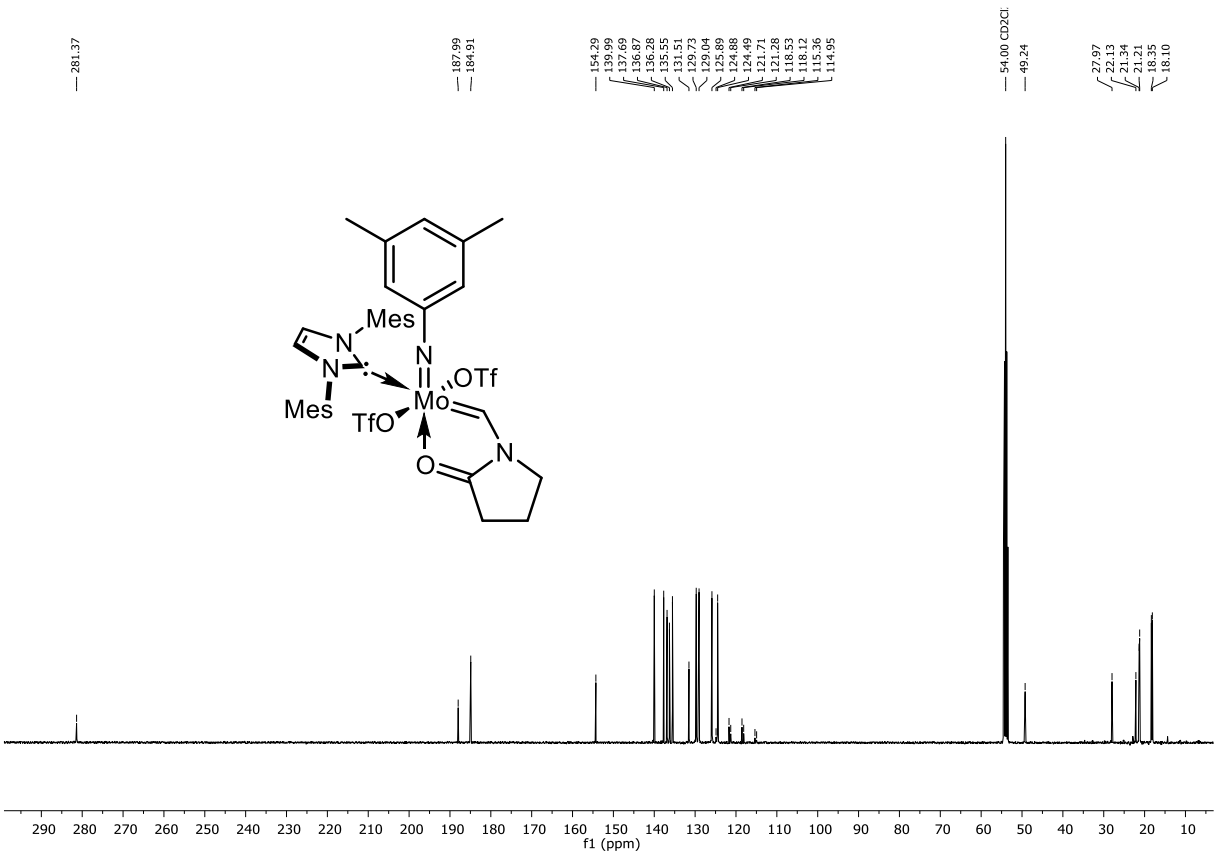

Figure 97. ^{13}C NMR spectrum of **Mo-7** (101 MHz, CD_2Cl_2).

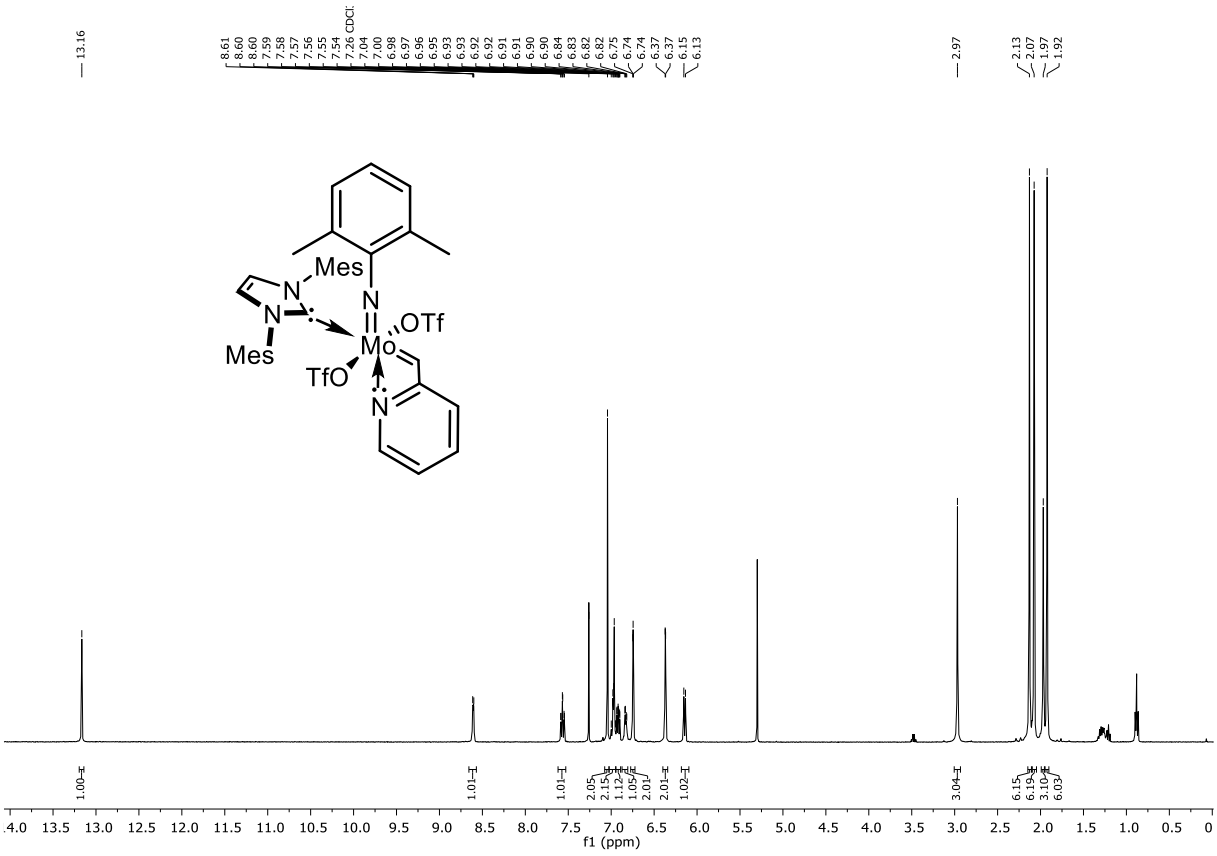

Figure 98. ^{1}H NMR spectrum of **Mo-8** (400 MHz, $CDCl_3$).

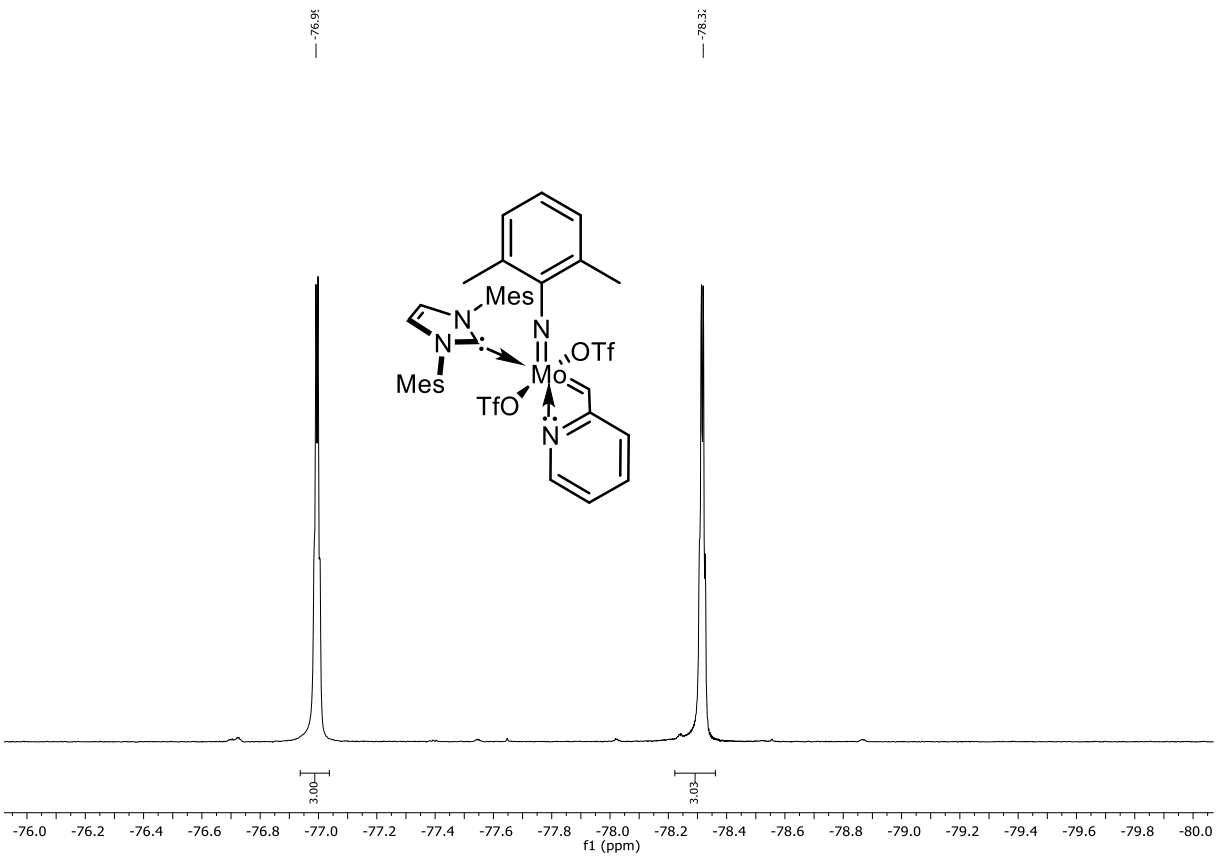

Figure 99. ^{19}F NMR spectrum of **Mo-8** (376 MHz, $CDCl_3$).

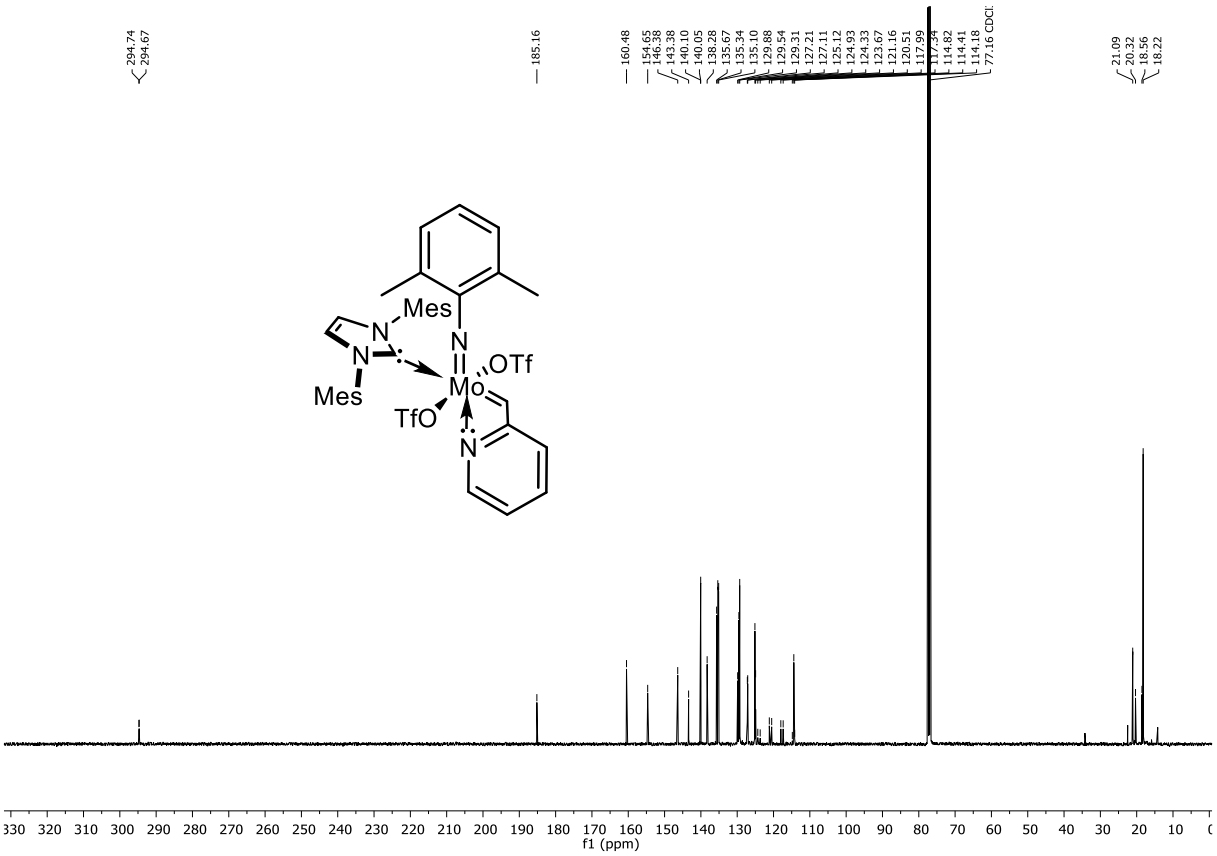

Figure 100. ^{13}C NMR spectrum of **Mo-8** (101 MHz, $CDCl_3$).

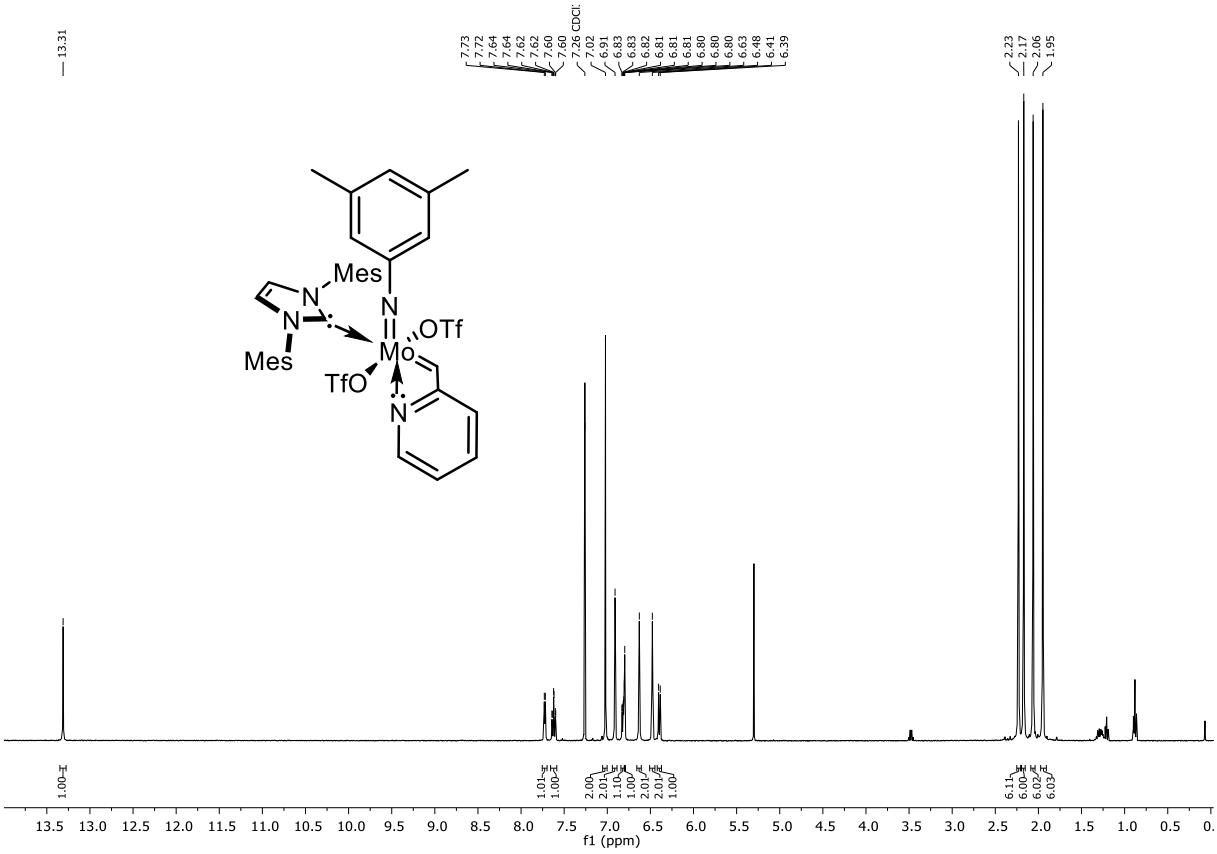

Figure 101. ^{1}H NMR spectrum of **Mo-9** (400 MHz, CD_2Cl_2).

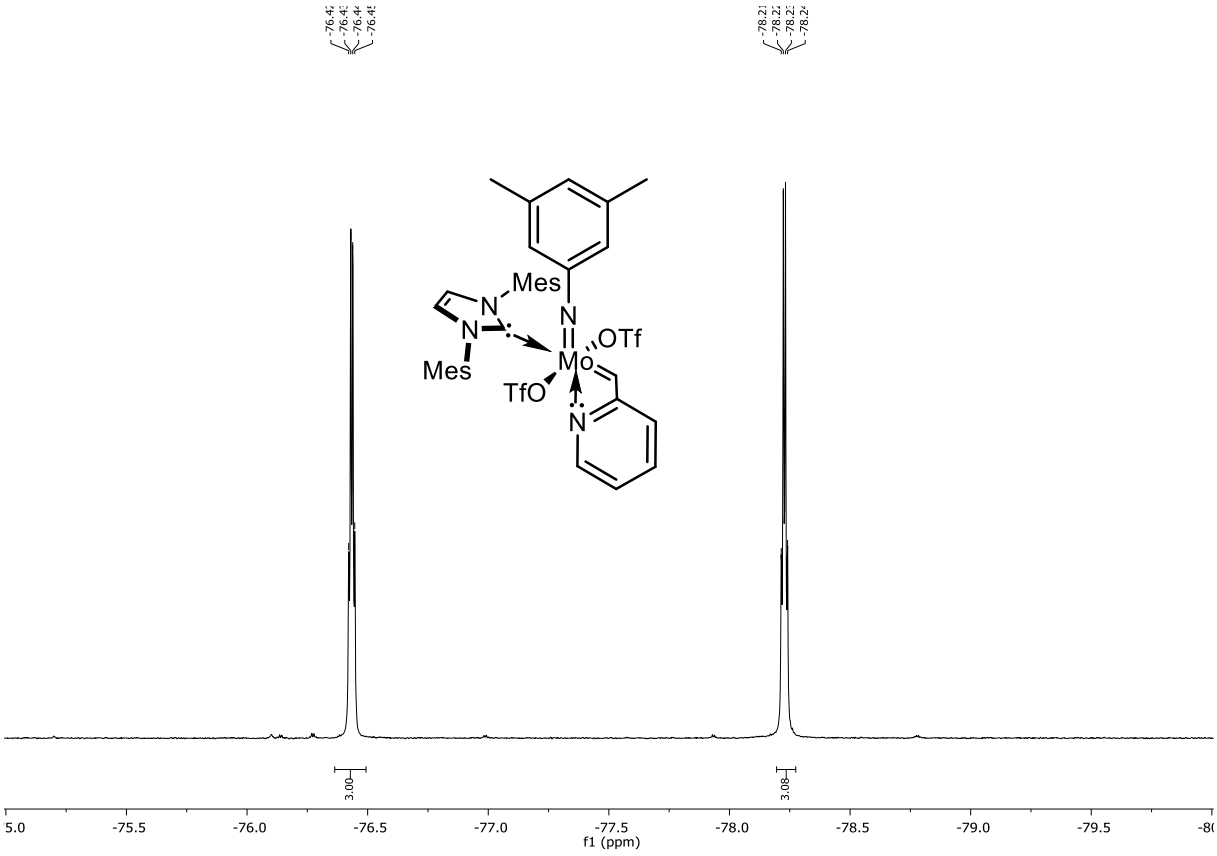

Figure 102. ^{19}F NMR spectrum of **Mo-9** (376 MHz, CD_2Cl_2).

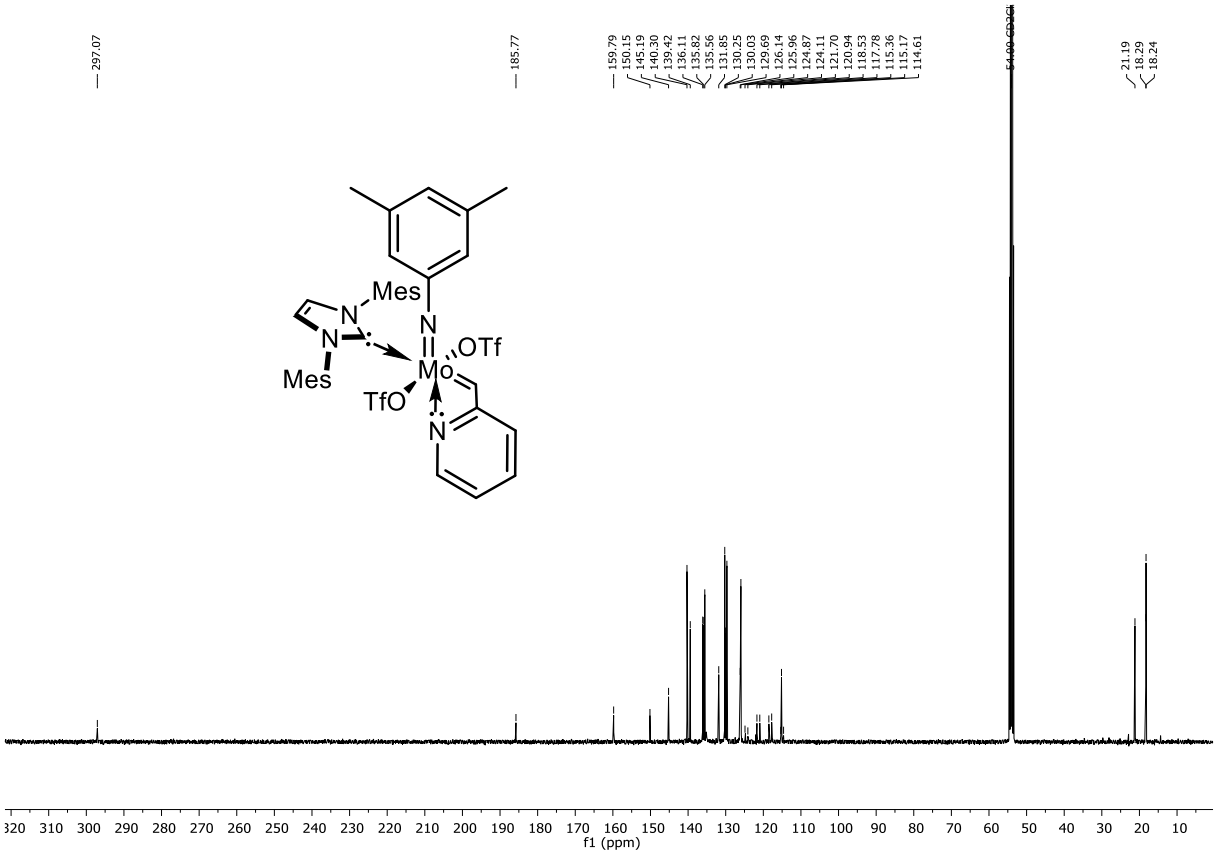

Figure 103. ^{13}C NMR spectrum of **Mo-9** (101 MHz, CD_2Cl_2).

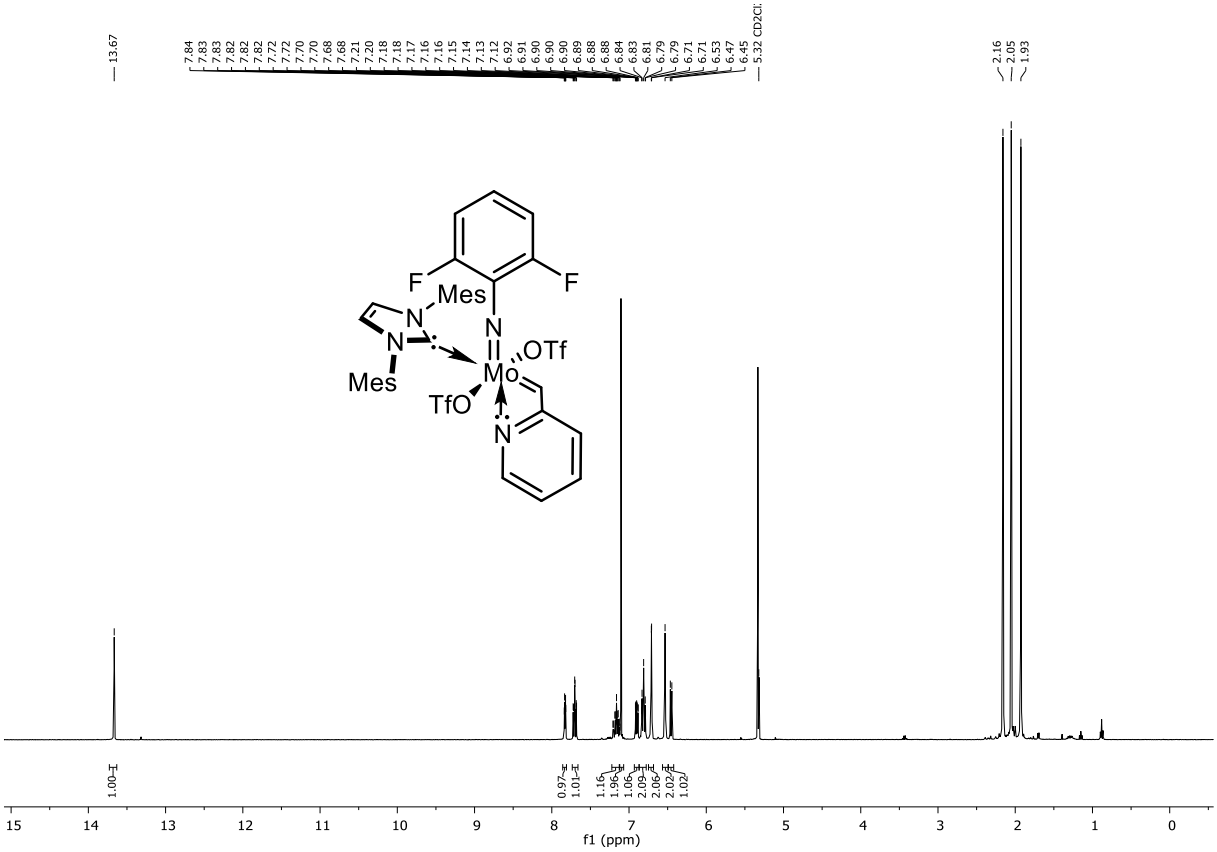

Figure 104. ^{1}H NMR spectrum of **Mo-10** (400 MHz, CD_2Cl_2).

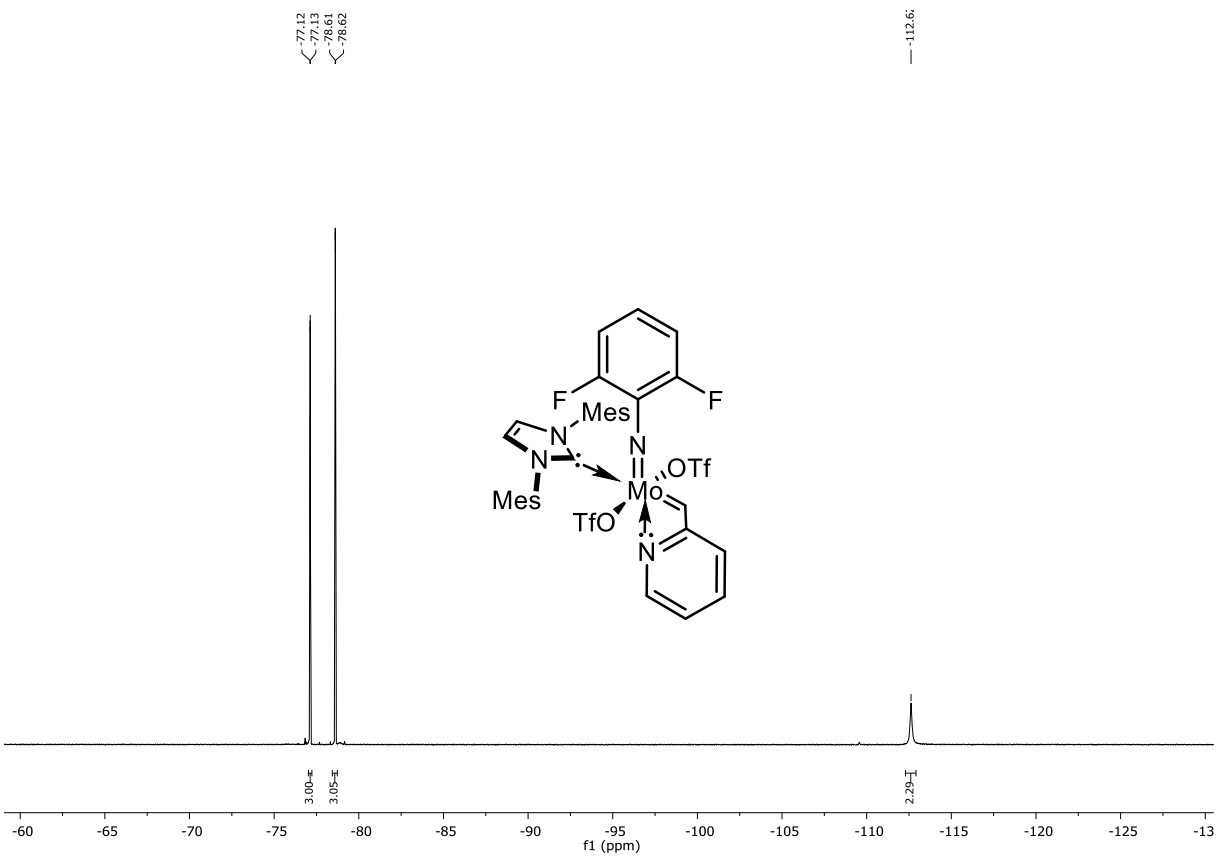

Figure 105. ^{19}F NMR spectrum of **Mo-10** (376 MHz, CD_2Cl_2).

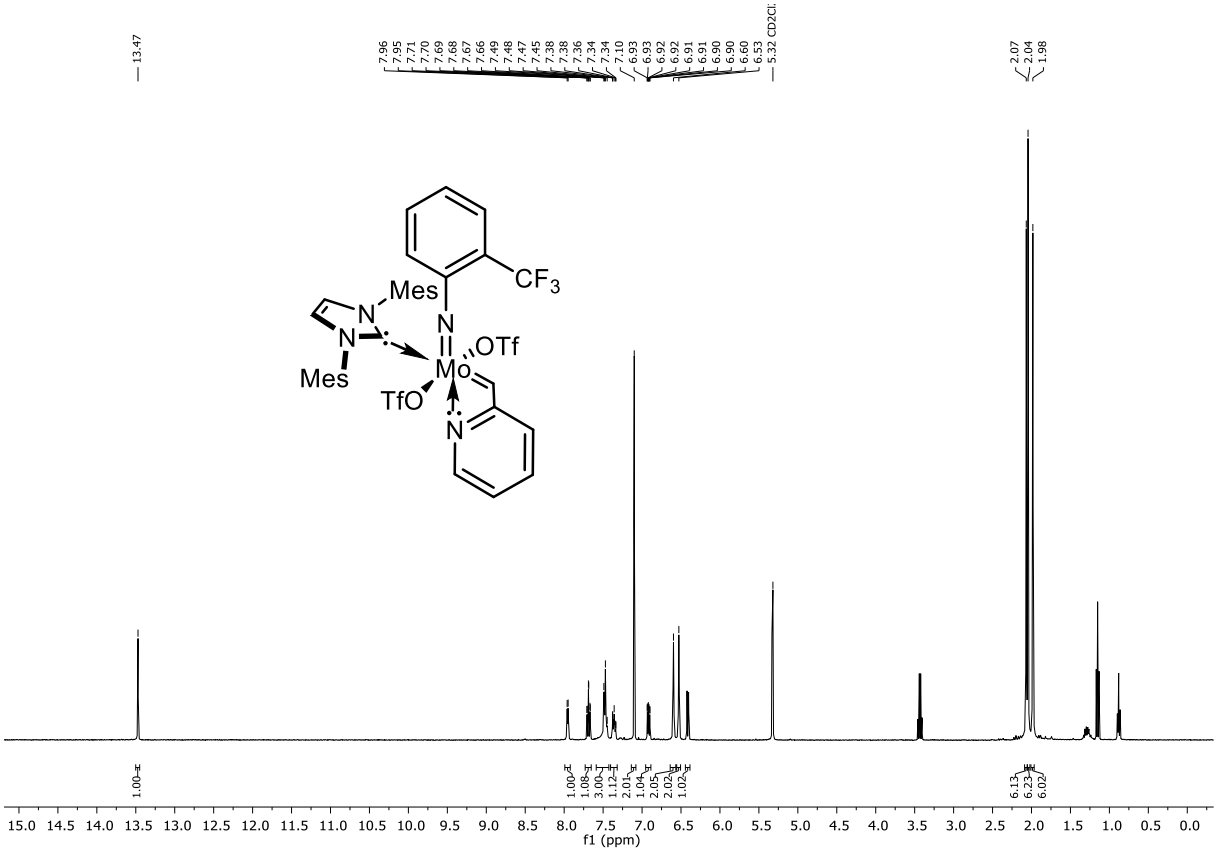

Figure 106. ^{1}H NMR spectrum of **Mo-11** (400 MHz, CD_2Cl_2).

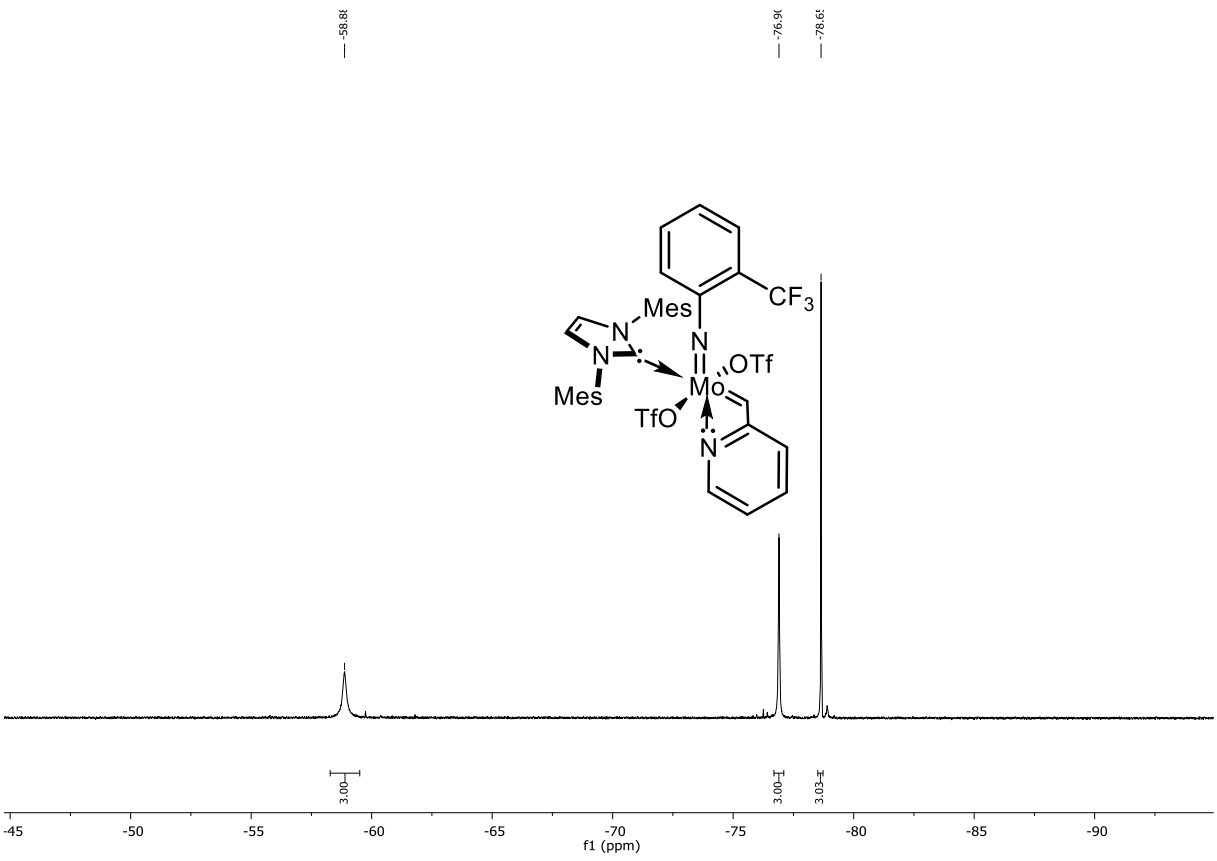

Figure 107. ^{19}F NMR spectrum of **Mo-11** (376 MHz, CD_2Cl_2).

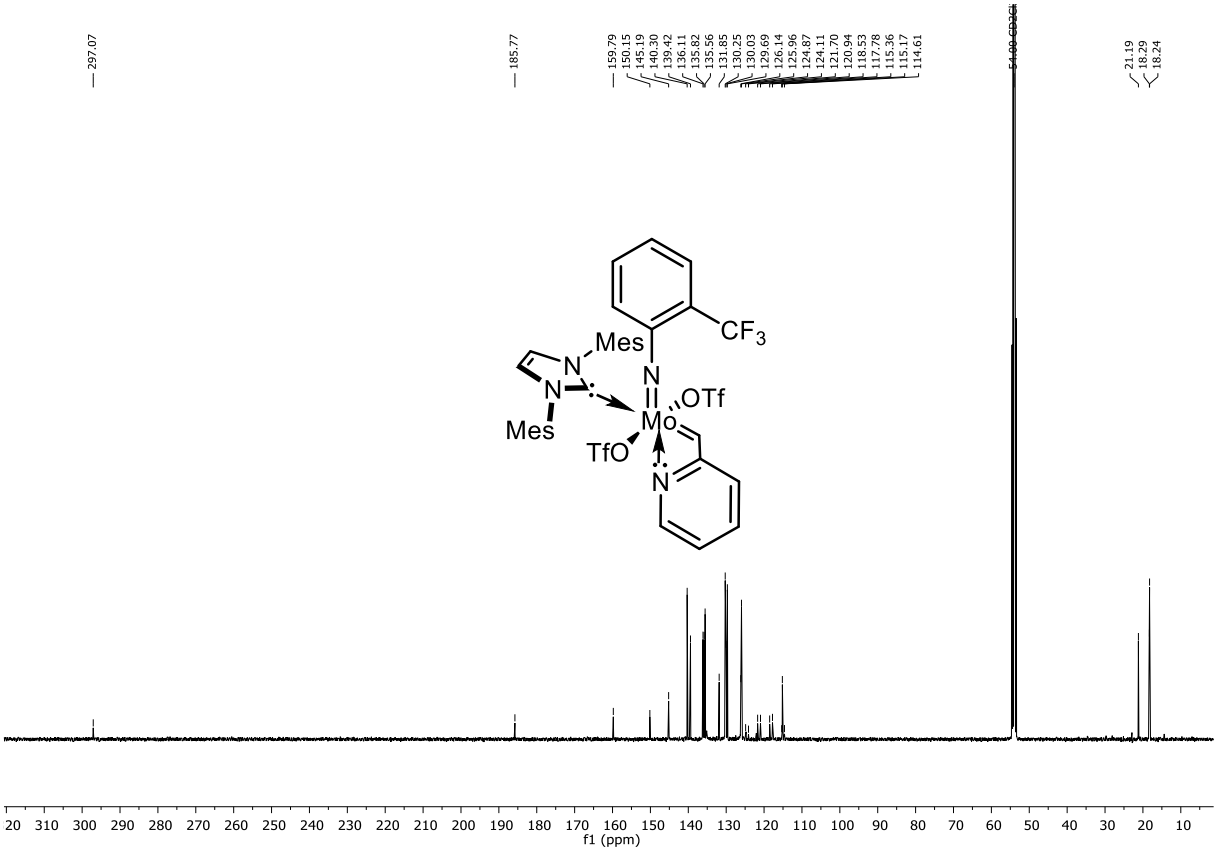

Figure 108. ^{13}C NMR spectrum of **Mo-11** (101 MHz, CD_2Cl_2).

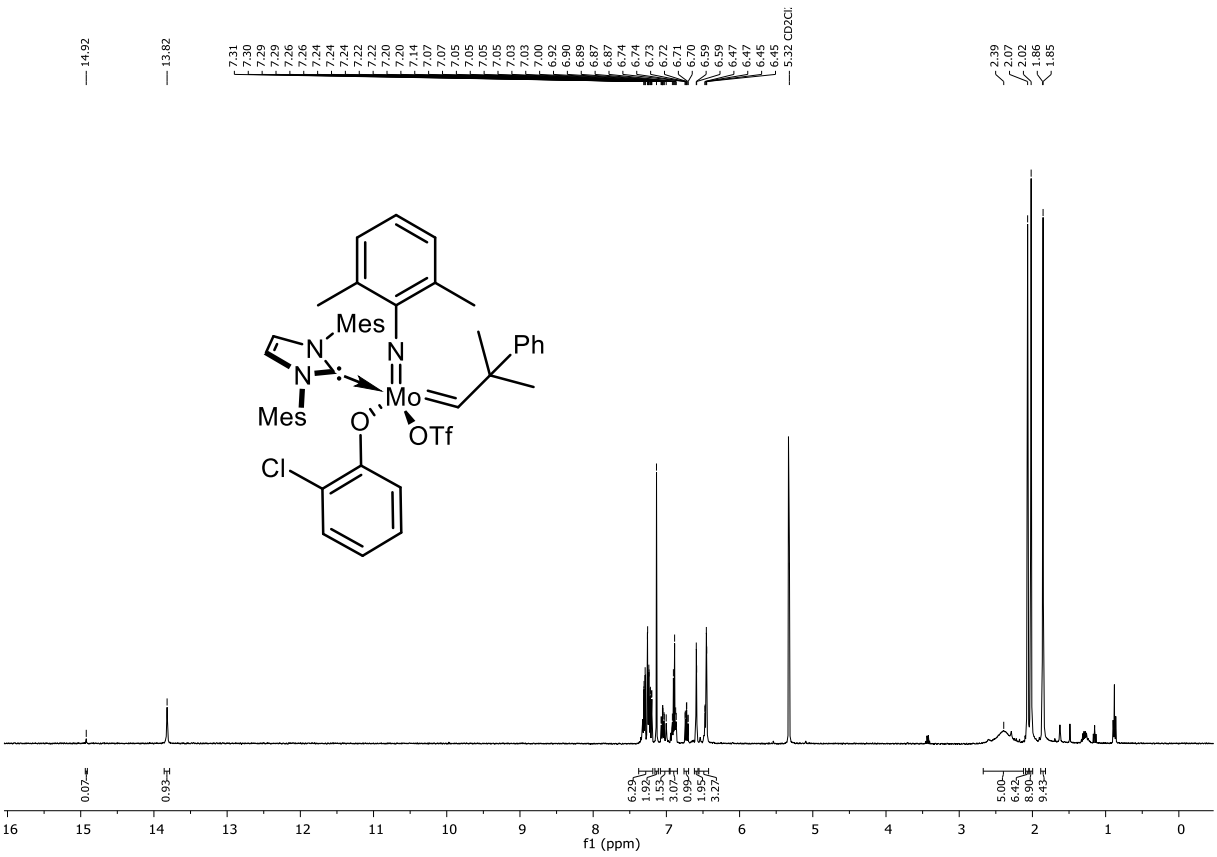

Figure 109. ^{1}H NMR spectrum of **Mo-12** (400 MHz, CD_2Cl_2).

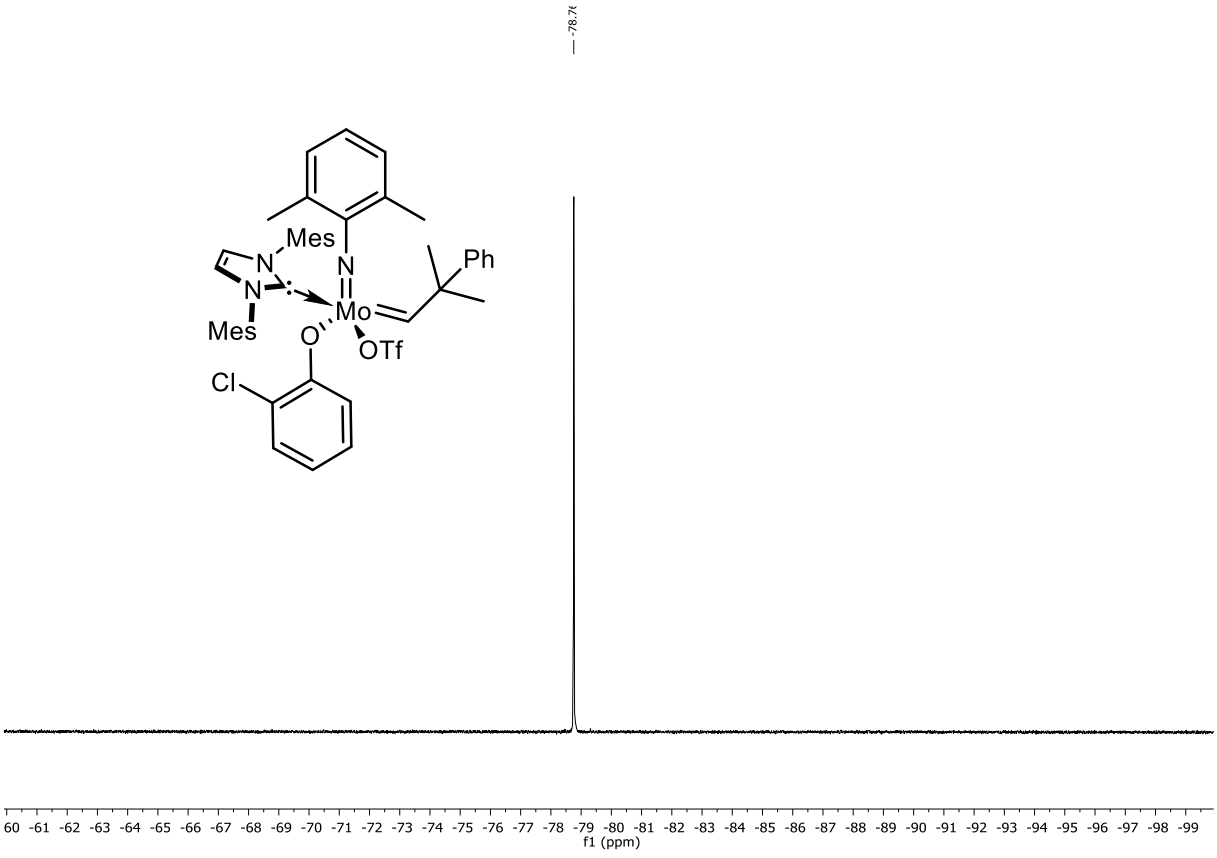

Figure 110. ^{19}F NMR spectrum of **Mo-12** (376 MHz, CD_2Cl_2).

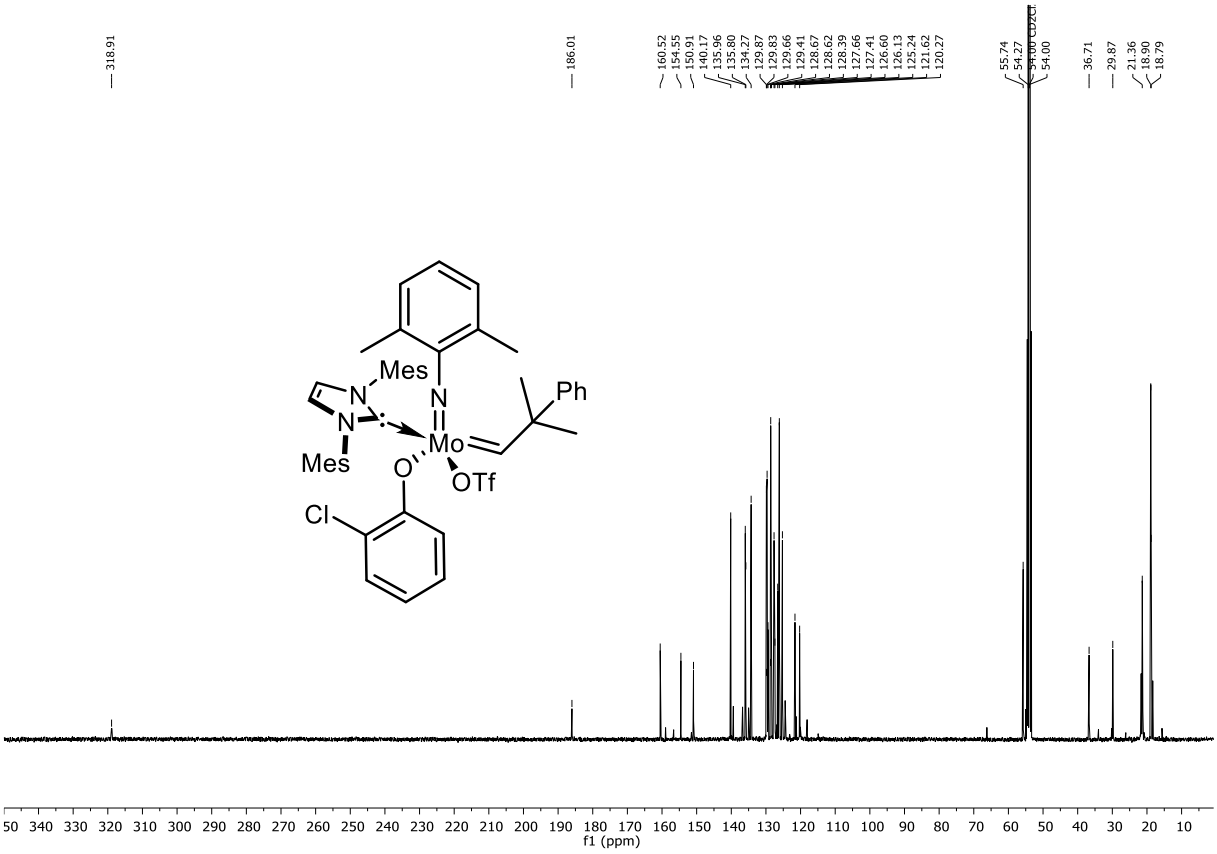

Figure 111. ^{13}C NMR spectrum of **Mo-12** (101 MHz, CD_2Cl_2).

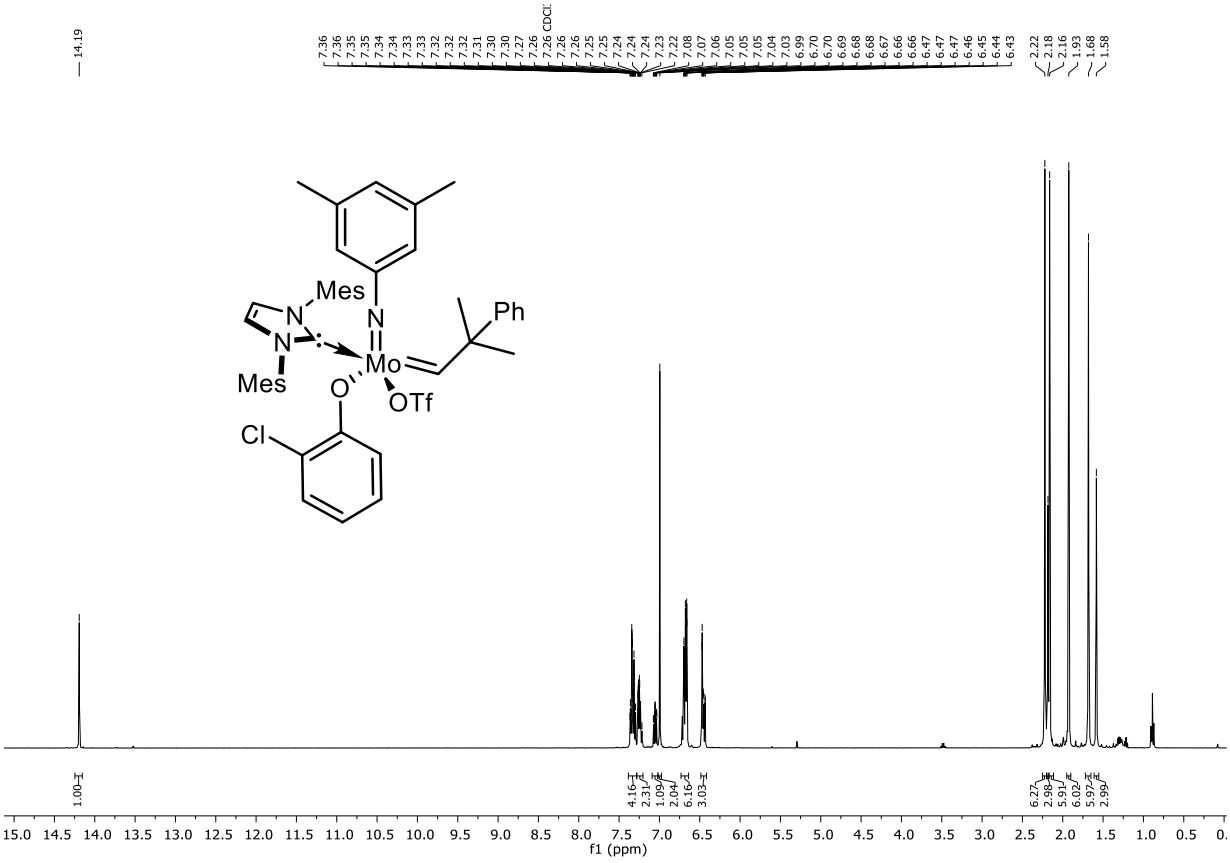

Figure 112. ^{1}H NMR spectrum of **Mo-13** (400 MHz, $CDCl_3$).

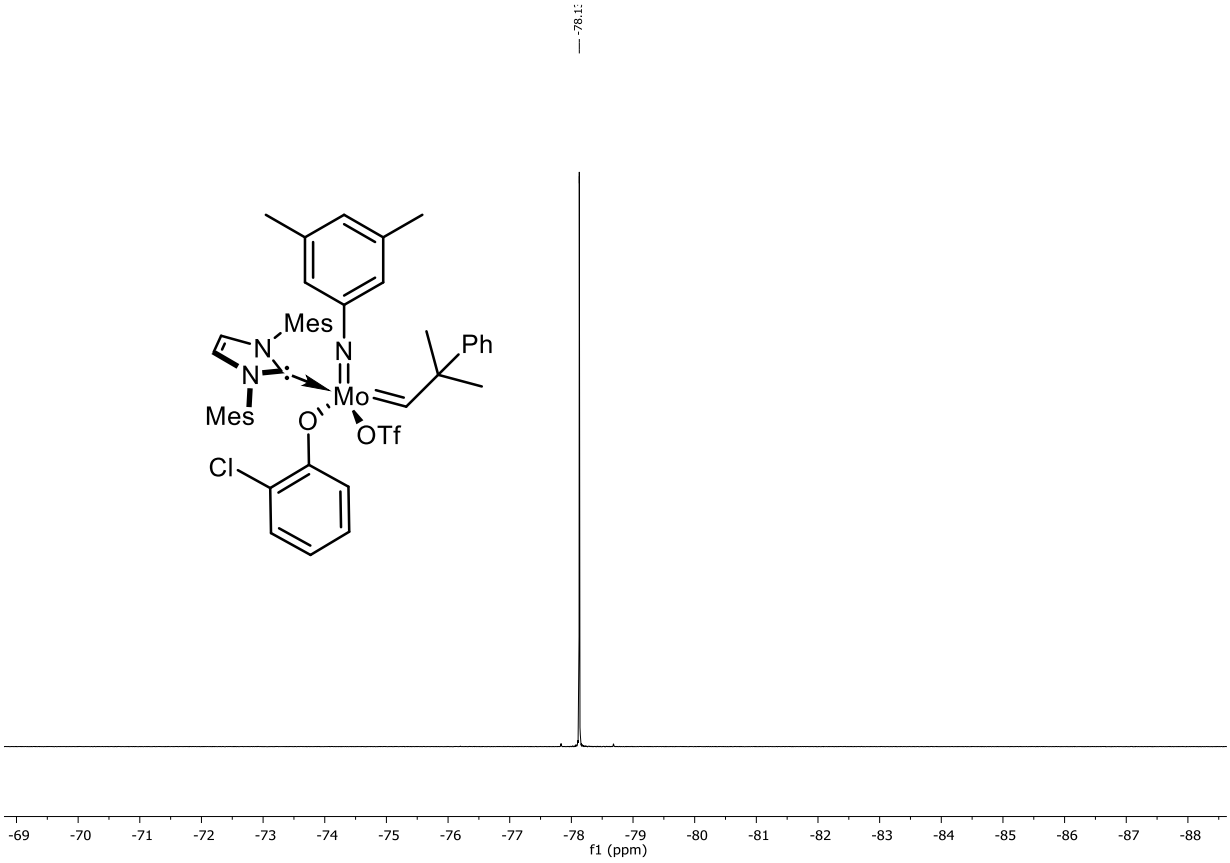

Figure 113. ^{19}F NMR spectrum of **Mo-13** (376 MHz, $CDCl_3$).

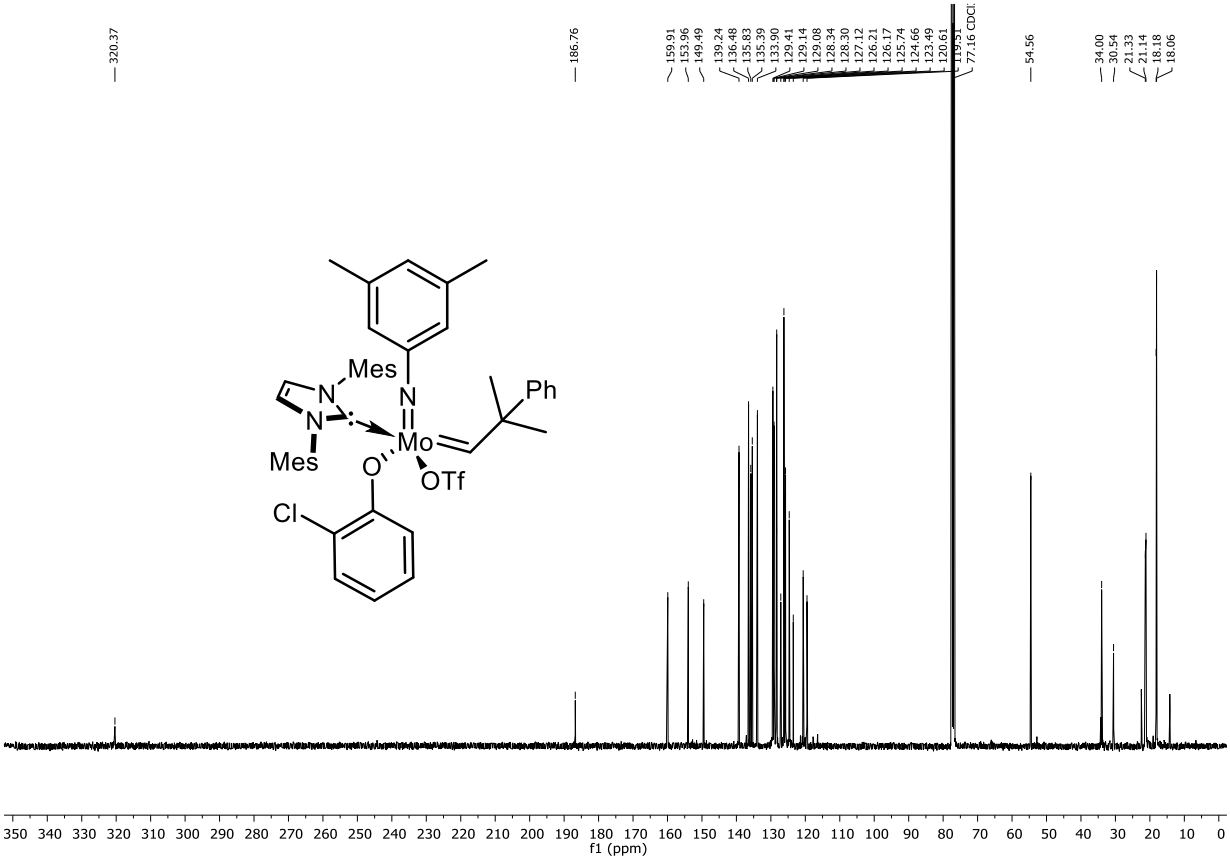

Figure 114. ^{13}C NMR spectrum of **Mo-13** (101 MHz, $CDCl_3$).

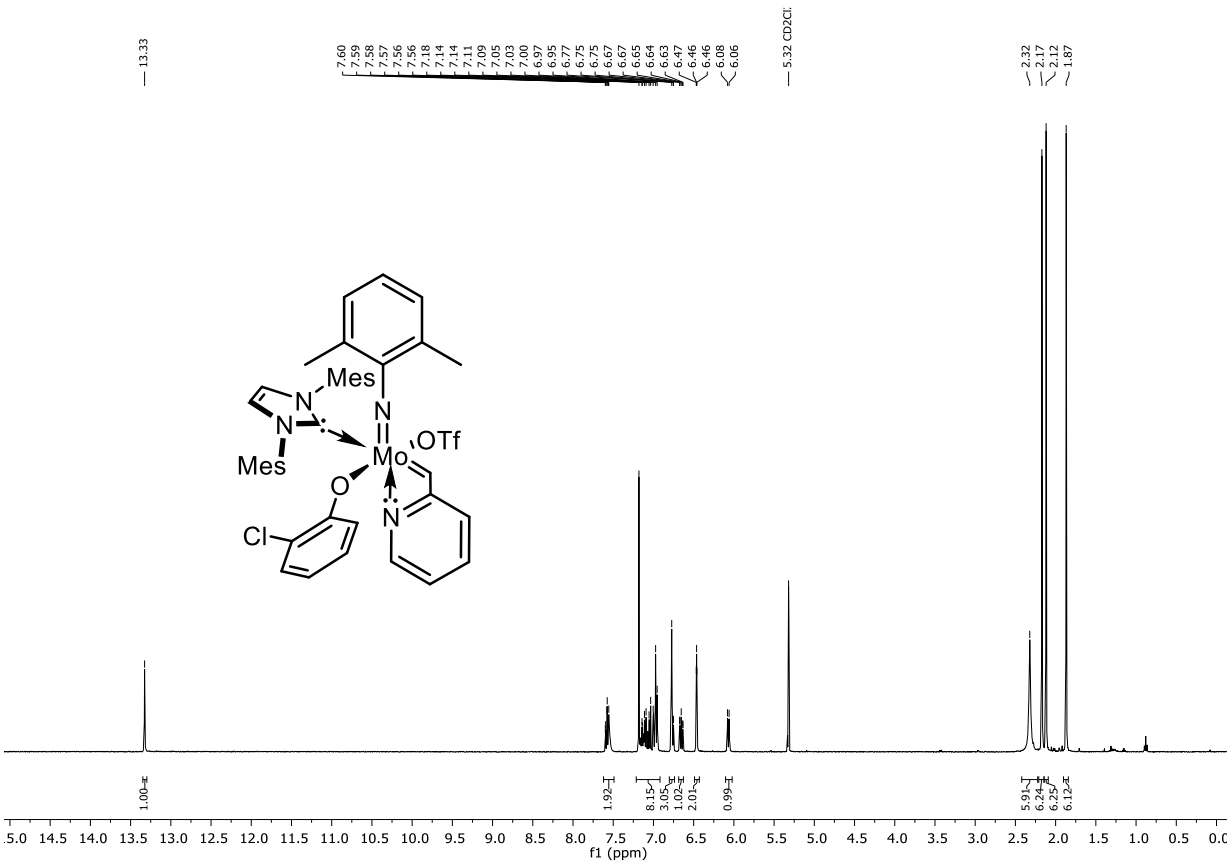

Figure 115. ^{1}H NMR spectrum of **Mo-14** (400 MHz, CD_2Cl_2).

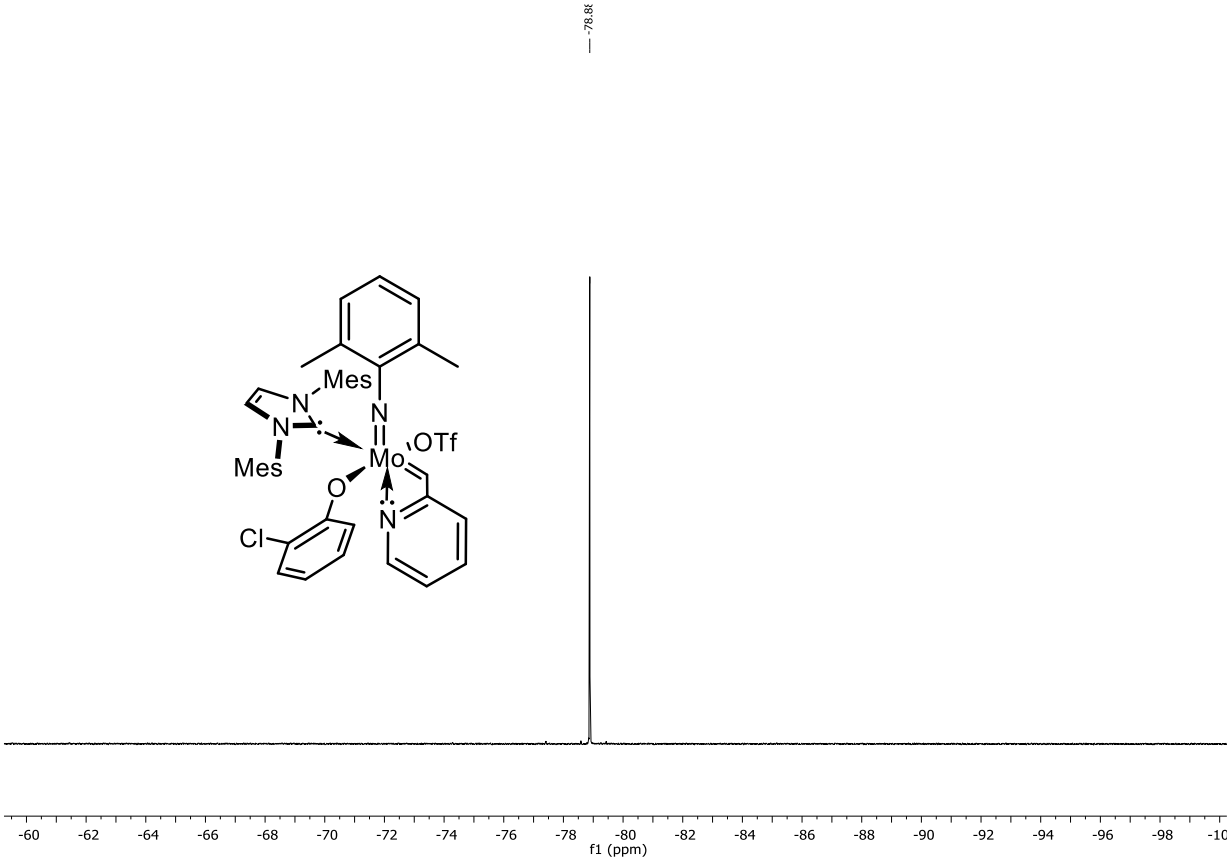

Figure 116. ^{19}F NMR spectrum of **Mo-14** (376 MHz, CD_2Cl_2).

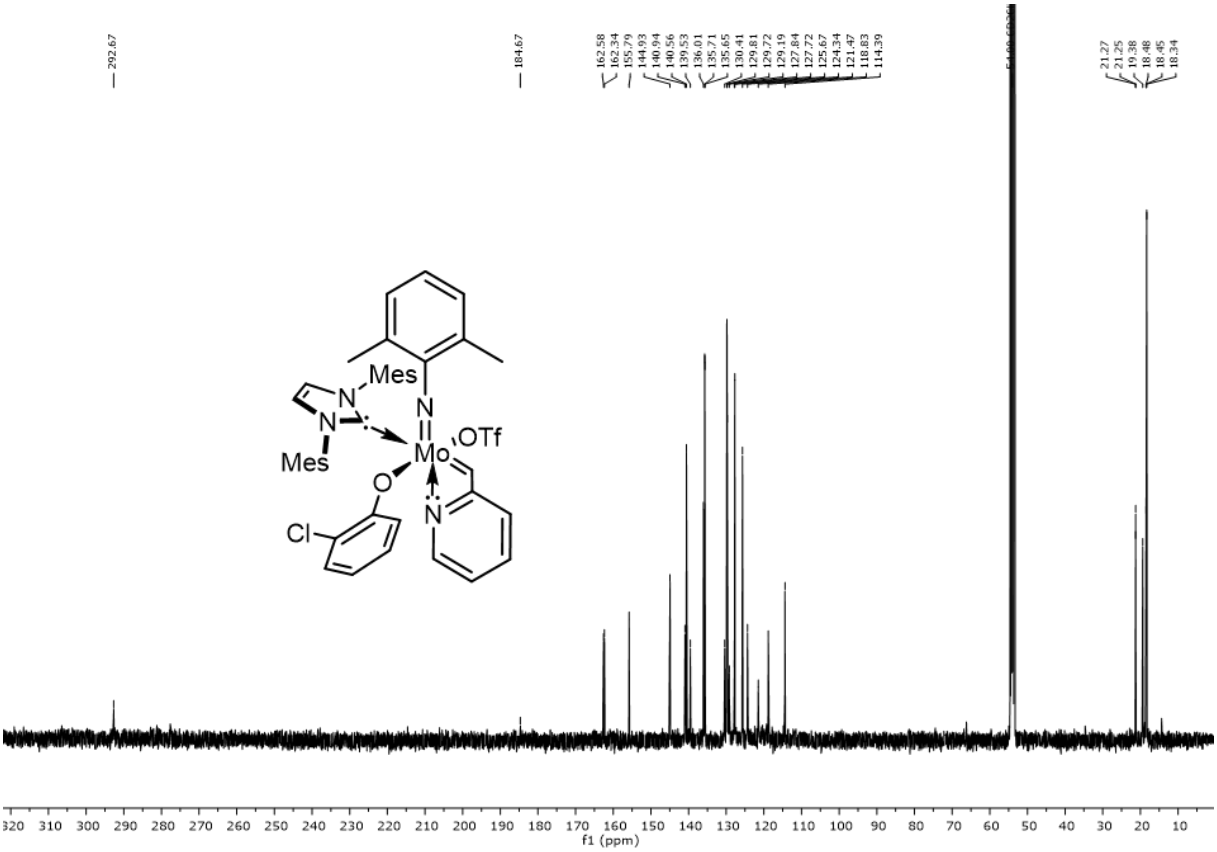

Figure 117. ^{13}C NMR spectrum of **Mo-14** (101 MHz, CD_2Cl_2).

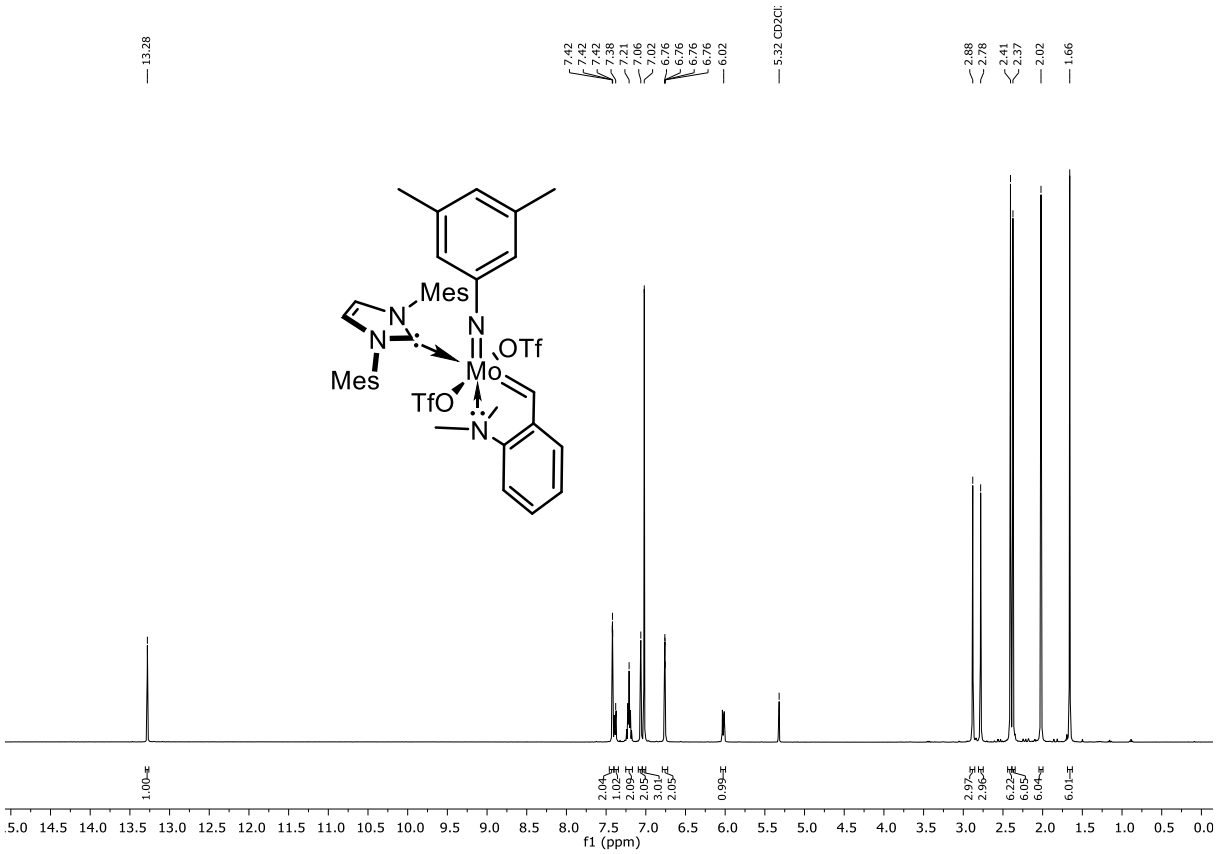

Figure 118. ^{1}H NMR spectrum Catalyst **Mo-15** (400 MHz, CD_2Cl_2).

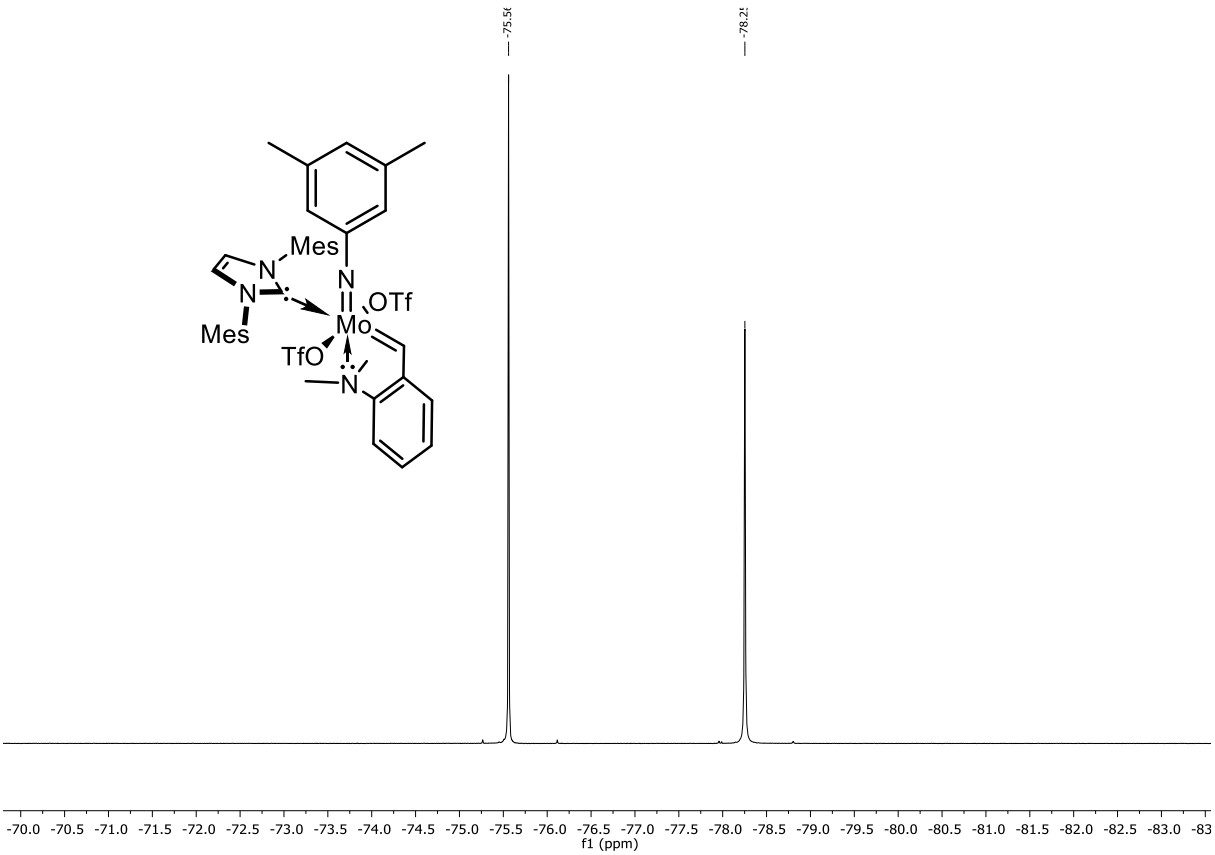

Figure 119. ^{19}F NMR spectrum of **Mo-15** (376 MHz, CD_2Cl_2).

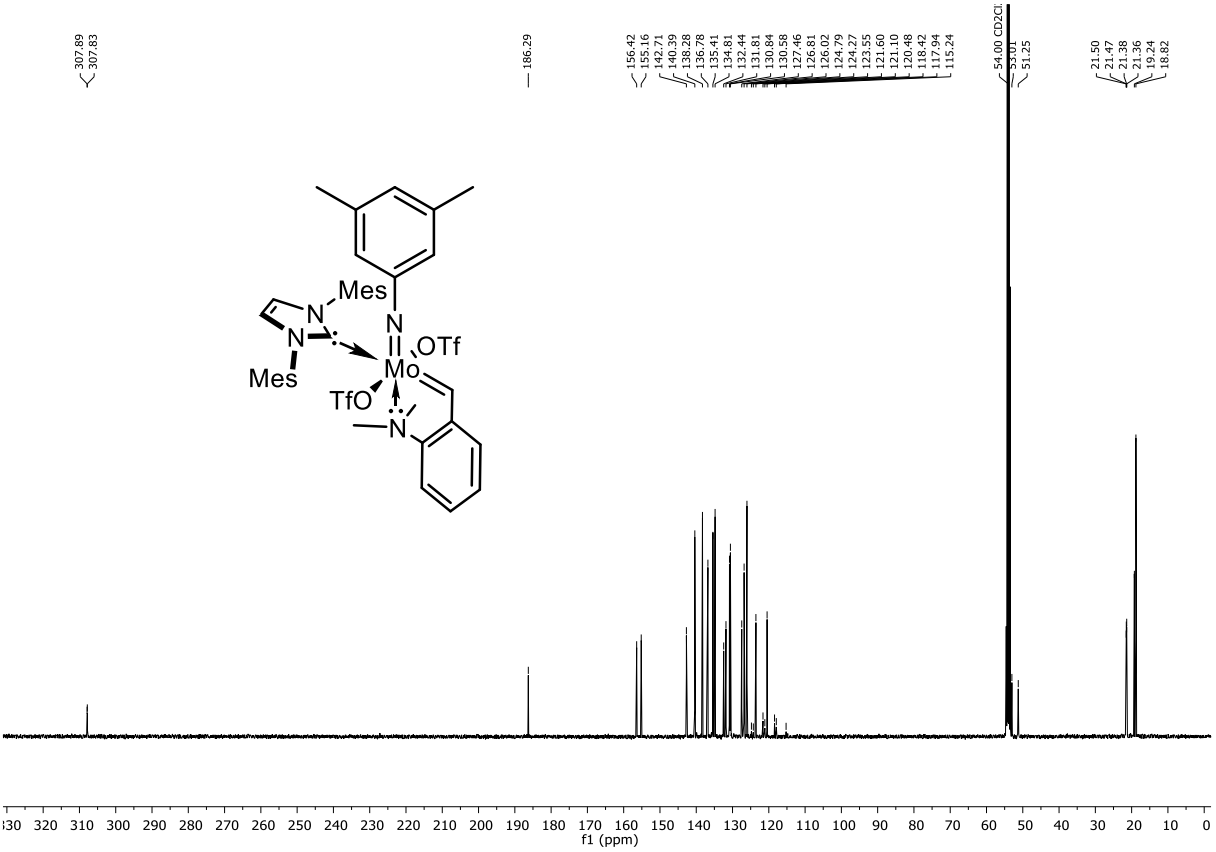

Figure 120. ^{13}C NMR spectrum of **Mo-15** (101 MHz, CD_2Cl_2).

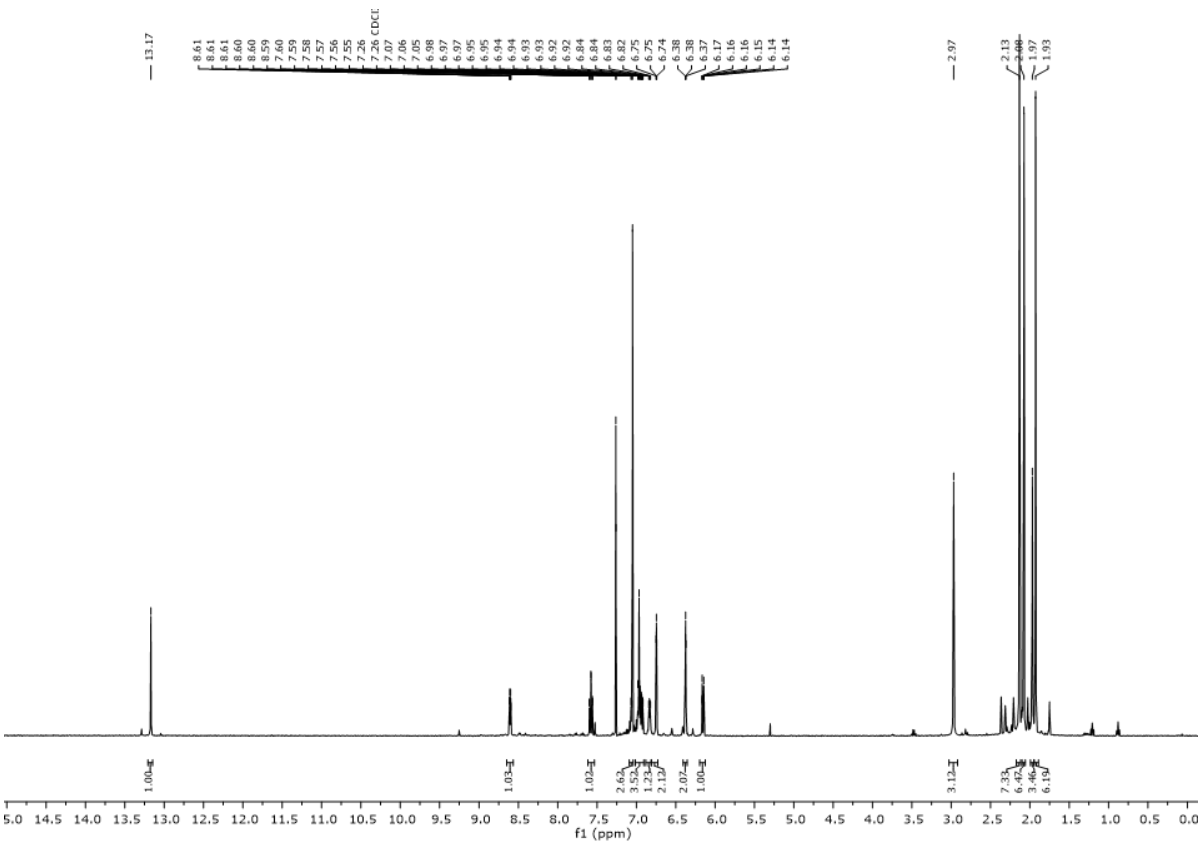

Figure 121. ^{1}H NMR spectrum of **Mo-8** in $CDCl_3$ after storage in air for 12 h. Virtually air stable, no decomposition was observed.

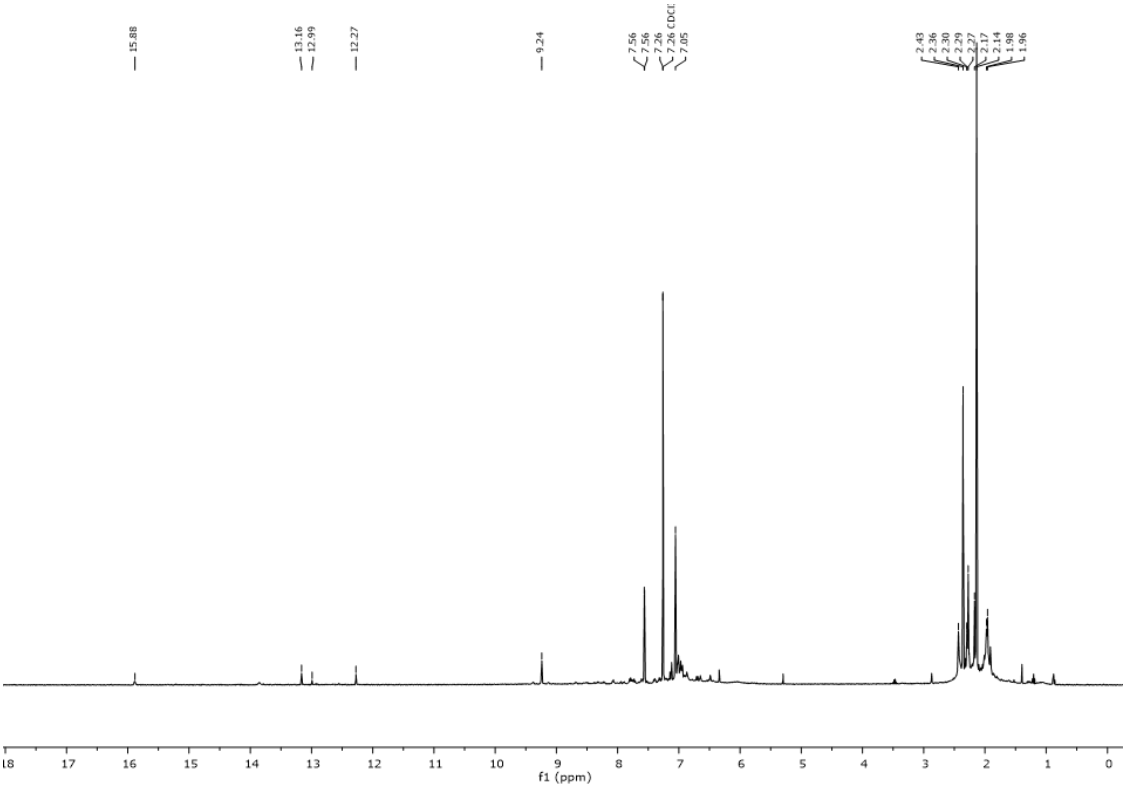

Figure 122. ^{1}H NMR spectrum of **Mo-9** in $CDCl_3$ after storage in air for 12 h. Multiple alkylidene signals were observed.

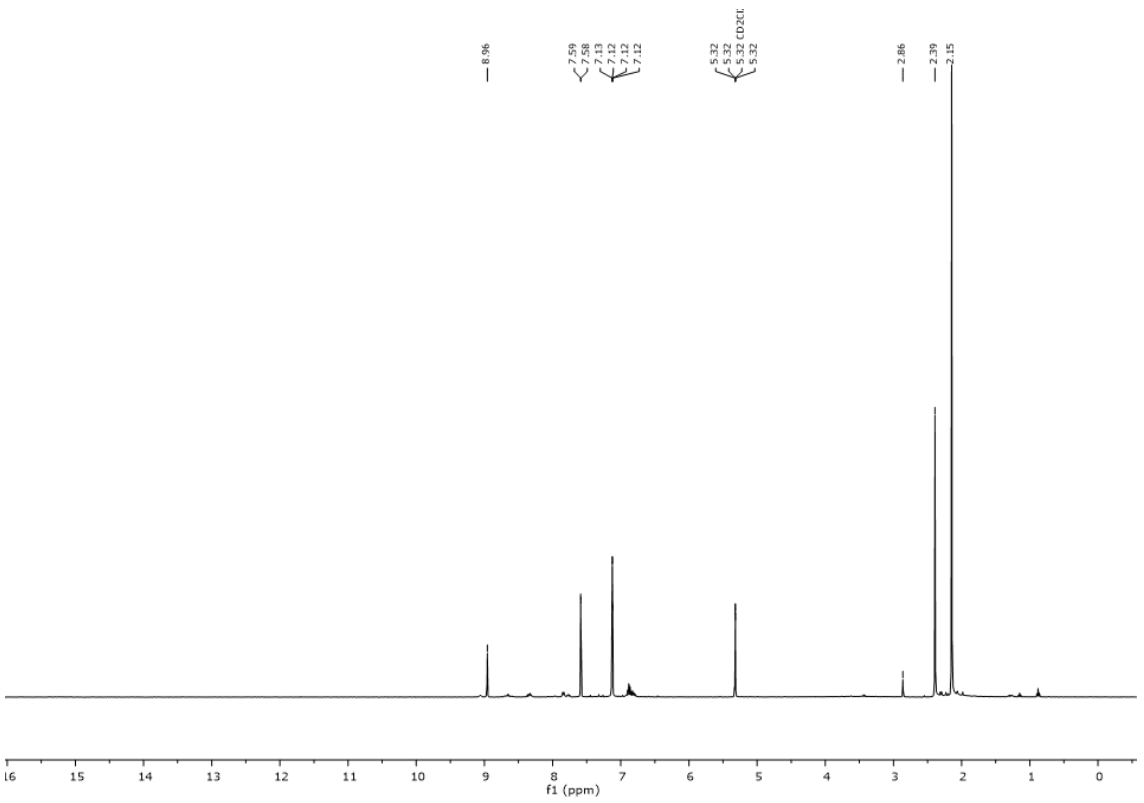

Figure 123. ^{1}H NMR spectrum of **Mo-10** in $CDCl_3$ after storage in air for 12 h. No alkylidene signal was observed.

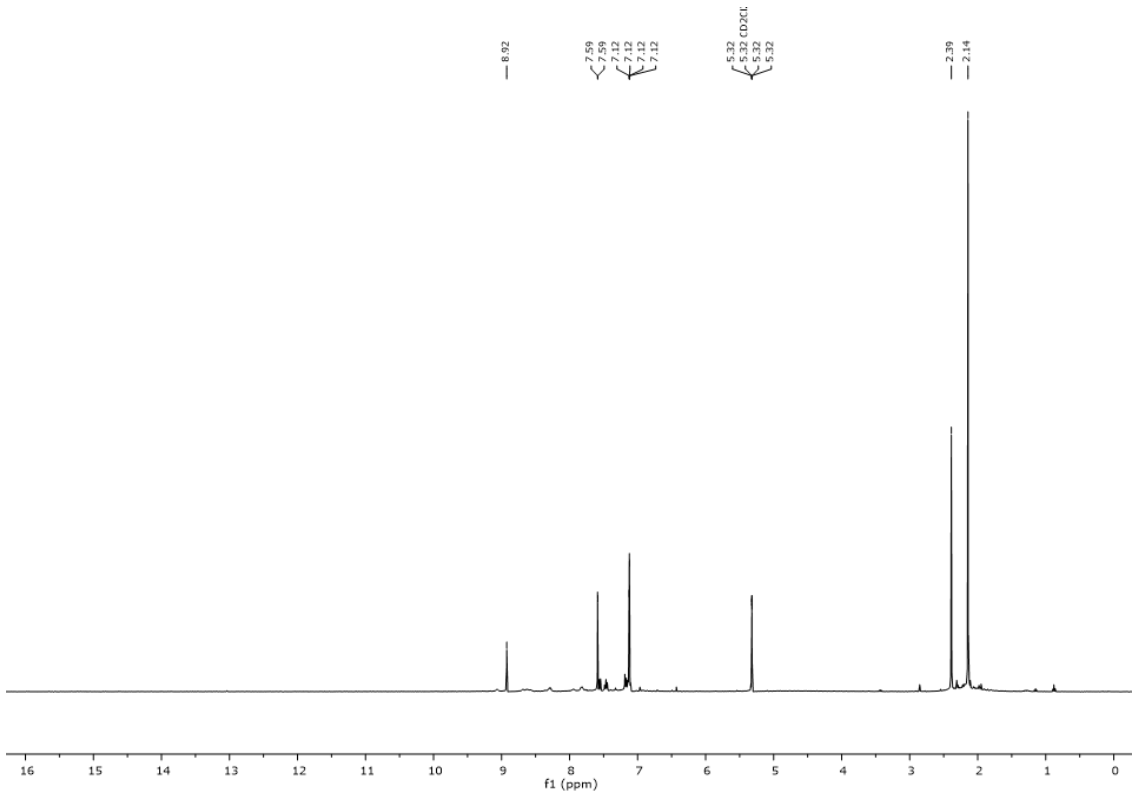

Figure 124. ^{1}H NMR spectrum of **Mo-11** in $CDCl_3$ after storage in air for 12 h. No alkylidene signal was observed.

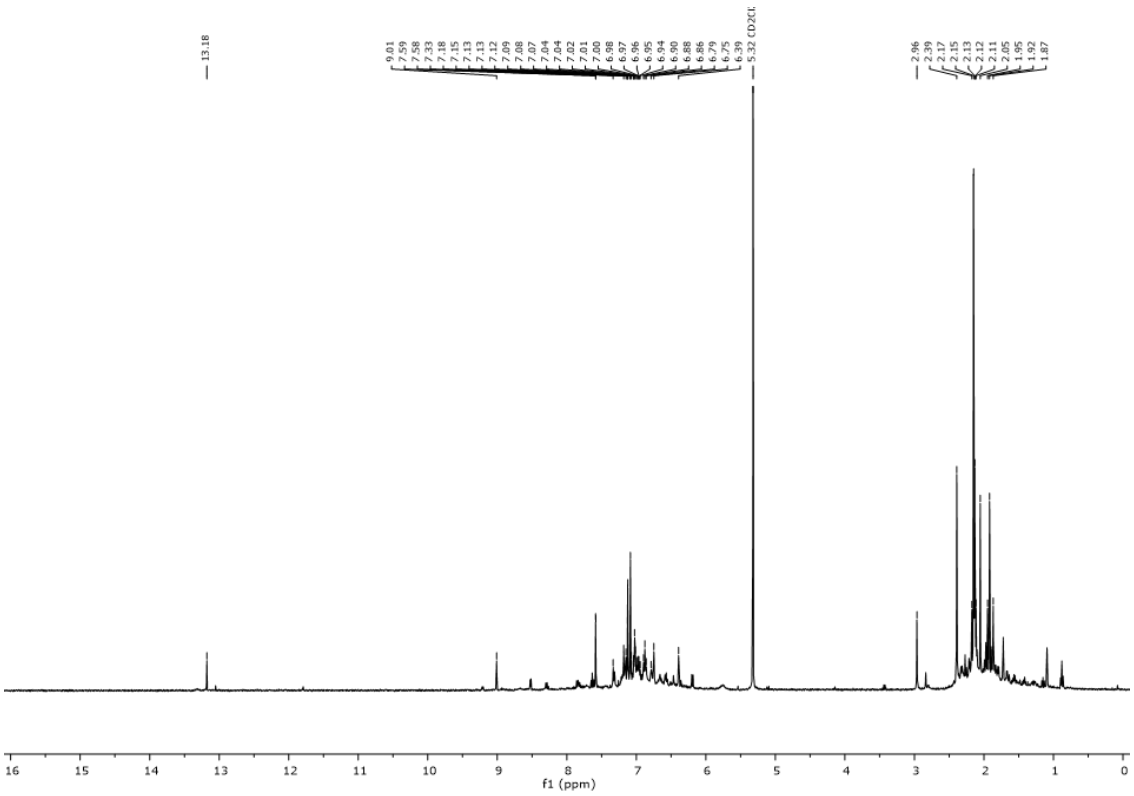

Figure 125. ^{1}H NMR spectrum of **Mo-14** in $CDCl_3$ after storage in air for 12 h. Alkylidene signal was observed along with decomposition.

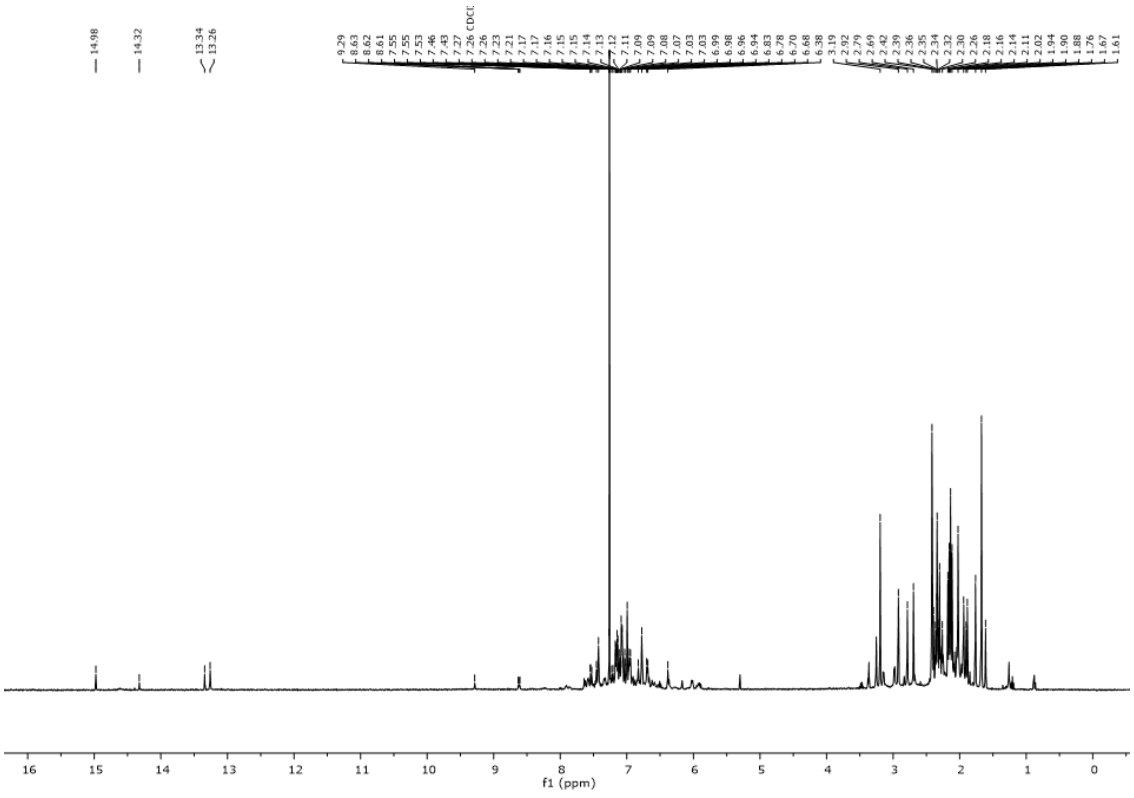

Figure 126. ^{1}H NMR spectrum of **Mo-15** in $CDCl_3$ after storage in air for 12 h. Multiple alkylidene signals were observed.

7.3 2,6-Difluorophenylimido Molybdenum Alkylidene NHC Complexes: Air Stable, Functional Group Tolerant Catalysts

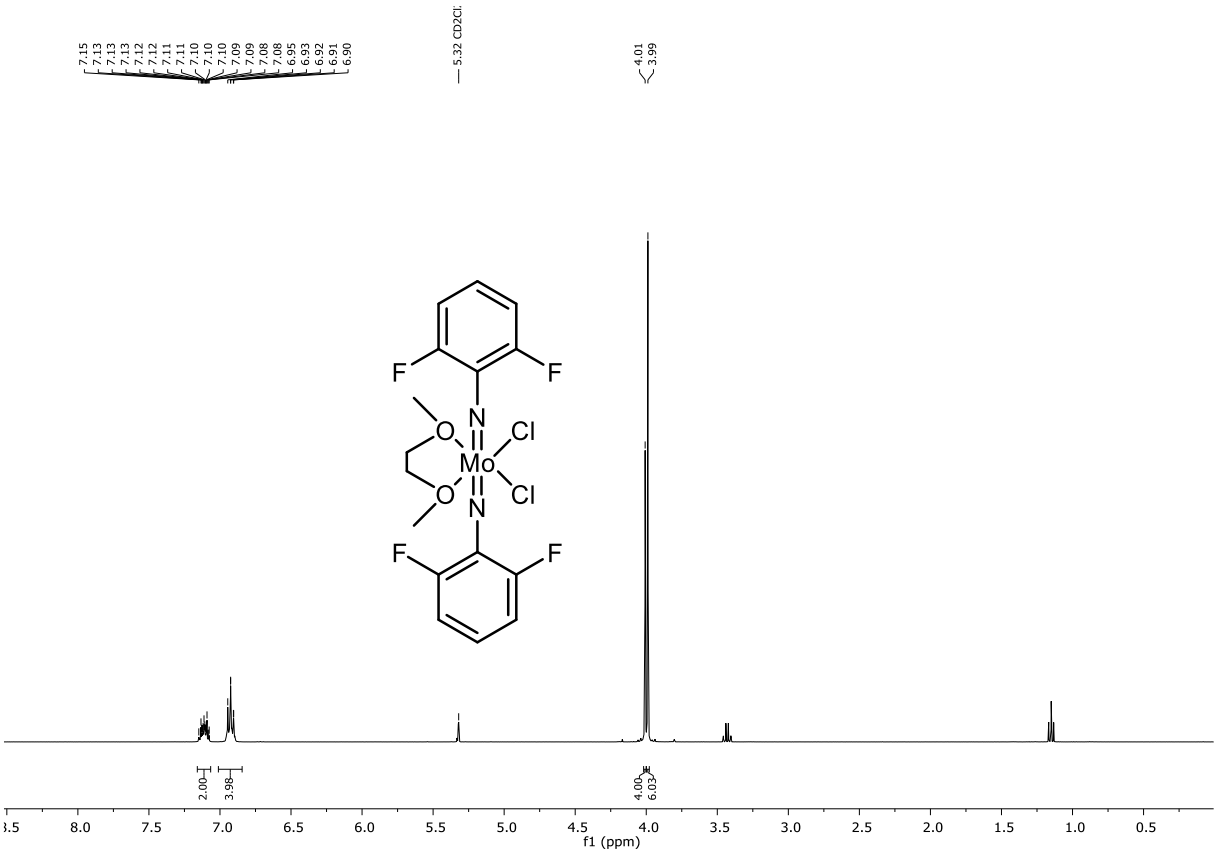

Figure 127. ^{1}H NMR spectrum of **Mo-16** (400 MHz, CD_2Cl_2).

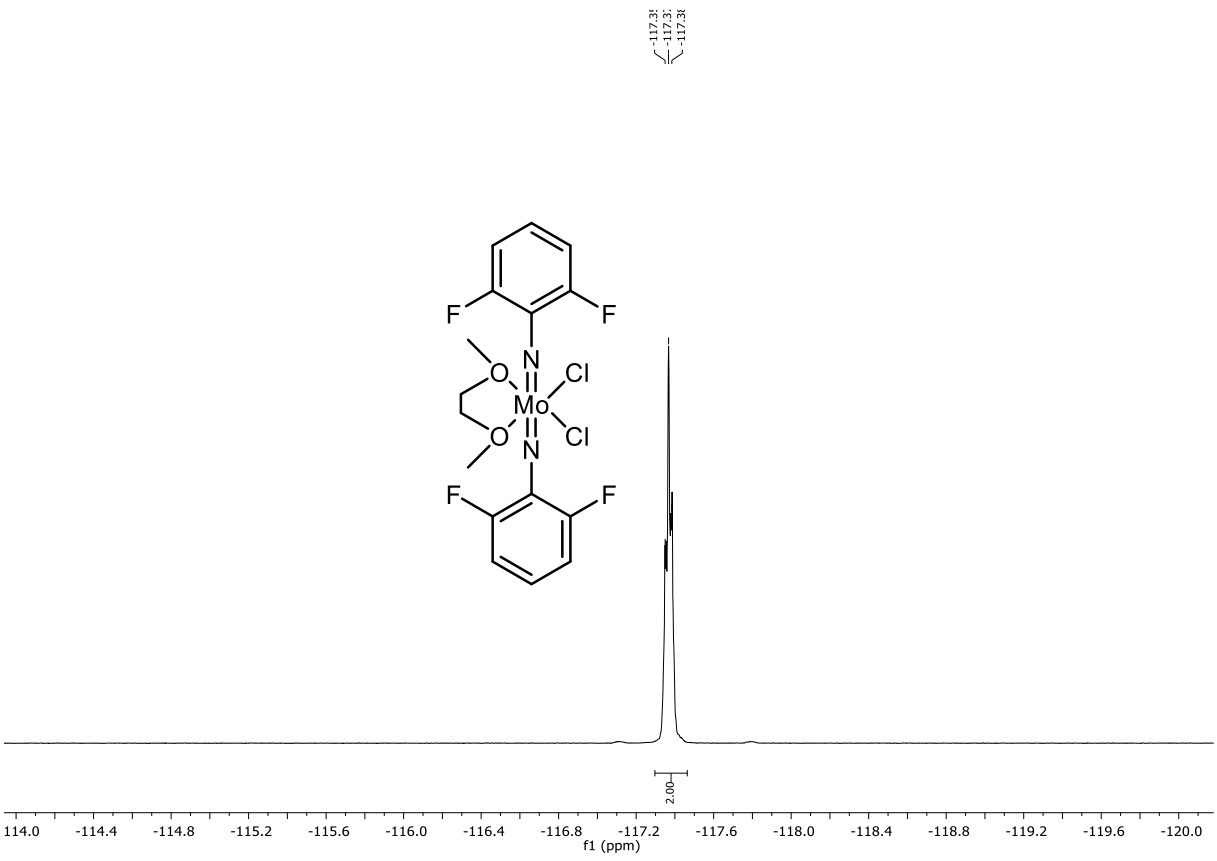

Figure 128. ^{19}F NMR spectrum of **Mo-16** (376 MHz, CD_2Cl_2).

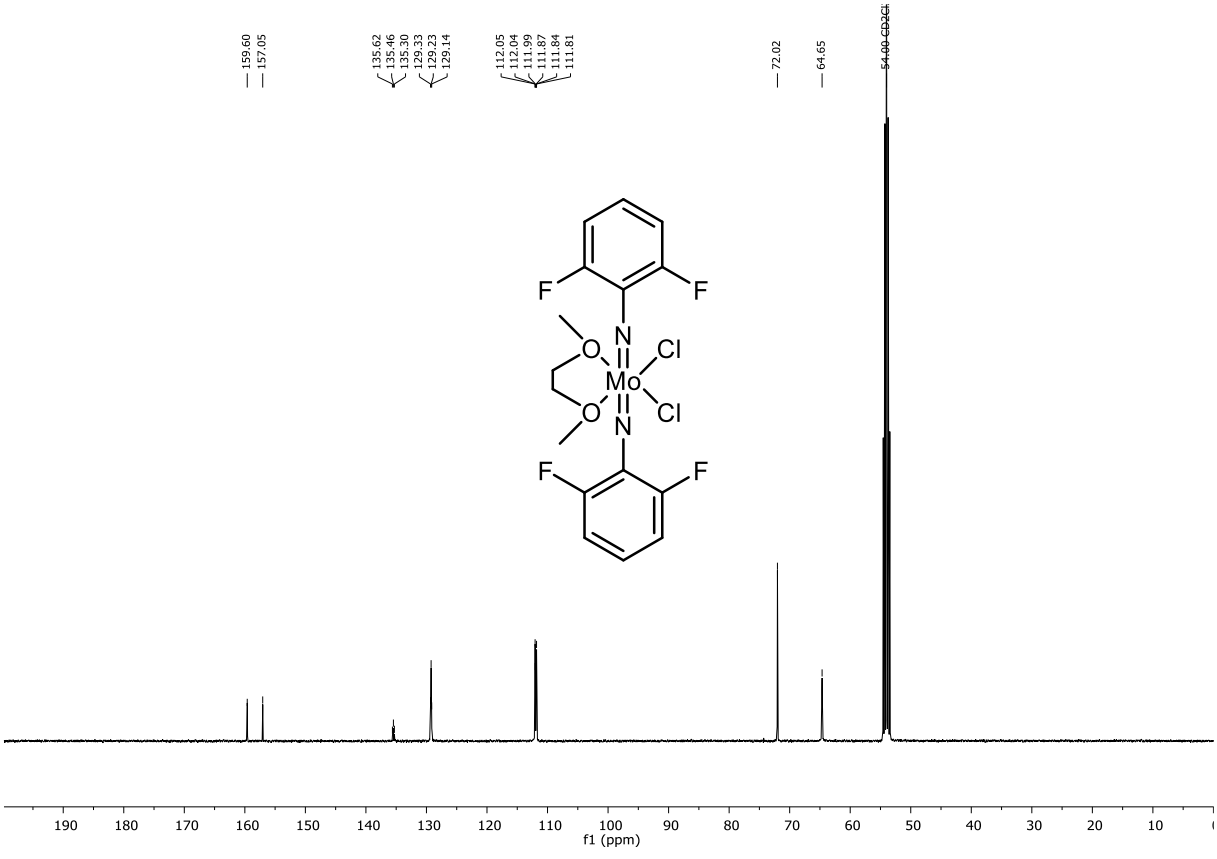

Figure 129. ^{13}C NMR spectrum of **Mo-16** (101 MHz, CD_2Cl_2).

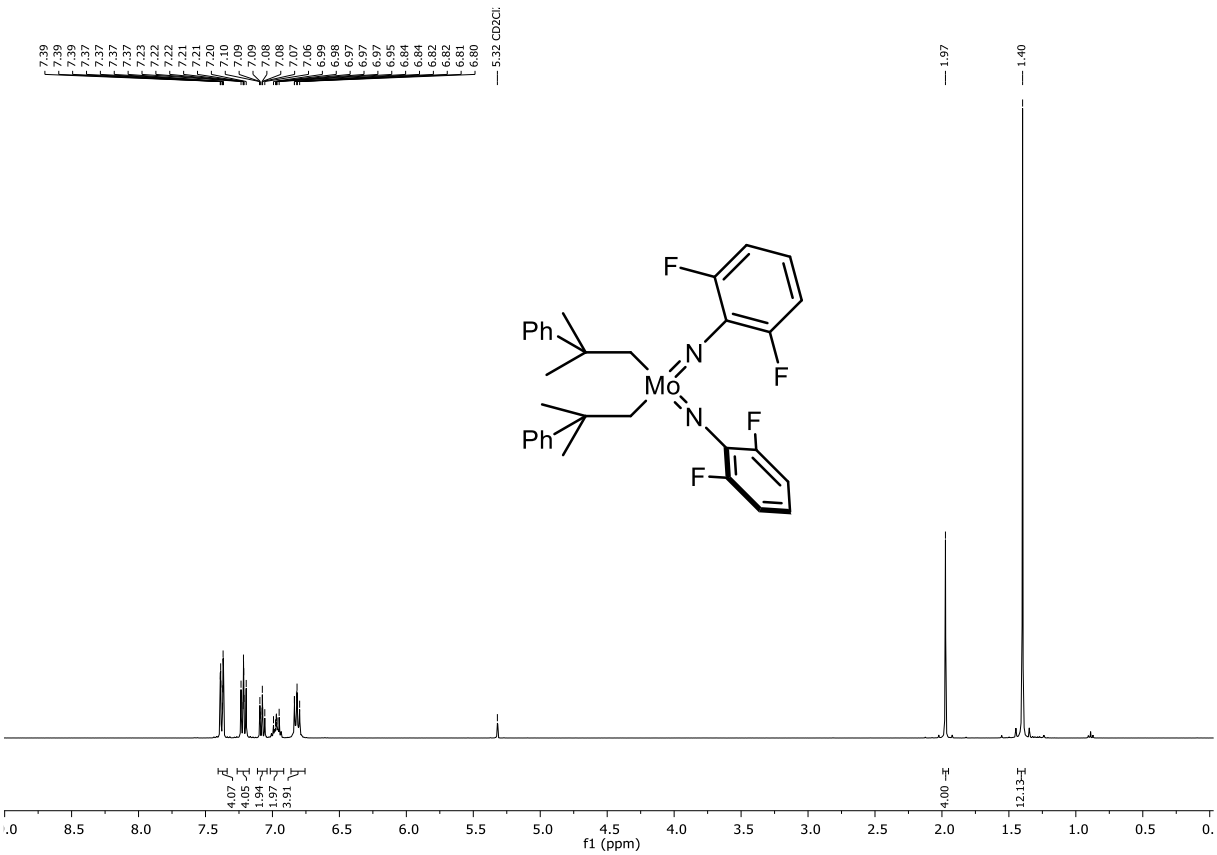

Figure 130. ^{1}H NMR spectrum of **Mo-17** (400 MHz, CD_2Cl_2).

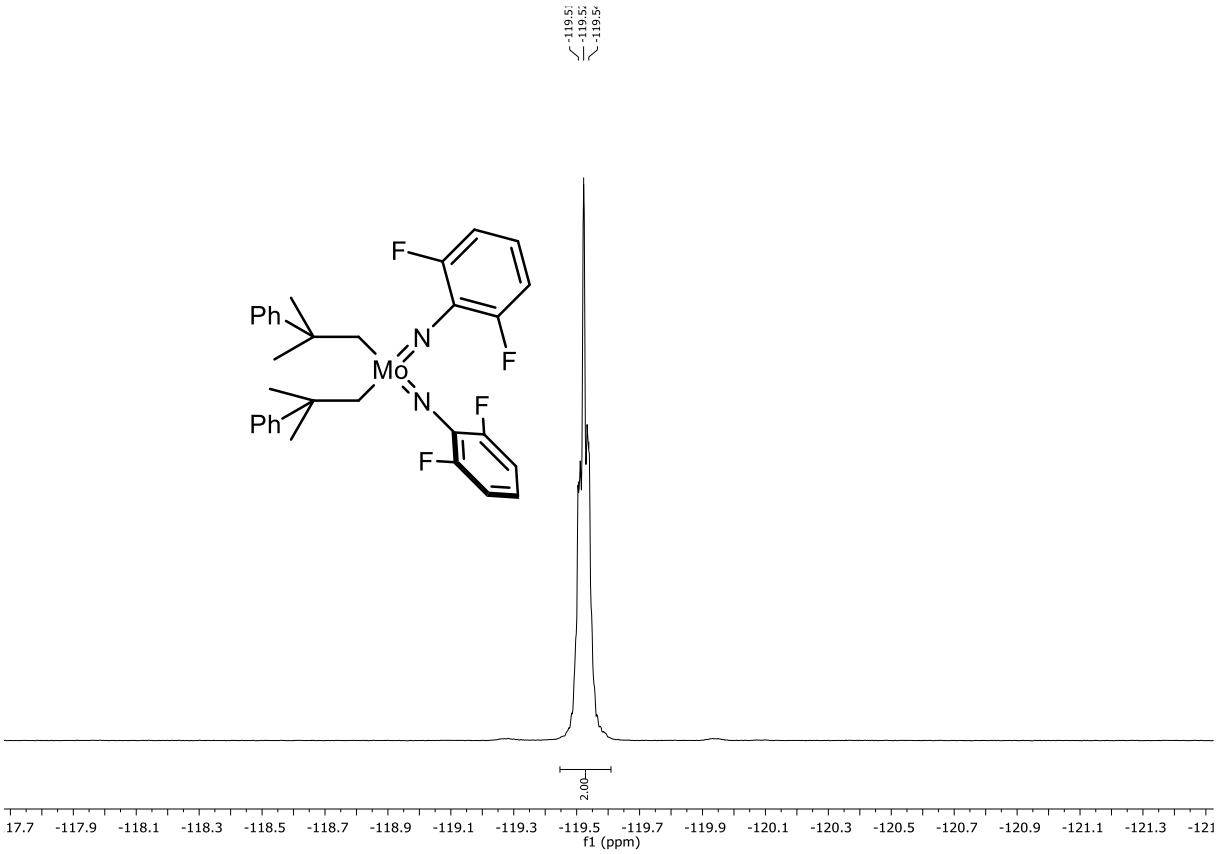

Figure 131. ^{19}F NMR spectrum of **Mo-17** (376 MHz, CD_2Cl_2).

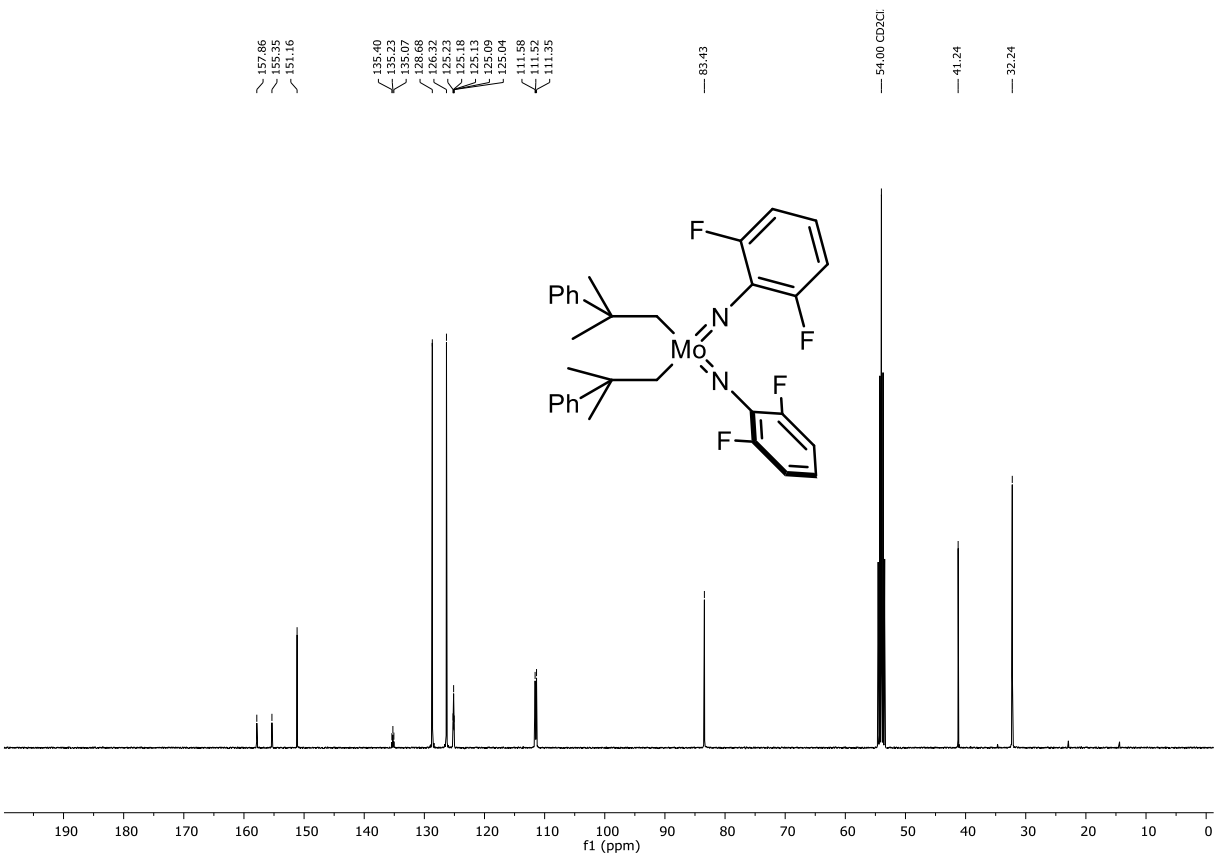

Figure 132. ^{13}C NMR spectrum of **Mo-17** (101 MHz, CD_2Cl_2).

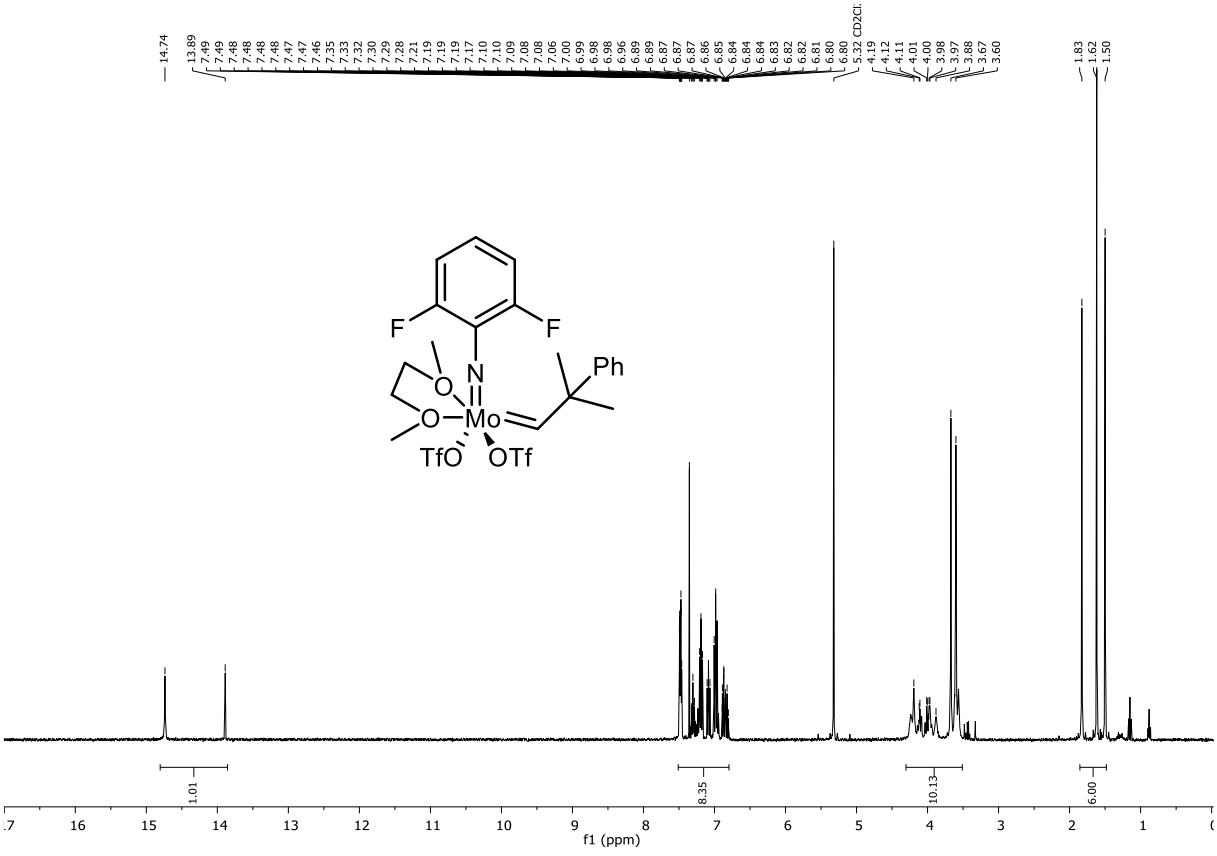

Figure 133. ^{1}H NMR spectrum of **Mo-18** (400 MHz, CD_2Cl_2).

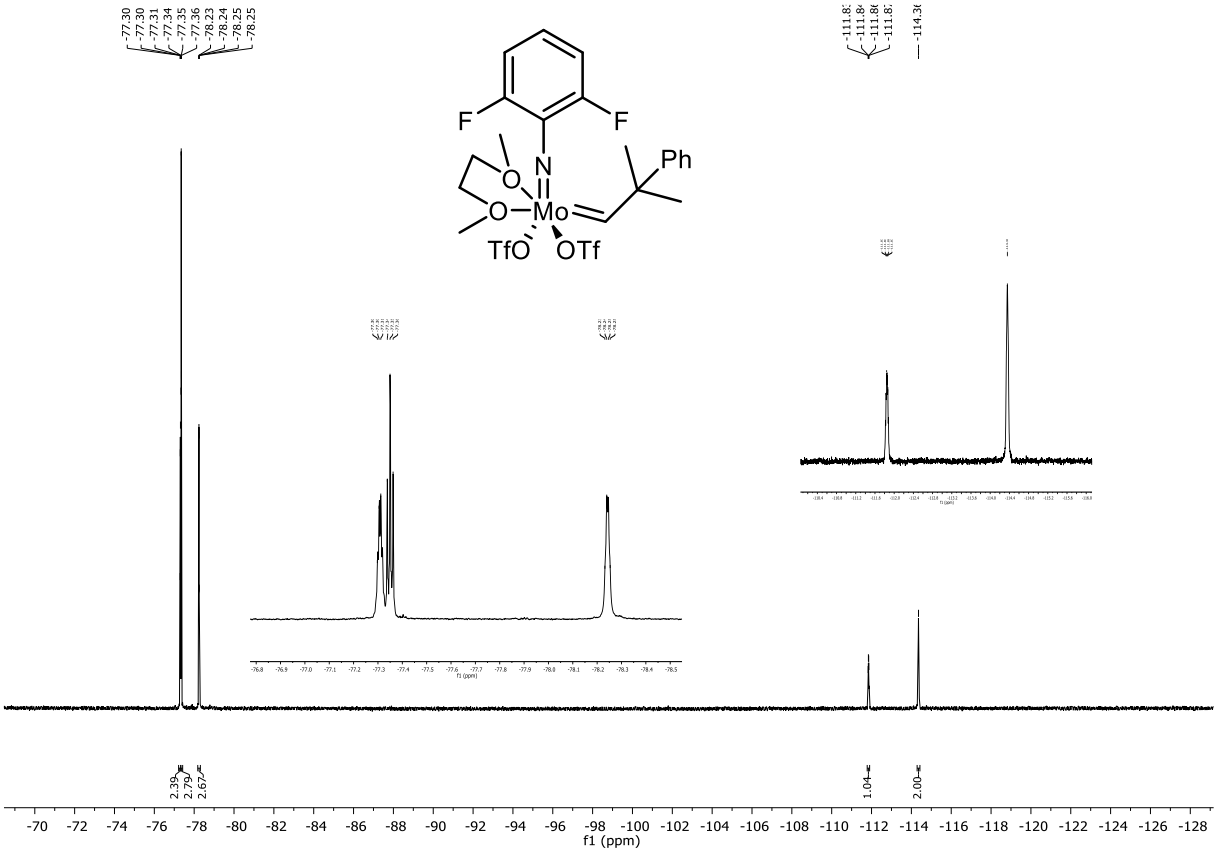

Figure 134. ^{19}F NMR spectrum of **Mo-18** (376 MHz, CD_2Cl_2).

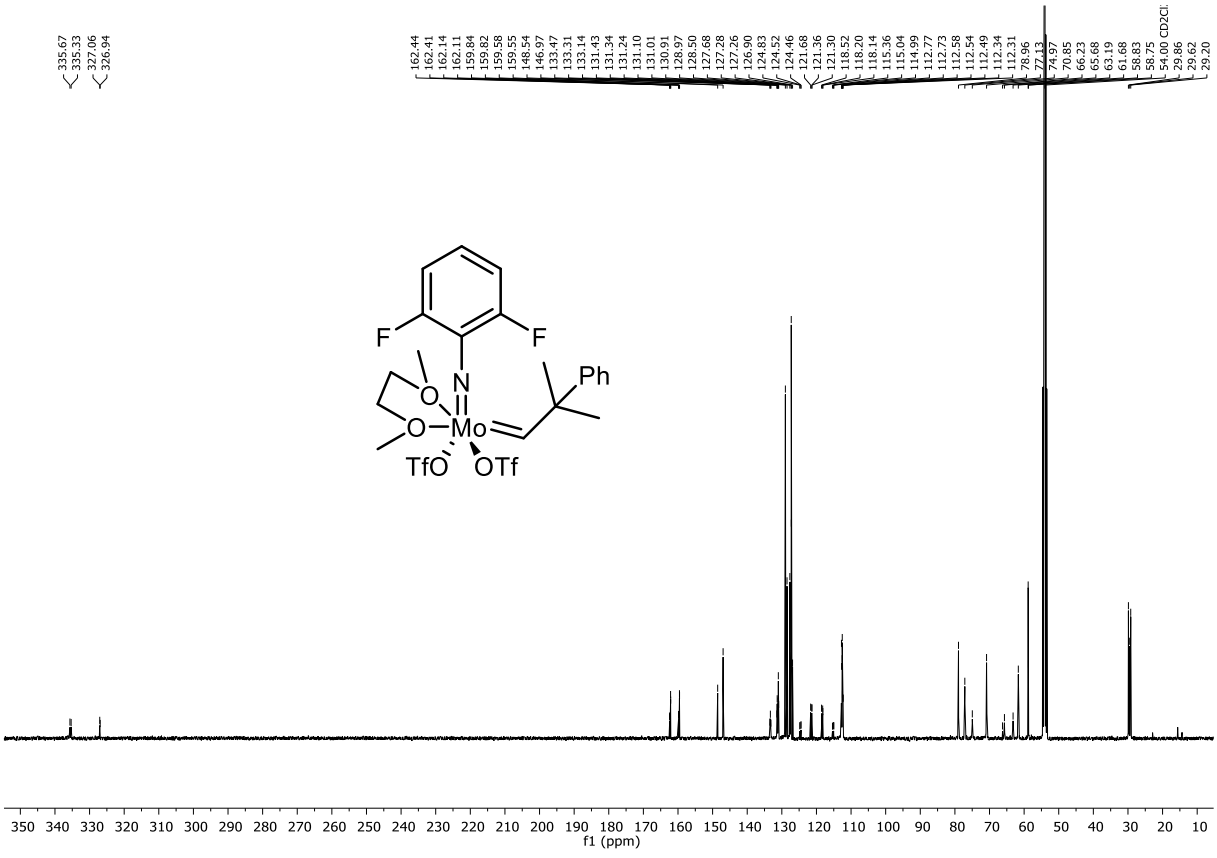

Figure 135. ^{13}C NMR spectrum of **Mo-18** (101 MHz, CD_2Cl_2).

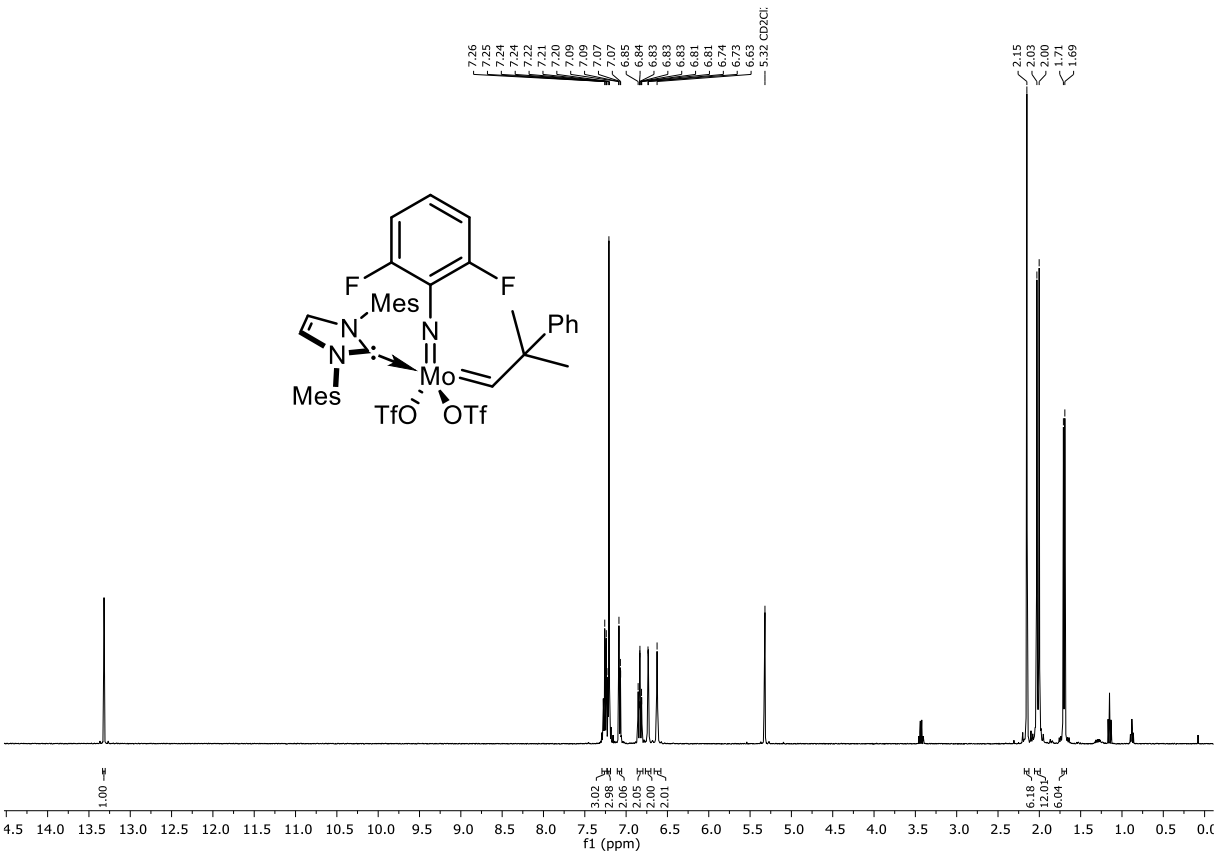

Figure 136. ^{1}H NMR spectrum of **Mo-19** (400 MHz, CD_2Cl_2).

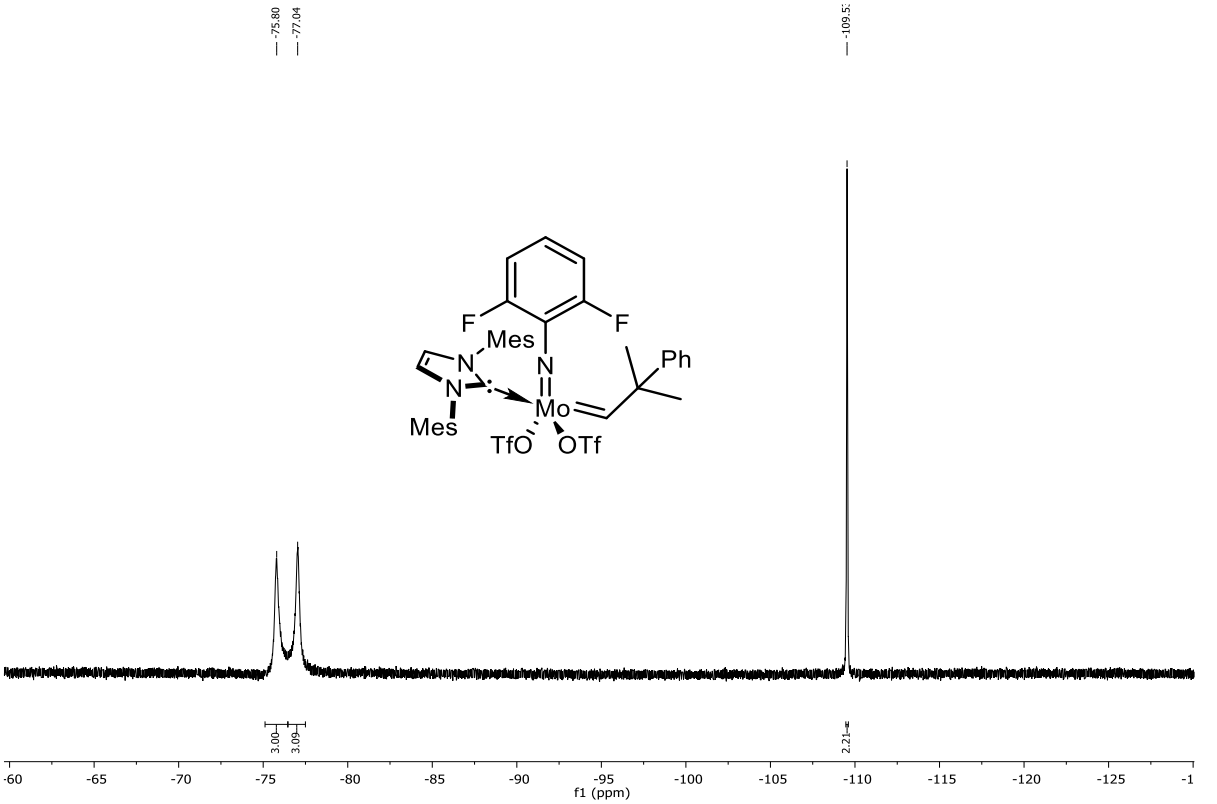

Figure 137. ^{19}F NMR spectrum of **Mo-19** (376 MHz, CD_2Cl_2).

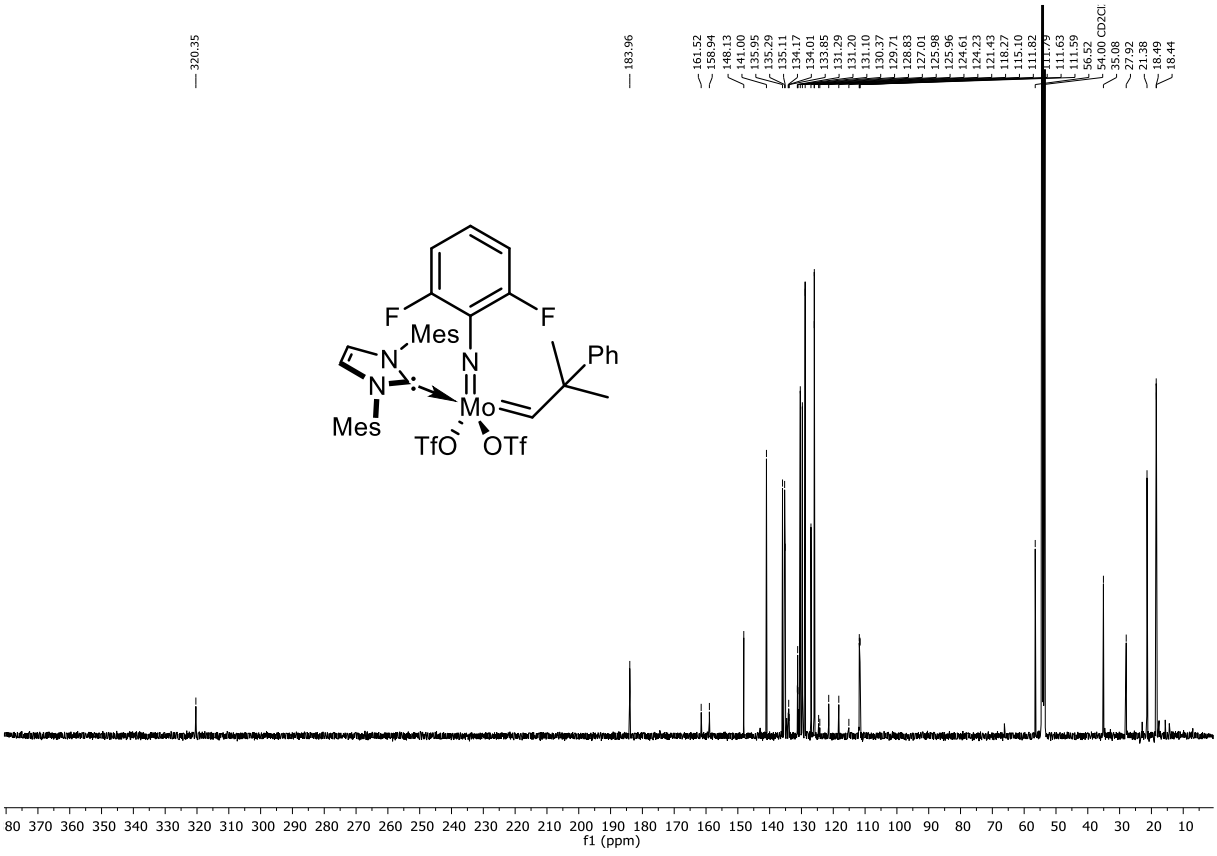

Figure 138. ^{13}C NMR spectrum of **Mo-19** (101 MHz, CD_2Cl_2).

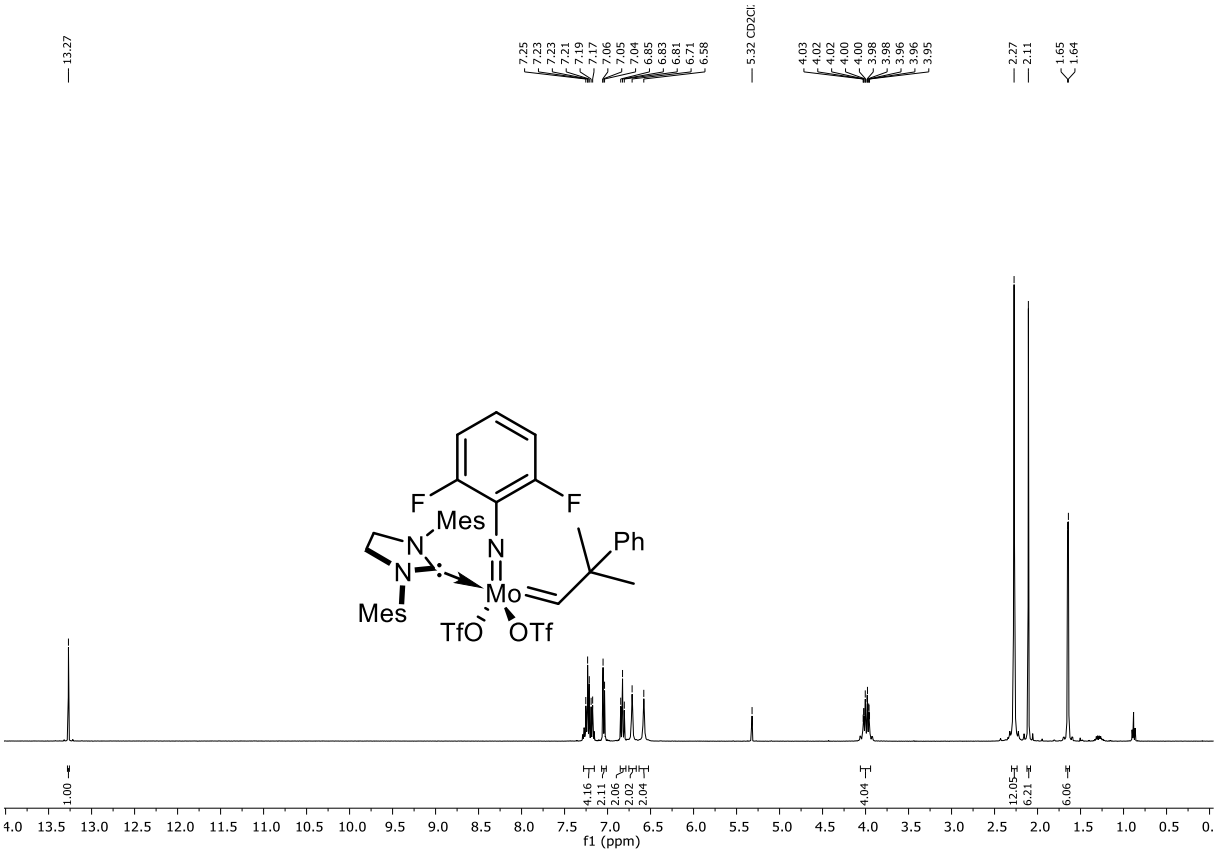

Figure 139. ^{1}H NMR spectrum of **Mo-20** (400 MHz, CD_2Cl_2).

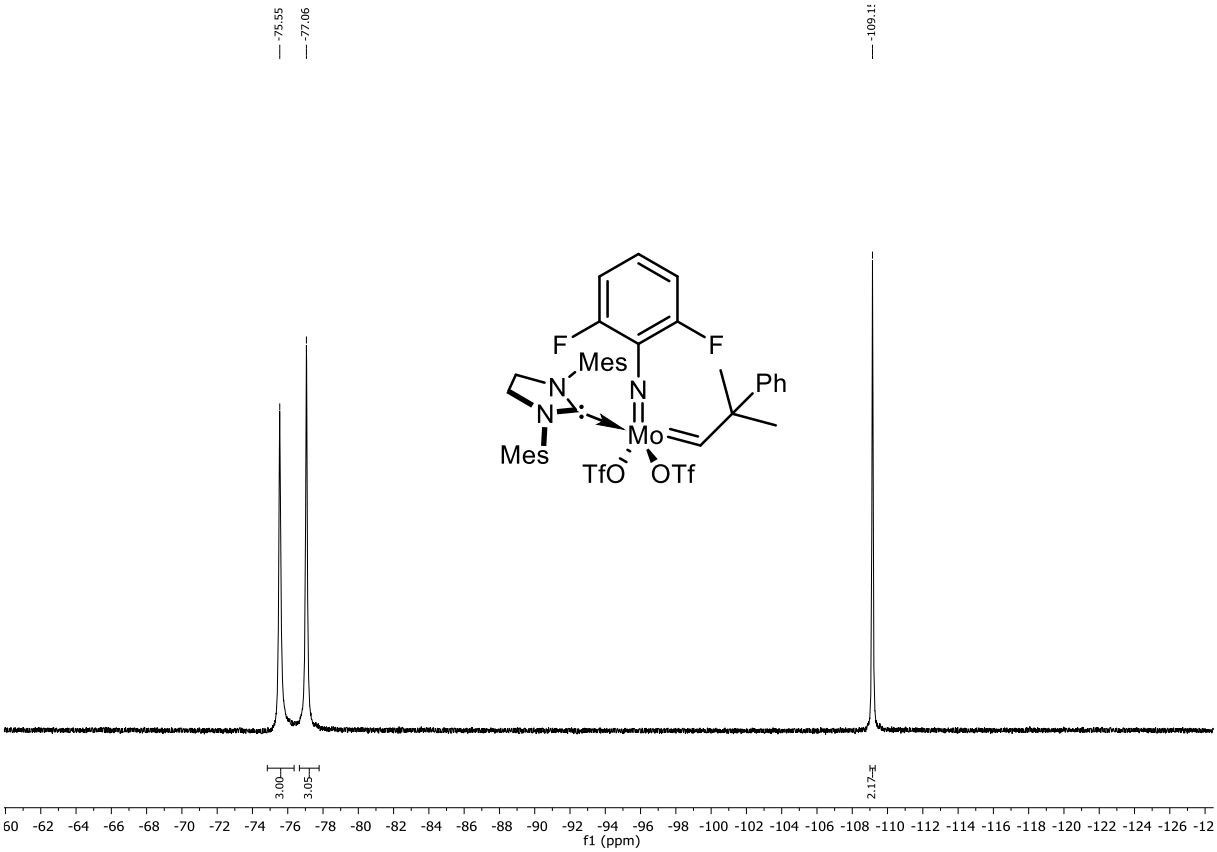

Figure 140. ^{19}F NMR spectrum of **Mo-20** (376 MHz, CD_2Cl_2).

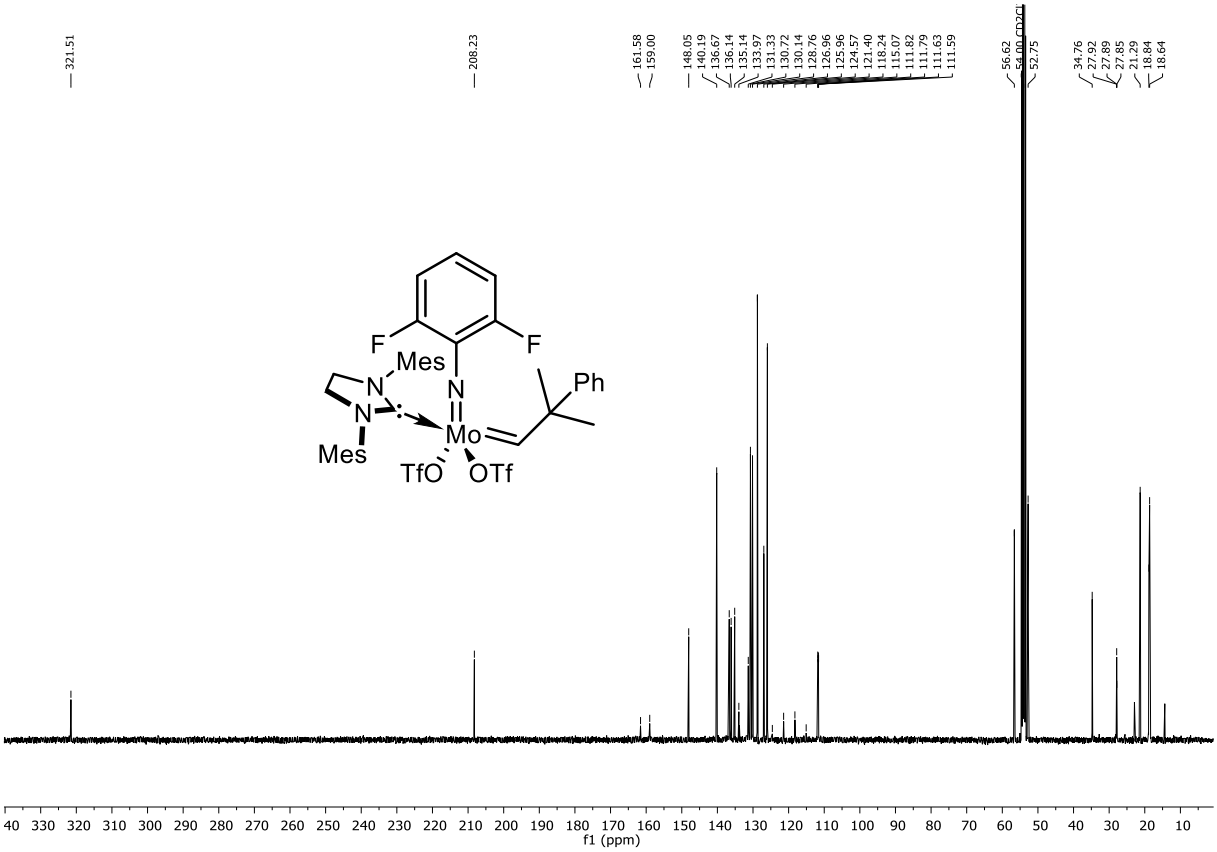

Figure 141. ^{13}C NMR spectrum of **Mo-20** (101 MHz, CD_2Cl_2).

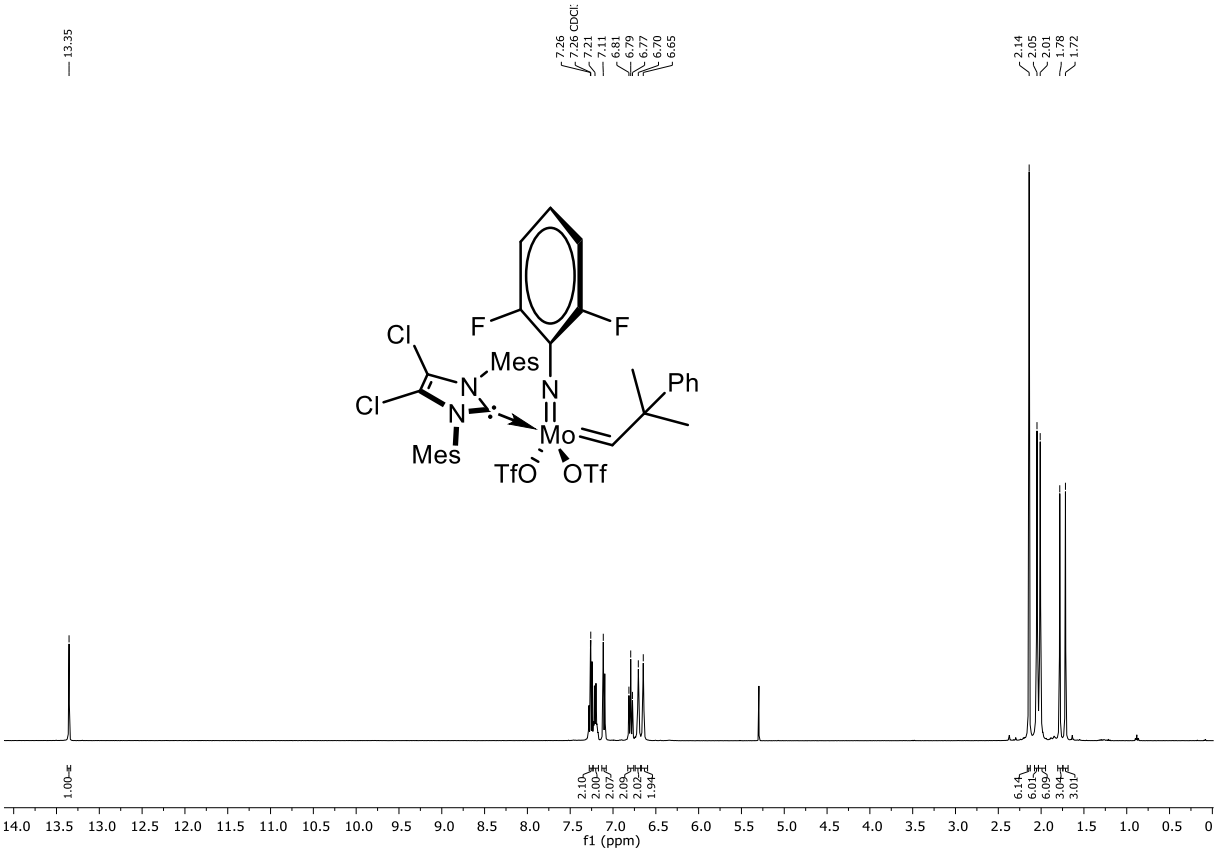

Figure 142. ^{1}H NMR spectrum of **Mo-21** (400 MHz, CD_2Cl_2).

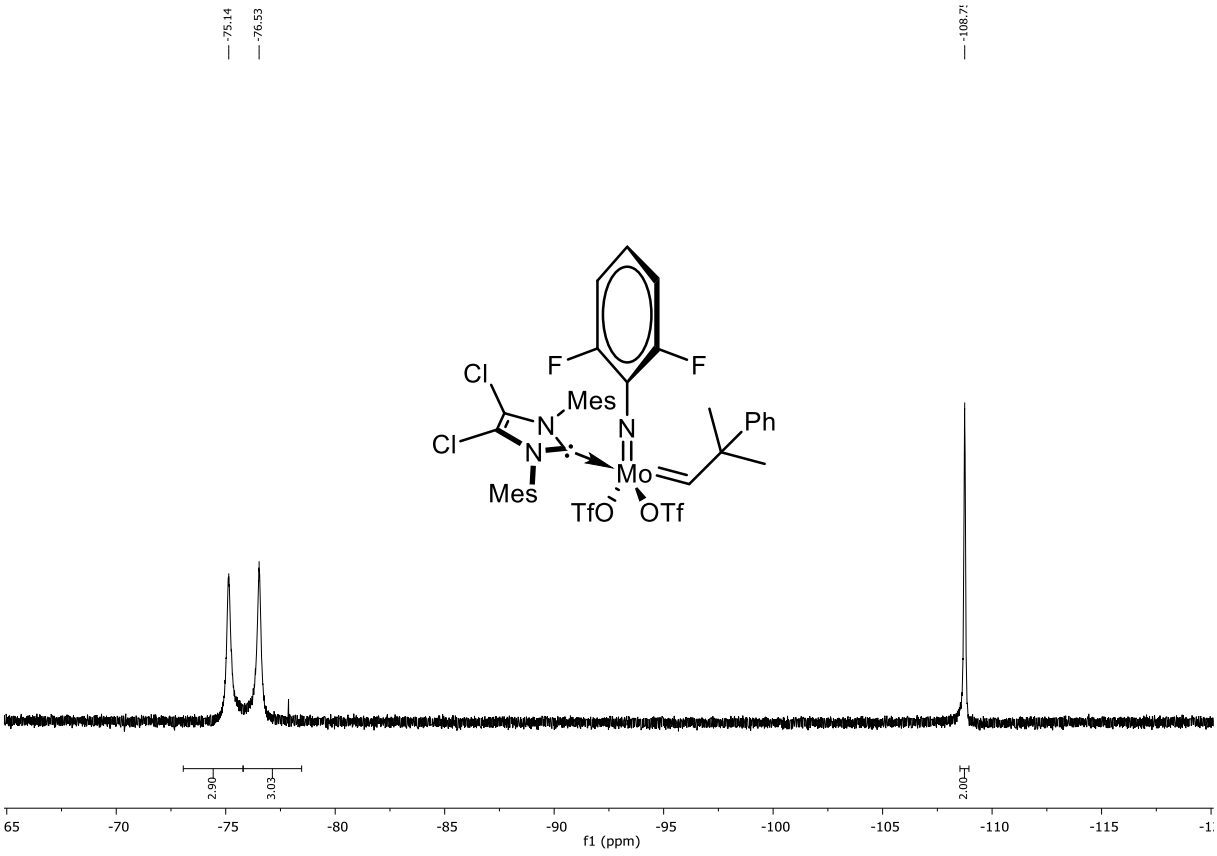

Figure 143. ^{19}F NMR spectrum of **Mo-21** (376 MHz, CD_2Cl_2).

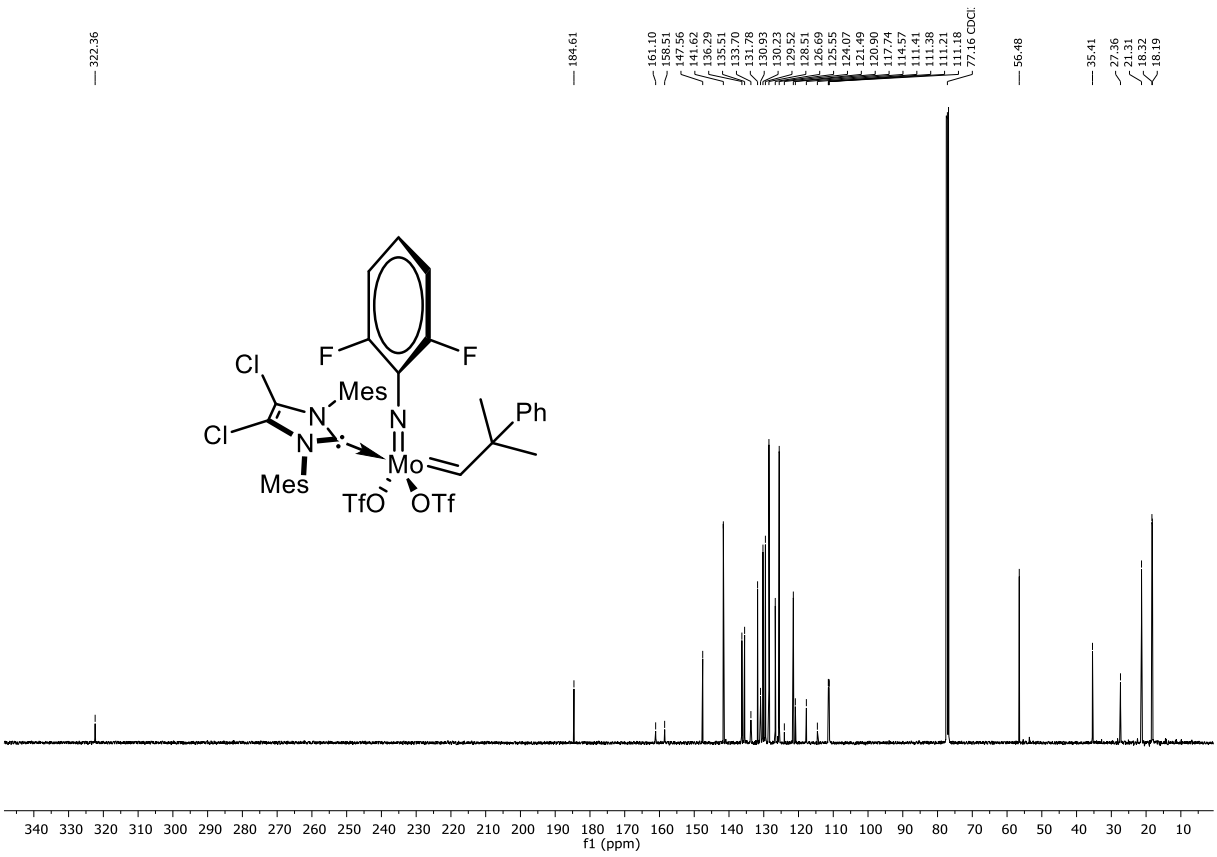

Figure 144. ^{13}C NMR spectrum of **Mo-21** (101 MHz, CD_2Cl_2).

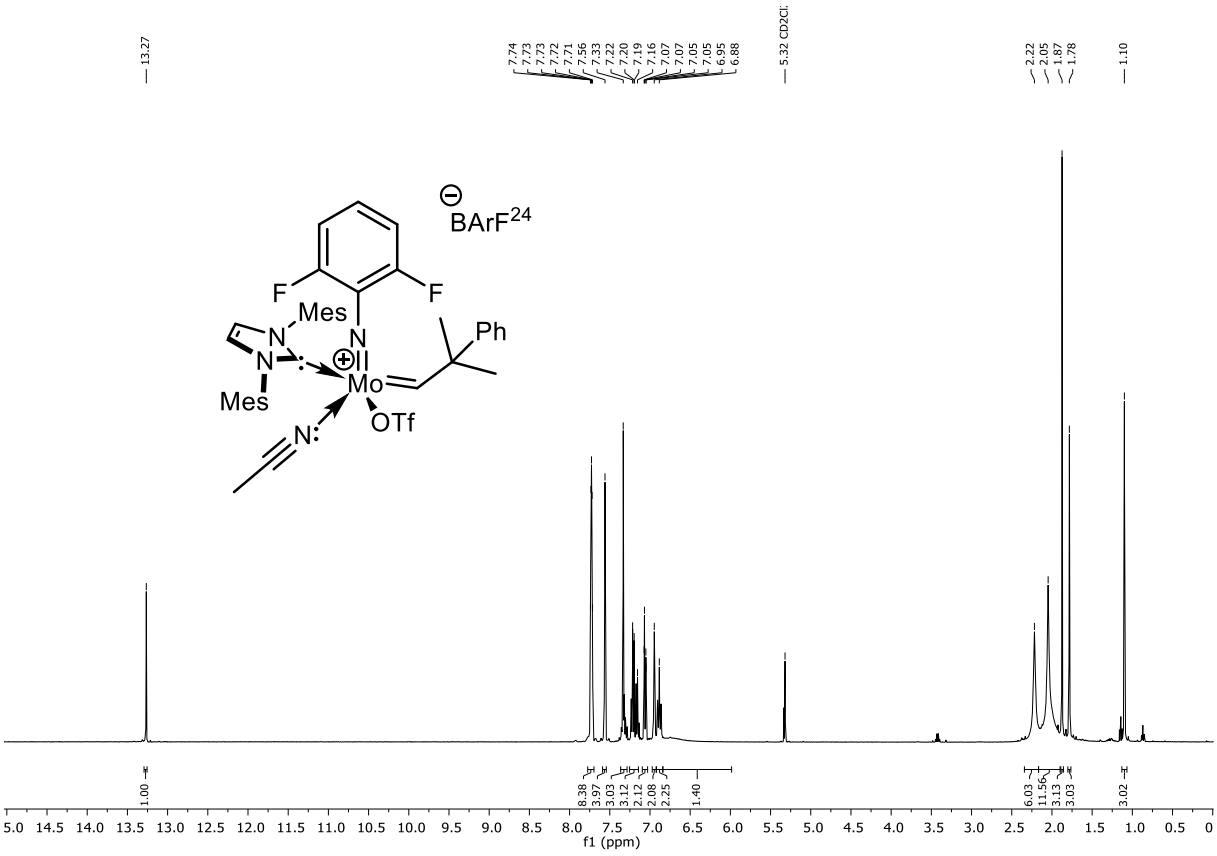

Figure 145. ^{1}H NMR spectrum of **Mo-22** (400 MHz, CD_2Cl_2).

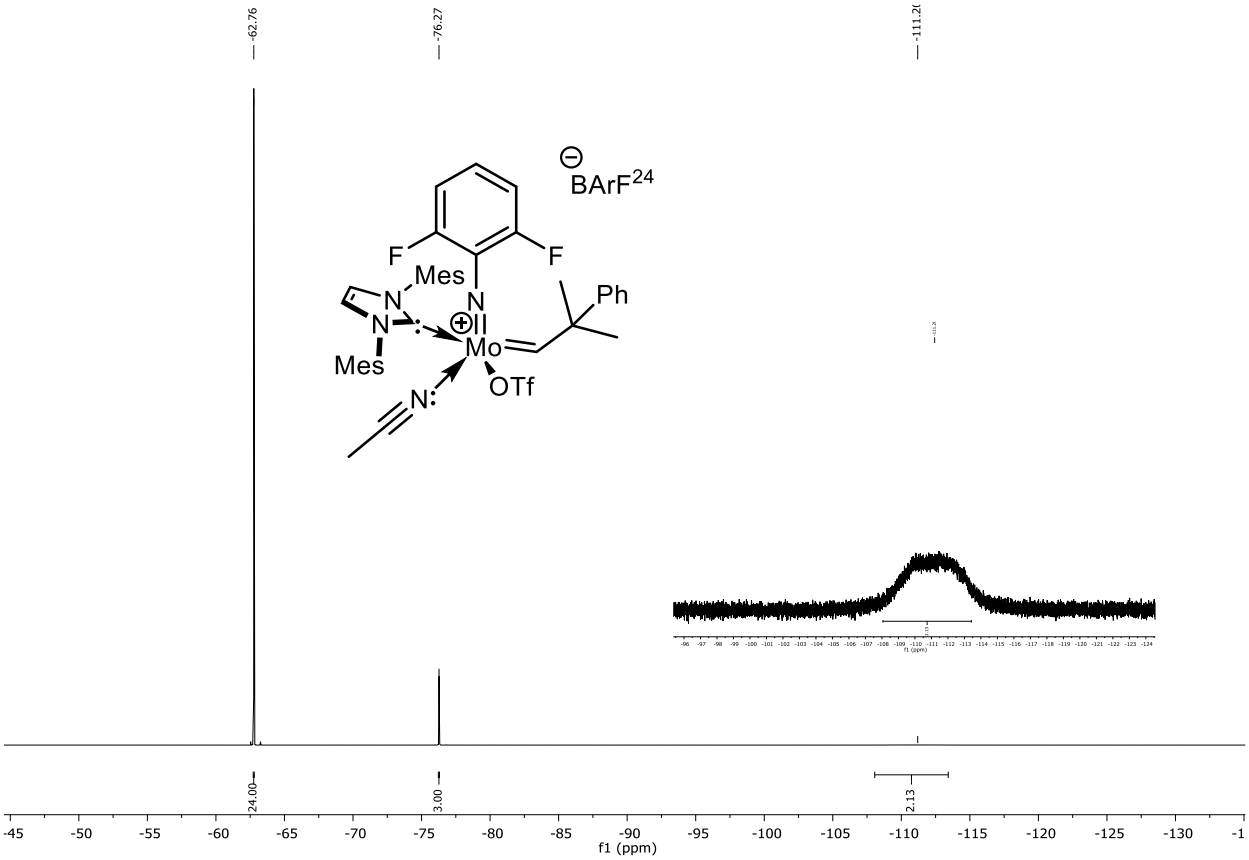

Figure 146. ^{19}F NMR spectrum of **Mo-22** (376 MHz, CD_2Cl_2).

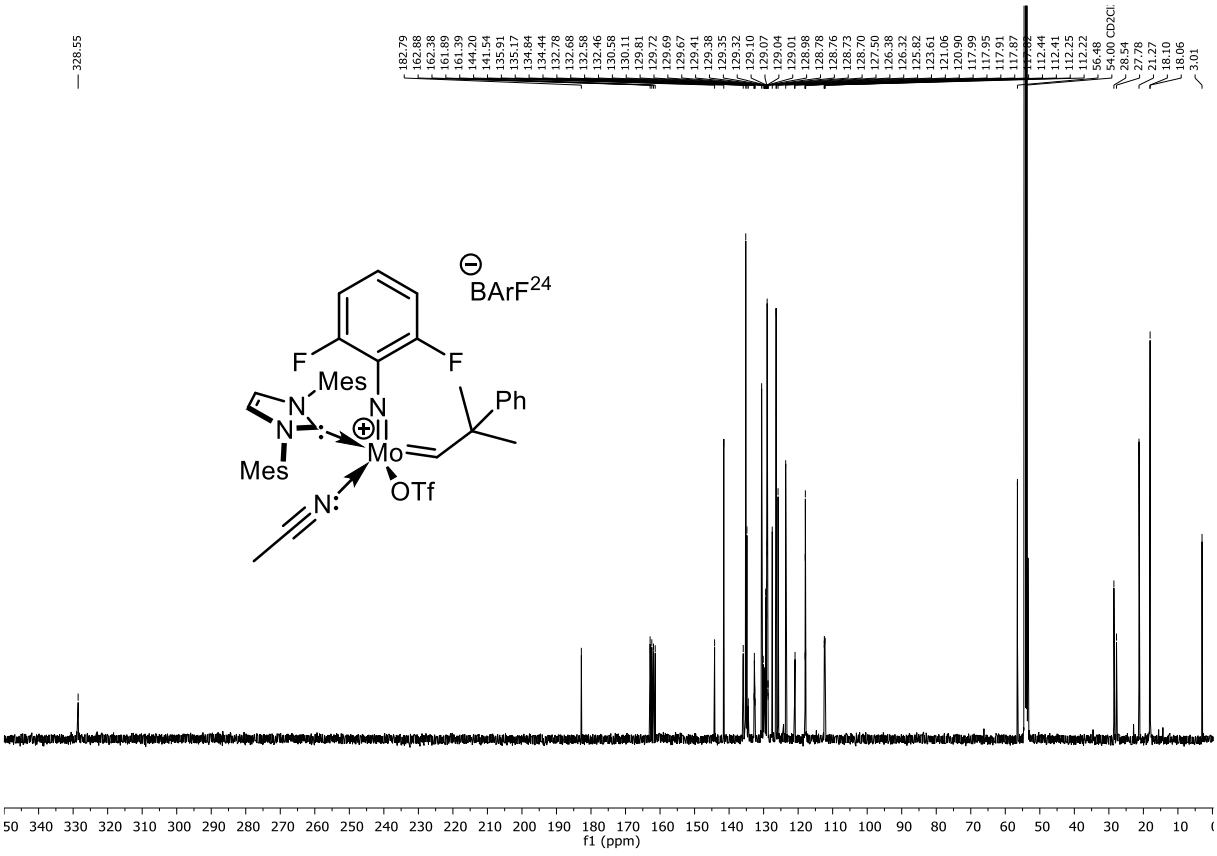

Figure 147. ^{13}C NMR spectrum of **Mo-22** (101 MHz, CD_2Cl_2).

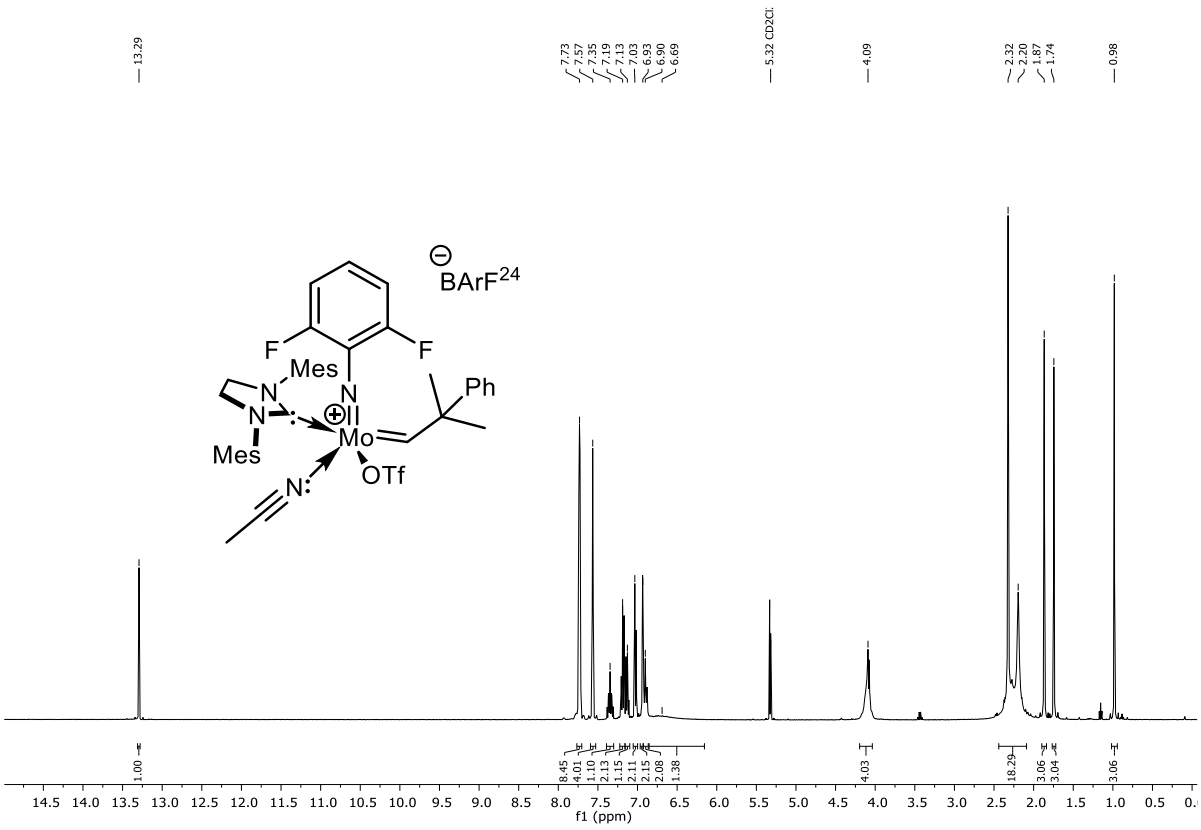

Figure 148. ^{1}H NMR spectrum of **Mo-23** (400 MHz, CD_2Cl_2).

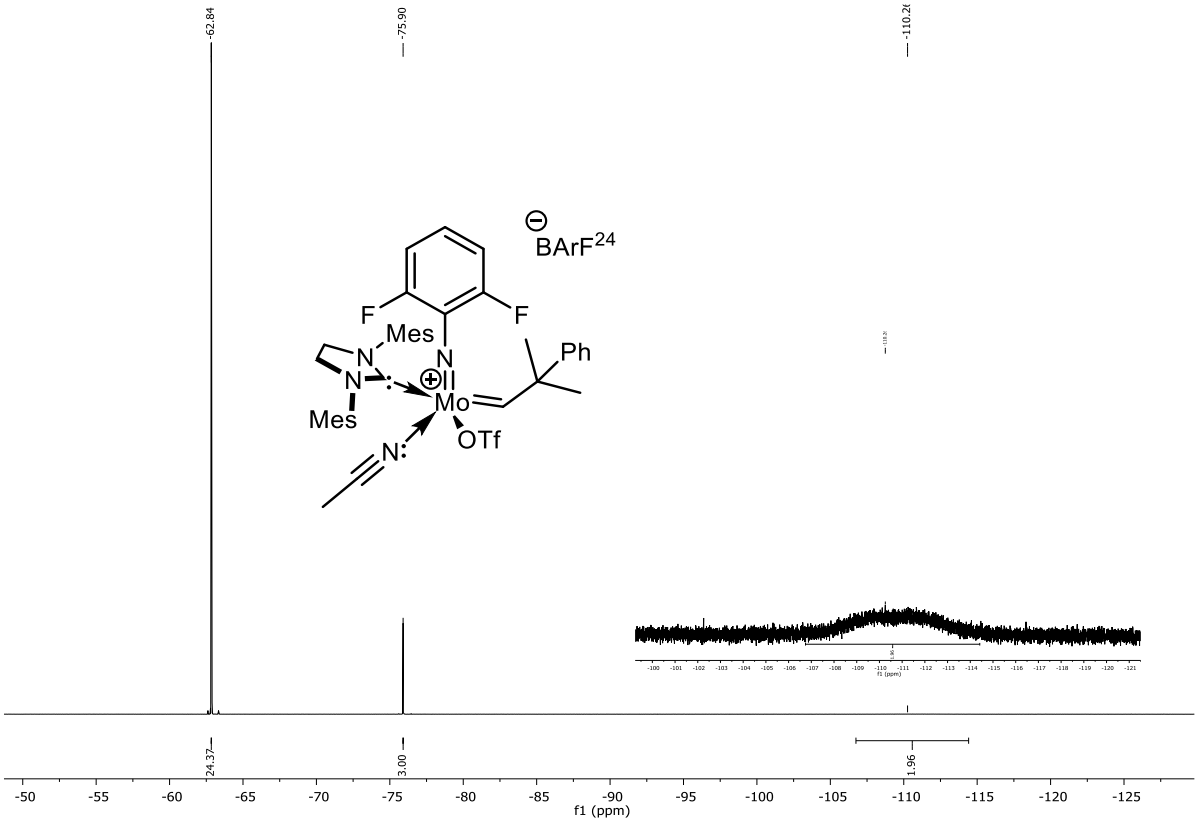

Figure 149. ^{19}F NMR spectrum of **Mo-23** (376 MHz, CD_2Cl_2).

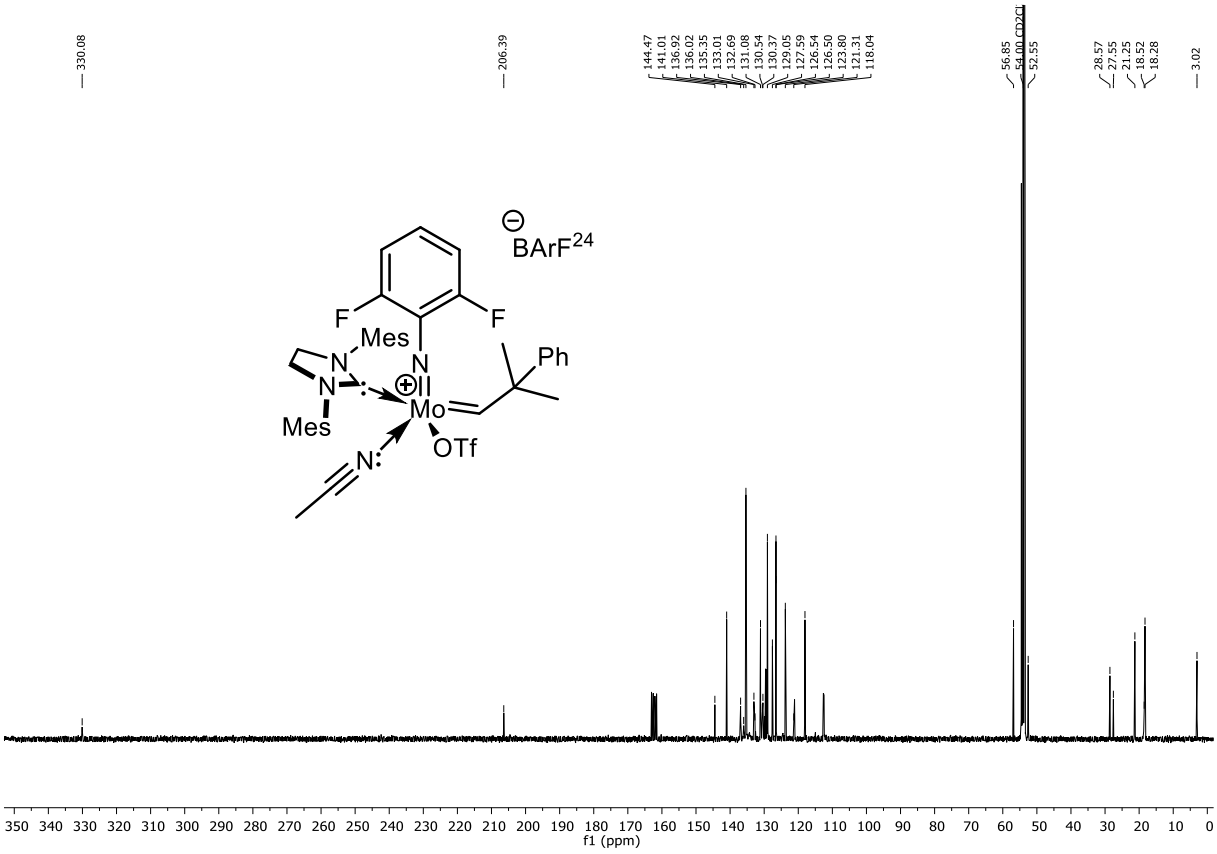

Figure 150. ^{13}C NMR spectrum of **Mo-23** (101 MHz, CD_2Cl_2).

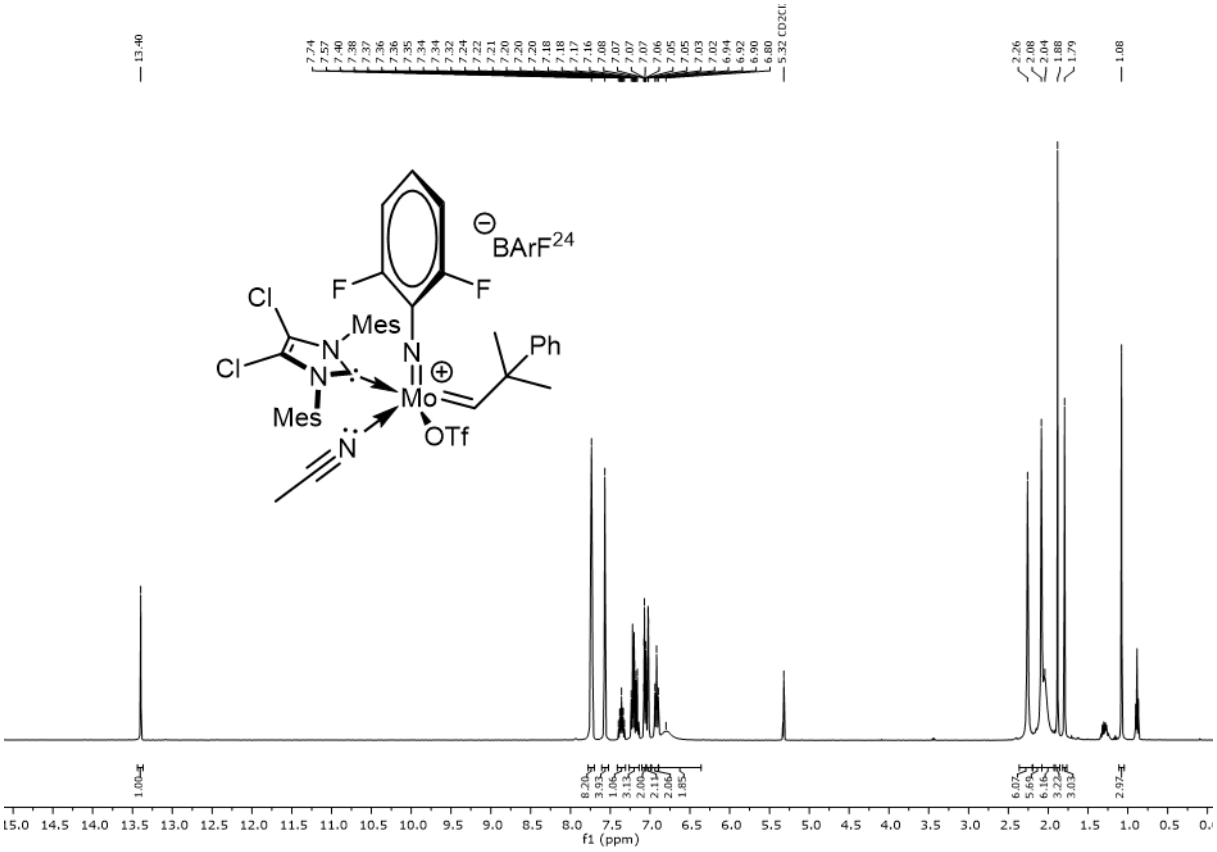

Figure 151. ^{1}H NMR spectrum of **Mo-24** (400 MHz, CD_2Cl_2).

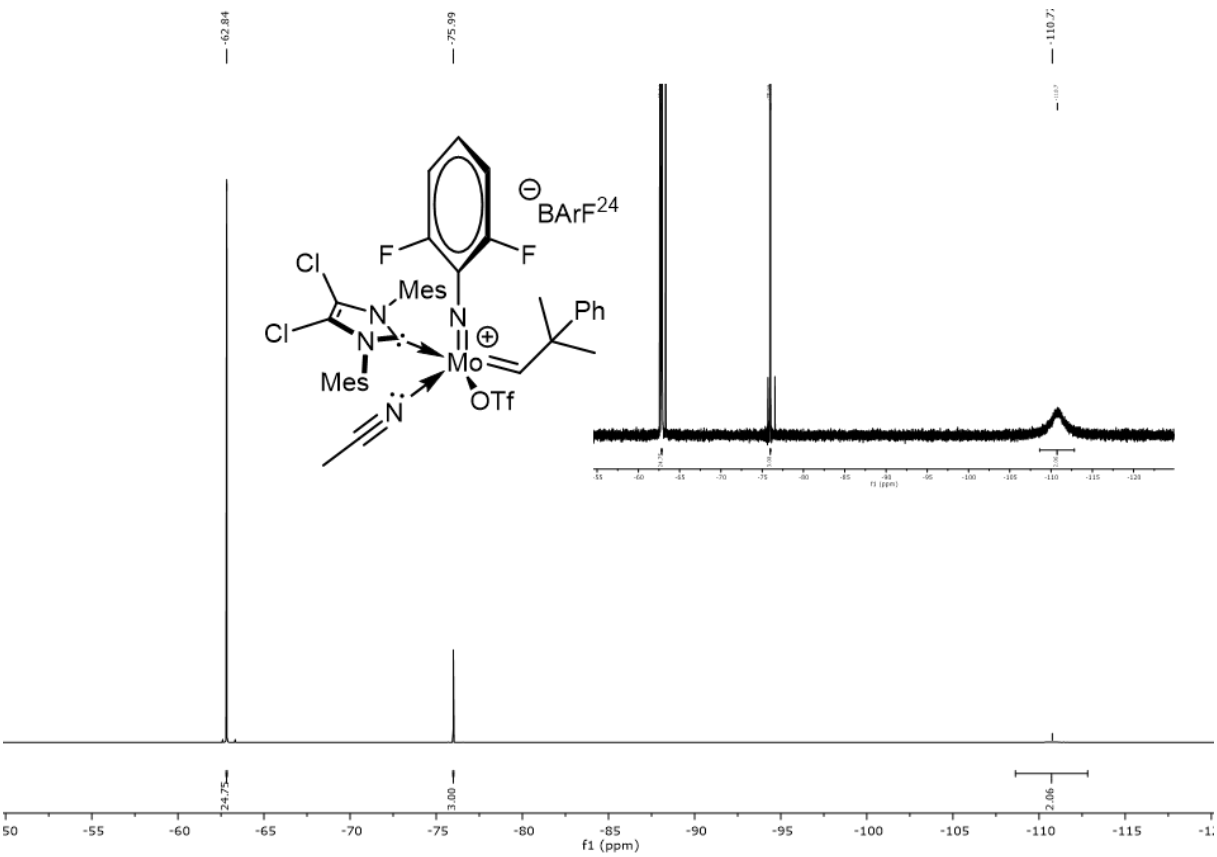

Figure 152. ^{19}F NMR spectrum of **Mo-24** (376 MHz, CD_2Cl_2).

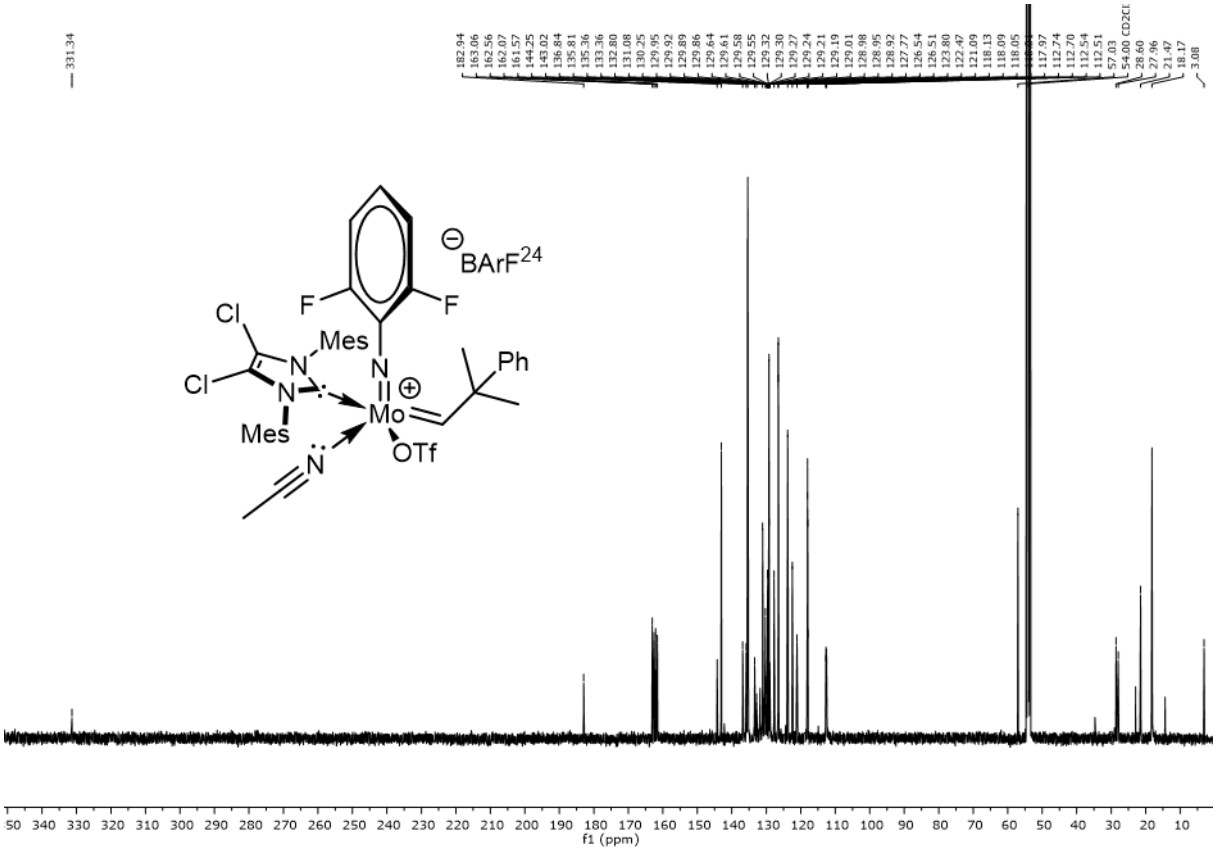

Figure 153. ^{13}C NMR spectrum of **Mo-24** (101 MHz, CD_2Cl_2).

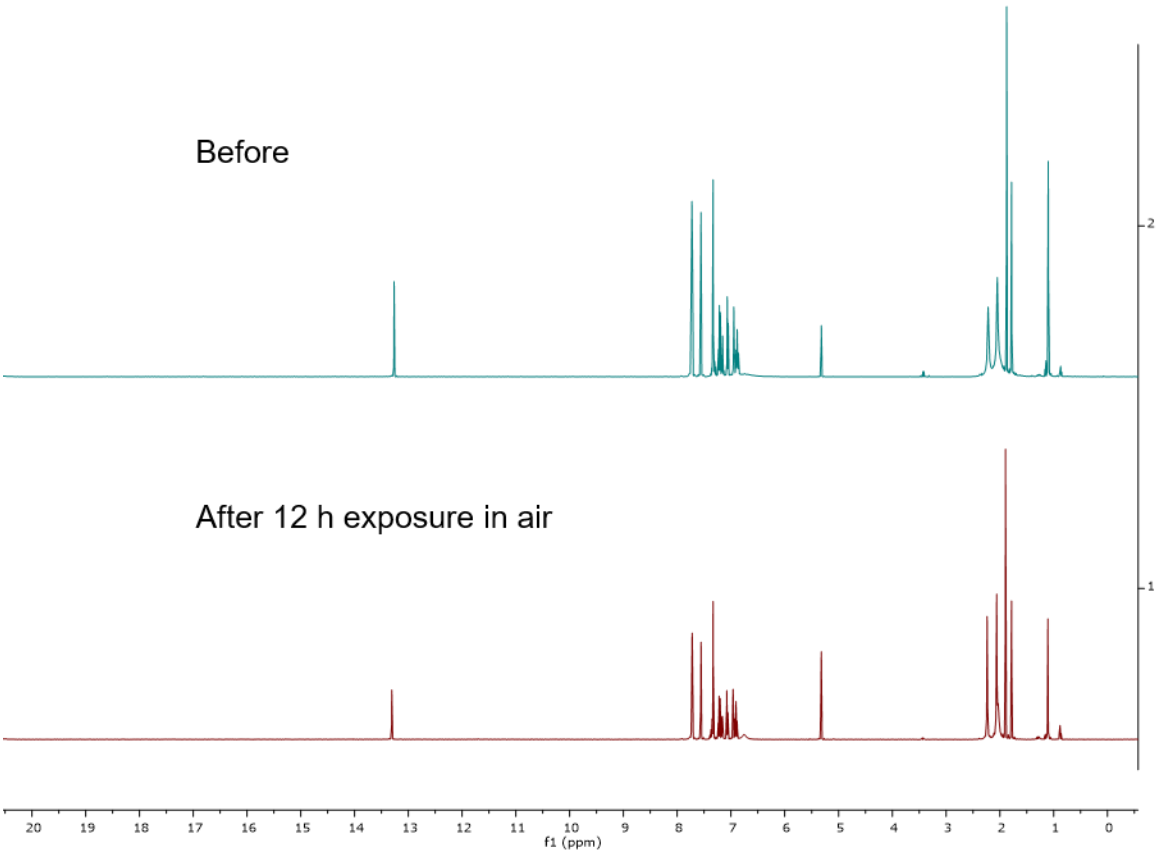

Figure 154. ^{1}H NMR spectrum of **Mo-22** (400 MHz, CD_2Cl_2) – air stability study.

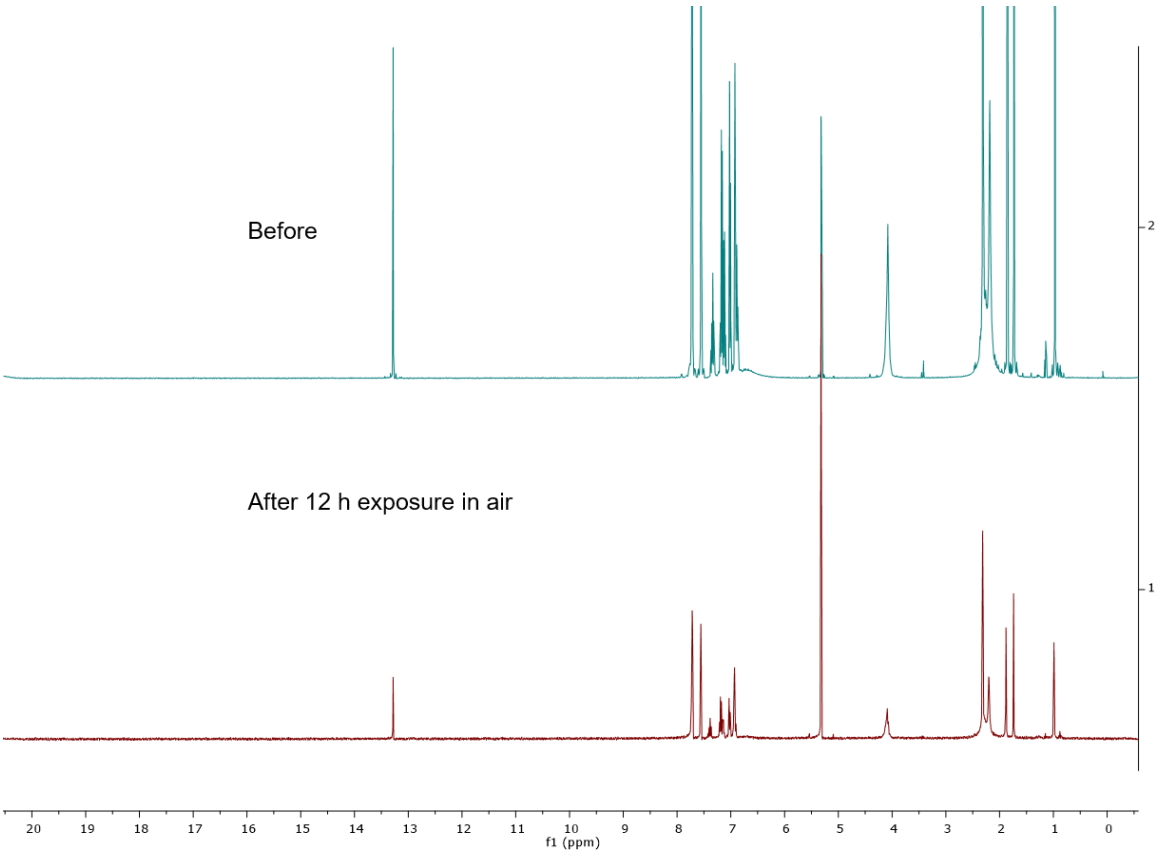

Figure 155. ^{1}H NMR spectrum of **Mo-23** (400 MHz, CD_2Cl_2) – air stability study.

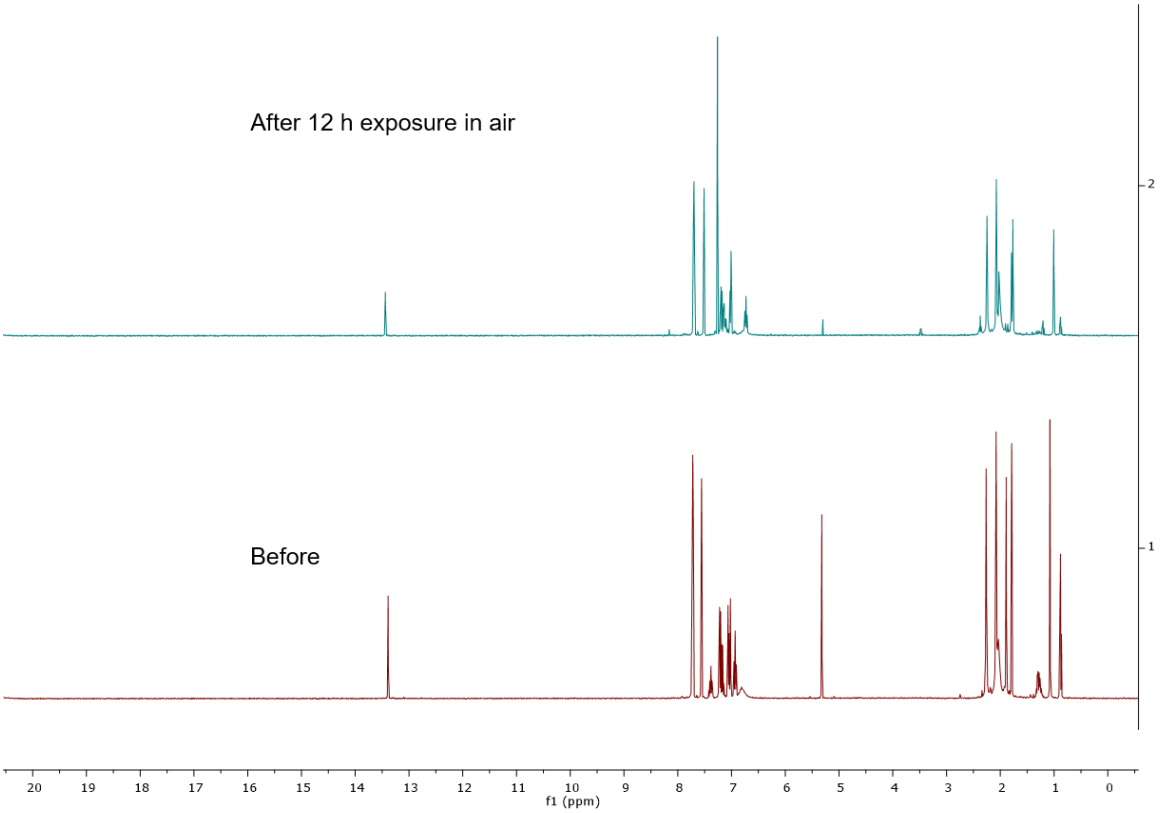

Figure 156. ^{1}H NMR spectrum of **Mo-24** (400 MHz, CD_2Cl_2) – air stability study.

7.4 Crystallographic Data for Chapter 2

Table 8. Crystal data and structure refinement for Complex Mo(*N*-3,5-$Me_2C_6H_3$)(CHCMe_2Ph)(IMesH_2)(OCPh(CF_3)$_2$)$^+$B(Ar^F)$_4^-$, **Mo-5-CAN**.

Identification code	Buch259
Empirical formula	$C_{82}H_{67}BF_{30}MoN_4O$
Formula weight	1801.14
Temperature	135(2) K
Wavelength	0.71073 Å
Crystal system, space group	Triclinic, P-1
Unit cell dimensions	a = 11.5737(4) Å, α = 100.763(2)°
	b = 17.2734(6) Å, β = 102.462(2)°
	c = 20.4304(7) Å, γ = 92.2840(10)°
Volume	3904.3(2) Å^3
Z, Calculated density	2, 1.532 mg/m^3
Absorption coefficient	0.289 mm^{-1}
F(000)	1824
Crystal size	0.450 x 0.389 x 0.367 mm
Theta range for data collection	1.743 to 33.281°
Limiting indices	-17<=h<=11, -26<=k<=26, -31<=l<=31
Reflections collected / unique	107992 / 29806 [R(int) = 0.0257]
Completeness to θ = 25.242	99.9 %
Absorption correction	Semi-empirical from equivalents
Max. and min. transmission	0.7465 and 0.7136
Refinement method	Full-matrix least-squares on F^2
Data / restraints / parameters	29806 / 12 / 1087
Goodness-of-fit on F^2	1.037
Final R indices [I>2σ(I)]	R1 = 0.0355, wR2 = 0.0974
R indices (all data)	R1 = 0.0474, wR2 = 0.1029
Extinction coefficient	n/a
Largest diff. peak and hole	0.881 and -0.656 e. Å^{-3}

7.5 Crystallographic Data for Chapter 3

Table 9. Crystal data and structure refinement for Mo(*N*-2,6-Me_2-C_6H_3)(CHC_4H_6NO)(IMes)($OTf)_2$, **Mo-6**.

Identification code	Buch308
Empirical formula	$C_{37}H_{42}Cl_2F_6MoN_4O_7S_2$
Formula weight	999.70
Temperature	140(2) K
Wavelength	0.71073 Å
Crystal system, space group	Triclinic, P-1
Unit cell dimensions	a = 11.3965(5) Å, α = 76.514(2)°
	b = 11.5325(5) Å, β = 75.379(2)°
	c = 17.7735(7) Å, γ = 84.558(2)°
Volume	2196.40(16) $Å^3$
Z, Calculated density	2, 1.512 mg/m^3
Absorption coefficient	0.591 mm^{-1}
F(000)	1020
Crystal size	0.284 x 0.194 x 0.161 mm
Theta range for data collection	1.82 to 26.45°
Limiting indices	-14<=h<=14, -14<=k<=14, -18<=l<=22
Reflections collected / unique	33974 / 8980 [R(int) = 0.0313]
Completeness to θ = 25.242	99.4 %
Absorption correction	Semi-empirical from equivalents
Max. and min. transmission	0.7454 and 0.7072
Refinement method	Full-matrix least-squares on F^2
Data / restraints / parameters	8980 / 80 / 621
Goodness-of-fit on F^2	1.048
Final R indices [I>2σ(I)]	R1 = 0.0389, wR2 = 0.1037
R indices (all data)	R1 = 0.0567, wR2 = 0.1115
Extinction coefficient	n/a
Largest diff. peak and hole	0.753 and -0.614 e.$Å^{-3}$

Table 10. Crystal data and structure refinement for Mo(*N*-3,5-Me_2-C_6H_3)(CHC_4H_6NO)(IMes)($OTf)_2$, **Mo-7**.

Identification code	Buch309
Empirical formula	$C_{37}H_{42}Cl_2F_6MoN_4O_7S_2$
Formula weight	999.70
Temperature	140(2) K
Wavelength	0.71073 Å
Crystal system, space group	Monoclinic, $P2_1/c$
Unit cell dimensions	a = 13.4276(10) Å, α = 90°
	b = 16.6453(13) Å, β = 91.984(4)°
	c = 18.7362(14) Å, γ = 90°
Volume	4185.2(5) $Å^3$
Z, Calculated density	4, 1.587 mg/m^3
Absorption coefficient	0.620 mm^{-1}
F(000)	2040
Crystal size	0.320 x 0.240 x 0.153 mm
Theta range for data collection	1.517 to 28.465°.
Limiting indices	-17<=h<=17, -22<=k<=21, -24<=l<=25
Reflections collected / unique	61655 / 10443 [R(int) = 0.0742]
Completeness to θ = 25.242	99.8 %
Absorption correction	Numerical
Max. and min. transmission	0.9912 and 0.6007
Refinement method	Full-matrix least-squares on F^2
Data / restraints / parameters	10443 / 0 / 540
Goodness-of-fit on F^2	1.038
Final R indices [I>2σ(I)]	R1 = 0.0532, wR2 = 0.1380
R indices (all data)	R1 = 0.0828, wR2 = 0.1513
Extinction coefficient	n/a
Largest diff. peak and hole	1.140 and -1.874 $e.A^{-3}$

Table 11. Crystal data and structure refinement for Mo(*N*-2,6-Me_2-C_6H_3)(CHC_5H_4N)(IMes)($OTf)_2$, **Mo-8**.

Identification code	Buch304
Empirical formula	$C_{38}H_{40}Cl_2F_6MoN_4O_6S_2$
Formula weight	993.70
Temperature	140(2) K
Wavelength	0.71073 Å
Crystal system, space group	Monoclinic, $P2_1/n$
Unit cell dimensions	a = 13.7867(7) Å, α = 90°
	b = 10.5984(5) Å, β = 93.105(2)°
	c = 29.5738(14) Å, γ= 90°
Volume	4314.9(4) $Å^3$
Z, Calculated density	4, 1.530 mg/m^3
Absorption coefficient	0.599 mm^{-1}
F(000)	2024
Crystal size	0.979 x 0.580 x 0.478 mm
Theta range for data collection	1.598 to 33.161°.
Limiting indices	-19<=h<=21, -16<=k<=9, -45<=l<=45
Reflections collected / unique	66546 / 16406 [R(int) = 0.0236]
Completeness to θ = 25.242	99.9 %
Absorption correction	Semi-empirical from equivalents
Max. and min. transmission	0.7465 and 0.6662
Refinement method	Full-matrix least-squares on F^2
Data / restraints / parameters	16406 / 36 / 569
Goodness-of-fit on F^2	1.022
Final R indices [I>2σ(I)]	R1 = 0.0396, wR2 = 0.1090
R indices (all data)	R1 = 0.0487, wR2 = 0.1141
Extinction coefficient	0.0029(2)
Largest diff. peak and hole	0.891 and -0.661 e.$Å^{-3}$

Table 12. Crystal data and structure refinement for Mo(*N*-3,5-Me_2-C_6H_3)(CHC_5H_4N)(IMes)($OTf)_2$, **Mo-9**.

Identification code	Buch305
Empirical formula	$C_{38}H_{40}Cl_2F_6MoN_4O_6S_2$
Formula weight	993.70
Temperature	140(2) K
Wavelength	0.71073 Å
Crystal system, space group	Orthorhombic, $P2_12_12_1$
Unit cell dimensions	a = 11.8955(9) Å, α = 90°.
	b = 17.3338(13) Å, β = 90°.
	c = 21.6389(18) Å, γ = 90°.
Volume	4461.8(6) $Å^3$
Z, Calculated density	4, 1.479 mg/m^3
Absorption coefficient	0.580 mm^{-1}
F(000)	2024
Crystal size	0.559 x 0.370 x 0.224 mm
Theta range for data collection	1.505 to 30.590°.
Limiting indices	-15<=h<=17, -24<=k<=18, -30<=l<=30
Reflections collected / unique	62997 / 13641 [R(int) = 0.0521]
Completeness to θ = 25.242	100.0 %
Absorption correction	Numerical
Max. and min. transmission	0.8977 and 0.7557
Refinement method	Full-matrix least-squares on F^2
Data / restraints / parameters	13641 / 221 / 605
Goodness-of-fit on F^2	1.026
Final R indices [I>2σ(I)]	R1 = 0.0408, wR2 = 0.0812
R indices (all data)	R1 = 0.0598, wR2 = 0.0869
Absolute structure parameter	-0.035(11)
Extinction coefficient	0.00058(16)
Largest diff. peak and hole	0.570 and -0.494 e. $Å^{-3}$

Table 13. Crystal data and structure refinement for Mo(N-2,6-Me_2-C_6H_3)(CHCMe_2Ph)(OTf)(*O*-2-Cl-C_6H_4)(IMes), **Mo-12**.

Identification code	Buch307
Empirical formula	$C_{46}H_{48.88}ClF_{3.12}MoN_3O_4S$
Formula weight	930.58
Temperature	140(2) K
Wavelength	0.71073 Å
Crystal system, space group	Monoclinic, $P2_1/n$
Unit cell dimensions	a = 11.3995(4) Å, α = 90°
	b = 19.1476(9) Å, β = 100.502(2)°
	c = 20.5676(9) Å, γ = 90°
Volume	4414.1(3) $Å^3$
Z, Calculated density	4, 1.400 mg/m^3
Absorption coefficient	0.464 mm^{-1}
F(000)	1924
Crystal size	0.469 x 0.232 x 0.194 mm
Theta range for data collection	1.910 to 28.323°
Limiting indices	-14<=h<=15, -25<=k<=25, -26<=l<=27
Reflections collected / unique	49216 / 10987 [R(int) = 0.0498]
Completeness to θ = 25.242	99.9 %
Absorption correction	Semi-empirical from equivalents
Max. and min. transmission	0.7457 and 0.7066
Refinement method	Full-matrix least-squares on F^2
Data / restraints / parameters	10987 / 24 / 554
Goodness-of-fit on F^2	1.047
Final R indices [I>2σ(I)]	R1 = 0.0438, wR2 = 0.0984
R indices (all data)	R1 = 0.0809, wR2 = 0.1095
Extinction coefficient	n/a
Largest diff. peak and hole	0.727 and -0.695 e. $Å^{-3}$

****

REMARK: On the phenyl-moiety of the ether ligand there is in the ortho-position a disordered fluoro atom (with only 12.5 % population, but nevertheless evident and free refineable)
****

Table 14. Crystal data and structure refinement for Mo(*N*-3,5-Me_2-C_6H_3)(CH(-2-*N*(Me_2)-C_6H_4)(IMes)$(OTf)_2$, **Mo-15**.

Identification code	Buch314
Empirical formula	$C_{41}H_{46}Cl_2F_6MoN_4O_6S_2$
Formula weight	1035.78
Temperature	140(2) K
Wavelength	0.71073 Å
Crystal system, space group	Triclinic, P-1
Unit cell dimensions	a = 11.4440(5) Å, α = 77.638(3)°
	b = 12.2031(6) Å, β = 78.969(3)°
	c = 17.6394(8) Å, γ = 71.747(2)°
Volume	2264.59(19) $Å^3$
Z, Calculated density	2, 1.519 mg/m^3
Absorption coefficient	0.574 mm^{-1}
F(000)	1060
Crystal size	0.220 x 0.185 x 0.134 mm
Theta range for data collection	1.782 to 28.310°
Limiting indices	-15<=h<=15, -16<=k<=15, -23<=l<=22
Reflections collected / unique	42453 / 10833 [R(int) = 0.0623]
Completeness to θ = 25.242	98.3 %
Absorption correction	Semi-empirical from equivalents
Max. and min. transmission	0.7457 and 0.6852
Refinement method	Full-matrix least-squares on F^2
Data / restraints / parameters	10833 / 0 / 572
Goodness-of-fit on F^2	1.017
Final R indices [I>2σ (I)]	R1 = 0.0487, wR2 = 0.0916
R indices (all data)	R1 = 0.1082, wR2 = 0.1066
Extinction coefficient	n/a
Largest diff. peak and hole	0.589 and -0.953 e. $Å^{-3}$

Table 15. Crystal data and structure refinement for the **Mo-imido alkylidene NHC olefin complex (MOC)**.

Identification code	Buch283
Empirical formula	$C_{43}H_{44}ClF_3MoN_4O_4S$
Formula weight	901.27
Temperature	135(2) K
Wavelength	1.54178 Å
Crystal system space group	Triclinic, P-1
Unit cell dimensions	a = 10.2546(6) Å, α = 72.382(6)°
	b = 19.5156(15) Å, β = 79.241(6)°
	c = 23.721(2) Å, γ = 75.826(5)°
Volume	4354.1(6) $Å^3$
Z, Calculated density	4, 1.375 mg/m^3
Absorption coefficient	3.960 mm^{-1}
F(000)	1856
Crystal size	0.107 x 0.060 x 0.025 mm
Theta range for data collection	6.566 to 62.497°
Limiting indices	-11<=h<=11 -22<=k<=22 -27<=l<=24
Reflections collected / unique	46034 / 13659 [R(int) = 0.2006]
Completeness to θ = 62.497	98.3 %
Absorption correction	Semi-empirical from equivalents
Max. and min. transmission	0.7523 and 0.5852
Refinement method	Full-matrix least-squares on F^2
Data / restraints / parameters	13659 / 171 / 1123
Goodness-of-fit on F^2	1.034
Final R indices [I>2σ(I)]	R1 = 0.0759 wR2 = 0.1519
R indices (all data)	R1 = 0.1514 wR2 = 0.1710
Extinction coefficient	0.00254(12)
Largest diff. peak and hole	0.710 and -0.860 $e.Å^{-3}$

****

Remark: bad crystal quality: R(int) ~ 0.20 -> check_cif: B-Alert

1. However, it is not further restrictive, since R-value and standard deviations of the geometry parameters are sufficiently good. -> check cif_report

2. Disordered solvent (diethyl ether) was removed with PLATON (subroutine squeeze).

3. A triflate counterion is strongly disordered.

4. Two independent complexes (conformers) in the asymmetric unit

****

Table 16. Atomic coordinates (x 10^4) and equivalent isotropic displacement parameters (A^2 x 10^3) for the **MOC**. U(eq) is defined as one third of the trace of the orthogonalized U_{ij} tensor.

	x	y	z	U(eq)
Mo(1A)	8805(1)	4130(1)	1987(1)	32(1)
Cl(1A)	11395(2)	3882(1)	1532(1)	42(1)
O(1A)	9502(5)	3110(3)	2473(2)	35(1)
N(1A)	5952(6)	3613(4)	2328(3)	32(2)
C(1A)	6901(7)	3889(5)	2489(4)	34(2)
N(2A)	6394(6)	3884(4)	3071(3)	33(2)
C(2A)	4967(8)	3438(5)	2799(4)	41(2)
N(3A)	8511(6)	4089(4)	1309(3)	30(2)
C(3A)	5233(8)	3603(5)	3263(4)	39(2)
N(4A)	9915(6)	4502(4)	2560(3)	37(2)
C(4A)	5991(7)	3460(5)	1776(4)	37(2)
C(5A)	6570(7)	2749(5)	1710(4)	37(2)
C(6A)	6496(8)	2611(6)	1179(5)	50(3)
C(7A)	5849(9)	3134(6)	729(5)	53(3)
C(8A)	5279(9)	3827(6)	798(4)	51(3)
C(9A)	5304(7)	4003(5)	1319(4)	36(2)
C(10A)	7235(9)	2179(5)	2211(5)	51(3)
C(11A)	5790(10)	2953(7)	147(5)	76(4)
C(12A)	4583(8)	4741(5)	1424(5)	51(3)
C(13A)	6976(7)	4146(5)	3457(4)	35(2)
C(14A)	7940(8)	3654(5)	3821(4)	38(2)
C(15A)	8499(8)	3944(6)	4162(4)	44(2)
C(16A)	8160(8)	4667(6)	4152(4)	45(2)
C(17A)	7135(8)	5119(6)	3829(4)	45(2)
C(18A)	6507(8)	4872(5)	3479(4)	38(2)
C(19A)	8302(9)	2850(5)	3853(4)	46(2)
C(20A)	8877(10)	4973(6)	4510(5)	59(3)
C(21A)	5292(8)	5353(5)	3180(4)	43(2)
C(22A)	11828(7)	3008(5)	2024(4)	36(2)
C(23A)	10805(7)	2743(5)	2436(4)	33(2)
C(24A)	11166(8)	2042(5)	2834(4)	47(2)
C(25A)	12477(9)	1653(6)	2789(5)	56(3)
C(26A)	13479(9)	1933(6)	2348(5)	56(3)
C(27A)	13155(8)	2604(5)	1972(4)	44(2)
C(28A)	8614(8)	4037(5)	733(4)	40(2)
C(29A)	9201(7)	3356(5)	595(4)	42(2)
C(30A)	9159(9)	3312(6)	13(4)	49(3)
C(31A)	8618(9)	3911(6)	-411(4)	50(3)
C(32A)	8124(8)	4574(6)	-286(4)	46(2)
C(33A)	8112(8)	4667(5)	270(4)	40(2)

C(34A)	9856(8)	2708(5)	1047(4)	46(2)
C(35A)	7590(11)	5404(5)	393(5)	58(3)
C(36A)	9930(7)	5184(5)	2167(4)	34(2)
C(37A)	10744(8)	5634(5)	2217(4)	44(2)
C(38A)	11551(9)	5372(6)	2667(4)	50(2)
C(39A)	11564(8)	4683(6)	3066(4)	47(2)
C(40A)	10719(8)	4262(5)	2992(4)	41(2)
C(41A)	8990(8)	5301(5)	1744(4)	37(2)
C(42A)	7643(8)	5248(5)	1964(4)	37(2)
S(1A)	8174(2)	7710(1)	952(1)	45(1)
O(2A)	8877(6)	8150(4)	445(3)	54(2)
O(3A)	7217(6)	8110(4)	1332(3)	58(2)
O(4A)	8992(6)	7020(3)	1263(3)	51(2)
C(43A)	7031(10)	7407(5)	608(4)	49(2)
F(1A)	6386(5)	6908(3)	1016(2)	59(2)
F(2A)	6088(5)	7957(3)	366(3)	62(2)
F(3A)	7694(5)	7078(4)	193(3)	70(2)
Mo(1B)	3749(1)	8470(1)	2607(1)	34(1)
Cl(1B)	5975(2)	9021(1)	2141(1)	40(1)
O(1B)	3705(5)	9148(3)	3111(3)	41(1)
C(1B)	1782(8)	8377(5)	3112(4)	40(2)
N(1B)	518(6)	8771(4)	2943(3)	38(2)
N(2B)	1448(6)	8017(4)	3693(3)	37(2)
C(2B)	-512(8)	8646(5)	3404(4)	48(2)
N(3B)	3190(6)	8981(4)	1924(3)	37(2)
C(3B)	39(7)	8168(5)	3881(4)	47(2)
N(4B)	5422(6)	7686(4)	3164(3)	38(2)
C(4B)	238(7)	9247(5)	2365(4)	35(2)
C(5B)	-72(7)	8957(5)	1945(4)	38(2)
C(6B)	-393(8)	9428(5)	1405(4)	46(2)
C(7B)	-365(8)	10163(6)	1268(4)	49(3)
C(8B)	-41(8)	10438(5)	1696(5)	47(2)
C(9B)	242(7)	9981(5)	2257(4)	36(2)
C(10B)	-205(9)	8163(5)	2107(5)	51(3)
C(11B)	-642(10)	10679(6)	658(4)	61(3)
C(12B)	522(9)	10294(5)	2724(4)	50(2)
C(13B)	2379(8)	7480(5)	4071(4)	42(2)
C(14B)	2537(8)	6737(5)	4094(4)	39(2)
C(15B)	3530(8)	6239(5)	4423(4)	38(2)
C(16B)	4273(8)	6445(5)	4752(4)	37(2)
C(17B)	3978(9)	7167(6)	4761(4)	46(2)
C(18B)	3025(8)	7702(5)	4427(4)	38(2)
C(19B)	1641(9)	6479(5)	3803(4)	48(2)
C(20B)	5323(8)	5902(5)	5104(4)	49(2)
C(21B)	2680(9)	8481(5)	4479(4)	49(2)
C(22B)	4676(8)	9510(5)	3086(4)	38(2)
C(23B)	5778(8)	9532(5)	2656(4)	41(2)

C(24B)	6754(8)	9940(5)	2608(5)	46(2)
C(25B)	6628(8)	10323(5)	3023(4)	48(2)
C(26B)	5569(9)	10294(5)	3470(4)	50(2)
C(27B)	4576(9)	9906(5)	3506(4)	46(2)
C(28B)	3190(7)	9384(5)	1332(4)	40(2)
C(29B)	3086(8)	9046(6)	901(4)	49(3)
C(30B)	3108(9)	9461(7)	315(5)	60(3)
C(31B)	3166(11)	10186(8)	157(5)	75(4)
C(32B)	3260(9)	10524(6)	584(5)	61(3)
C(33B)	3243(8)	10127(6)	1172(4)	51(3)
C(34B)	2935(9)	8255(6)	1059(5)	58(3)
C(35B)	3380(9)	10515(6)	1618(5)	53(3)
C(36B)	5949(8)	7332(5)	2736(4)	39(2)
C(37B)	7269(8)	6930(5)	2712(5)	47(2)
C(38B)	7991(9)	6867(6)	3160(4)	52(3)
C(39B)	7469(9)	7196(5)	3607(5)	49(3)
C(40B)	6164(8)	7621(5)	3592(4)	43(2)
C(41B)	4939(8)	7498(5)	2324(4)	41(2)
C(42B)	3631(8)	7359(5)	2583(5)	45(2)
S(1B)	2324(2)	2651(2)	4574(1)	64(1)
O(2B)	2758(12)	2657(8)	5117(5)	92(3)
O(3B)	1052(9)	2414(7)	4680(6)	77(3)
O(4B)	2556(14)	3235(7)	4073(6)	106(3)
O(2C)	3310(20)	3050(14)	4581(13)	99(3)
O(3C)	1028(15)	2751(16)	4914(11)	87(3)
O(4C)	2340(30)	2830(19)	3930(5)	103(4)
C(43B)	3467(12)	1797(6)	4513(6)	146(7)
F(1B)	4686(14)	1963(10)	4303(8)	161(4)
F(2B)	3212(16)	1390(10)	4215(8)	163(4)
F(3B)	3462(18)	1387(9)	5088(6)	171(4)
F(1C)	4782(15)	1597(18)	4545(14)	166(4)
F(2C)	2920(30)	1217(13)	4766(16)	167(4)
F(3C)	3370(30)	1960(20)	3924(8)	162(4)

Table 17. Bond lengths [Å] and angles [°] for the **MOC**.

Mo(1A)-N(3A)	1.718(6)
Mo(1A)-O(1A)	2.006(5)
Mo(1A)-C(1A)	2.167(8)
Mo(1A)-C(42A)	2.206(9)
Mo(1A)-C(41A)	2.228(9)
Mo(1A)-N(4A)	2.292(7)
Mo(1A)-Cl(1A)	2.6577(19)
Cl(1A)-C(22A)	1.757(9)
O(1A)-C(23A)	1.353(9)
N(1A)-C(2A)	1.378(10)
N(1A)-C(1A)	1.380(10)

N(1A)-C(4A)	1.422(10)
C(1A)-N(2A)	1.379(10)
N(2A)-C(3A)	1.376(10)
N(2A)-C(13A)	1.446(10)
C(2A)-C(3A)	1.328(12)
C(2A)-H(2A)	0.9500
N(3A)-C(28A)	1.382(11)
C(3A)-H(3A)	0.9500
N(4A)-C(40A)	1.337(10)
N(4A)-C(36A)	1.376(11)
C(4A)-C(5A)	1.411(12)
C(4A)-C(9A)	1.420(12)
C(5A)-C(6A)	1.385(12)
C(5A)-C(10A)	1.498(13)
C(6A)-C(7A)	1.376(14)
C(6A)-H(6A)	0.9500
C(7A)-C(8A)	1.382(14)
C(7A)-C(11A)	1.539(13)
C(8A)-C(9A)	1.384(12)
C(8A)-H(8A)	0.9500
C(9A)-C(12A)	1.520(12)
C(10A)-H(10A)	0.9800
C(10A)-H(10B)	0.9800
C(10A)-H(10C)	0.9800
C(11A)-H(11A)	0.9800
C(11A)-H(11B)	0.9800
C(11A)-H(11C)	0.9800
C(12A)-H(12A)	0.9800
C(12A)-H(12B)	0.9800
C(12A)-H(12C)	0.9800
C(13A)-C(18A)	1.394(12)
C(13A)-C(14A)	1.413(12)
C(14A)-C(15A)	1.383(12)
C(14A)-C(19A)	1.503(12)
C(15A)-C(16A)	1.361(13)
C(15A)-H(15A)	0.9500
C(16A)-C(17A)	1.380(13)
C(16A)-C(20A)	1.542(12)
C(17A)-C(18A)	1.390(12)
C(17A)-H(17A)	0.9500
C(18A)-C(21A)	1.513(11)
C(19A)-H(19A)	0.9800
C(19A)-H(19B)	0.9800
C(19A)-H(19C)	0.9800
C(20A)-H(20A)	0.9800
C(20A)-H(20B)	0.9800
C(20A)-H(20C)	0.9800

C(21A)-H(21A)	0.9800
C(21A)-H(21B)	0.9800
C(21A)-H(21C)	0.9800
C(22A)-C(23A)	1.378(11)
C(22A)-C(27A)	1.400(11)
C(23A)-C(24A)	1.414(12)
C(24A)-C(25A)	1.376(12)
C(24A)-H(24A)	0.9500
C(25A)-C(26A)	1.406(14)
C(25A)-H(25A)	0.9500
C(26A)-C(27A)	1.347(13)
C(26A)-H(26A)	0.9500
C(27A)-H(27A)	0.9500
C(28A)-C(29A)	1.426(12)
C(28A)-C(33A)	1.437(12)
C(29A)-C(30A)	1.417(12)
C(29A)-C(34A)	1.493(13)
C(30A)-C(31A)	1.366(13)
C(30A)-H(30A)	0.9500
C(31A)-C(32A)	1.370(13)
C(31A)-H(31A)	0.9500
C(32A)-C(33A)	1.383(12)
C(32A)-H(32A)	0.9500
C(33A)-C(35A)	1.502(13)
C(34A)-H(34A)	0.9800
C(34A)-H(34B)	0.9800
C(34A)-H(34C)	0.9800
C(35A)-H(35A)	0.9800
C(35A)-H(35B)	0.9800
C(35A)-H(35C)	0.9800
C(36A)-C(37A)	1.394(11)
C(36A)-C(41A)	1.449(11)
C(37A)-C(38A)	1.370(13)
C(37A)-H(37A)	0.9500
C(38A)-C(39A)	1.390(13)
C(38A)-H(38A)	0.9500
C(39A)-C(40A)	1.395(12)
C(39A)-H(39A)	0.9500
C(40A)-H(40A)	0.9500
C(41A)-C(42A)	1.400(11)
C(41A)-H(41A)	0.95(2)
C(42A)-H(42A)	0.94(2)
C(42A)-H(42B)	0.94(2)
S(1A)-O(2A)	1.434(6)
S(1A)-O(3A)	1.452(6)
S(1A)-O(4A)	1.463(6)
S(1A)-C(43A)	1.837(10)

C(43A)-F(2A)	1.320(11)
C(43A)-F(3A)	1.328(11)
C(43A)-F(1A)	1.352(10)
Mo(1B)-N(3B)	1.742(7)
Mo(1B)-O(1B)	2.022(6)
Mo(1B)-C(1B)	2.164(8)
Mo(1B)-C(41B)	2.207(9)
Mo(1B)-C(42B)	2.220(10)
Mo(1B)-N(4B)	2.317(7)
Mo(1B)-Cl(1B)	2.670(2)
Cl(1B)-C(23B)	1.753(9)
O(1B)-C(22B)	1.337(9)
C(1B)-N(2B)	1.366(11)
C(1B)-N(1B)	1.397(10)
N(1B)-C(2B)	1.380(11)
N(1B)-C(4B)	1.438(11)
N(2B)-C(3B)	1.416(10)
N(2B)-C(13B)	1.440(11)
C(2B)-C(3B)	1.345(13)
C(2B)-H(2B)	0.9500
N(3B)-C(28B)	1.387(11)
C(3B)-H(3B)	0.9500
N(4B)-C(40B)	1.336(11)
N(4B)-C(36B)	1.356(11)
C(4B)-C(9B)	1.376(12)
C(4B)-C(5B)	1.403(12)
C(5B)-C(6B)	1.374(13)
C(5B)-C(10B)	1.514(12)
C(6B)-C(7B)	1.380(13)
C(6B)-H(6B)	0.9500
C(7B)-C(8B)	1.402(13)
C(7B)-C(11B)	1.523(13)
C(8B)-C(9B)	1.396(13)
C(8B)-H(8B)	0.9500
C(9B)-C(12B)	1.517(13)
C(10B)-H(10D)	0.9800
C(10B)-H(10E)	0.9800
C(10B)-H(10F)	0.9800
C(11B)-H(11D)	0.9800
C(11B)-H(11E)	0.9800
C(11B)-H(11F)	0.9800
C(12B)-H(12D)	0.9800
C(12B)-H(12E)	0.9800
C(12B)-H(12F)	0.9800
C(13B)-C(18B)	1.384(12)
C(13B)-C(14B)	1.404(12)
C(14B)-C(15B)	1.394(12)

C(14B)-C(19B)	1.500(12)
C(15B)-C(16B)	1.382(12)
C(15B)-H(15B)	0.9500
C(16B)-C(17B)	1.373(12)
C(16B)-C(20B)	1.490(12)
C(17B)-C(18B)	1.400(12)
C(17B)-H(17B)	0.9500
C(18B)-C(21B)	1.512(12)
C(19B)-H(19D)	0.9800
C(19B)-H(19E)	0.9800
C(19B)-H(19F)	0.9800
C(20B)-H(20D)	0.9800
C(20B)-H(20E)	0.9800
C(20B)-H(20F)	0.9800
C(21B)-H(21D)	0.9800
C(21B)-H(21E)	0.9800
C(21B)-H(21F)	0.9800
C(22B)-C(23B)	1.373(11)
C(22B)-C(27B)	1.412(12)
C(23B)-C(24B)	1.393(12)
C(24B)-C(25B)	1.375(13)
C(24B)-H(24B)	0.9500
C(25B)-C(26B)	1.367(13)
C(25B)-H(25B)	0.9500
C(26B)-C(27B)	1.387(12)
C(26B)-H(26B)	0.9500
C(27B)-H(27B)	0.9500
C(28B)-C(33B)	1.394(13)
C(28B)-C(29B)	1.406(13)
C(29B)-C(30B)	1.380(14)
C(29B)-C(34B)	1.514(14)
C(30B)-C(31B)	1.364(16)
C(30B)-H(30B)	0.9500
C(31B)-C(32B)	1.391(16)
C(31B)-H(31B)	0.9500
C(32B)-C(33B)	1.376(14)
C(32B)-H(32B)	0.9500
C(33B)-C(35B)	1.518(14)
C(34B)-H(34D)	0.9800
C(34B)-H(34E)	0.9800
C(34B)-H(34F)	0.9800
C(35B)-H(35D)	0.9800
C(35B)-H(35E)	0.9800
C(35B)-H(35F)	0.9800
C(36B)-C(37B)	1.389(12)
C(36B)-C(41B)	1.468(12)
C(37B)-C(38B)	1.365(13)

C(37B)-H(37B)	0.9500
C(38B)-C(39B)	1.361(14)
C(38B)-H(38B)	0.9500
C(39B)-C(40B)	1.391(12)
C(39B)-H(39B)	0.9500
C(40B)-H(40B)	0.9500
C(41B)-C(42B)	1.421(12)
C(41B)-H(41B)	0.96(2)
C(42B)-H(42C)	0.97(2)
C(42B)-H(42D)	0.95(2)
S(1B)-O(4B)	1.404(8)
S(1B)-O(3C)	1.423(10)
S(1B)-O(2C)	1.424(10)
S(1B)-O(3B)	1.443(8)
S(1B)-O(2B)	1.445(8)
S(1B)-O(4C)	1.458(10)
S(1B)-C(43B)	1.817(9)
O(4C)-F(3C)	1.77(5)
C(43B)-F(2B)	1.308(9)
C(43B)-F(2C)	1.314(10)
C(43B)-F(1C)	1.318(10)
C(43B)-F(1B)	1.336(9)
C(43B)-F(3C)	1.353(10)
C(43B)-F(3B)	1.355(9)

N(3A)-Mo(1A)-O(1A)	109.0(3)
N(3A)-Mo(1A)-C(1A)	97.7(3)
O(1A)-Mo(1A)-C(1A)	81.5(3)
N(3A)-Mo(1A)-C(42A)	98.6(3)
O(1A)-Mo(1A)-C(42A)	148.2(3)
C(1A)-Mo(1A)-C(42A)	79.4(3)
N(3A)-Mo(1A)-C(41A)	99.2(3)
O(1A)-Mo(1A)-C(41A)	144.9(3)
C(1A)-Mo(1A)-C(41A)	115.6(3)
C(42A)-Mo(1A)-C(41A)	36.8(3)
N(3A)-Mo(1A)-N(4A)	151.7(3)
O(1A)-Mo(1A)-N(4A)	85.4(2)
C(1A)-Mo(1A)-N(4A)	108.7(3)
C(42A)-Mo(1A)-N(4A)	77.1(3)
C(41A)-Mo(1A)-N(4A)	60.6(3)
N(3A)-Mo(1A)-Cl(1A)	84.0(2)
O(1A)-Mo(1A)-Cl(1A)	77.61(15)
C(1A)-Mo(1A)-Cl(1A)	158.4(2)
C(42A)-Mo(1A)-Cl(1A)	121.8(2)
C(41A)-Mo(1A)-Cl(1A)	85.2(2)
N(4A)-Mo(1A)-Cl(1A)	75.24(16)
C(22A)-Cl(1A)-Mo(1A)	95.6(3)

C(23A)-O(1A)-Mo(1A)	125.6(5)
C(2A)-N(1A)-C(1A)	111.0(7)
C(2A)-N(1A)-C(4A)	122.1(6)
C(1A)-N(1A)-C(4A)	126.7(6)
N(2A)-C(1A)-N(1A)	101.6(6)
N(2A)-C(1A)-Mo(1A)	129.8(5)
N(1A)-C(1A)-Mo(1A)	128.2(6)
C(3A)-N(2A)-C(1A)	113.1(7)
C(3A)-N(2A)-C(13A)	121.4(6)
C(1A)-N(2A)-C(13A)	125.5(6)
C(3A)-C(2A)-N(1A)	108.6(7)
C(3A)-C(2A)-H(2A)	125.7
N(1A)-C(2A)-H(2A)	125.7
C(28A)-N(3A)-Mo(1A)	166.0(5)
C(2A)-C(3A)-N(2A)	105.6(7)
C(2A)-C(3A)-H(3A)	127.2
N(2A)-C(3A)-H(3A)	127.2
C(40A)-N(4A)-C(36A)	119.1(7)
C(40A)-N(4A)-Mo(1A)	143.7(6)
C(36A)-N(4A)-Mo(1A)	94.4(5)
C(5A)-C(4A)-C(9A)	120.6(8)
C(5A)-C(4A)-N(1A)	120.0(8)
C(9A)-C(4A)-N(1A)	119.0(8)
C(6A)-C(5A)-C(4A)	117.9(9)
C(6A)-C(5A)-C(10A)	122.8(8)
C(4A)-C(5A)-C(10A)	119.3(8)
C(7A)-C(6A)-C(5A)	122.2(9)
C(7A)-C(6A)-H(6A)	118.9
C(5A)-C(6A)-H(6A)	118.9
C(6A)-C(7A)-C(8A)	119.5(9)
C(6A)-C(7A)-C(11A)	120.2(10)
C(8A)-C(7A)-C(11A)	120.3(10)
C(7A)-C(8A)-C(9A)	121.5(9)
C(7A)-C(8A)-H(8A)	119.3
C(9A)-C(8A)-H(8A)	119.3
C(8A)-C(9A)-C(4A)	118.2(8)
C(8A)-C(9A)-C(12A)	122.3(9)
C(4A)-C(9A)-C(12A)	119.4(8)
C(5A)-C(10A)-H(10A)	109.5
C(5A)-C(10A)-H(10B)	109.5
H(10A)-C(10A)-H(10B)	109.5
C(5A)-C(10A)-H(10C)	109.5
H(10A)-C(10A)-H(10C)	109.5
H(10B)-C(10A)-H(10C)	109.5
C(7A)-C(11A)-H(11A)	109.5
C(7A)-C(11A)-H(11B)	109.5
H(11A)-C(11A)-H(11B)	109.5

C(7A)-C(11A)-H(11C)	109.5
H(11A)-C(11A)-H(11C)	109.5
H(11B)-C(11A)-H(11C)	109.5
C(9A)-C(12A)-H(12A)	109.5
C(9A)-C(12A)-H(12B)	109.5
H(12A)-C(12A)-H(12B)	109.5
C(9A)-C(12A)-H(12C)	109.5
H(12A)-C(12A)-H(12C)	109.5
H(12B)-C(12A)-H(12C)	109.5
C(18A)-C(13A)-C(14A)	122.2(8)
C(18A)-C(13A)-N(2A)	118.3(7)
C(14A)-C(13A)-N(2A)	119.5(8)
C(15A)-C(14A)-C(13A)	116.7(8)
C(15A)-C(14A)-C(19A)	121.6(8)
C(13A)-C(14A)-C(19A)	121.6(8)
C(16A)-C(15A)-C(14A)	122.6(9)
C(16A)-C(15A)-H(15A)	118.7
C(14A)-C(15A)-H(15A)	118.7
C(15A)-C(16A)-C(17A)	119.0(8)
C(15A)-C(16A)-C(20A)	120.7(9)
C(17A)-C(16A)-C(20A)	120.3(9)
C(16A)-C(17A)-C(18A)	122.0(9)
C(16A)-C(17A)-H(17A)	119.0
C(18A)-C(17A)-H(17A)	119.0
C(17A)-C(18A)-C(13A)	116.9(8)
C(17A)-C(18A)-C(21A)	121.1(8)
C(13A)-C(18A)-C(21A)	121.8(8)
C(14A)-C(19A)-H(19A)	109.5
C(14A)-C(19A)-H(19B)	109.5
H(19A)-C(19A)-H(19B)	109.5
C(14A)-C(19A)-H(19C)	109.5
H(19A)-C(19A)-H(19C)	109.5
H(19B)-C(19A)-H(19C)	109.5
C(16A)-C(20A)-H(20A)	109.5
C(16A)-C(20A)-H(20B)	109.5
H(20A)-C(20A)-H(20B)	109.5
C(16A)-C(20A)-H(20C)	109.5
H(20A)-C(20A)-H(20C)	109.5
H(20B)-C(20A)-H(20C)	109.5
C(18A)-C(21A)-H(21A)	109.5
C(18A)-C(21A)-H(21B)	109.5
H(21A)-C(21A)-H(21B)	109.5
C(18A)-C(21A)-H(21C)	109.5
H(21A)-C(21A)-H(21C)	109.5
H(21B)-C(21A)-H(21C)	109.5
C(23A)-C(22A)-C(27A)	123.1(8)
C(23A)-C(22A)-Cl(1A)	117.1(6)

C(27A)-C(22A)-Cl(1A)	119.8(7)
O(1A)-C(23A)-C(22A)	123.9(7)
O(1A)-C(23A)-C(24A)	119.4(7)
C(22A)-C(23A)-C(24A)	116.7(7)
C(25A)-C(24A)-C(23A)	120.1(9)
C(25A)-C(24A)-H(24A)	120.0
C(23A)-C(24A)-H(24A)	120.0
C(24A)-C(25A)-C(26A)	121.3(10)
C(24A)-C(25A)-H(25A)	119.3
C(26A)-C(25A)-H(25A)	119.3
C(27A)-C(26A)-C(25A)	119.2(8)
C(27A)-C(26A)-H(26A)	120.4
C(25A)-C(26A)-H(26A)	120.4
C(26A)-C(27A)-C(22A)	119.5(8)
C(26A)-C(27A)-H(27A)	120.2
C(22A)-C(27A)-H(27A)	120.2
N(3A)-C(28A)-C(29A)	120.3(8)
N(3A)-C(28A)-C(33A)	120.2(8)
C(29A)-C(28A)-C(33A)	119.5(8)
C(30A)-C(29A)-C(28A)	118.1(9)
C(30A)-C(29A)-C(34A)	120.7(9)
C(28A)-C(29A)-C(34A)	121.2(8)
C(31A)-C(30A)-C(29A)	121.2(9)
C(31A)-C(30A)-H(30A)	119.4
C(29A)-C(30A)-H(30A)	119.4
C(30A)-C(31A)-C(32A)	120.4(9)
C(30A)-C(31A)-H(31A)	119.8
C(32A)-C(31A)-H(31A)	119.8
C(31A)-C(32A)-C(33A)	122.4(9)
C(31A)-C(32A)-H(32A)	118.8
C(33A)-C(32A)-H(32A)	118.8
C(32A)-C(33A)-C(28A)	118.2(9)
C(32A)-C(33A)-C(35A)	121.3(9)
C(28A)-C(33A)-C(35A)	120.5(8)
C(29A)-C(34A)-H(34A)	109.5
C(29A)-C(34A)-H(34B)	109.5
H(34A)-C(34A)-H(34B)	109.5
C(29A)-C(34A)-H(34C)	109.5
H(34A)-C(34A)-H(34C)	109.5
H(34B)-C(34A)-H(34C)	109.5
C(33A)-C(35A)-H(35A)	109.5
C(33A)-C(35A)-H(35B)	109.5
H(35A)-C(35A)-H(35B)	109.5
C(33A)-C(35A)-H(35C)	109.5
H(35A)-C(35A)-H(35C)	109.5
H(35B)-C(35A)-H(35C)	109.5
N(4A)-C(36A)-C(37A)	121.5(8)

N(4A)-C(36A)-C(41A)	107.7(7)
C(37A)-C(36A)-C(41A)	130.9(8)
C(38A)-C(37A)-C(36A)	117.9(9)
C(38A)-C(37A)-H(37A)	121.1
C(36A)-C(37A)-H(37A)	121.1
C(37A)-C(38A)-C(39A)	121.8(8)
C(37A)-C(38A)-H(38A)	119.1
C(39A)-C(38A)-H(38A)	119.1
C(38A)-C(39A)-C(40A)	117.4(8)
C(38A)-C(39A)-H(39A)	121.3
C(40A)-C(39A)-H(39A)	121.3
N(4A)-C(40A)-C(39A)	122.4(9)
N(4A)-C(40A)-H(40A)	118.8
C(39A)-C(40A)-H(40A)	118.8
C(42A)-C(41A)-C(36A)	118.4(8)
C(42A)-C(41A)-Mo(1A)	70.7(5)
C(36A)-C(41A)-Mo(1A)	95.0(6)
C(42A)-C(41A)-H(41A)	108(6)
C(36A)-C(41A)-H(41A)	133(6)
Mo(1A)-C(41A)-H(41A)	108(6)
C(41A)-C(42A)-Mo(1A)	72.5(5)
C(41A)-C(42A)-H(42A)	119(5)
Mo(1A)-C(42A)-H(42A)	118(5)
C(41A)-C(42A)-H(42B)	123(6)
Mo(1A)-C(42A)-H(42B)	115(6)
H(42A)-C(42A)-H(42B)	107(7)
O(2A)-S(1A)-O(3A)	115.5(4)
O(2A)-S(1A)-O(4A)	115.6(4)
O(3A)-S(1A)-O(4A)	115.5(4)
O(2A)-S(1A)-C(43A)	102.5(4)
O(3A)-S(1A)-C(43A)	101.5(4)
O(4A)-S(1A)-C(43A)	103.1(4)
F(2A)-C(43A)-F(3A)	108.4(8)
F(2A)-C(43A)-F(1A)	107.1(7)
F(3A)-C(43A)-F(1A)	105.9(8)
F(2A)-C(43A)-S(1A)	112.0(7)
F(3A)-C(43A)-S(1A)	112.1(6)
F(1A)-C(43A)-S(1A)	111.1(7)
N(3B)-Mo(1B)-O(1B)	109.8(3)
N(3B)-Mo(1B)-C(1B)	97.6(3)
O(1B)-Mo(1B)-C(1B)	82.4(3)
N(3B)-Mo(1B)-C(41B)	97.6(3)
O(1B)-Mo(1B)-C(41B)	144.4(3)
C(1B)-Mo(1B)-C(41B)	116.9(3)
N(3B)-Mo(1B)-C(42B)	99.5(4)
O(1B)-Mo(1B)-C(42B)	147.4(3)
C(1B)-Mo(1B)-C(42B)	79.7(3)

C(41B)-Mo(1B)-C(42B)	37.5(3)
N(3B)-Mo(1B)-N(4B)	150.9(3)
O(1B)-Mo(1B)-N(4B)	85.1(2)
C(1B)-Mo(1B)-N(4B)	109.4(3)
C(41B)-Mo(1B)-N(4B)	60.8(3)
C(42B)-Mo(1B)-N(4B)	75.6(3)
N(3B)-Mo(1B)-Cl(1B)	83.5(2)
O(1B)-Mo(1B)-Cl(1B)	77.25(16)
C(1B)-Mo(1B)-Cl(1B)	158.6(3)
C(41B)-Mo(1B)-Cl(1B)	83.9(2)
C(42B)-Mo(1B)-Cl(1B)	121.3(2)
N(4B)-Mo(1B)-Cl(1B)	75.39(16)
C(23B)-Cl(1B)-Mo(1B)	94.8(3)
C(22B)-O(1B)-Mo(1B)	125.9(5)
N(2B)-C(1B)-N(1B)	101.9(7)
N(2B)-C(1B)-Mo(1B)	130.1(6)
N(1B)-C(1B)-Mo(1B)	127.3(6)
C(2B)-N(1B)-C(1B)	111.9(7)
C(2B)-N(1B)-C(4B)	121.1(7)
C(1B)-N(1B)-C(4B)	127.0(7)
C(1B)-N(2B)-C(3B)	112.9(7)
C(1B)-N(2B)-C(13B)	125.0(6)
C(3B)-N(2B)-C(13B)	121.8(7)
C(3B)-C(2B)-N(1B)	108.1(7)
C(3B)-C(2B)-H(2B)	126.0
N(1B)-C(2B)-H(2B)	126.0
C(28B)-N(3B)-Mo(1B)	161.4(5)
C(2B)-C(3B)-N(2B)	105.2(8)
C(2B)-C(3B)-H(3B)	127.4
N(2B)-C(3B)-H(3B)	127.4
C(40B)-N(4B)-C(36B)	119.5(7)
C(40B)-N(4B)-Mo(1B)	143.7(6)
C(36B)-N(4B)-Mo(1B)	92.8(5)
C(9B)-C(4B)-C(5B)	122.7(8)
C(9B)-C(4B)-N(1B)	118.0(8)
C(5B)-C(4B)-N(1B)	119.3(8)
C(6B)-C(5B)-C(4B)	118.3(8)
C(6B)-C(5B)-C(10B)	120.7(8)
C(4B)-C(5B)-C(10B)	120.6(8)
C(5B)-C(6B)-C(7B)	121.2(9)
C(5B)-C(6B)-H(6B)	119.4
C(7B)-C(6B)-H(6B)	119.4
C(6B)-C(7B)-C(8B)	119.2(9)
C(6B)-C(7B)-C(11B)	121.4(9)
C(8B)-C(7B)-C(11B)	119.4(9)
C(9B)-C(8B)-C(7B)	121.2(9)
C(9B)-C(8B)-H(8B)	119.4

C(7B)-C(8B)-H(8B)	119.4
C(4B)-C(9B)-C(8B)	117.4(8)
C(4B)-C(9B)-C(12B)	122.2(8)
C(8B)-C(9B)-C(12B)	120.4(8)
C(5B)-C(10B)-H(10D)	109.5
C(5B)-C(10B)-H(10E)	109.5
H(10D)-C(10B)-H(10E)	109.5
C(5B)-C(10B)-H(10F)	109.5
H(10D)-C(10B)-H(10F)	109.5
H(10E)-C(10B)-H(10F)	109.5
C(7B)-C(11B)-H(11D)	109.5
C(7B)-C(11B)-H(11E)	109.5
H(11D)-C(11B)-H(11E)	109.5
C(7B)-C(11B)-H(11F)	109.5
H(11D)-C(11B)-H(11F)	109.5
H(11E)-C(11B)-H(11F)	109.5
C(9B)-C(12B)-H(12D)	109.5
C(9B)-C(12B)-H(12E)	109.5
H(12D)-C(12B)-H(12E)	109.5
C(9B)-C(12B)-H(12F)	109.5
H(12D)-C(12B)-H(12F)	109.5
H(12E)-C(12B)-H(12F)	109.5
C(18B)-C(13B)-C(14B)	121.8(8)
C(18B)-C(13B)-N(2B)	119.3(8)
C(14B)-C(13B)-N(2B)	118.7(8)
C(15B)-C(14B)-C(13B)	117.1(8)
C(15B)-C(14B)-C(19B)	120.9(8)
C(13B)-C(14B)-C(19B)	121.9(8)
C(16B)-C(15B)-C(14B)	122.7(8)
C(16B)-C(15B)-H(15B)	118.7
C(14B)-C(15B)-H(15B)	118.7
C(17B)-C(16B)-C(15B)	117.5(8)
C(17B)-C(16B)-C(20B)	120.7(8)
C(15B)-C(16B)-C(20B)	121.7(8)
C(16B)-C(17B)-C(18B)	123.0(8)
C(16B)-C(17B)-H(17B)	118.5
C(18B)-C(17B)-H(17B)	118.5
C(13B)-C(18B)-C(17B)	117.2(8)
C(13B)-C(18B)-C(21B)	121.8(8)
C(17B)-C(18B)-C(21B)	120.9(8)
C(14B)-C(19B)-H(19D)	109.5
C(14B)-C(19B)-H(19E)	109.5
H(19D)-C(19B)-H(19E)	109.5
C(14B)-C(19B)-H(19F)	109.5
H(19D)-C(19B)-H(19F)	109.5
H(19E)-C(19B)-H(19F)	109.5
C(16B)-C(20B)-H(20D)	109.5

C(16B)-C(20B)-H(20E)	109.5
H(20D)-C(20B)-H(20E)	109.5
C(16B)-C(20B)-H(20F)	109.5
H(20D)-C(20B)-H(20F)	109.5
H(20E)-C(20B)-H(20F)	109.5
C(18B)-C(21B)-H(21D)	109.5
C(18B)-C(21B)-H(21E)	109.5
H(21D)-C(21B)-H(21E)	109.5
C(18B)-C(21B)-H(21F)	109.5
H(21D)-C(21B)-H(21F)	109.5
H(21E)-C(21B)-H(21F)	109.5
O(1B)-C(22B)-C(23B)	123.1(8)
O(1B)-C(22B)-C(27B)	119.9(7)
C(23B)-C(22B)-C(27B)	117.1(8)
C(22B)-C(23B)-C(24B)	123.3(9)
C(22B)-C(23B)-Cl(1B)	118.6(7)
C(24B)-C(23B)-Cl(1B)	118.1(7)
C(25B)-C(24B)-C(23B)	118.3(8)
C(25B)-C(24B)-H(24B)	120.8
C(23B)-C(24B)-H(24B)	120.8
C(26B)-C(25B)-C(24B)	120.1(9)
C(26B)-C(25B)-H(25B)	119.9
C(24B)-C(25B)-H(25B)	119.9
C(25B)-C(26B)-C(27B)	121.5(9)
C(25B)-C(26B)-H(26B)	119.3
C(27B)-C(26B)-H(26B)	119.3
C(26B)-C(27B)-C(22B)	119.6(9)
C(26B)-C(27B)-H(27B)	120.2
C(22B)-C(27B)-H(27B)	120.2
N(3B)-C(28B)-C(33B)	119.9(8)
N(3B)-C(28B)-C(29B)	119.5(9)
C(33B)-C(28B)-C(29B)	120.6(9)
C(30B)-C(29B)-C(28B)	118.0(10)
C(30B)-C(29B)-C(34B)	119.6(10)
C(28B)-C(29B)-C(34B)	122.4(9)
C(31B)-C(30B)-C(29B)	121.5(11)
C(31B)-C(30B)-H(30B)	119.3
C(29B)-C(30B)-H(30B)	119.3
C(30B)-C(31B)-C(32B)	120.6(11)
C(30B)-C(31B)-H(31B)	119.7
C(32B)-C(31B)-H(31B)	119.7
C(33B)-C(32B)-C(31B)	119.5(11)
C(33B)-C(32B)-H(32B)	120.3
C(31B)-C(32B)-H(32B)	120.3
C(32B)-C(33B)-C(28B)	119.8(10)
C(32B)-C(33B)-C(35B)	117.4(10)
C(28B)-C(33B)-C(35B)	122.7(8)

C(29B)-C(34B)-H(34D)	109.5
C(29B)-C(34B)-H(34E)	109.5
H(34D)-C(34B)-H(34E)	109.5
C(29B)-C(34B)-H(34F)	109.5
H(34D)-C(34B)-H(34F)	109.5
H(34E)-C(34B)-H(34F)	109.5
C(33B)-C(35B)-H(35D)	109.5
C(33B)-C(35B)-H(35E)	109.5
H(35D)-C(35B)-H(35E)	109.5
C(33B)-C(35B)-H(35F)	109.5
H(35D)-C(35B)-H(35F)	109.5
H(35E)-C(35B)-H(35F)	109.5
N(4B)-C(36B)-C(37B)	121.7(8)
N(4B)-C(36B)-C(41B)	108.4(7)
C(37B)-C(36B)-C(41B)	129.8(9)
C(38B)-C(37B)-C(36B)	117.2(9)
C(38B)-C(37B)-H(37B)	121.4
C(36B)-C(37B)-H(37B)	121.4
C(39B)-C(38B)-C(37B)	122.2(9)
C(39B)-C(38B)-H(38B)	118.9
C(37B)-C(38B)-H(38B)	118.9
C(38B)-C(39B)-C(40B)	118.0(8)
C(38B)-C(39B)-H(39B)	121.0
C(40B)-C(39B)-H(39B)	121.0
N(4B)-C(40B)-C(39B)	121.3(9)
N(4B)-C(40B)-H(40B)	119.3
C(39B)-C(40B)-H(40B)	119.3
C(42B)-C(41B)-C(36B)	116.5(8)
C(42B)-C(41B)-Mo(1B)	71.8(5)
C(36B)-C(41B)-Mo(1B)	94.3(6)
C(42B)-C(41B)-H(41B)	113(5)
C(36B)-C(41B)-H(41B)	126(4)
Mo(1B)-C(41B)-H(41B)	121(4)
C(41B)-C(42B)-Mo(1B)	70.8(5)
C(41B)-C(42B)-H(42C)	130(5)
Mo(1B)-C(42B)-H(42C)	118(5)
C(41B)-C(42B)-H(42D)	114(5)
Mo(1B)-C(42B)-H(42D)	101(5)
H(42C)-C(42B)-H(42D)	112(7)
O(3C)-S(1B)-O(2C)	121.0(18)
O(4B)-S(1B)-O(3B)	118.8(8)
O(4B)-S(1B)-O(2B)	116.0(9)
O(3B)-S(1B)-O(2B)	112.2(7)
O(3C)-S(1B)-O(4C)	116.5(16)
O(2C)-S(1B)-O(4C)	98.2(17)
O(4B)-S(1B)-C(43B)	111.5(8)
O(3C)-S(1B)-C(43B)	128.4(13)

O(2C)-S(1B)-C(43B)	98.3(13)
O(3B)-S(1B)-C(43B)	99.0(7)
O(2B)-S(1B)-C(43B)	95.3(7)
O(4C)-S(1B)-C(43B)	86.2(14)
S(1B)-O(4C)-F(3C)	90.3(14)
F(2C)-C(43B)-F(1C)	108.2(12)
F(2B)-C(43B)-F(1B)	109.6(10)
F(2C)-C(43B)-F(3C)	105.9(14)
F(1C)-C(43B)-F(3C)	104.1(14)
F(2B)-C(43B)-F(3B)	106.3(10)
F(1B)-C(43B)-F(3B)	110.0(11)
F(2B)-C(43B)-S(1B)	121.5(12)
F(2C)-C(43B)-S(1B)	113.2(16)
F(1C)-C(43B)-S(1B)	129.3(19)
F(1B)-C(43B)-S(1B)	106.1(10)
F(3C)-C(43B)-S(1B)	91.6(16)
F(3B)-C(43B)-S(1B)	102.9(10)
C(43B)-F(3C)-O(4C)	91.5(17)

Table 18. Anisotropic displacement parameters (A^2 x 10^3) for the **MOC**. The anisotropic displacement factor exponent takes the form: $-2\pi^2 [h^2 a^{*2} U_{11} + ... + 2 h k a^* b^* U_{12}]$.

	U_{11}	U_{22}	U_{33}	U_{23}	U_{13}	U_{12}
Mo(1A)	20(1)	44(1)	33(1)	-8(1)	-2(1)	-13(1)
Cl(1A)	25(1)	55(1)	44(1)	-10(1)	3(1)	-16(1)
O(1A)	22(3)	46(4)	36(3)	-8(3)	-4(2)	-9(2)
N(1A)	16(3)	54(5)	28(4)	-11(3)	4(3)	-14(3)
C(1A)	21(4)	47(6)	42(5)	-20(4)	-9(4)	-6(4)
N(2A)	26(3)	43(4)	31(4)	-8(3)	3(3)	-12(3)
C(2A)	28(4)	56(6)	44(6)	-18(5)	7(4)	-19(4)
N(3A)	24(3)	48(4)	22(4)	-13(3)	7(3)	-19(3)
C(3A)	29(4)	58(6)	35(5)	-14(5)	5(4)	-23(4)
N(4A)	23(3)	50(5)	35(4)	-7(4)	4(3)	-13(3)
C(4A)	20(4)	59(6)	40(5)	-18(5)	6(4)	-24(4)
C(5A)	22(4)	46(6)	48(6)	-16(5)	4(4)	-15(4)
C(6A)	21(4)	77(7)	70(7)	-47(6)	15(5)	-22(5)
C(7A)	30(5)	90(9)	56(7)	-35(6)	-3(5)	-23(5)
C(8A)	36(5)	86(8)	36(6)	-16(5)	-1(4)	-25(5)
C(9A)	22(4)	57(6)	39(5)	-15(5)	1(4)	-24(4)
C(10A)	36(5)	47(6)	77(7)	-24(5)	-6(5)	-11(4)
C(11A)	51(6)	129(11)	72(8)	-60(8)	6(6)	-32(7)
C(12A)	25(4)	66(7)	68(7)	-17(6)	-12(4)	-19(4)
C(13A)	19(4)	56(6)	31(5)	-10(4)	-2(3)	-12(4)
C(14A)	30(4)	56(6)	33(5)	-17(4)	4(4)	-19(4)
C(15A)	36(5)	75(8)	26(5)	-7(5)	0(4)	-29(5)
C(16A)	33(5)	72(7)	39(5)	-14(5)	-2(4)	-30(5)
C(17A)	38(5)	74(7)	33(5)	-22(5)	4(4)	-29(5)
C(18A)	34(4)	41(6)	31(5)	-4(4)	6(4)	-10(4)

C(19A)	38(5)	53(6)	40(5)	-4(5)	-2(4)	-11(4)
C(20A)	51(6)	86(8)	57(7)	-33(6)	-11(5)	-24(5)
C(21A)	32(4)	66(7)	35(5)	-15(5)	-2(4)	-18(4)
C(22A)	23(4)	45(5)	43(5)	-14(4)	-3(4)	-11(4)
C(23A)	26(4)	40(5)	33(5)	0(4)	-10(4)	-17(4)
C(24A)	34(5)	55(7)	55(6)	-15(5)	-2(4)	-16(4)
C(25A)	37(5)	52(6)	85(8)	-29(6)	-18(5)	0(5)
C(26A)	32(5)	51(7)	90(8)	-32(6)	2(5)	-9(5)
C(27A)	20(4)	59(7)	58(6)	-20(5)	-3(4)	-18(4)
C(28A)	25(4)	54(6)	47(6)	-14(5)	3(4)	-24(4)
C(29A)	20(4)	67(7)	47(6)	-23(5)	7(4)	-22(4)
C(30A)	39(5)	72(7)	48(6)	-26(6)	12(5)	-35(5)
C(31A)	41(5)	80(8)	40(6)	-18(6)	-2(4)	-32(5)
C(32A)	37(5)	76(8)	28(5)	-6(5)	0(4)	-29(5)
C(33A)	28(4)	56(6)	35(5)	0(5)	-4(4)	-21(4)
C(34A)	31(5)	49(6)	53(6)	-9(5)	-5(4)	-3(4)
C(35A)	69(7)	56(7)	54(6)	-11(5)	-22(5)	-18(5)
C(36A)	26(4)	45(6)	41(5)	-17(5)	-3(4)	-22(4)
C(37A)	43(5)	49(6)	45(6)	-15(5)	-2(4)	-17(4)
C(38A)	42(5)	58(7)	57(6)	-20(6)	-4(5)	-22(5)
C(39A)	26(4)	76(8)	49(6)	-24(6)	-13(4)	-12(5)
C(40A)	31(4)	57(6)	38(5)	-14(5)	-6(4)	-13(4)
C(41A)	32(4)	45(6)	37(5)	-14(5)	1(4)	-15(4)
C(42A)	22(4)	48(6)	41(6)	-11(5)	3(4)	-12(4)
S(1A)	37(1)	54(2)	47(1)	-14(1)	-1(1)	-18(1)
O(2A)	46(4)	61(4)	50(4)	-7(3)	10(3)	-23(3)
O(3A)	60(4)	65(5)	61(4)	-39(4)	10(3)	-17(3)
O(4A)	43(3)	51(4)	60(4)	-10(3)	-14(3)	-9(3)
C(43A)	51(6)	49(6)	46(6)	-13(5)	8(5)	-15(5)
F(1A)	53(3)	64(4)	63(4)	-7(3)	-3(3)	-33(3)
F(2A)	47(3)	57(4)	75(4)	4(3)	-20(3)	-18(3)
F(3A)	50(3)	110(5)	67(4)	-44(4)	6(3)	-30(3)
Mo(1B)	20(1)	44(1)	41(1)	-9(1)	-2(1)	-13(1)
Cl(1B)	26(1)	48(1)	47(1)	-13(1)	2(1)	-16(1)
O(1B)	26(3)	53(4)	48(4)	-14(3)	-5(3)	-16(3)
C(1B)	22(4)	44(6)	45(6)	-1(5)	-5(4)	-2(4)
N(1B)	21(3)	50(5)	41(4)	-6(4)	1(3)	-16(3)
N(2B)	29(4)	45(5)	36(4)	-7(4)	-5(3)	-10(3)
C(2B)	26(4)	52(6)	59(6)	-12(5)	5(4)	-6(4)
N(3B)	19(3)	47(5)	41(4)	-3(4)	-7(3)	-7(3)
C(3B)	13(4)	68(7)	58(6)	-19(5)	4(4)	-8(4)
N(4B)	23(3)	37(4)	50(5)	-2(4)	-2(3)	-15(3)
C(4B)	17(4)	43(6)	44(5)	-11(4)	4(4)	-10(4)
C(5B)	17(4)	49(6)	52(6)	-14(5)	-7(4)	-9(4)
C(6B)	24(4)	55(7)	62(7)	-16(5)	-6(4)	-11(4)
C(7B)	24(4)	59(7)	59(6)	-5(5)	-14(4)	-4(4)
C(8B)	24(4)	50(6)	71(7)	-14(5)	-5(4)	-17(4)

C(9B)	18(4)	47(6)	47(6)	-15(5)	-3(4)	-11(4)
C(10B)	33(5)	50(6)	72(7)	-12(5)	-2(5)	-19(4)
C(11B)	56(6)	70(8)	54(7)	-4(6)	-21(5)	-10(5)
C(12B)	33(5)	59(7)	54(6)	-12(5)	-4(4)	-7(4)
C(13B)	22(4)	55(6)	47(6)	-9(5)	3(4)	-17(4)
C(14B)	34(5)	48(6)	42(5)	-16(4)	3(4)	-22(4)
C(15B)	40(5)	33(5)	38(5)	-7(4)	-5(4)	-8(4)
C(16B)	33(4)	46(6)	31(5)	-11(4)	2(4)	-8(4)
C(17B)	39(5)	75(8)	28(5)	-9(5)	-5(4)	-23(5)
C(18B)	35(5)	42(6)	31(5)	-5(4)	5(4)	-12(4)
C(19B)	40(5)	56(6)	50(6)	-13(5)	-6(4)	-18(4)
C(20B)	34(5)	59(6)	49(6)	-8(5)	-7(4)	-8(4)
C(21B)	56(6)	53(6)	44(6)	-24(5)	-1(5)	-14(5)
C(22B)	25(4)	43(6)	48(6)	-9(4)	-3(4)	-13(4)
C(23B)	27(4)	44(6)	50(6)	-10(5)	-3(4)	-11(4)
C(24B)	23(4)	38(6)	71(7)	-7(5)	-4(4)	-8(4)
C(25B)	32(5)	51(6)	70(7)	-26(5)	-7(5)	-12(4)
C(26B)	40(5)	57(7)	60(6)	-15(5)	-17(5)	-15(5)
C(27B)	39(5)	40(6)	59(6)	-17(5)	-11(4)	-4(4)
C(28B)	18(4)	62(7)	39(5)	-8(5)	-10(4)	-9(4)
C(29B)	28(5)	79(8)	38(6)	-14(5)	-13(4)	-4(5)
C(30B)	28(5)	89(9)	59(7)	-21(7)	-9(5)	-2(5)
C(31B)	62(7)	101(11)	46(7)	-6(7)	-2(5)	-11(7)
C(32B)	41(6)	63(7)	66(8)	5(6)	-4(5)	-15(5)
C(33B)	21(4)	71(8)	48(6)	4(5)	-2(4)	-14(4)
C(34B)	46(6)	78(8)	62(7)	-34(6)	-8(5)	-16(5)
C(35B)	41(5)	61(7)	62(7)	-14(5)	-13(5)	-16(5)
C(36B)	24(4)	36(5)	56(6)	-10(5)	4(4)	-16(4)
C(37B)	31(5)	43(6)	72(7)	-16(5)	-5(5)	-14(4)
C(38B)	30(5)	62(7)	56(7)	-1(5)	0(5)	-19(4)
C(39B)	34(5)	51(6)	63(7)	-1(5)	-22(5)	-17(4)
C(40B)	30(5)	59(6)	35(5)	6(4)	-3(4)	-22(4)
C(41B)	29(4)	50(6)	47(6)	-14(5)	-7(4)	-13(4)
C(42B)	24(4)	55(6)	61(7)	-15(5)	0(4)	-21(4)
S(1B)	39(1)	82(2)	65(2)	-10(2)	-4(1)	-17(1)
O(2B)	76(4)	111(5)	93(5)	-24(4)	-5(4)	-33(4)
O(3B)	52(4)	102(6)	83(6)	-20(5)	-9(4)	-31(4)
O(4B)	84(5)	111(5)	107(5)	-4(4)	1(4)	-29(4)
O(2C)	81(4)	110(5)	101(5)	-15(4)	-4(4)	-35(4)
O(3C)	65(4)	107(6)	89(5)	-18(4)	-5(4)	-29(4)
O(4C)	88(5)	106(6)	103(6)	-10(5)	-2(5)	-26(5)
C(43B)	147(9)	162(9)	140(9)	-40(6)	-40(6)	-35(6)
F(1B)	155(5)	157(6)	161(6)	-47(5)	-15(4)	-12(5)
F(2B)	166(5)	154(6)	167(6)	-50(5)	-17(5)	-21(5)
F(3B)	166(6)	161(6)	170(6)	-37(5)	-18(5)	-16(5)
F(1C)	160(6)	160(6)	166(6)	-43(5)	-16(5)	-13(5)
F(2C)	168(6)	157(6)	169(6)	-45(5)	-18(5)	-21(5)

F(3C)	161(5)	156(6)	164(6)	-49(5)	-16(4)	-19(4)

Table 19. Hydrogen coordinates (x 10^4) and isotropic displacement parameters (A^2 x 10^3) for the **MOC**.

	x	y	z	U(eq)
H(2A)	4222	3233	2792	49
H(3A)	4728	3540	3648	47
H(6A)	6906	2141	1123	61
H(8A)	4860	4192	481	61
H(10A)	6547	2048	2549	77
H(10B)	7899	2375	2333	77
H(10C)	7695	1742	2078	77
H(11A)	6713	2796	-34	114
H(11B)	5332	3391	-130	114
H(11C)	5288	2558	235	114
H(12A)	4401	5098	1041	76
H(12B)	5158	4912	1618	76
H(12C)	3726	4689	1681	76
H(15A)	9146	3626	4413	53
H(17A)	6850	5614	3848	53
H(19A)	9161	2631	4020	68
H(19B)	8394	2788	3452	68
H(19C)	7586	2607	4108	68
H(20A)	8748	4710	4933	89
H(20B)	8492	5497	4458	89
H(20C)	9848	4907	4366	89
H(21A)	5352	5286	2782	64
H(21B)	5275	5868	3145	64
H(21C)	4460	5215	3420	64
H(24A)	10502	1841	3132	57
H(25A)	12710	1185	3062	67
H(26A)	14375	1651	2316	67
H(27A)	13823	2803	1674	52
H(30A)	9515	2859	-83	59
H(31A)	8585	3867	-796	60
H(32A)	7776	4985	-592	56
H(34A)	9797	2256	962	69
H(34B)	9392	2718	1445	69
H(34C)	10811	2726	1028	69
H(35A)	8349	5595	442	86
H(35B)	6949	5353	759	86
H(35C)	7129	5744	58	86
H(37A)	10739	6108	1949	53
H(38A)	12117	5670	2707	60
H(39A)	12127	4504	3377	57
H(40A)	10715	3788	3259	49
H(41A)	9050(90)	5480(50)	1322(11)	60(30)

H(42A)	6980(60)	5450(40)	1700(30)	30(20)
H(42B)	7230(80)	5320(50)	2340(20)	60(30)
H(2B)	-1447	8860	3387	58
H(3B)	-420	7974	4261	56
H(6B)	-638	9243	1121	56
H(8B)	-14	10943	1602	57
H(10D)	-1078	8107	2349	77
H(10E)	532	7852	2335	77
H(10F)	-155	8015	1743	77
H(11D)	-508	10391	370	92
H(11E)	-18	11020	530	92
H(11F)	-1578	10955	682	92
H(12D)	-126	10182	3083	75
H(12E)	428	10827	2568	75
H(12F)	1446	10075	2824	75
H(15B)	3702	5739	4422	45
H(17B)	4443	7310	5004	56
H(19D)	753	6478	4043	72
H(19E)	2055	5981	3771	72
H(19F)	1530	6809	3403	72
H(20D)	6049	6143	5115	73
H(20E)	5701	5499	4918	73
H(20F)	4911	5706	5511	73
H(21D)	2649	8824	4080	73
H(21E)	3373	8560	4674	73
H(21F)	1795	8565	4717	73
H(24B)	7488	9953	2297	55
H(25B)	7277	10607	2998	58
H(26B)	5513	10546	3762	60
H(27B)	3831	9908	3812	55
H(30B)	3082	9236	15	72
H(31B)	3142	10464	-247	90
H(32B)	3335	11024	469	74
H(34D)	2127	8187	1348	86
H(34E)	3738	7932	1234	86
H(34F)	2843	8134	699	86
H(35D)	4301	10606	1555	80
H(35E)	3199	10206	2024	80
H(35F)	2728	10983	1563	80
H(37B)	7653	6709	2397	57
H(38B)	8889	6584	3161	62
H(39B)	7980	7137	3920	59
H(40B)	5793	7870	3891	52
H(41B)	5130(70)	7500(40)	1912(13)	30(20)
H(42C)	2890(60)	7320(50)	2400(40)	54
H(42D)	3580(80)	7110(40)	2996(13)	40(20)

Table 21. Torsion angles [°] for the **MOC**.

C(2A)-N(1A)-C(1A)-N(2A)	-1.6(9)
C(4A)-N(1A)-C(1A)-N(2A)	-176.7(8)
C(2A)-N(1A)-C(1A)-Mo(1A)	171.5(6)
C(4A)-N(1A)-C(1A)-Mo(1A)	-3.5(12)
N(1A)-C(1A)-N(2A)-C(3A)	1.8(9)
Mo(1A)-C(1A)-N(2A)-C(3A)	-171.2(6)
N(1A)-C(1A)-N(2A)-C(13A)	-177.7(7)
Mo(1A)-C(1A)-N(2A)-C(13A)	9.2(12)
C(1A)-N(1A)-C(2A)-C(3A)	1.0(10)
C(4A)-N(1A)-C(2A)-C(3A)	176.3(8)
O(1A)-Mo(1A)-N(3A)-C(28A)	-78(3)
C(1A)-Mo(1A)-N(3A)-C(28A)	-162(3)
C(42A)-Mo(1A)-N(3A)-C(28A)	118(3)
C(41A)-Mo(1A)-N(3A)-C(28A)	81(3)
N(4A)-Mo(1A)-N(3A)-C(28A)	39(3)
Cl(1A)-Mo(1A)-N(3A)-C(28A)	-3(3)
N(1A)-C(2A)-C(3A)-N(2A)	0.2(10)
C(1A)-N(2A)-C(3A)-C(2A)	-1.3(10)
C(13A)-N(2A)-C(3A)-C(2A)	178.3(8)
C(2A)-N(1A)-C(4A)-C(5A)	-81.5(9)
C(1A)-N(1A)-C(4A)-C(5A)	93.0(10)
C(2A)-N(1A)-C(4A)-C(9A)	91.3(10)
C(1A)-N(1A)-C(4A)-C(9A)	-94.2(9)
C(9A)-C(4A)-C(5A)-C(6A)	2.7(11)
N(1A)-C(4A)-C(5A)-C(6A)	175.4(7)
C(9A)-C(4A)-C(5A)-C(10A)	-177.4(7)
N(1A)-C(4A)-C(5A)-C(10A)	-4.7(11)
C(4A)-C(5A)-C(6A)-C(7A)	-1.9(12)
C(10A)-C(5A)-C(6A)-C(7A)	178.2(8)
C(5A)-C(6A)-C(7A)-C(8A)	1.7(13)
C(5A)-C(6A)-C(7A)-C(11A)	-179.8(8)
C(6A)-C(7A)-C(8A)-C(9A)	-2.2(13)
C(11A)-C(7A)-C(8A)-C(9A)	179.3(8)
C(7A)-C(8A)-C(9A)-C(4A)	2.9(12)
C(7A)-C(8A)-C(9A)-C(12A)	-174.8(8)
C(5A)-C(4A)-C(9A)-C(8A)	-3.2(11)
N(1A)-C(4A)-C(9A)-C(8A)	-175.9(7)
C(5A)-C(4A)-C(9A)-C(12A)	174.6(7)
N(1A)-C(4A)-C(9A)-C(12A)	1.9(10)
C(3A)-N(2A)-C(13A)-C(18A)	-86.9(10)
C(1A)-N(2A)-C(13A)-C(18A)	92.6(9)
C(3A)-N(2A)-C(13A)-C(14A)	89.8(9)
C(1A)-N(2A)-C(13A)-C(14A)	-90.7(10)
C(18A)-C(13A)-C(14A)-C(15A)	-6.0(11)
N(2A)-C(13A)-C(14A)-C(15A)	177.5(7)
C(18A)-C(13A)-C(14A)-C(19A)	171.8(7)

N(2A)-C(13A)-C(14A)-C(19A)	-4.7(11)
C(13A)-C(14A)-C(15A)-C(16A)	-0.4(12)
C(19A)-C(14A)-C(15A)-C(16A)	-178.2(8)
C(14A)-C(15A)-C(16A)-C(17A)	5.7(13)
C(14A)-C(15A)-C(16A)-C(20A)	-176.1(8)
C(15A)-C(16A)-C(17A)-C(18A)	-4.9(12)
C(20A)-C(16A)-C(17A)-C(18A)	176.9(8)
C(16A)-C(17A)-C(18A)-C(13A)	-1.1(12)
C(16A)-C(17A)-C(18A)-C(21A)	173.6(8)
C(14A)-C(13A)-C(18A)-C(17A)	6.7(11)
N(2A)-C(13A)-C(18A)-C(17A)	-176.7(7)
C(14A)-C(13A)-C(18A)-C(21A)	-168.0(7)
N(2A)-C(13A)-C(18A)-C(21A)	8.5(11)
Mo(1A)-Cl(1A)-C(22A)-C(23A)	1.4(7)
Mo(1A)-Cl(1A)-C(22A)-C(27A)	179.3(7)
Mo(1A)-O(1A)-C(23A)-C(22A)	-4.3(11)
Mo(1A)-O(1A)-C(23A)-C(24A)	176.1(6)
C(27A)-C(22A)-C(23A)-O(1A)	-176.7(8)
Cl(1A)-C(22A)-C(23A)-O(1A)	1.1(11)
C(27A)-C(22A)-C(23A)-C(24A)	2.9(12)
Cl(1A)-C(22A)-C(23A)-C(24A)	-179.3(6)
O(1A)-C(23A)-C(24A)-C(25A)	178.1(8)
C(22A)-C(23A)-C(24A)-C(25A)	-1.6(13)
C(23A)-C(24A)-C(25A)-C(26A)	-0.7(14)
C(24A)-C(25A)-C(26A)-C(27A)	1.7(15)
C(25A)-C(26A)-C(27A)-C(22A)	-0.5(14)
C(23A)-C(22A)-C(27A)-C(26A)	-1.9(13)
Cl(1A)-C(22A)-C(27A)-C(26A)	-179.7(7)
Mo(1A)-N(3A)-C(28A)-C(29A)	71(3)
Mo(1A)-N(3A)-C(28A)-C(33A)	-110(3)
N(3A)-C(28A)-C(29A)-C(30A)	173.8(7)
C(33A)-C(28A)-C(29A)-C(30A)	-5.3(11)
N(3A)-C(28A)-C(29A)-C(34A)	-7.0(11)
C(33A)-C(28A)-C(29A)-C(34A)	173.9(7)
C(28A)-C(29A)-C(30A)-C(31A)	2.3(12)
C(34A)-C(29A)-C(30A)-C(31A)	-176.9(8)
C(29A)-C(30A)-C(31A)-C(32A)	1.2(13)
C(30A)-C(31A)-C(32A)-C(33A)	-1.7(13)
C(31A)-C(32A)-C(33A)-C(28A)	-1.4(12)
C(31A)-C(32A)-C(33A)-C(35A)	178.8(8)
N(3A)-C(28A)-C(33A)-C(32A)	-174.2(7)
C(29A)-C(28A)-C(33A)-C(32A)	4.9(11)
N(3A)-C(28A)-C(33A)-C(35A)	5.7(11)
C(29A)-C(28A)-C(33A)-C(35A)	-175.2(7)
C(40A)-N(4A)-C(36A)-C(37A)	-1.3(12)
Mo(1A)-N(4A)-C(36A)-C(37A)	-166.6(7)
C(40A)-N(4A)-C(36A)-C(41A)	179.2(7)

Mo(1A)-N(4A)-C(36A)-C(41A)	13.9(6)
N(4A)-C(36A)-C(37A)-C(38A)	1.0(12)
C(41A)-C(36A)-C(37A)-C(38A)	-179.6(9)
C(36A)-C(37A)-C(38A)-C(39A)	-0.4(13)
C(37A)-C(38A)-C(39A)-C(40A)	0.0(14)
C(36A)-N(4A)-C(40A)-C(39A)	0.9(12)
Mo(1A)-N(4A)-C(40A)-C(39A)	155.6(7)
C(38A)-C(39A)-C(40A)-N(4A)	-0.3(13)
N(4A)-C(36A)-C(41A)-C(42A)	56.5(10)
C(37A)-C(36A)-C(41A)-C(42A)	-123.0(10)
N(4A)-C(36A)-C(41A)-Mo(1A)	-14.3(7)
C(37A)-C(36A)-C(41A)-Mo(1A)	166.2(8)
C(36A)-C(41A)-C(42A)-Mo(1A)	-85.2(8)
O(2A)-S(1A)-C(43A)-F(2A)	-67.5(7)
O(3A)-S(1A)-C(43A)-F(2A)	52.1(7)
O(4A)-S(1A)-C(43A)-F(2A)	172.0(6)
O(2A)-S(1A)-C(43A)-F(3A)	54.5(8)
O(3A)-S(1A)-C(43A)-F(3A)	174.2(7)
O(4A)-S(1A)-C(43A)-F(3A)	-65.9(7)
O(2A)-S(1A)-C(43A)-F(1A)	172.8(6)
O(3A)-S(1A)-C(43A)-F(1A)	-67.5(7)
O(4A)-S(1A)-C(43A)-F(1A)	52.3(7)
N(2B)-C(1B)-N(1B)-C(2B)	-0.2(10)
Mo(1B)-C(1B)-N(1B)-C(2B)	-171.7(7)
N(2B)-C(1B)-N(1B)-C(4B)	-179.1(8)
Mo(1B)-C(1B)-N(1B)-C(4B)	9.5(13)
N(1B)-C(1B)-N(2B)-C(3B)	0.8(10)
Mo(1B)-C(1B)-N(2B)-C(3B)	172.0(7)
N(1B)-C(1B)-N(2B)-C(13B)	174.6(8)
Mo(1B)-C(1B)-N(2B)-C(13B)	-14.2(13)
C(1B)-N(1B)-C(2B)-C(3B)	-0.5(11)
C(4B)-N(1B)-C(2B)-C(3B)	178.4(8)
O(1B)-Mo(1B)-N(3B)-C(28B)	91(2)
C(1B)-Mo(1B)-N(3B)-C(28B)	175(2)
C(41B)-Mo(1B)-N(3B)-C(28B)	-66(2)
C(42B)-Mo(1B)-N(3B)-C(28B)	-104(2)
N(4B)-Mo(1B)-N(3B)-C(28B)	-27(2)
Cl(1B)-Mo(1B)-N(3B)-C(28B)	17(2)
N(1B)-C(2B)-C(3B)-N(2B)	0.9(10)
C(1B)-N(2B)-C(3B)-C(2B)	-1.1(11)
C(13B)-N(2B)-C(3B)-C(2B)	-175.2(8)
C(2B)-N(1B)-C(4B)-C(9B)	90.0(9)
C(1B)-N(1B)-C(4B)-C(9B)	-91.3(10)
C(2B)-N(1B)-C(4B)-C(5B)	-87.8(10)
C(1B)-N(1B)-C(4B)-C(5B)	90.9(10)
C(9B)-C(4B)-C(5B)-C(6B)	-0.5(11)
N(1B)-C(4B)-C(5B)-C(6B)	177.3(7)

C(9B)-C(4B)-C(5B)-C(10B)	-173.6(7)
N(1B)-C(4B)-C(5B)-C(10B)	4.1(11)
C(4B)-C(5B)-C(6B)-C(7B)	2.4(12)
C(10B)-C(5B)-C(6B)-C(7B)	175.5(8)
C(5B)-C(6B)-C(7B)-C(8B)	-1.9(13)
C(5B)-C(6B)-C(7B)-C(11B)	176.5(8)
C(6B)-C(7B)-C(8B)-C(9B)	-0.5(12)
C(11B)-C(7B)-C(8B)-C(9B)	-178.9(8)
C(5B)-C(4B)-C(9B)-C(8B)	-1.8(11)
N(1B)-C(4B)-C(9B)-C(8B)	-179.6(7)
C(5B)-C(4B)-C(9B)-C(12B)	177.5(7)
N(1B)-C(4B)-C(9B)-C(12B)	-0.3(11)
C(7B)-C(8B)-C(9B)-C(4B)	2.3(12)
C(7B)-C(8B)-C(9B)-C(12B)	-177.0(7)
C(1B)-N(2B)-C(13B)-C(18B)	93.1(11)
C(3B)-N(2B)-C(13B)-C(18B)	-93.7(10)
C(1B)-N(2B)-C(13B)-C(14B)	-91.0(10)
C(3B)-N(2B)-C(13B)-C(14B)	82.2(10)
C(18B)-C(13B)-C(14B)-C(15B)	-9.5(12)
N(2B)-C(13B)-C(14B)-C(15B)	174.7(7)
C(18B)-C(13B)-C(14B)-C(19B)	167.7(8)
N(2B)-C(13B)-C(14B)-C(19B)	-8.1(12)
C(13B)-C(14B)-C(15B)-C(16B)	4.6(12)
C(19B)-C(14B)-C(15B)-C(16B)	-172.7(8)
C(14B)-C(15B)-C(16B)-C(17B)	1.8(12)
C(14B)-C(15B)-C(16B)-C(20B)	179.6(8)
C(15B)-C(16B)-C(17B)-C(18B)	-3.7(12)
C(20B)-C(16B)-C(17B)-C(18B)	178.4(8)
C(14B)-C(13B)-C(18B)-C(17B)	7.8(12)
N(2B)-C(13B)-C(18B)-C(17B)	-176.4(7)
C(14B)-C(13B)-C(18B)-C(21B)	-169.6(7)
N(2B)-C(13B)-C(18B)-C(21B)	6.1(12)
C(16B)-C(17B)-C(18B)-C(13B)	-0.9(12)
C(16B)-C(17B)-C(18B)-C(21B)	176.5(8)
Mo(1B)-O(1B)-C(22B)-C(23B)	7.9(11)
Mo(1B)-O(1B)-C(22B)-C(27B)	-173.5(6)
O(1B)-C(22B)-C(23B)-C(24B)	176.4(8)
C(27B)-C(22B)-C(23B)-C(24B)	-2.2(13)
O(1B)-C(22B)-C(23B)-Cl(1B)	-3.6(12)
C(27B)-C(22B)-C(23B)-Cl(1B)	177.8(6)
Mo(1B)-Cl(1B)-C(23B)-C(22B)	-0.8(7)
Mo(1B)-Cl(1B)-C(23B)-C(24B)	179.2(7)
C(22B)-C(23B)-C(24B)-C(25B)	2.0(13)
Cl(1B)-C(23B)-C(24B)-C(25B)	-178.0(7)
C(23B)-C(24B)-C(25B)-C(26B)	0.4(13)
C(24B)-C(25B)-C(26B)-C(27B)	-2.4(14)
C(25B)-C(26B)-C(27B)-C(22B)	2.2(14)

O(1B)-C(22B)-C(27B)-C(26B)	-178.6(8)
C(23B)-C(22B)-C(27B)-C(26B)	0.1(13)
Mo(1B)-N(3B)-C(28B)-C(33B)	-80(2)
Mo(1B)-N(3B)-C(28B)-C(29B)	102(2)
N(3B)-C(28B)-C(29B)-C(30B)	-179.1(7)
C(33B)-C(28B)-C(29B)-C(30B)	3.2(12)
N(3B)-C(28B)-C(29B)-C(34B)	1.6(12)
C(33B)-C(28B)-C(29B)-C(34B)	-176.0(8)
C(28B)-C(29B)-C(30B)-C(31B)	-3.0(13)
C(34B)-C(29B)-C(30B)-C(31B)	176.3(9)
C(29B)-C(30B)-C(31B)-C(32B)	2.6(15)
C(30B)-C(31B)-C(32B)-C(33B)	-2.4(15)
C(31B)-C(32B)-C(33B)-C(28B)	2.7(13)
C(31B)-C(32B)-C(33B)-C(35B)	178.7(9)
N(3B)-C(28B)-C(33B)-C(32B)	179.2(7)
C(29B)-C(28B)-C(33B)-C(32B)	-3.1(12)
N(3B)-C(28B)-C(33B)-C(35B)	3.4(12)
C(29B)-C(28B)-C(33B)-C(35B)	-178.9(7)
C(40B)-N(4B)-C(36B)-C(37B)	-3.3(12)
Mo(1B)-N(4B)-C(36B)-C(37B)	159.2(8)
C(40B)-N(4B)-C(36B)-C(41B)	-179.7(7)
Mo(1B)-N(4B)-C(36B)-C(41B)	-17.2(7)
N(4B)-C(36B)-C(37B)-C(38B)	4.1(13)
C(41B)-C(36B)-C(37B)-C(38B)	179.6(9)
C(36B)-C(37B)-C(38B)-C(39B)	-1.7(14)
C(37B)-C(38B)-C(39B)-C(40B)	-1.4(14)
C(36B)-N(4B)-C(40B)-C(39B)	0.0(12)
Mo(1B)-N(4B)-C(40B)-C(39B)	-149.5(8)
C(38B)-C(39B)-C(40B)-N(4B)	2.3(13)
N(4B)-C(36B)-C(41B)-C(42B)	-53.7(10)
C(37B)-C(36B)-C(41B)-C(42B)	130.4(10)
N(4B)-C(36B)-C(41B)-Mo(1B)	18.1(7)
C(37B)-C(36B)-C(41B)-Mo(1B)	-157.9(9)
C(36B)-C(41B)-C(42B)-Mo(1B)	85.7(7)
O(3C)-S(1B)-O(4C)-F(3C)	-128(2)
O(2C)-S(1B)-O(4C)-F(3C)	101.3(19)
C(43B)-S(1B)-O(4C)-F(3C)	3.4(15)
O(4B)-S(1B)-C(43B)-F(2B)	-83.1(14)
O(3B)-S(1B)-C(43B)-F(2B)	42.7(13)
O(2B)-S(1B)-C(43B)-F(2B)	156.2(13)
O(3C)-S(1B)-C(43B)-F(2C)	9(2)
O(2C)-S(1B)-C(43B)-F(2C)	150(2)
O(4C)-S(1B)-C(43B)-F(2C)	-113(2)
O(3C)-S(1B)-C(43B)-F(1C)	-134(2)
O(2C)-S(1B)-C(43B)-F(1C)	8(2)
O(4C)-S(1B)-C(43B)-F(1C)	105(2)
O(4B)-S(1B)-C(43B)-F(1B)	42.8(13)

O(3B)-S(1B)-C(43B)-F(1B)	168.7(11)
O(2B)-S(1B)-C(43B)-F(1B)	-77.8(11)
O(3C)-S(1B)-C(43B)-F(3C)	117(2)
O(2C)-S(1B)-C(43B)-F(3C)	-102.2(19)
O(4C)-S(1B)-C(43B)-F(3C)	-4.5(19)
O(4B)-S(1B)-C(43B)-F(3B)	158.3(12)
O(3B)-S(1B)-C(43B)-F(3B)	-75.8(11)
O(2B)-S(1B)-C(43B)-F(3B)	37.7(11)
F(2C)-C(43B)-F(3C)-O(4C)	118(2)
F(1C)-C(43B)-F(3C)-O(4C)	-128(2)
S(1B)-C(43B)-F(3C)-O(4C)	3.7(16)
S(1B)-O(4C)-F(3C)-C(43B)	-5(2)

7.6 Crystallographic Data for Chapter 4

Table 22. Crystal data and structure refinement for [Mo(N-2,6-F_2-C_6H_3)(CHCMe_2Ph)(DME)$(OTf)_2$], **Mo-18**.

Identification code	Buch265
Empirical formula	$C_{22}H_{25}F_8MoNO_8S_2$
Formula weight	743.49
Temperature	135(2) K
Wavelength	0.71073 Å
Crystal system, space group	Orthorhombic, Pbca
Unit cell dimensions	a = 13.3548(4) Å, α = 90°
	b = 16.4916(5) Å, β = 90°
	c = 26.2501(8) Å, γ = 90°
Volume	5781.4(3) $Å^3$
Z, Calculated density	8, 1.708 mg/m^3
Absorption coefficient	0.695 mm^{-1}
F(000)	2992
Crystal size	0.284 x 0.186 x 0.146 mm
Theta range for data collection	1.551 to 30.542°
Limiting indices	-19<=h<=19, -23<=k<=23, -17<=l<=37
Reflections collected / unique	77941 / 8841 [R(int) = 0.0366]
Completeness to θ = 25.242	99.9 %
Absorption correction	Numerical
Max. and min. transmission	0.9772 and 0.9104
Refinement method	Full-matrix least-squares on F^2
Data / restraints / parameters	8841 / 0 / 383
Goodness-of-fit on F^2	1.032
Final R indices [I>2σ(I)]	R1 = 0.0268, wR2 = 0.0633
R indices (all data)	R1 = 0.0402, wR2 = 0.0671
Extinction coefficient	n/a
Largest diff. peak and hole	0.436 and -0.415 e. $Å^{-3}$

Table 23. Crystal data and structure refinement for [Mo(N-2,6-F_2-C_6H_3)(CHCMe_2Ph)(IMes)$(OTf)_2$], **Mo-19**.

Identification code	Buch299
Empirical formula	$C_{39}H_{39}F_8MoN_3O_6S_2$
Formula weight	957.79
Temperature	140(2) K
Wavelength	0.71073 Å
Crystal system, space group	Monoclinic, $P2_1/n$
Unit cell dimensions	a = 10.3321(7) Å, α = 90°
	b = 17.9429(12) Å, β = 91.499(3)°
	c = 21.8141(14) Å, γ = 90°
Volume	4042.7(5) $Å^3$
Z, Calculated density	4, 1.574 mg/m^3
Absorption coefficient	0.515 mm^{-1}
F(000)	1952
Crystal size	0.565 x 0.396 x 0.290 mm
Theta range for data collection	2.160 to 33.142°
Limiting indices	-15<=h<=15, -12<=k<=27, -33<=l<=33
Reflections collected / unique	71536 / 15388 [R(int) = 0.0323]
Completeness to θ = 25.242	99.9 %
Absorption correction	Semi-empirical from equivalents
Max. and min. transmission	0.7465 and 0.7062
Refinement method	Full-matrix least-squares on F^2
Data / restraints / parameters	15388 / 0 / 545
Goodness-of-fit on F^2	1.042
Final R indices [I>2σ(I)]	R1 = 0.0300, wR2 = 0.0706
R indices (all data)	R1 = 0.0457, wR2 = 0.0756
Extinction coefficient	0.00042(12)
Largest diff. peak and hole	0.670 and -0.588 e. $Å^{-3}$

Table 24. Crystal data and structure refinement for [Mo(N-2,6-F_2-C_6H_3)(CHCMe_2Ph)(IMesCl_2)(OTf)$_2$], **Mo-21**.

Identification code	Buch300
Empirical formula	$C_{40}H_{39}Cl_4F_8MoN_3O_6S_2$
Formula weight	1111.60
Temperature	140(2) K
Wavelength	0.71073 Å
Crystal system, space group	Monoclinic, $P2_1/c$
Unit cell dimensions	a = 12.1004(4) Å, α = 90°
	b = 17.5629(7) Å, β = 98.083(2)°
	c = 21.8833(8) Å, γ = 90°
Volume	4604.4(3) $Å^3$
Z, Calculated density	4, 1.604 mg/m^3
Absorption coefficient	0.689 mm^{-1}
F(000)	2248
Crystal size	0.195 x 0.132 x 0.101 mm
Theta range for data collection	1.493 to 28.353°
Limiting indices	-16<=h<=16, -23<=k<=23, -28<=l<=28
Reflections collected / unique	54228 / 11398 [R(int) = 0.0680]
Completeness to θ = 25.242	100.0 %
Absorption correction	Numerical
Max. and min. transmission	0.9967 and 0.9617
Refinement method	Full-matrix least-squares on F^2
Data / restraints / parameters	11398 / 0 / 584
Goodness-of-fit on F^2	1.028
Final R indices [I>2σ(I)]	R1 = 0.0455, wR2 = 0.0919
R indices (all data)	R1 = 0.0870, wR2 = 0.1010
Extinction coefficient	n/a
Largest diff. peak and hole	0.976 and -0.754 e. $Å^{-3}$

Table 25. Crystal data and structure refinement for [Mo(N-2,6-F_2-C_6H_3)-(CHCMe_2Ph)(IMes)(OTf)(MeCN)][B(Ar^F)$_4$], **Mo-22**.

Identification code	Buch256
Empirical formula	$C_{72}H_{54}BF_{29}MoN_4O_3S$
Formula weight	1713.00
Temperature	135(2) K
Wavelength	0.71073 Å
Crystal system, space group	Triclinic, P-1
Unit cell dimensions	a = 12.7917(5) Å, α = 64.059(2)°
	b = 18.1854(7) Å, β = 73.654(2)°
	c = 18.6054(8) Å, γ = 70.333(2)°
Volume	3618.6(3) Å^3
Z, Calculated density	2, 1.572 mg/m^3
Absorption coefficient	0.335 mm^{-1}
F(000)	1724
Crystal size	0.643 x 0.470 x 0.461 mm
Theta range for data collection	1.712 to 33.254°
Limiting indices	-19<=h<=17, -28<=k<=21, -28<=l<=28
Reflections collected / unique	109223 / 27676 [R(int) = 0.0317]
Completeness to θ = 25.242	100.0 %
Absorption correction	Semi-empirical from equivalents
Max. and min. transmission	0.7465 and 0.7150
Refinement method	Full-matrix least-squares on F^2
Data / restraints / parameters	27676 / 168 / 1084
Goodness-of-fit on F^2	1.046
Final R indices [I>2σ(I)]	R1 = 0.0399 wR2, = 0.0969
R indices (all data)	R1 = 0.0640 wR2, = 0.1065
Extinction coefficient	n/a
Largest diff. peak and hole	0.672 and -0.590 e. Å^{-3}